Investigation of skeletal and cardiac muscle metabolism in patients with cardiovascular disease.

Sarah Maria Birkhoelzer

MD, PGCertMedEd, MRCP

Christ Church

Division of Cardiovascular Medicine

Radcliffe Department of Medicine

University of Oxford

A thesis submitted for the degree of

Doctor of Philosophy in Medical Sciences

Trinity Term 2025

Declaration

I hereby declare that this thesis and all results herein are entirely my work, unless otherwise indicated. The present results have not been submitted, either wholly or substantially, for another degree at this university, or a degree at any other institution. I have acknowledged assistance from colleagues and collaborators where relevant.

The total word count is 52284 words.

Abstract

Despite advances in treatment, heart failure (HF) remains a leading cause of morbidity and mortality worldwide. This thesis demonstrates the use of magnetic resonance imaging (MRI) and multinuclear magnetic resonance spectroscopy (^{31}P, ^{1}H, ^{13}C MRS) techniques to examine three structurally and metabolic different phenotypes of HF: non-ischaemic cardiomyopathy with reduced ejection fraction and iron deficiency (**Chapter 3 IRON HEART**), metabolic HF with preserved ejection fraction (**Chapter 4 DICE**), and pressure overload induced HF (**Chapter 5 HYPER HEART**). The overarching aim was to characterise myocardial and skeletal muscle energetics in each phenotype and examine the effect of three targeted interventions – intravenous iron, Ninerafaxstat, and aortic valve intervention, on substrate metabolism, mitochondrial function and functional outcomes.

Chapter 3 described the first study (**IRON HEART)** combing cardiac and skeletal muscle energetic assessment following intravenous ferric carboxymaltose in non-ischaemic cardiomyopathy and iron deficiency. Intravenous iron has shown benefits in large trials, reducing symptoms, improving exercise capacity, and lowering hospitalisation rates, though mechanisms remain unclear. The results demonstrated a significant improvement in ejection fraction, exercise capacity, and skeletal muscle mitochondrial capacity without an improvement in myocardial energetics. These findings suggest a combined benefit of iron on cardiac and skeletal muscle, warranting larger trials.

Chapter 4 (**DICE**) demonstrates a proof of concept for metabolic modulation in HFpEF and the potential for cardiac mitotropes to become an additional pillar in the treatment of metabolic HFpEF. The novel mitotrope, Ninerafaxstat, as a partial fatty acid inhibitor, was safe and improved cardiac energetics by restoring metabolic flexibility. The energetic improvement was linked to increased exercise capacity and symptoms. It is the first of its kind and might offer potential as a targeted therapy in a phenotype with limited treatment options.

Chapter 5 (HYPER HEART) explored the metabolic adaptations before and after pressure unloading in severe aortic stenosis. The study revealed a dissociation between structural and metabolic recovery post valve intervention. It highlighted the potential role of multinuclear magnetic resonance spectroscopy and imaging to guide timing of valve intervention, in particularly in asymptomatic patients who already display structural remodelling.

Table of Contents

List of Figures

List of Tables

List of Abbreviations and Definition of Terms

Abbreviation	Definition
1H	Proton/hydrogen
13C	Carbon 13
3D-CSI	Three-dimensional chemical shift imaging
3-KAT	3-ketoacyl-coenzyme A thiolase
6-MWT	Six-minute Walk test
6-MWD	6-minute walk distance
31P	Phosphorus
°C	Degrees Celsius
µg	Microgram
ACC	American Heart Association
Acetyl-CoA	Acetyl coenzyme A
ADP	Adenosine diphosphate
AE	Adverse event
AF	Atrial fibrillation
AHA	American Heart Association
AGE	Glycation end-products
ALT	Alanine aminotransferase
ANOVA	Analysis of variance
API	Active Pharmaceutical Ingredient
AS	Aortic stenosis
ASL	Arterial spin labelling
AST	Aspartate aminotransferase
ATP	Adenosine triphosphate

AUC	Area under the curve
AVR	Aortic Valve Replacement
ß-OHB	ß hydroxybutyrate
BID	Twice daily
BMI	Body mass index
BP	Blood pressure
bpm	Beats per minute
bSSFP	Balanced steady-state free precession
BUN	Blood Urea Nitrogen
CABG	Coronary artery bypass grafting
CAD	Coronary artery disease
CHF	Chronic heart failure
CI	Confidence interval
CK	Creatine kinase
CKMB	Myofibrillar creatine kinase
CKmito	Mitochondrial creatine kinase
CKD	Chronic kidney disease
ClinRO	Clinician-reported outcome
Cmax	Maximum observed plasma concentration
CMR	Cardiac magnetic resonance
CO	Cardiac output
CoA	Coenzyme A
CRLB	Cramer-Rao lower bounds
CRP	C-reactive protein
CRT	Cardiac Resynchronisation Therapy
CT	Computer Tomography

CW	Continuous wave
DbCM	Diabetic cardiomyopathy
DCA	Dichloroacetic acid
DICOM	Digital Imaging and Communications in Medicine
DPG	Diphosphoglycerate
DRESS	Depth resolved surface coil spectroscopy
e’	Early diastolic mitral annulus velocity
E	Early diastolic mitral inflow velocity
EAT	Epicardial adipose tissue
ECG	Electrocardiogram
ECV	Extracellular volume
eCRF	Electronic case report form
EDC	Electronic data capture
EDV	End-diastolic volume
EDTA	Ethylenediaminetetraacetic acid
EF	Ejection fraction
eGFR	Estimated glomerular filtration rate
EOA	Effective orifices area
EOS	End of study
EOT	End of treatment
ESC	European Society of Cardiology
ETC	Electron transport chain
FA	Fatty acid
FADH2	dihydro flavin adenine dinucleotide
FAO	Fatty acid oxidation
FAT / CD36	Fatty acid translocase

FCM	Ferric carboxymaltose
FFA	Free fatty acid
FOV	Field of view
FSH	Follicle-stimulating hormone
GBCA	Gadolinium-based contrast agent
GCP	Good Clinical Practice
Gd	Gadolinium
GP	General practitioner
GRE	Gradient echo
GTP	Guanosine triphosphate
γ-GT	Gamma Glutamyl Transferase
H2FPEF	Heavy, Hypertensive, Atrial Fibrillation, Pulmonary Hypertension, Elder, Filling Pressure
HbA1c	Glycated haemoglobin A1c
HDL	High-Density Lipoprotein
HF	Heart failure
HFA	Heart Failure Association
HFpEF	Heart failure with preserved ejection fraction
HFrEF	Heart failure with reduced ejection fraction
HLA	Horizontal long axis
HR	Heart rate
HOMA2-%B	Homeostatic model assessment-beta cell output of insulin
HOMA-S	Homeostatic model assessment-insulin sensitivity
hs-cTn	High-sensitivity cardiac troponin
ICA	Invasive coronary angiograph
ICF	Informed consent form
IEC	Independent Ethics Committee

IHD	Ischaemic heart disease
IMP	Investigational medicinal product
IQR	Interquartile range
IR	Immediate release
IR	Inversion recovery
IU	International Units
IV	Intravenous
JMRUI	Java-based Magnetic Resonance User Interface
Kcal	kilocalorie
KCCQ-23	23-item Kansas City Cardiomyopathy Questionnaire
LA	Left atrium (atrial)
LAVI	Left atrial volume index
LAEF	Left atrial ejection fraction
LDH	Lactate dehydrogenase
LDL	Low-Density Lipoprotein
LGE	Late gadolinium enhancement
LV	Left ventricle (ventricular)
LVEDVi	Left ventricular end diastolic volume index
LVEF	Left ventricular ejection fraction
LVESV	Left ventricular end-systolic volume
LVMi	Left ventricular mass index
LVOT	Left ventricular outflow tract
MBF	Myocardial blood flow
MBV	Myocardial blood volume
MDT	Multidisciplinary Team Meeting
mg	Milligram

Min	Minute/ minutes
ml	Milliliter
mmHg	Millimetre mercury
mmol	Millimole
MPI/MPS	Myocardial perfusion imaging/scan
MR	Magnetic resonance
MRI	Magnetic resonance imaging
MRS	Magnetic resonance spectroscopy
ms	Millisecond
MS	Mass spectroscopy
MTG	Myocardial triglyceride/triglycerides
µmol	micromole
NAD+	Oxidised form of nicotinamide adenine dinucleotide
NADH	Reduced form of nicotinamide adenine dinucleotide
NF	National Formulary
ng	Nanogram
NHS	National Health Service
NICM	Non-ischaemic cardiomyopathy
NMR	Nuclear magnetic resonance
NT-proBNP	N-terminal pro-brain natriuretic peptide
NYHA	New York Heart Association
OCMR	Oxford Centre for Clinical Magnetic Resonance Research
OMT	Optimal medical treatment
OUH	Oxford University Hospitals NHS Foundation Trust
OXSA	OXford Spectroscopy Analysis
PALS	Pulsed arterial spin labelling

PCr	Phosphocreatine
PCr/ATP	Phosphocreatine to adenosine triphosphate ratio
PDE	Phosphodiester
PDFF	Proton density fat fraction
PDH	Pyruvate dehydrogenase
PET	Positron Emission Tomography
PGI-C	Patient Global Impression of Change
PGI-S	Patient Global Impression of Severity
pmol	Picomole
PK	Pharmacokinetic(s)
PP	Per Protocol
PPARα	Peroxisome proliferator-activated receptor-α
PRESS	Point RESolved Spectroscopy
PRO	Patient-reported outcome
PW	Pulsed wave
QC	Quality control
QoL	Quality of life
QTcF	Heart rate-corrected QT interval using Fridericia's formula
QUICKI	Quantitative insulin sensitivity check index
RAAS	Renin angiotensin aldosterone system
REC	Research ethics committee
RF	Radiofrequency
ROI	Region of interest
ROS	Reactive oxygen species
RV	Right ventricular
RVEF	Right ventricular ejection fraction

SA	Short axis
SAE	Serious adverse event
SAVR	Surgical Aortic Valve Replacement
SBP	Systolic blood pressure
SCMR	Society for Cardiovascular Magnetic Resonance
SD	Standard deviation
SE	Standard error
SEM	Standard error of the mean
SFP	Sterile fluid pathway
SSFP	Steady-state free precession
SGLT2i	Sodium glucose transporter 2 inhibitor
SUSAR	Suspected Unexpected Serious Adverse Reaction
SPECT	Single-photon emission computed tomography
SV	Stroke volume
T	Tesla
T1	Longitudinal or spin-lattice relaxation
T2	Transverse or spin-spin relaxation
T2DM	Type 2 Diabetes Mellitus
TAVI	Transcatheter Aortic Valve Implantation
TASQ	Toronto Aortic Stenosis QoL Questionnaire
TD	Trigger delay
TCA	Tricarboxylic acid cycle
TE	Echo time
TI	Inversion time
TMZ	Trimetazidine
TTE	Transthoracic echocardiography

Ttl	Total
UACR	Urinary albumin-creatinine ratio
UK	United Kingdom
ULN	Upper limit of normal
USA	United States of America
VLA	Vertical Long Axis
W	Watt
WOCBP	Woman of childbearing potential
WSVD	Whitened singular value decomposition

Acknowledgements

First and foremost, I would like to express my deepest gratitude to **Professor Stefan Neubaue**r for offering me the opportunity to pursue a DPhil in OCMR. His unwavering support and leadership fostered an environment where I felt psychologically safe and empowered to excel beyond my imagination.

I am profoundly thankful to **Professor Damian Tyler**, for his guidance as a supervisor and for serving as a role model of a compassionate leader and a devoted parent.

My heartfelt appreciation goes to **Professor Oliver Rider** for sharing his profound wisdom on myocardial metabolism and for offering invaluable life support as I navigated the challenges of a professional career while striving to be a good parent. Our shared passion for making the world a better place has been a source of inspiration.

To **Professor Ladislav Valkovič**, your patience and belief in my abilities has been an incredible gift. Thank you for your kindness and encouragement.

I am deeply grateful to **Dr. Jenny Rayner**, one of the few female cardiologists who have supported my career and served as a genuine role model. Your support meant a lot.

Dr. Ferenc Mózes, your kindness and intellect have left a lasting impression on me. You taught me the value of embracing diverse perspectives and showed me how this drives excellence.

Dr. Jordan McGing, **Dr. Aaron Axford** and **Dr. James Grist** our teamwork extended to so many areas of my DPhil. Thank you for helping with areas that were beyond my capabilities.

I would also like to thank the radiographer team, led by **Rebecca Mills**, whose "can-do" attitude helped overcome numerous challenges during my DPhil. Thank you, **Joana Leal Pelado**, for your assistance with the DICE visits; **Neil Fox**, for bringing joy to our scanning and reporting sessions; and **Arun Thumbolil Muyyayil**, for facilitating the HYPER HEART visits and navigating the challenges of the MRI scanner.

To my clinical colleagues in the '**TAVI team**' and in the '**Heart Failure Team**', thank you for supporting my recruitment efforts.

I am grateful to the **British Heart Foundation** and the **Wellcome Trust** for their generous support and funding of my research facilitating my academic journey.

I extend my heartfelt gratitude to my professional coach, US colleague and friend **Dr. Deborah Lockwood**, whose unwavering support helped me forgive those who hurt me, release the burden of motherly guilt, reshape my mindset and goals, and navigate the challenges of both my professional and personal life with renewed strength and clarity.

A special thanks to my dear friends **Dr. Alicja Jasińska Piadlo** and **Dr. Anna Merz**, who lifted me up during life's challenges, offered comfort in moments of vulnerability, and gave me the strength to keep going.

To my husband, **Dr. Francis Gardner**, your unwavering support of my past, present, and future career aspirations—no matter how ambitious or seemingly delusional—you have been my rock. To

my children, **Charlotte** and **Benjamin**, you are my lifeline, my external batteries, and the greatest joy of my life. You are the ultimate reason I have made it to where I am today, giving me the energy and purpose to live my dreams.

My DPhil has been so much more than research—three transformative years of personal development as a researcher, public speaker, doctor, and parent. These years have been shaped by freedom, creativity, and connection with incredible people who have broadened my perspective and helped me become a better person. Finally, I wish to express my deepest gratitude to my supervisors, who not only supported my research and thesis writing but also served as moral compasses during life's challenges.

Thank you all for being part of this incredible journey.

1 Introduction

The prevalence of HF is rising worldwide [1] due to increasing cardiovascular risk factors, including physical inactivity, poor diet, obesity, T2DM, hypertension (HTN), and aortic stenosis (AS). [2] Around 200.000 new diagnosis of HF occur yearly in the UK leading to a prevalence of over 1 million. HF is classified into preserved (HFpEF), mildly reduced (HFmrEF), and reduced ejection fraction (HFrEF). It is characterised by multiple aetiologies often associated with obesity, type 2 diabetes (T2DM) and iron deficiency. [3] Magnetic resonance imaging (MRI) and multinuclear magnetic resonance spectroscopy (^{31}P, ^{1}H, ^{13}C MRS) offer detailed assessment of structural and metabolic changes offering an early diagnostic and therapeutic insight. Although these techniques are primarily research tools, they hold potential for providing risk stratification and personalised therapeutic options.

1.1 Heart failure overview

The HF syndrome is characterised by shortness of breath, fluid overload, and fatigue, where the heart fails to deliver the body's demand of oxygen and nutrients. Its aetiology can be divided into intra-myocardial causes (for example ischaemia, non-ischaemic cardiomyopathy or valve disease) and extra-myocardial causes (for example metabolic syndrome, T2DM, cardiac amyloidosis). [4] The assessment of cardiovascular biomarkers like N-terminal pro B-type natriuretic peptide (NTproBNP) support the diagnosis [5] and often trigger referral pathways for specialist evaluation. Subsequent cardiac imaging is performed to assess structural changes including ejection fraction (EF) or increased left ventricular (LV) filling pressures and led to classification of HF with reduced ejection fraction (HFrEF, EF <40%), HF with preserved EF (HFpEF, EF >50%), HF with mildly reduced EF (HFmrEF, EF 41-49%). [6] The pathophysiological origin is characterised by distinct alterations in structure, function and metabolism. HFpEF is commonly driven by an extra-myocardial cause including obesity, hypertension and diabetes, whereas HFrEF is more commonly associated with

intra-myocardial pathology. [4] HFpEF is characterised by concentric LV hypertrophy, impaired relaxation resulting in pressure overload, as opposed to the eccentric remodelling in HFrEF due to volume overload with subsequent LV dilatation. [7] Structural changes are seen across the spectrum of HF and are linked to changes in myocardial metabolism, however the degree of interaction and subsequent impact on clinical outcomes remains understudied. [8]

1.2 Metabolism and Energetics

Metabolism refers to the cellular pathways that 'transform/change' [9] the energy stored in the chemical bonds of different fuels into the high energy intermediates (Adenosine Triphosphate, ATP). In the heart, the main substrates for ATP production are glucose and fatty acids. Three pathways may be used for ATP production depending on oxygen and substrate availability: glycolysis (in the cytosol), the tricarboxylic acid cycle (TCA cycle, also known as the citric acid cycle or Krebs cycle) and oxidative phosphorylation (OXPHOS in the mitochondria). [10] (See **Figure 1.1**) The biochemical principles of these pathways were established through seminal discoveries recognised by the 1953 Nobel Prize in Physiology or Medicine, awarded jointly to Sir Hans Adolf Krebs and Fritz Albert Lipmann. Sir Hans Adolf Krebs [11] was a German doctor who studied at the University of Munich, Germany, under Dr. Otto Warburg who first described the 'Warburg effect', the increase in anaerobic glycolysis in cancer cells in 1920. [12] Fritz Albert Lipmann was a German-American doctor [13], who discovered coenzyme A. Together Krebs and Lipman discovered the cyclic nature of the TCA cycle (Krebs cycle) and identified coenzyme A as a key carrier of acyl groups in energy metabolism — a discoveries that form the cornerstone of our understanding of cellular and cardiac bioenergetics. [14] Earlier Prof. Albert von Szent-Györgyi, who was awarded the Nobel Prize in Medicine in 1937 [15], discovered the role of biological oxidation, thereby laying the groundwork for Krebs and Lipman.

Glycolysis converts one glucose molecule (containing 6 carbon) into two nicotinamide adenine dinucleotide (NADH) molecules, two ATP molecules and two Pyruvate molecules. Depending on the type of fatty acid, fatty acid metabolism including fatty acid oxidation (FAO) or β -oxidation, the TCA cycle and the electron transport chain (ETC), converts one fatty acid molecule (12-18 carbon) into one acetyl coenzyme A (Acetyl-CoA), one NADH, and Flavin Adenine Dinucleotide ($FADH_2$) per cycle of β-oxidation, therefore producing 8 of each undergoing seven cycles of β -oxidation for one palmitic acid molecule of 16 carbons. [16] The last enzyme of the β-oxidation is 3-Ketoacyl-CoA thiolase [17] which is inhibited by Trimetazidine [18] and Trimetazidine precursor Ninerafaxstat (as discussed in **Improve Di**abetic **C**ardiac **E**nergetic (IMPROVE-DiCE)-2 Study **'DICE' Chapter 4**). Acetyl-CoA gets further oxidised in the TCA cycle to produce NADH which together with $FADH_2$ donates electrons to the four proteins of the ETC to generate a proton gradient across the inner mitochondrial membrane. Iron is an essential cofactor for the enzymes of the ETC (complex I, complex II, complex III, cytochrome C, and complex IV) [19], which if absent may contribute to reduced energy production (as discussed in **IRON Chapter 3**). The proton gradient between the matrix of the mitochondria and the inter-membrane space of the mitochondria provides energy for ATP production by phosphorylation of adenosine diphosphate (ADP). [20] The phosphate of ATP is subsequently shuttled, via the creatine kinase (CK) shuttle to the myocytes to power muscle contraction. [21] Each pathway has a different phosphorylation to oxidation ratio (P/O ratio), i.e. the amount of ATP generated per oxygen molecule consumed by the mitochondria. [22] The complete oxidation of fatty acids in the mitochondria requires around 30% more oxygen than complete glucose oxidation. [16] Therefore pathological states like LVH or HF may promote a switch from fatty acid metabolism to glycolysis as an oxygen independent pathway of ATP production [23] (as discussed in **HYPER-HEART Chapter 5**).

The term "Energetics" is used to describe the energy balance at the cellular level concerning the ratio of a number of molecules like ATP/ADP, nicotinamide adenine dinucleotide ($NADH/NAD^+$),

and Phosphocreatine/Creatine (PCr/Cr). [24] After the production of ATP from ADP and phosphate in the mitochondria, the high energy phosphate bond is transferred from creatine to form Phosphocreatine (PCr) which is transported to the myofibrils where its energy is used for contraction and relaxation through sarcoendoplasmic reticulum Ca^{2+}-ATPase (SERCA). [25, 26] The ratio between PCr and creatine serves as an indicator of the energetic state of the heart [27], with a reduced PCr/ATP ratio reflecting compromised myocardial energy reserves and efficiency. [25] The value of PCr/ATP is typically around 2 in athletes and sedentary controls, but is reduced in many cardiac pathologies like DCM [28], hypertrophic cardiomyopathy (HCM) [29], and HF [25, 30] to around 1 in patients with HFpEF.[31]

Therapeutic interventions to modulate cardiac energetic and improve cardiac performance are limited. [32] This thesis presents three distinct interventions and their effect on cardiac energetics (PCr/ATP) and are examined in three different heart failure populations. In **Chapter 3 (IRON HEART),** the effects of intravenous (i.v.) Ferric carboxymaltose (FCM) in non-ischaemic cardiomyopathy with reduced EF and iron deficiency are assessed. In **Chapter 4 (DICE),** the partial fatty acid oxidation inhibitor, Ninerafaxstat, is examined in cohort of HFpEF, obesity and T2DM, and in **Chapter 5 (HYPER-HEART),** the effect of pressure load and removal in patients with severe aortic stenosis (AS) undergoing transcatheter aortic valve implantation (TAVI) is evaluated.

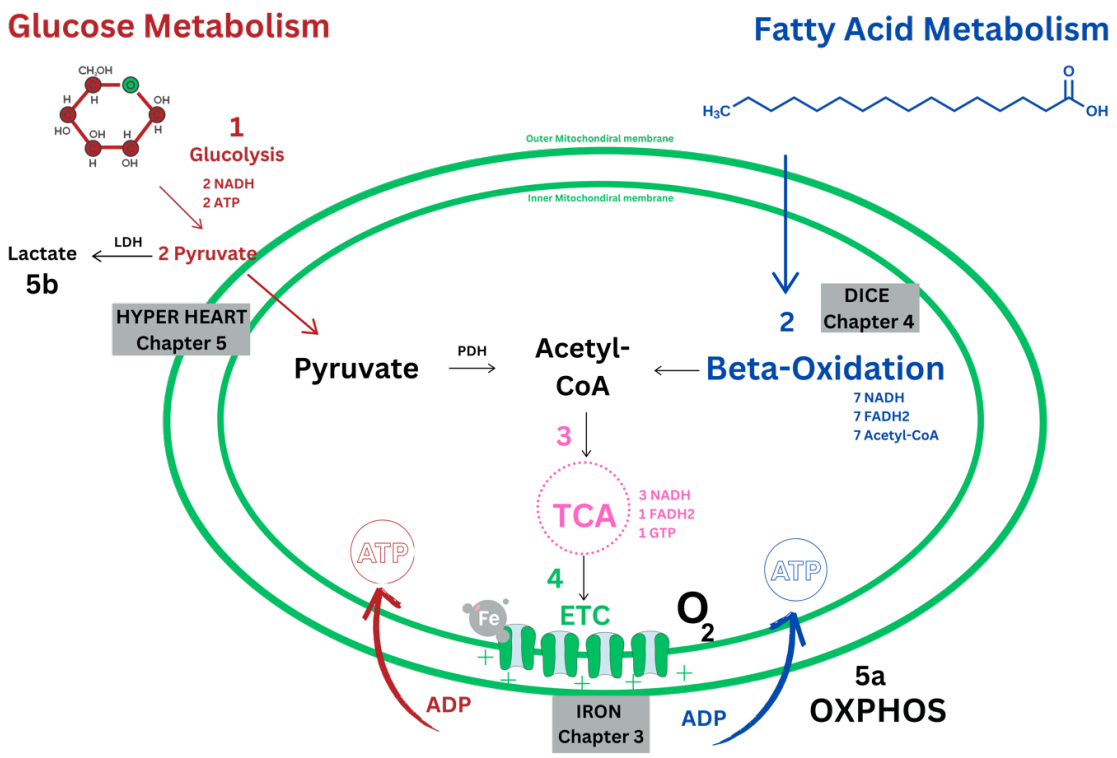

Figure 1.1 Overview of cellular metabolism and associated thesis chapters

There is a link between alterations in cardiac metabolism and cardiovascular disease, however there are few therapeutics which target these pathways with the aim to improve cardiovascular disease. There are two main substrate pathways for ATP production: Glucose metabolism via glycolysis (1), Tricarboxylic acid (TCA) cycle and Electron Transport Chain (ETC), which produces two NADH, two ATP and two Pyruvate, and Fatty acid metabolism of for example palmitate via β-oxidation (2) into ~7 Acetyl-CoA, ~7 NADH, ~7 $FADH_2$. Acetyl-CoA enters the TCA cycle (3) where its oxidation produces three NADH and one $FADH_2$ and one Guanosine triphosphate (GTP) per cycle. NADH and $FADH_2$ donate electrons to the ETC (4) to generate an electrochemical proton gradient (+) across the mitochondrial inner membrane. ATP is produced (5a) via oxidative phosphorylation (OXPHOS). 3-Ketoacyl-CoA thiolase is last enzyme of the β -oxidation and inhibited by Trimetazidine the main working substance in Ninerafaxstat (see DICE Chapter 4). Iron is an essential cofactor for the enzymes of the ETC (complex I, complex II, complex III, cytochrome C, and complex IV) (see IRON Chapter 3). Reduction in oxygen availability as seen in cardiovascular disease like heart failure and/or left ventricular hypertrophy reduces aerobic pathway via Pyruvate dehydrogenase (PDH) and promotes the anaerobic pathway (5b) of ATP production via Lactate dehydrogenase (LDH) (see HYPER HEART Chapter 5).

1.2.1 Metabolism in Healthy Muscle

The utilization of different substrates changes with age and disease. The foetal heart utilizes glucose and lactate [33] and becomes increasingly metabolically flexible, due to the increasing presence of oxygen and fatty acids, and generates ATP from fatty acids, glucose, lactate, and ketone bodies. [27] With abundance of oxygen, the heart predominantly uses β-oxidation to process short, medium and long chain fatty acids for energy production. [27] Depending on the type of fatty acid, the complete oxidation of one fatty acid molecule may generate over 100 ATP molecules [34] and therefore has the highest yield of ATP production at the expense of the greatest oxygen consumption.[35] In contrast, during glycolysis, the oxidation of one molecule of glucose may only produce between 32-38 molecules of ATP. Outside the mitochondria 2 ATP, 2 NADH (producing a further 5 ATP molecules), and 2 molecules of pyruvate are produced per glucose molecule. Inside the mitochondria, out of each molecule of pyruvate, a further 12 ATP are produced via the Krebs Cycle and ETC.

In the skeletal muscle, substrate utilisation depends on the type of muscle [36] and the degree of activity i.e. resting state, high intensity activity, or endurance. Slow muscle fibres are well perfused to deliver oxygen to oxidative enzymes generating ATP via aerobic metabolism. Fast muscle fibres generate ATP predominantly via anaerobic metabolism. [37] The degree of aerobic and anaerobic metabolism to produce ATP in the skeletal muscle depends on the intensity and duration of exercise. [38]

1.2.2 Metabolism in heart failure

Depending on the type of HF (HFpEF, HFrEF), the aetiology of HF (diabetic cardiomyopathy, hypertrophy or ischaemia) and the severity of HF (compensated or decompensated heart failure), substrate utilization and the contribution of energy production from myocardial fatty acid oxidation and glycolysis varies. [25] The metabolism of fatty acid oxidation (FAO) and glycolysis is tightly

regulated by the Glucose Fatty-Acid Cycle first described by Randle et. al. [39] The degree of metabolic remodelling depends on the type of cardiac structural remodelling, the type and degree of heart failure [40] and additional systemic metabolic disorders (overweight, obesity, T2DM) [31, 41, 42]. In addition, increases in body mass index (BMI), age and LV mass negatively contribute to cardiac energetic state. [31]

1.2.2.1 Metabolic Alterations in Heart Failure with Reduced Ejection Fraction

The metabolic modulation in HFrEF is often simply described as a switch to oxygen independent glycolysis [23], which originated from original studies in ischaemic cardiomyopathy [34]. However, all three key stages of cardiac energy metabolism; substrate utilisation, oxidative phosphorylation, and ATP transfer by the Creatine Kinase (CK) energy shuttle, may be affected. [27]

Metabolic studies with Positron Emission Tomography (PET) demonstrated that in HFrEF myocardial glucose uptake is increased while fatty-acid uptake was attenuated. [43] However, the metabolic phenotype of non-ischaemia cardiomyopathy is better described as relative augmentation of glucose utilisation with impaired metabolic flexibility, rather than a universal 'switch' to anaerobic glycolysis. Fatty acid metabolism in HF represents a dynamic and multifactorial process rather than a single, uniform alteration. Lopaschuk et al [34] highlights that FAO reflects a finely balanced interplay between substrate availability, intracellular signalling, and mitochondrial function. (see **Table 1.1**)

Plasma levels of free fatty acids are increased in HFrEF in comparison to heart failure with mildly reduced ejection fraction or preserved ejection fraction. [44] Despite this fatty acid uptake and FAO are reduced [45], processes regulated by the nuclear transcription factor peroxisome proliferator-activated receptor-α (PPARα), which modulates the expression and activity of key enzymes involved in FAO. In HFrEF, PPARα is downregulated, leading to suppression across all steps of myocardial fatty acid metabolism. [46] Furthermore, a suppression in pyruvate dehydrogenase

(PDH) activity by PDH kinase (PDK) results in uncoupling of glycolysis and glucose oxidation with increased lactate production. [45] Beyond substrate metabolism, mitochondrial dysfunction, increased mitochondrial apoptosis [47], increased oxidative stress and decreased production of enzymes of the respiratory chain [48] contribute further to the metabolic derangement seen in HF.

The third step of cardiac energy metabolism is referred to as ATP transfer and utilisation, which is commonly measured as Creatinine Kinase (CK) flux. Although reduction in CK flux is associated with worse outcomes in heart failure, the mechanism behind CK reduction is less well understood and may be attributed to mitochondrial dysfunction, limitation in creatine availability, or altered creatine kinase activity.[49]

Mechanism contributing to impaired metabolic flexibility in Heart Failure with Reduced Ejection Fraction

Substrate availability	Plasma free fatty acids are elevated in HFrEF versus heart failure with mildly reduced or preserved ejection fraction. [44]
	Reduced fatty acid uptake [45]
Modulation of enzyme activity	PPARα downregulation: suppression of of cardiac fatty acid metabolism. [46]
	Reduction in PDH activity resulting in uncoupling of glycolysis and glucose oxidation. [45]
Mitochondria dysfunction	Mitochondrial dysfunction and apoptosis, increased oxidative stress [50]
Reduced CK flux	Mitochondrial insufficiency, limitation in creatine availability, altered creatine kinase activity.

Table 1.1 Overview of metabolic alterations in HFrEF

HFrEF: Heart Failure with reduced ejection fraction; PPARα: peroxisome proliferator-activated receptor-α; PDH: pyruvate dehydrogenase; CK: Creatine Kinase

The totality of current literature suggests that in HFrEF, if free fatty acid availability is limited, baseline myocardial glucose uptake is increased (see **Figure 1.2**) and metabolic flexibility is decreased. [49]

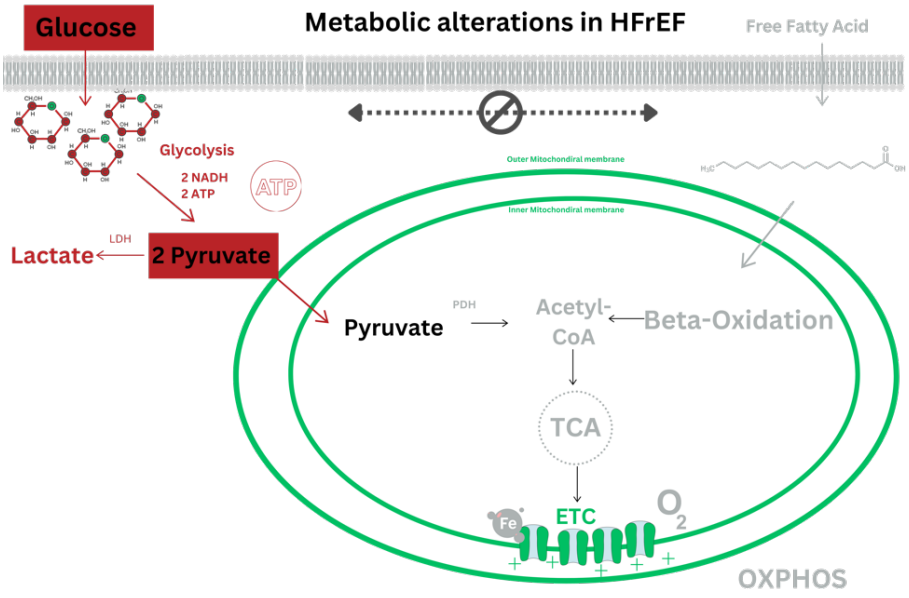

Figure 1.2 Metabolic alterations in HFrEF

Substrate availability is regulated by the Glucose Fatty-Acid Cycle resulting in the inhibition of glucose metabolism by fatty acids in the muscle and inhibition of fatty acid metabolism in the adipose tissue with increased concentrations of glucose (dotted arrow). Reduced fatty acid availability (grey) results in increased myocardial glucose uptake (red).

Iron deficiency (ID) is common in HFrEF. [51] Iron modulates many steps involved in mitochondrial function and energy production via oxidative phosphorylation [52]. Myocardial iron deficiency is linked to impaired mitochondrial function [53] and reduction of ATP production via oxidative phosphorylation and an increase in glycolysis and lactate formation. [54] This results in impaired cardiac [55] and skeletal muscle oxidative metabolism. [56] Iron supplementation leads to increased NADH formation and oxygen consumption, boosting ATP production through oxidative

phosphorylation. [52] Clinically, i.v. iron replacement results in an improvement of symptoms, Quality of Life (QoL), and exercise capacity. [57-65] However, the benefits of iron repletion on cardiac and skeletal muscle mitochondrial function are understudied. A recent small randomised controlled trial [66] demonstrated an improvement in skeletal muscle oxidative capacity (reduction in lactate production) and exercise capacity of patients with HFrEF after iron repletion, which supports the hypothesis that iron repletion augments skeletal muscle mitochondrial oxidative capacity. [67]

The **IRON-HEART** study (**Chapter 3**) is the first to examine the effect of i.v. Ferric carboxymaltose (FCM) on cardiac metabolism and skeletal muscle oxidative capacity, perfusion and function with the aim to establish a potential mechanism of the known clinical benefit of i.v. FCM.

1.2.2.2 Metabolic Alterations in Heart Failure with Preserved Ejection Fraction

Precise energetic adaptations associated with HFpEF are less well understood, partially due to the complicating contribution of insulin resistance and diabetes which commonly coexist. In HFpEF, progressive insulin resistance activates peroxisome proliferator activated receptor-α (PPARα) [68] which results in increased levels of circulating free fatty acids (FFA) and subsequent increased myocardial uptake and metabolism of FFA [69] at the expense of increased oxygen consumption. In addition, insulin resistance results in a downregulation of insulin-regulated glucose transporter 4 (GLUT4) and inhibition of pyruvate dehydrogenase (PDH) which catalyses the decarboxylation of pyruvate into acetyl-CoA resulting in increased lactate production by uncoupling of glycolysis from glucose oxidation. [70] (See **Figure 1.3**) As a result metabolic HFpEF, obesity, insulin resistance, T2DM, and LVH, which are commonly linked, display a reduction in myocardial energetics. [71]

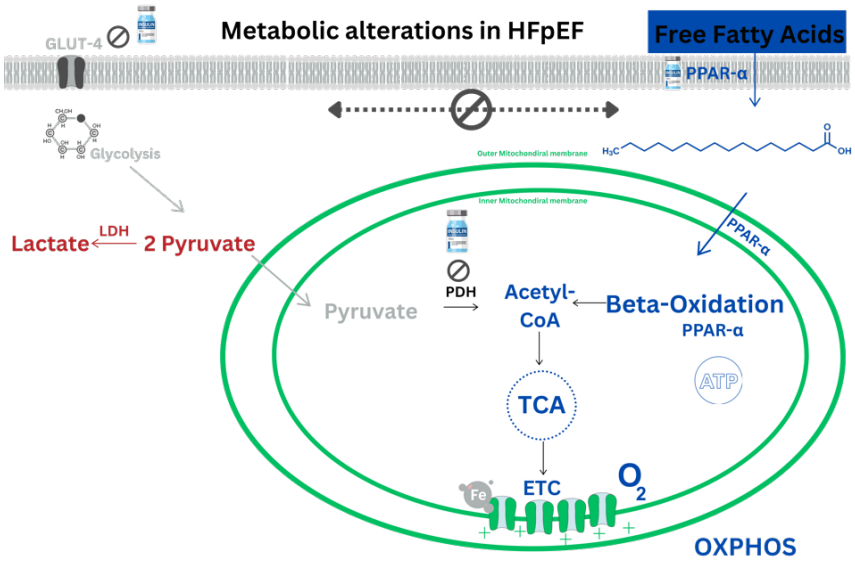

Figure 1.3 Metabolic alterations in HFpEF

Insulin resistance activates peroxisome proliferator activated receptor-α (PPARα) resulting in increased Free Fatty Acids (FFA) uptake, metabolism and oxygen consumption (blue). Insulin resistance results in inhibition of insulin-regulated glucose transporter 4 (GLUT4) and pyruvate dehydrogenase (PDH) (grey) resulting in increased lactate production by uncoupling of glycolysis from glucose oxidation (red).

Ninerafaxstat was designed to counteract the undesirable consequences of increased myocardial fatty acid uptake and metabolism. Its two key compounds include the partial fatty acid oxidation (FAO) inhibitor Trimetazidine (TMZ), its structural analogue carboxy-8814 [72] and nicotinic acid [73]. It was initially studied in participants at risk of HFpEF with obesity and diabetes (IMPROVE DiCE) [74] to demonstrate its mechanistic effect in shifting substrate metabolism towards glucose metabolism (TMZ) and demonstrate increase cardiac metabolic efficiency by increasing the synthesis of NAD^+ to improve mitochondrial function [75]. In this mechanistic trial [74] it highlighted its potential to improve myocardial energetics and augmentation of PDH flux was demonstrated resulting in improved PCr/ATP and diastolic function. In this thesis the follow up trial (IMPROVE-DiCE-2, **Chapter 4**) is presented, aiming to confirm mechanistic effect in patient with obesity, diabetes and HFpEF.

1.2.2.3 Metabolic Alteration in pressure overload

Aortic stenosis and subsequent pressure load leads to left ventricular (LV) remodelling, LVH [76] and changes in metabolism [77]. This may lead to a shift of myocardial metabolism away from oxidative metabolism and FAO towards glycolysis [77] and increased myocardial uptake of ketone bodies [78]. However, the pre-clinical evidence is inconclusive (see **Table 1.2**) and is discussed in more details in **Chapter 5.1.1**. Human studies in AS have demonstrated a shift from FAO towards glucose metabolism with increased glucose update and glycolysis but no increase in glucose oxidation overall resulting in a reduction in PCr/ATP. [79] Increasing diastolic pressures in AS [80] and LVH [79] are linked to decreased PCr/ATP and systolic function [81]. However, in AS regardless of diastolic pressure, energy reserve measured by total PCr [41], PCr/ATP [81], and CK flux [81] is reduced.

Animal studies			**Human studies [49, 82-84]**
spontaneous hypertensive rats [85]	Hyperthyroid rats [86]	abdominal aortic banding [87]	
↑ Glucose metabolism No change in anaerobic glycolysis ↑ Glucose oxidation	↓ PDH flux ↓ Glucose oxidation	↑ Lactate production (uncoupling of glycolytic metabolism from glucose oxidation)	↓ FAO ↑ Glucose uptake ↑ Glycolysis No change in glucose oxidation

Table 1.2 Metabolic alterations in left ventricular hypertrophy

PDH= Pyruvate dehydrogenase; FAO= fatty acid oxidation

The purpose of the HYPER HEART study (**Chapter 5**) was multifold. Firstly, to assess cardiac metabolism and left ventricular remodelling in patients with LV pressure load, and to confirm that severe AS results in reduced cardiac energetics as shown in previous studies [79, 88] and is linked to pressure overload [80]. Secondly, to verify the reversibility of energetic impairment with pressure removal, which has been shown with aortic valve replacement. [89] Thirdly, to investigate the long-term effects of transcatheter aortic valve implantation (TAV) on LVH regression and energetic recovery. [84]

1.3 Magnetic Resonance Spectroscopy and Metabolism

Magnetic resonance spectroscopy (MRS) is an advanced technique that complements magnetic resonance imaging (MRI) and offers insight into the biochemical and metabolic status of tissues. [90] This thesis aims to showcase its application in muscle metabolism to gain insight into physiological and pathological states of skeletal and cardiac muscle metabolism during health and cardiovascular disease. For this purpose, the key isotopes ^{31}P, ^{1}H and ^{13}C have been used to display metabolic processes in HF and LVH.

The clinical and research applications of MRS and MRI are built upon the pioneering work of Paul C. Lauterbur and Sir Peter Mansfield, who were awarded the 2003 Nobel Prize in Physiology or Medicine for their development of magnetic resonance imaging [91], which has transformed medical diagnostics. Lauterbur introduced the concept of spatial encoding using magnetic field gradients for signal localisation. [92] The British Physicist Peter Mansfield developed the mathematical framework to produce anatomical cross-sectional nuclear magnetic resonance images and laid the foundation for fast high-resolution imaging techniques used today. [93] Their work underpins all modern MRI and MRS techniques facilitating structural, functional and metabolic imaging used in clinical practise and research.

Phosphorus magnetic resonance spectroscopy (^{31}P-MRS) (see **1.3.1**) allows the assessment of ATP and PCr *in vivo*, providing critical insights into the change of the energetic status of the cardiac and skeletal muscle, and the effect of systemic diseases like HF on skeletal muscle energetics. For the assessment of skeletal muscle dynamic ^{31}P-MRS is used; this includes measurements at rest, during submaximal muscle contraction and consecutive recovery. [94]

Similarly, proton magnetic resonance spectroscopy (^{1}H-MRS) (see **1.3.2**) is used for the quantification of intramyocardial triglyceride content, offering insights into lipid oxidation and lipid storage.[95] It is predominantly used in research to explore the effect of interventions like exercise and medications on muscle metabolism.

Hyperpolarised carbon-13 (^{13}C-MRS) (see **1.3.3**) is a novel molecular imaging technique which provides unique insights into metabolic processes [82] allowing the assessment of pyruvate metabolism into bicarbonate, lactate and alanine. [83, 96]

In all three studies presented in this thesis ^{31}P- and ^{1}H-MRS were performed as described in **Chapter 2** (Methods). Cardiac ^{31}P-MRS was used to assess cardiac PCr/ATP and ^{1}H-MRS used to assess lipid metabolism in health and disease states like HF. In addition, in **Chapter 3** (IRON HEART) skeletal muscle ^{31}P-MRS was used for the dynamic assessment of skeletal muscle metabolism, with **Chapter 5** (HYPER HEART) also including hyperpolarised ^{13}C-MRS to assess pyruvate metabolism. Collectively, these MRS techniques offer a comprehensive, non-invasive approach which provides valuable understanding of muscular and cardiovascular diseases, potentially leading to more targeted therapeutic strategies, which are highlighted in this thesis. Each of these approaches is described in more detail in the following sections.

1.3.1 Phosphorus magnetic resonance spectroscopy to assess muscle metabolism

^{31}P-MRS was first described in 1977 in an *ex vivo* experiment in rodents. [97] Since then, it has developed into a non-invasive tool to quantify intracellular metabolites of cardiac [98] and skeletal muscle [99]. It enables assessment of phosphorus containing compounds such as ATP, PCr, and inorganic phosphate (Pi), as well as intracellular pH, which all provide vital insight into cardiac and skeletal muscle health. (See **Figure 1.4**) The evaluation of the absolute levels and ratios of these metabolites aids the understanding of the energetic state of the resting and dynamic cardiac and skeletal muscle in health and disease.

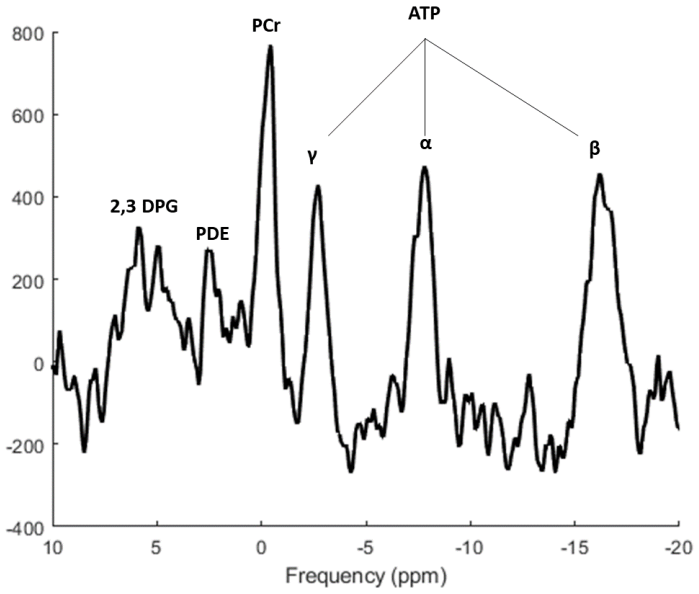

Figure 1.4 Representative example of Cardiac ^{31}P-MRS Spectrum

31-Phoshorus magnetic resonance spectrum displayed in part per million (ppm) demonstrating the peaks for 2, 3 diphosphoglycerate (2,3 DPG), phosphodiesters (PDE), phosphocreatine (PCr), and the three (γ, α, β) adenosine triphosphate (ATP) peaks (left to right).

^{31}P-MRS uses the magnetic field of an MR scanner and radiofrequency pulses to excite phosphorus nuclei (^{31}P) in tissue. [100] When placed inside the MR scanner, ^{31}P-nuclei align either with or

against the magnetic field and when a radiofrequency pulse is applied, the direction of this alignment is changed. As they return to their baseline equilibrium, the nuclei generate electromagnetic fields which can be detected by a spectroscopy MR coil. Depending on the chemical environment of each phosphorous nuclei, i.e. bound to adenosine in the form of adenosine triphosphate (ATP), creatine (PCr), or free (inorganic phosphate [Pi)]), it resonates at a distinct frequency. [101] The signal detected from PCr is used as a frequency reference value at 0 parts per million (ppm), and is displayed in the centre of the spectrum. [101] The area under the peak is proportional to the relative concentrations of these metabolites, which allows calculation of ratios of metabolites (for example PCr/ATP) to aid understanding of the energetic state of cardiac muscle. [25] Furthermore, ^{31}P-MRS has been shown to correlate with left-ventricular biopsy measures of enzyme activity, such as creatine-kinase (CK) flux and activity, supporting its validity as a non-invasive tool for assessing myocardial energetics. [81]

In contrast to that, in the dynamic assessment of skeletal muscle metabolism absolute values of PCr, Pi and pH are used and plotted over time i.e. during rest, exercise, and recovery. [99] PCr depletion, production of Pi and PCr recovery (rate) are the main components to assess skeletal muscle metabolism. [102] (For more details see **Chapter 3.1.2**)

MRS is currently a research tool which if translated into clinical practice may contribute to diagnosis, treatment, and monitoring of cardiac and skeletal muscle pathologies. [103] Various sequences are available to perform phosphorus spectroscopy two of which were used in this thesis: Depth resolved surface coil spectroscopy (DRESS) [104] in IRON HEART (**Chapter 3**) and three-dimensional MRS imaging (3D-MRSI) [105] in DICE (**Chapter 4**) and HYPER HEART (**Chapter 5**). DRESS has a short acquisition time (4 mins) and uses a single selection slab obliquely over the septum parallel to the surface coil. The MRSI acquisition is significantly longer (8 mins) and uses a voxel grid aligned over the inter-ventricular septum and allows spectroscopic assessment of each

individual voxel. In both, saturation bands are placed over the skeletal muscle of the chest wall (higher PCr/ATP than myocardium) and liver (no PCr). [106] (Please see **Chapter 2.8.** for more details on ^{31}P-MRS and scan parameters.)

1.3.2 Proton magnetic resonance spectroscopy to assess lipid metabolism

Proton magnetic resonance spectroscopy (^{1}H-MRS) can detect concentrations of hydrogen nuclei (protons) in different chemical environments due to the difference in chemical shift i.e., change in frequency, based on its surrounding molecular environment. [107] (See **Chapter 2.8.3.** for ^{1}H-MRS spectrum) It allows quantification of intracellular lipid content and lipid metabolism for example in myocardial and skeletal muscle tissue. [108, 109] It offers insights into the biochemical changes associated with heart disease. In normal weight, healthy adults, myocardial triglyceride content is approximately 1.3% fat/water [95] and increases with age and in the context of obesity and diabetes [110]. Elevation of intermediates from lipid metabolism are linked to various types of heart disease although a direct cause-and-effect relationship in patients with HF has not been defined. [111] However, intramyocardial lipid accumulation and toxicity is often seen in obesity and T2DM and negatively impacts cellular function contributing to the pathogenesis of HF. [112] Spectroscopy allows *in vivo* analysis without the need for tissue biopsies making it a crucial tool in translational research. Its validity has been demonstrated by Bakermans et al [113], who showed significant correlation between in vivo 1H-MRS- derived myocardial creatine and triglyceride content and ex vivo biochemical assays from myocardial biopsies, confirming the accuracy of localised cardiac MRS for quantifying myocardial metabolites. Proton spectroscopy supports the understanding of cardiac lipid metabolism, potentially becoming an early diagnostic tool and vehicle to inform targeted therapeutic strategies in metabolic and cardiovascular disorders like heart failure. In this thesis, ^{1}H-MRS was used to investigate the metabolic effects of therapeutic interventions like Ninerafaxstat (DICE **Chapter 4**) and aortic valve replacement (HYPER HEART **Chapter 5**). [114, 115]

1.3.3 Carbon-13 magnetic resonance spectroscopy to assess cardiac metabolism

Hyperpolarised carbon-13 magnetic resonance spectroscopy (^{13}C-MRS) gives insight into myocardial glucose and fatty acid metabolism by tracing ^{13}C-labelled pyruvate and its incorporation into metabolic products like bicarbonate, lactate and alanine. [96] This allows understanding of substrate utilisation and changes in metabolic flux via pyruvate dehydrogenase (PDH), lactate dehydrogenase, and alanine transaminase in cardiac tissue during health and cardiovascular disease. [116] Like other spectroscopy methods, it can be applied in the assessment of therapeutic interventions and how those may modulate cardiac metabolism of glucose and fat. In cardiovascular medicine its use is reserved to very few centres around the world, however in oncology ^{13}C-MRS is more established in research of cancer and its management. [117] In this thesis ^{13}C-MRS was used in selected cases of aortic stenosis and is described in more detail in **Chapter 5** (HYPER HEART).

1.4 Aims

In summary, this thesis demonstrates how advanced MR techniques can be used to assess the metabolic effects of three different interventions in HF.

The **IRON HEART study (Chapter 3)** aims to demonstrate the beneficial effects of i.v. FCM in patients with non-ischaemic cardiomyopathy, reduced EF, and iron deficiency on cardiac and skeletal metabolism and to offer a mechanistic link between clinical, structural and metabolic impact of iron repletion.

The **DICE study (Chapter 4)** showcases the role of CMR in a mechanistic phase 2a clinical drug trial using Ninerafaxstat to modulate substrate utilisation and downstream metabolism to improve cardiac energetics, function and exercise capacity in obesity, diabetes and HFpEF.

The purpose of the **HYPER HEART study (Chapter 5**) was to assess the reversibility of cardiac metabolic impairment and left ventricular remodelling in patients with and without pressure loading and assess the long-term effects of transcatheter aortic valve implantation (TAVI) on clinical, structural and energetic recovery. This study aimed to showcase the benefits of advanced MR spectroscopy to reveal metabolic alterations and inform novel treatment targets.

2 Chapter 2 Methods

2.1 Clinical Assessment

All participants underwent focused clinical assessment and assessment of inclusion and exclusion criteria, MRI safety questionnaire, drug history including allergies, and assessment of fasting including time of last food intake. The following procedures were performed: height (cm), weight (kg), vital signs (blood pressure, heart rate, respiratory rate, body temperature), resting 12-lead electrocardiogram (ECG), a brief physical examination targeted to patient's symptoms. Participants in the DICE study (**Chapter 4**) were also asked to provide a spot urine sample for measurement of urine-albumin-creatinine-ratio (uACR).

2.2 Blood Sampling

Blood sampling took place from participants in the DICE (**Chapter 4**) and HYPER-HEART (**Chapter 5**) studies. Participants were fasted to assess fasting insulin, glucose, lipid profile, and ketone bodies alongside clinical chemistry, haematology and coagulation. Samples for clinical chemistry, haematology, coagulation and biomarkers were sent for analysis to the laboratory of Oxford Hospitals NHS Trust. Women of childbearing potential (WOCBP) were required to have a negative serum pregnancy test. Estimated glomerular filtration rate (eGFR) was calculated using the Modification of Diet in Renal Disease (MDRD) equation; eGFR (mL/min/1.73 m^2) = 175 x $(SCr)^{-1.154}$ x $(age)^{-0.203}$ x 0.742 (if female) x 1.212 (if black) where, SCr is serum creatinine (mg/dL). Urinary albumin-creatinine ratio (UACR) was calculated using the formula UACR (mg/g) = urine albumin (mg/dL)/urine creatinine (g/dL).

2.3 Electrocardiogram

A twelve-lead ECG was conducted at every imaging visit in all three studies. In addition, an ECG was performed at the screening visit of the DICE study (**Chapter 4**). The ECG was reviewed for rate and rhythm, and particularly for evidence of AF, and to exclude potential contraindications to dobutamine administration. These include arrhythmia, evidence of acute myocardial infarction, signs of electrolyte disturbances.

2.4 New York Heart Association (NYHA) Functional Assessment

NYHA functional class [118] was assessed in all three studies. (See **Table 2.1**).

NYHA Class	Patient Symptoms
I	No limitation of physical activity. Ordinary physical activity does not cause undue fatigue, palpitation, dyspnoea (shortness of breath).
II	Slight limitation of physical activity. Comfortable at rest. Ordinary physical activity results in fatigue, palpitation, dyspnoea (shortness of breath).
III	Marked limitation of physical activity. Comfortable at rest. Less than ordinary activity causes fatigue, palpitation, or dyspnoea.
IV	Unable to carry on any physical activity without discomfort. Symptoms of heart failure at rest. If any physical activity is undertaken, discomfort increases.

Table 2.1 New York Heart Association Functional Class Assessment

2.5 Patient Reported Outcomes

Patient reported outcomes were assessed in all three studies. The Kansas City Cardiomyopathy Questionnaire (KCCQ) was used in the IRON-HEART (**Chapter 3**) and DICE (**Chapter 4**) studies. The Toronto aortic stenosis quality of life questionnaire (TASQ) was used in the HYPER HEART study (**Chapter 5**). Patient global impression scores (PGI) were used in the DICE (**Chapter 4**) and the HYPER-HEART (**Chapter 5**) studies.

2.5.1 Kansas City Cardiomyopathy Questionnaire (KCCQ)

The 23-item KCCQ (see **Appendix 1**) was used to assess symptoms (frequency, severity, recent changes), limitations (physical, social, emotional), quality of life (QoL), and self-efficacy (understanding to manage complication). [119] The maximum score is 100, the health status can be divided into: 0 to 24 very poor to poor; 25 to 49 poor to fair: 50 to 74 fair to good; 75 to 100 good to excellent. Summary scores of different components of the KCCQ were calculated: the total Symptom Score (TSS), the Clinical Summary Score (CSS), and the Overall Summary Score (OSS). TSS includes frequency, burden, and stability of symptoms. The CSS focuses on physical limitation and symptoms (frequency and burden). The OSS excludes questions on the patient's ability to manage their HF. (see **Table 2.2**)

Symptoms		**Limitations**		**Quality of Life**	**Self-efficacy**
Frequency Burden Stability	Physical	Social	Emotional		HF management
Total Symptom Score (TSS)					
Clinical Summary Score (CSS)					
Overall Summary Score (OSS)					

Table 2.2 Components of the Kansas City Cardiomyopathy Questionnaire score

The generally accepted minimal clinically important difference (MCID) in KCCQ score was set at a threshold of 5-point change to detect a small improvement. [120] However, more recent trials have suggested a change in the overall score lower than 5 points might also be clinically relevant. [121] The 23-item KCCQ was used in the DICE study (**Chapter 4**) at enrolment (Visit 2), at the non-imaging visit (Visit 3), end of treatment (EOT, Visit 4), and end of study (EOS, Visit 5). For IRON-HEART (**Chapter 3**) a shorter, 12-item KCCQ [122] was used. [123] Participants were given the questionnaires at baseline and at 6 weeks post iron administration. The maximum score of the short KCCQ is 64 points.

2.5.2 Toronto Aortic Stenosis Quality of Life Questionnaire (TASQ)

The TASQ was designed to assess patients undergoing aortic valve replacement [124, 125]. It assesses physical symptoms and limitations, the emotional impact of aortic stenosis, social limitation and health expectations. [124] The 16 questions result in a maximum total score of 112 points indicating highest quality of life (QoL). [124] Participants of HYPER-HEART (**Chapter 5**) were asked to complete the questionnaire at each study visit. (see **Appendix 2**)

2.5.3 Patient Global Impression of Change (PGI-C) and Severity (PGI-S)

In DICE (**Chapter 4**) participants were asked to complete the PGI of change (PGI-C) and PGI of Severity (PGI-S) surveys at enrolment (Visit 2), at the non-imaging visit (Visit 3), end of treatment (EOT, Visit 4), and end of study (EOS, Visit 5). In HYPER-HEART (**Chapter 5**) participants were asked to complete the surveys at each study visit. The PGI-C and PGI-S scales used a 5-point Likert scale. Participants were asked to choose the response that best described the overall clinical status between non (0 points), mild (1 point), moderate (2 points), severe (3 points), very severe (4 points) and overall change in the severity of their HF symptoms since starting the study. [126] (see **Appendix 3**)

2.6 Six-Minute Walk Test

In all three studies, participants performed a six-minute walk test (6-MWT) at the imaging assessment. They walked along a flat, 20-meter-long corridor. (See **Figure 2.1)** Previously published guidance [127] was followed to perform the test. The 6-minute walk distance (6-MWD) covered was recorded in meters.

Figure 2.1 Six minute-walk test

A six-minute walk test was performed along a dedicated, flat, 20-meter-long corridor

2.6.1.1 The Borg Rating of Perceived Exertion and Dyspnoea Score

The rating of perceived exertion category scale and the Borg dyspnoea scale rating of perceived exertion and fatigue [128] were recorded prior to and after the 6-MWT. (see **Appendix 4**) At the beginning of the 6MWT, the scale was displayed, and the patient questioned: “Please grade your level of fatigue using this scale” followed by “Please grade your level of shortness of breath using this scale”. At the end of the 6MWT, the patient was asked to grade their level of fatigue and breathing level again.

2.7 Echocardiogram

Transthoracic echocardiography (TTE) was performed in the DICE (**Chapter 4**) and HYPER-HEART (**Chapter 5**) studies for the evaluation of cardiac structure and function. TTE assessment was performed on a GE Vivid I system (GE, Boston, USA).

- Participants in the DICE study (**Chapter 4**) underwent TTE assessment at screening (Visit 1) and EOT (Visit 4).
- Participants in HYPER-HEART study (**Chapter 5**) underwent TTE assessment at rest only at each visit.

Depending on the body habitus and mobility of the participant resting TTE was performed in the left lateral decubitus position (see **Figure 2.2A**) or sitting on a chair (see **Figure 2.2B**). For the stress assessment, the participant performed sub-maximal exercise by cycling on a foot pedal exerciser for 5 mins at 30 Watts (W) (see **Figure 2.2B**).

A TTE at rest

B TTE at sub-maximal exercise

Figure 2.2 Transthoracic Echocardiogram at rest and stress

(A) Transthoracic echocardiogram (TTE) at rest in left lateral decubitus position and (B) exercise sitting on a chair cycling on a foot pedal exerciser

A parasternal long axis (PLAX) view was used to assess left ventricular (LV) wall thickness, Interventricular septum diameter at end diastole (IVDd), LV posterior wall diameter at end diastole

(LVPWd) and LV end diastolic diameter (LVEDd). (see **Figure 2.3A**). A PLAX right ventricular (RV) influx view or apical four chamber view (see **Figure 2.3B**) was used to demonstrate tricuspid regurgitation (if present) and continuous wave doppler (CWD) was used to measure peak TR velocity. A parasternal short axis view (PSAX), apical 4, 2, 3 chamber view was used to assess LV function and regional wall motion abnormalities.

An apical 4 chamber view (A4C) (see **Figure 2.3C**) was performed to assess LV function, valve function and left atrial volume (see **Figure 2.3D**). Pulse wave doppler was used to measure peak velocity in early diastole (E_{max}), flow deceleration time (DT) from peak E wave to end of E wave signal, and if in sinus rhythm peak velocity in late diastole (A_{max}). (see **Figure 2.3D**) Tissue doppler imaging (TDI) was performed to assess left ventricular diastolic function (septal and lateral e'). Tissue doppler imaging (TDI) was measured at the lateral tricuspid annulus to assess basal RV contraction. (see **Figure 2.3E, 2.3F**) An M-Mode was aligned along the lateral tricuspid annulus to measure longitudinal motion of the annulus (total excursion of the tricuspid annulus, TAPSE).

A LV size and wall thickness

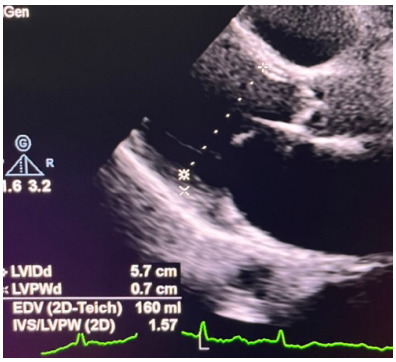

B TR

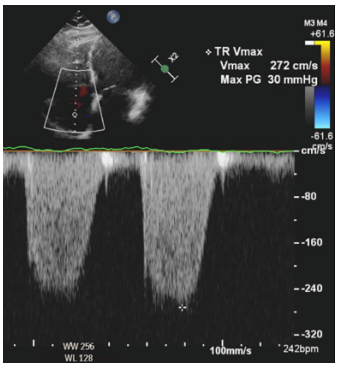

C LV function

D LA volume

E Diastolic function:

E-wave, A-wave, E/A

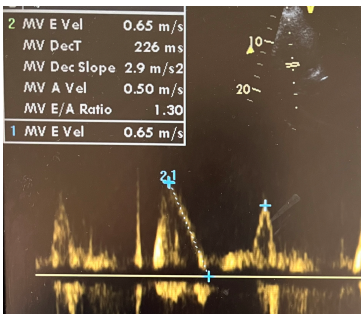

F Diastolic function:

septal e'

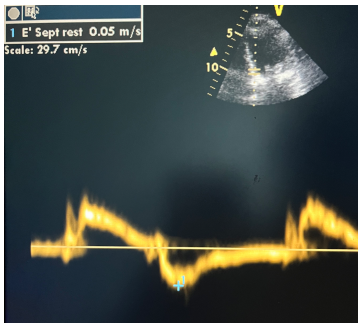

Figure 2.3 Representative views of transthoracic echocardiography

Parasternal long axis view to assess (A) left ventricular (LV) size and LV wall thickness; (B) apical four chamber view to assess tricuspid regurgitation (TR), and (C) LV function (C) and left atrial volume (D), diastolic function (E, F).

2.8 Cardiac MR Protocols and Analysis

2.8.1 Cardiac ^{31}P-MRS Spectral Acquisition

In all three studies of this thesis cardiac phosphorus spectroscopy (^{31}P-MRS) was performed using a 3 Tesla Magnetom PRISMA MRI scanner (Siemens Healthineers, Erlangen, Germany). Owing to variable coil availability, three different coils and respective sequences were used for the acquisition of phosphorus spectra (see **Table 2.3**). All spectroscopic assessments were performed after 6 hours (IRON HEART **Chapter 3**; HYPER HEART **Chapter 5**) and 9 hours (DICE **Chapter 4**) of fasting. Participants were moved headfirst into the scanner until their heart was at isocentre.

In the IRON HEART study (**Chapter 3**), spectra were acquired with a surface ^{1}H/^{31}P flex coil (11 cm in diameter for ^{31}P, Rapid Biomedical) in supine position. A non-gated, slice-selective Depth-resolved surface-coil spectroscopy (DRESS) sequence was used. ^{31}P-MRS was performed at rest and during dobutamine stress (at 65% of maximal heart rate).

For the DICE study (**Chapter 4**) a 3-element dual-tuned heart/liver ^{1}H/^{31}P surface coil (Siemens Medical, Erlangen, Germany) was used consisting of a large outer element (26 x 28 cm) which acts as ^{1}H transmit-receive and ^{31}P transmit, with a smaller loop/butterfly receive pair (12 x 15 cm loop and 23 x 12 cm butterfly) which receives ^{31}P signal. Participants were positioned in the prone position with their left ventricle positioned over the centre of the coil at the magnet iso-centre. A non-gated, 3D acquisition-weighted, ultra-short echo time (UTE) ^{31}P -magnetic resonance spectroscopic imaging (^{31}P-MRSI) sequence was used at rest only.

For the HYPER-HEART study (**Chapter 5**), a home-built prototype multi-layer coil (four conductor layers of 2 oz copper [0:07mm], separated by dielectric insulator layers of 0:127mm Kapton; 82mm to 125mm diameter) [129] was used. Participants were positioned supine with the centre of the coil over the left ventricular septum. A non-gated, 3D acquisition-weighted, ultra-short echo time

(UTE) ^{31}P-MRSI sequence was used at rest only. Although spectroscopic measurements appear unaffected by prior administration of gadolinium [130], all spectroscopic assessments in the HYPER-HEART study were performed prior to contrast administration.

^{31}P-MRS

Chapter Study	**Chapter 3 IRON HEART**	**Chapter 4 DICE**	**Chapter 5 HYPER HEART**
Coil	Surface ^{1}H/^{31}P flex coil (Rapid Biomedical, Rimpar, Germany)	3-element dual-tuned ^{1}H/^{31}P surface coil (Siemens Medical, Erlangen, Germany)	Home-built multilayer coil
Position	Supine	prone position (if able)	supine position
Sequence	Gated, slice selective Depth-Resolved Surface-coil Spectroscopy (DRESS) at rest and Dobutamine stress	Non-gated, 3D acquisition-weighted, ultra-short echo time (UTE) chemical shift imaging (CSI) at rest	Non-gated 3D acquisition-weighted ultra-short echo time (UTE) chemical shift imaging (CSI) at rest

Table 2.3 Coils and sequences used for ^{31}P-Magnetic Resonance Spectroscopy

Proton localisers were used to position the participant prior to spectroscopy. Localiser images were acquired to identify the position of a phenylphosphonic acid (PPA) fiducial and cod-liver oil phantoms to confirm correct coil positioning. To determine the loading of the coil, twelve free induction decay inversion recovery (IR-FID) curves with increasing inversion delay (50-1500 ms (**IRON HEART)** and 50 - 4000ms (**DICE, HYPER HEART**) were acquired. Vertical long axis (VLA), horizontal long axis (HLA) and short axis (SA) stack (3 slices) localiser images were acquired to position the DRESS selection slab (**IRON HEART**) or the CSI voxel grid (**DICE, HYPER HEART**) correctly. The DRESS selection slab (width 20mm) was placed in an oblique fashion over the septum (see **Figure 2.4**). The CSI voxel grid was aligned to position voxels within the inter-ventricular

septum (see **Figure 2.5**). Three saturation bands were placed over the anterior and lateral chest wall (to supress signal from skeletal muscle), and over the liver (to minimise signal contamination).

In IRON HEART (**Chapter 3**), Cardiac Slice Selective Depth Resolved Surface Coil spectroscopy (DRESS) (see **Figure 2.4**) was performed as previously described [104] with a 20 mm slab. A sinc-shaped RF pulse was centred between γ- and α- ATP resonances (by subtracting 250 Hz from the observed phosphocreatine frequency). [105] DRESS was performed at rest and during dobutamine stress. DRESS, rapid single-slice localisation method originally developed by Bottomley et al in 1984 [131], formed the basis for subsequent multivoxel chemical shift imaging (CSI) techniques [132]. Although CSI offers improved reproducibility and reduced contamination compared with DRESS [100], it was not available at the time the IRON HEART study commenced; hence, DRESS was used.

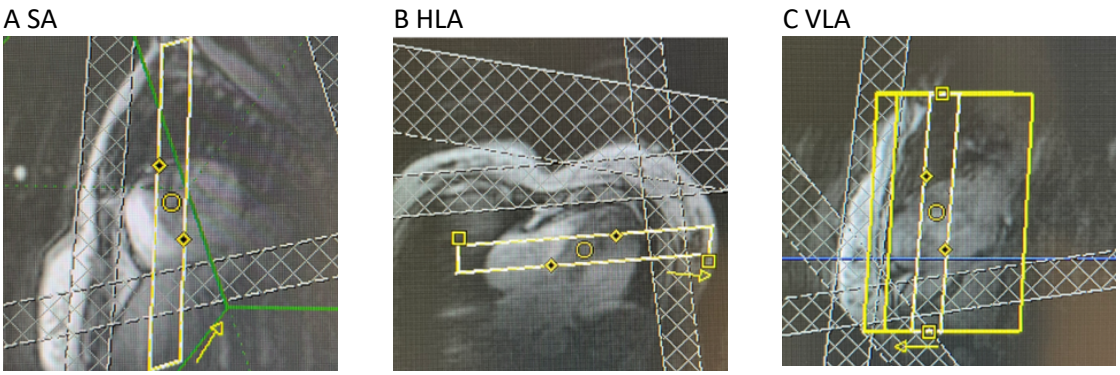

Figure 2.4 Position of selection lab for DRESS

Position of the slice selective Depth Resolved Surface Coil Spectroscopy (DRESS) selection slab (yellow) in oblique fashion over the septum in the (A) short axis (SA), (B) horizontal long axis (HLA), (C) vertical long axis (VLA) view parallel to the coil over the chest (white dot in A). Saturation bands (white) over the anterior and lateral chest wall and over the liver.

In **DICE** (**Chapter 4**) and **HYPER HEART** (**Chapter 5**) a non-gated 3-D acquisition-weighted MRS imaging (MRSI) [133] was used (see **Figure 2.5**)**.** The optimised RF pulse was centred between γ- and α- ATP resonances as described above.

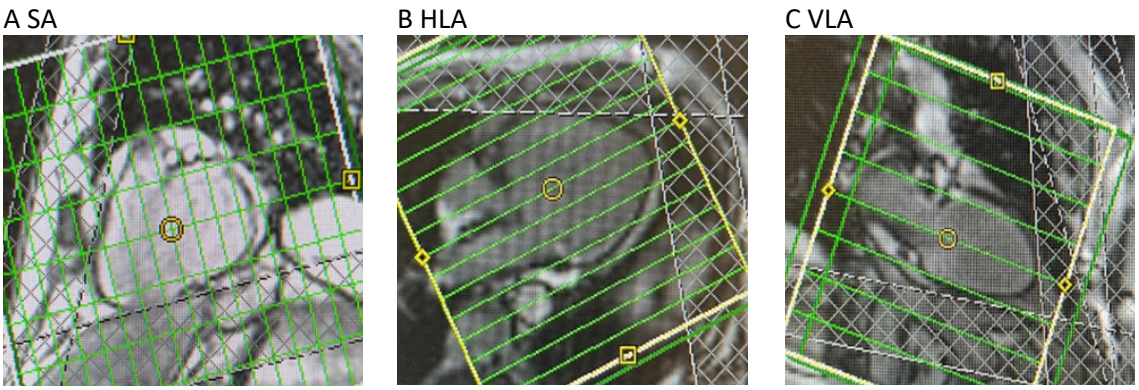

Figure 2.5 Voxel grid position for ^{31}P -Magnetic Resonance Spectroscopy Imaging

Position of the ^{31}P -Magnetic Resonance Spectroscopy Imaging (MRSI) voxel grid (green) with (A) precise position of at least one voxel over the basal septum in short axis view (SA), (B) parallel to the septum in (B) horizontal long axis view (HLA) and (C) vertical long axis view. Saturation bands (white) over the anterior and lateral chest wall and over the liver.

In addition to ^{31}P-MRS at rest, in **IRON HEART** (**Chapter 3**), ^{31}P-MRS was also performed during pharmacological stress with Dobutamine to investigate the effect of iron on the myocardial metabolic reserve. Dopamine, a sympathomimetic catecholamine, exerts positive inotropic effects at low doses (≤10 μg/kg/min) and chronotropic effects at higher doses [134] increasing cardiac output and oxygen consumption.[135] Its rapid onset, short half-life (120 seconds), and β-blockade offers ideal characteristics as a stress agent.[135] According to the Society of Cardiac Magnetic Resonance (SCMR) guidelines, escalating doses (2.5 to 40 μg/kg/min) are used for stress MRI.[136]

Prior to the administration of Dobutamine, a pre-infusion checklist excluded contraindications which are listed as follows:

- Severe outflow obstruction (aortic stenosis, hypertrophic cardiomyopathy)
- Acute Coronary Syndrome
- Left ventricular failure with symptoms at rest
- Significant arrhythmias
- Severe hypertension (>220/120 mmHg)
- Recent pulmonary embolus / infarction
- Thrombophlebitis or active deep vein thrombosis
- Known hypokalaemia
- Active endocarditis, myocarditis, pericarditis

Resting vitals and a good quality ECG was ensured. Dobutamine (5mg/ml) was administered via intra-venous infusion, starting at a dose of 5 μg/kg/min, with dose increments every 3 minutes to a maximum of 40 μg/kg/min or until the target heart rate of 65% of the maximal predicted heart rate (Age in years – 220) was achieved. A reversal agent (metoprolol, as a short acting β-blocker) was easily accessible during all scans.

2.8.2 ^{31}P-MRS Spectral Analysis

The acquired spectra were characterised offline using MATLAB (OXSA [137]). The spectral analysis of the non-localised DRESS sequence used in **IRON HEART** (**Chapter 3**) was fully automated, whereas the MRSI sequence used in **DICE** (**Chapter 4**) and **HYPER HEART** (**Chapter 5**) required a manual selection of a voxel which was the only user-dependent part of the analysis.

The ^{31}P-spectral analysis in MATLAB was performed in three steps:

(1) Fit inversion recovery free induction decay (IR FIDS)

(2) Fit coil position

(3) Manual selection of a voxel

The inversion recovery data and the localizer (see **Figure 2.6A**) containing the locations of the cod liver oil capsules (see **Figure 2.6B**), which were externally fixed to the coil, were used to calculate the actual flip angle at the selected voxel.

A Localiser

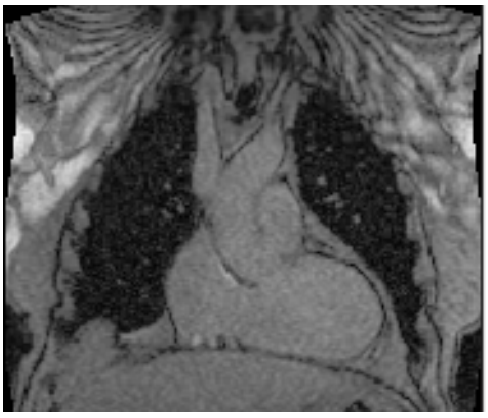

B Cod liver oil capsules

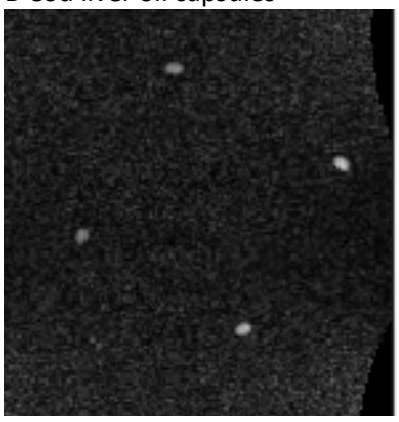

Figure 2.6 MATLAB Spectral analysis: Fitting of coil position

To fit the coil position in MATLAB the location of the (B) four cod liver oil capsules was identified on a (A) localiser image.

Once the voxel was selected, an automated spectral fitting algorithm AMARES (advanced method for accurate, robust, and efficient spectral) [138] was used to accurately fit the spectral resonances of phosphocreatine (PCr), alpha, beta, and gamma adenosine triphosphate (α, γ, β, – ATP), 2,3-diphosphoglycerate (2-3-DPG), and phosphodiesters (PDE). (See **Figure 2.7**) This was achieved by incorporating prior knowledge of relative peak frequencies, J-coupling configurations, relative peak amplitudes, relative phases, and assumed Lorentzian line shapes. Initial peak area correction was performed to account for radiofrequency (RF) saturation effects, employing the recorded R-R-interval, flip angles, and the longitudinal relaxation times (T1 values: PCr 3.8±0.3 s and γ-ATP 2.4±0.5 s). [139]

Correction of the ATP peaks due to blood contamination were made by subtracting 11% of the 2,3-DPG peak area. [28] Calculations of PCr/ATP ratios were conducted using an average value across all three ATP resonances. [105] Cramer-Rao lower bounds (CRLB) were used to assess the quality of spectral fits and to distinguish the spectra from noise. [140] Samples with a coefficient of variation greater than 30 % were excluded.

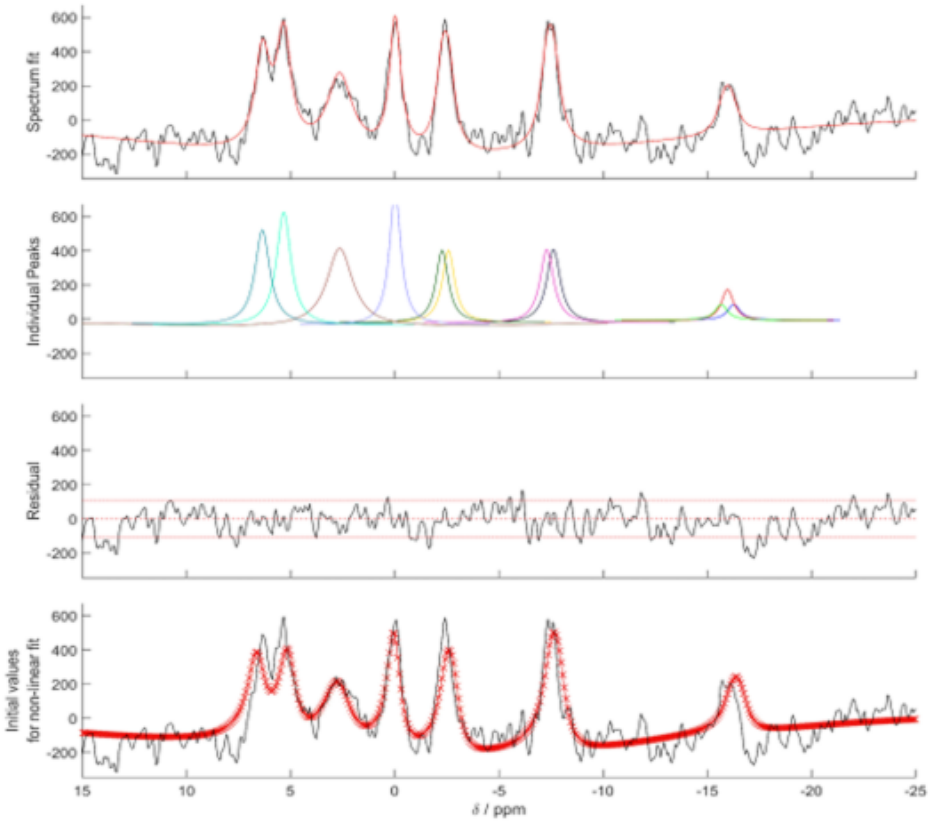

Figure 2.7 MATLAB Spectral fitting graph of cardiac muscle ^{31}P-MRS data at 3T

Top panel – Spectrum fit: black line represents the acquired spectral data showing peaks of different phosphorus-containing metabolites, red line represents the spectral fitting performed by the algorithm.

Second panel – Individual peaks: coloured curves represent the individual metabolic peaks, such as phosphocreatine (PCr), and the three ATP peaks for γ, α, β- ATP.

Third panel – Residual: Black line represents the difference between acquired spectral data and fitting, red line represents the confidence interval, which are used to assess the quality of spectral fitting.

Bottom panel – Initial values for non-linear fit: black line identical to top panel, red crosses represent the initial estimates used by the algorithm before optimisation.

2.8.3 Cardiac Proton Magnetic Resonance Spectroscopy

In the **DICE** (**Chapter 4**) and **HYPER HEART** (**Chapter 5**) studies, proton magnetic resonance spectroscopy (^{1}H-MRS) was used to assess myocardial lipid metabolism by measuring myocardial lipid content, as well as creatine, and choline levels. [141] ^{1}H-MRS was performed using a 30-channel surface coil (Siemens Healthineers, Erlangen, Germany) with the participant in the supine position. [109] Spectra were acquired with ECG gating in mid-diastole and in end expiration during a breath hold. A single voxel was placed over the basal septum. (see **Figure 2.8**)

A SA B HLA C VLA

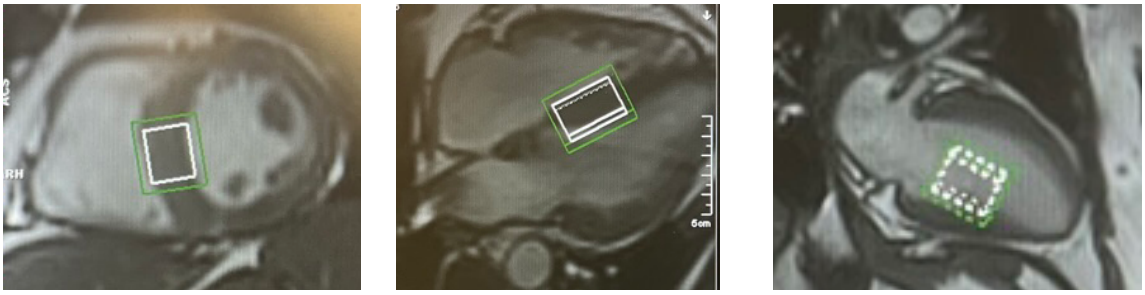

Figure 2.8 Voxel position for cardiac ^{1}H-Magnetic Resonance Spectroscopy

Position of voxel (white box) and adjustment volume (green box) over the basal septum in (A) short axis view (SA), (B) Horizontal long axis view (HLA) and (C) Vertical long axis (VLA) view

Five water-suppression cycling breath holds (see **Figure 2.9A**) were acquired using a spin echo sequences (Point RESolved Spectroscopy, PRESS) followed by one sequence without water suppression (see **Figure 2.9B**).[141] Spectra were analyzed with MATLAB and the AMARES algorithm within the OXSA toolbox.[137] Myocardial triglyceride (MTG) content was calculated as a percentage relative to water (signal amplitude of lipid/signal amplitude of water) and multiplied by 100 (% water). [142] MTG levels differ by cardiomyopathy type [143], while myocardial creatine content correlates with HF [144].

A Water suppression cycling on

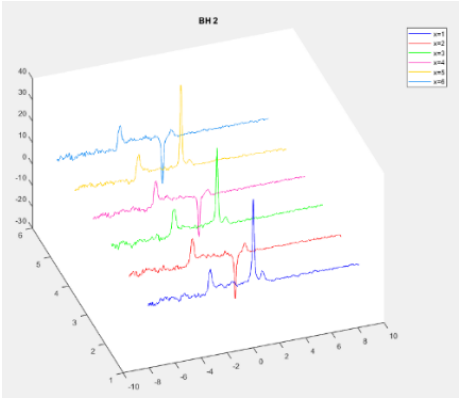

B Water suppression cycling off

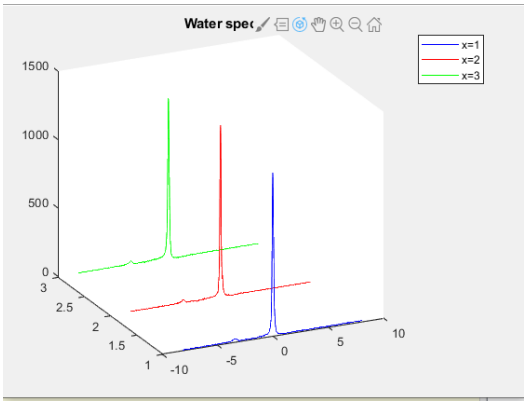

Figure 2.9 Representative 3D-plot of ^{1}H-Magnetic Resonance spectroscopy

x- axis = chemical shift in part per million (ppm); y-axis= signal amplitude; z-axis individual datasets; (A) water suppression to visualise the smaller peak of myocardial triglycerides (peaks on the right); (B) water suppression off show the dominant water signal due to its high concentration. The different coloured lines represent separate spectra.

2.8.4 Magnetic Resonance Imaging- Cardiac Volumes and Function

Cardiac Magnetic Resonance imaging was performed using a 3 Tesla MR Scanner to assess cardiac volumes and function. For **IRON HEART** and **DICE** studies, cardiac volumes were assessed on a Prisma (Siemens) MR system equipped with spine and 18-channel surface receive coils. For **HYPER HEART,** a GE Premier (General Electric Healthcare) was used equipped with a GE cardiac AIR^{TM} coil. Following localiser images, in all three studies cine images were acquired in the horizontal long axis (HLA), and vertical long axis (VLA). In addition, for **HYPER HEART** (coronal) left ventricular outflow tract views were obtained. Short axis cine phase-contrast MRI (CINES) were acquired in **IRON HEART** and **HYPER HEART** studies with electrocardiographic (ECG) gating and breath-holding. Retrospective ECG gating was used to acquire CINE images for participants in sinus rhythm and prospectively triggered ECG gating was used for participants in atrial fibrillation.

For the DICE study, cardiac volumes and function at rest were acquired with a highly accelerated, compressed sensing, free-breathing CINE imaging sequence to acquire a SA stack during exercise (~60 seconds). Bi-ventricular ejection fraction (%), end-diastolic and end-systolic volume index (mL/m^2) were quantified by semi-automatic planimetry of endocardial and epicardial borders in SA views using Circle Cardiovascular Imaging (cvi42, version 5.10.1, Circle Imaging, Calgary, Canada) in accordance with the Society for Cardiovascular Magnetic Resonance (SCMR) guidelines [136]. (see **Figure 2.10A**) The volumes at end-systole (ESV) and end-diastole (EDV) were measured and used to determine the stroke volume (SV) using the formula SV = EDV – ESV. EF was computed using the equation EF = SV/EDV. The LV mass was calculated by multiplying the total LV volume by the assumed myocardial density (1.05 g/ml).[145] Bi-atrial ejection fraction (%) were quantified by semi-automatic planimetry of endocardial and epicardial borders in the VLA view (see **Figure 2.10B**) and HLA view (**Figure 2.10C**) using cvi42. MR analysis was performed in a blinded fashion in all three studies.

A SA B VLA C HLA

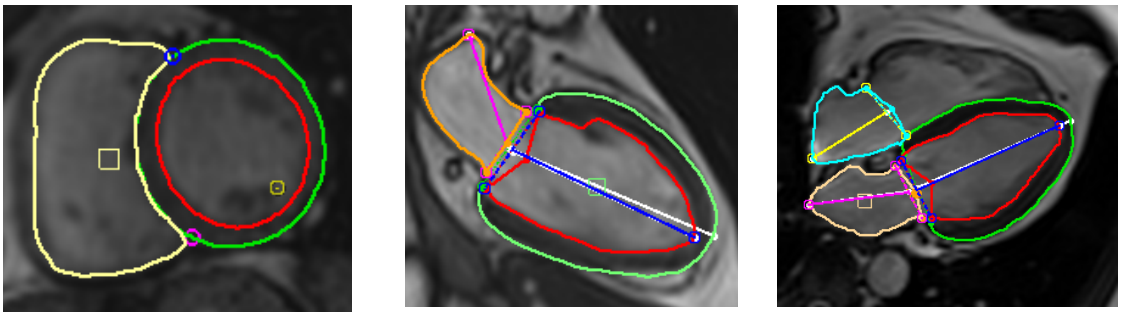

Figure 2.10 Image analysis in CVI42 for biventricular cardiac volumes

Endo-and epicardial borders of cardiac chambers in (A) short axis (SA) image; (B) Vertical Long Axis (VLA) view; (C) Horizontal long axis (HLA) view

2.9 Statistics

The statistical analysis for the three studies described in this thesis was performed with GraphPad Prism 10 and IBM SPSS Statistics 29.0.2.0. Most of the datasets comprised paired data points, particularly the analysis pre- and post-intervention (**IRON HEART:** intravenous iron, **DICE:** Ninerafaxstat, **HYPER HEART:** TAVI). Some data sets (**HYPER HEART**) involved two data points post-intervention (1-day and 6-months follow post TAVI). Not all data sets were normally distributed (IRON HEART). Across all three studies, demographic, and baseline data, was summarised together with all concomitant medications, safety/tolerability data, follow-up data, and laboratory data. Continuous variables were summarised using descriptive statistics for example mean and standard deviation for normally distributed data and median and interquartile range (IQR) for non-normally distributed data. Categorical variables were summarised using frequencies and percentages.

Statistical methods were applied as follows:

- Normality of distribution was assessed using the Shapiro–Wilks test.
- Paired t-tests were used to analyse normally distributed paired datasets, such as PCr/ATP pre-/post intervention.
- Mann-Whitney U tests were applied for paired datasets that were not normally distributed, such as changes in leg perfusion pre and post intravenous iron.
- Unpaired t-tests were used to compare two independent groups such as the participants without cardiovascular disease compared to the participants with aortic stenosis at baseline.
- Two-way Analysis of Variance (ANOVA) was used to analyse paired datasets at multiple time points, for example to assess the changes over two time points post intervention in patients with aortic stenosis who had undergone TAVI.

To assess correlations, the Pearson's rank coefficient was used. A power calculation was performed using the primary endpoint of change in cardiac PCr/ATP in the paired data set. To assess the effect size (d), the mean differences between the paired (pre/post) data was divided by the standard deviation of the differences. A significance level (α) of 0.05 was used. To reject the null hypothesis the threshold for power was defined at 80%.

For each individual statistic section please see:

Chapter 3.2.10 (**IRON HEART**), Chapter 4.2.14 (**DICE**), Chapter 5.2.7 (**HYPER HEART**).

3 IRON HEART

In this chapter the results of the **IRON HEART** study are presented, which investigates the effect of i.v. FCM on cardiac and skeletal muscle metabolism, perfusion and oxygenation in patients with symptomatic non-ischaemic cardiomyopathy, reduced EF, and iron deficiency.

3.1 Background

Iron deficiency (ID) in HF is a predictor of outcomes [146] and iron depletion may benefit exercise capacity, symptoms and hospitalisation [147]. Whether this is due to the beneficial effects of iron on the cardiac or skeletal muscle is poorly understood. The **IRON HEART** study was the first to explore the impact of intravenous iron repletion on cardiac and skeletal muscle function, metabolism, perfusion and oxygenation, using magnetic resonance imaging (MRI) and spectroscopy (MRS). **IRON HEART** examined the effects of iron repletion on cardiac function (ejection fraction), cardiac muscle energetics (PCr/ATP) at rest and during dobutamine stress, skeletal muscle oxidative capacity (PCr recovery rate), and skeletal muscle perfusion and oxygenation (ASL).

The hypothesis was that intravenous (i.v.) Ferric carboxymaltose (FCM) in patients with chronic non-ischaemic cardiomyopathy would enhance cardiac energy reserve, and skeletal muscle mitochondrial capacity. Understanding these mechanisms could optimise treatments for exercise intolerance in heart failure by targeting cardiac output, oxygen transport and utilisation to facilitate ATP production in cardiac and skeletal muscle.

3.1.1 Heart Failure and Iron Deficiency

There is a complex interplay between iron homeostasis, oxygen supply, and cellular energy metabolism. Iron is an essential trace element, plays a key part in erythropoiesis, and facilitates the

bond between oxygen and haemoglobin and subsequent tissue perfusion. [148] Independently of ID, HF affects tissue perfusion and oxygenation. [149-151] Iron is a cofactor for several key enzymes (complex I, complex II, coenzyme Q, complex III, cytochrome C, and complex IV) [19] and stimulates production of enzymes of the TCA cycle [152]. In addition, iron is required to catalyse the oxidation of NADH and $FADH_2$ an essential part of ATP production via the electron transport chain (ETC). [153, 154]. Hence, ID leads to a reduction of ATP production and an increase in glycolysis and lactate formation to compensate for decreased oxidative ATP production. [54]

As a multi-system disease affecting cardiac and skeletal muscle function and metabolism (see **Figure 3.1**), HF leads to impaired oxygen delivery to the skeletal muscles, leading to skeletal muscle myopathy [155], reduced oxidative capacity, and altered muscle metabolism. [156] Independent of the presence of HF, iron deficiency (ID) can occur due to insufficient dietary intake and/or absorption of iron, increased iron requirements, or blood loss. However, chronic diseases like HF can lead to reduction in absorption and utilization of iron [157] irrespective of anaemia. [158-160] In heart failure, ID is associated with worse symptoms and reduced survival. [59] The European Society of Cardiology (ESC) defines ID in heart failure (HF) as follows:

1) serum ferritin <100 mg/L (absolute ID) or

2) serum ferritin 100–299 mg/L and transferrin saturation (TSAT) <20% (functional ID). [161]

However, emerging evidence suggests that ID in HF is more complex than these definitions imply as ferritin and TSAT are influenced by inflammation, hypoxia, comorbidities, and medications such as SGLT2i. [162]

In patients with HF with an ejection fraction <45% and ID, intravenous (i.v.) iron replacement results in an improvement of symptoms, Quality of Life (QoL), and exercise capacity. [57-65] Therefore, the ESC Guidelines recommend screening all patients with HFrEF for ID and consider i.v. iron to improve quality of life and exercise capacity. [163]

Furthermore, non-anaemic iron deficiency exerts different effects on the myocardium, skeletal muscle and pulmonary vasculature independent of haemoglobin, reflecting the crucial role of intracellular iron supporting oxidative phosphorylation, oxygen sensing, myoglobin synthesis, and calcium handling. [162] Iron supplementation leads to increased NADH formation and oxygen consumption, boosting ATP production through oxidative phosphorylation. [52] Despite that, the effects of iron repletion on cardiac and skeletal muscle mitochondrial function in patients with HF are less well studied. Papalia et al. [55] proposed that ID was associated with reduced mitochondrial function in the cardiomyocytes. Menon et al. [56] showed that skeletal muscle oxidative metabolism was reduced in patients with HF. A recently published study [67] proposed that intravenous iron repletion in patients with HF improved skeletal muscle mitochondrial oxidative capacity.

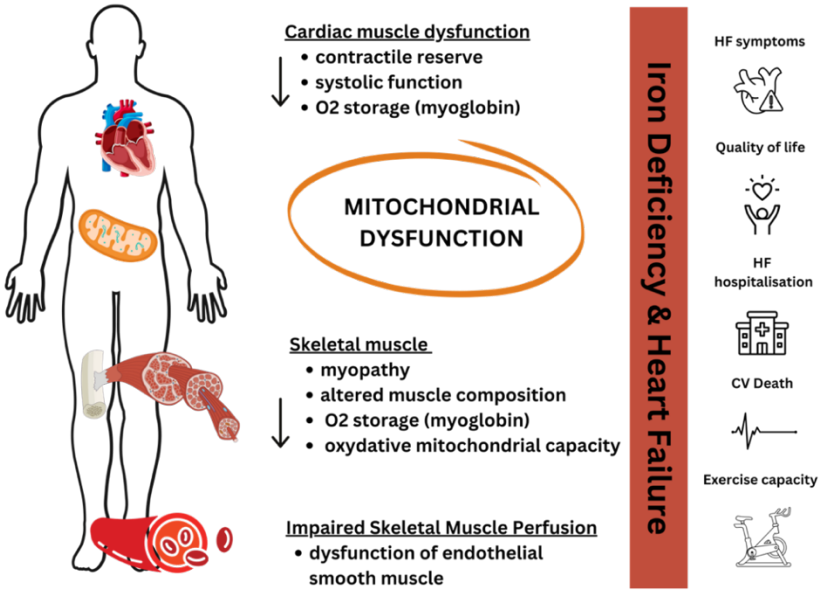

Figure 3.1 IRON HEART; Heart Failure and Iron deficiency

Heart Failure (HF) and iron deficiency affect cardiac and skeletal muscle function and skeletal muscle perfusion. In the heart, it results in reduction in contractile reserve, systolic function and oxygen (O2) storage via myoglobin. In the skeletal muscle it may contribute to myopathy, altered muscle composition and metabolism (oxidative mitochondrial capacity). Furthermore, iron affects endothelial smooth muscle function resulting in altered skeletal muscle perfusion. Iron repletion results in an improvement in HF symptoms, Quality of Life, and exercise capacity, and a reduction in HF hospitalisation and cardiovascular (CV) death.

3.1.2 Skeletal Muscle Physiology

Skeletal muscle plays a critical role in movement, metabolic health and energy balance. [164] In sedentary adults, dependent on sex (greater in men) and age (declines after fifth decade) skeletal muscle accounts for about 30-40% of body weight. [165] It also accounts for 25-30% of the resting metabolic state, and for up to 90% of whole-body oxygen consumption [166]. Its oxidative capacity depends on the muscle composition, available substrates, metabolic pathway used to produce ATP, and the intensity of exercise [167] Different skeletal muscle fibres co-exist and vary depending on age, health and training. [168] They are classified by myosin heavy chain (MHC) isoforms [168] catering for different demands of exercise: Type I (slow-twitch fibres with low maximal power but high endurance), and Type II. [169] Type II are divided in Type IIA and Type IIX (previously described as Type IIB [170]) and consists of fast twitch fibres with high power and low resistance to fatigue [171].

ATP production in the skeletal muscle occurs via three pathways: [172] high energy phosphagen system, anaerobic glycolytic system, oxidative phosphorylation. During an abundance of oxygen FFA are the predominant fuel source. With increasing exercise intensity and oxygen requirement, glycogen becomes the preferred substrate. [167] After the initiation of muscle contraction ATP is hydrolysed into ADP and P_i ($ATP + H_2O \rightarrow ADP + P_i + H^+$). [173]

During short duration exercise the phosphagen system produces the highest amount of ATP via the creatine kinase reaction [172] and phosphocreatine (PCr) shuttle. [174] Creatine kinase (CK) catalyses the phosphorylation of ADP by Phosphocreatine to generate ATP and Creatine ($PCr + ADP + H^+ \rightarrow ATP + Cr$). [173] The drop of PCr is inversely proportional to the rise in inorganic phosphate (Pi). [173] (See **Figure 3.2A**)

During short to moderate duration exercise, the anaerobic glycolytic system dominates the energy supply [174] with anaerobic glycolysis. This produces lactate and hydrogen ions, decreasing muscle

pH, which can be measured with ^{31}P-MR spectroscopy [175] by calculating the chemical shift, *δ,* between Pi and PCr. [94]

For longer duration activities, the aerobic oxidative system uses intermediates NADH and $FADH_2$ to generate ATP. [167] The oxidative pathway of ATP synthesis is referred to as Q and the maximal oxidative capacity as Q_{max}. [176] Q_{max} is dependent on the density and capacity of mitochondria and the availability of substrates and oxygen. [177] Q_{max} can be used to assess muscle oxidative capacity, endurance potential in athletes and the correlation with exercise capacity in patients with chronic disease. [178] A high Q_{max} indicates efficient mitochondrial activity, reduced Q_{max} values may signal mitochondrial dysfunction for example in HF. [179]

Muscle performance and fatigue is linked to PCr depletion and longer recovery time during which phosphocreatine (PCr) is replenished using intracellular inorganic phosphate (Pi) via an oxygen dependent process. [180] (See **Figure 3.2B**) The smaller the pH drop and the quicker the PCr recovery time, the larger the aerobic capacity. [181] The rate of PCr resynthesis after submaximal work is described as tau (t) and is independent of exercise intensity and end-exercise levels of PCr but is heavily dependent on the availability of oxygen and pH. [182] Prolonged tau is a sign of reduced muscle mitochondrial function and exercise capacity. [183] The impaired ability to recover PCr might contribute to the limited exercise capacity in HF [184], alongside reduced cardiac output, impaired oxygen perfusion (pulmonary congestion), transport (anaemia), and utilisation in the skeletal muscle. [185] Skeletal muscle metabolism plays a significant role in exercise performance, and alteration in skeletal muscle metabolism may be a key reason for exercise fatigue in HF. In addition, HF as a chronic inflammatory state, may negatively affect skeletal muscle function. [179]

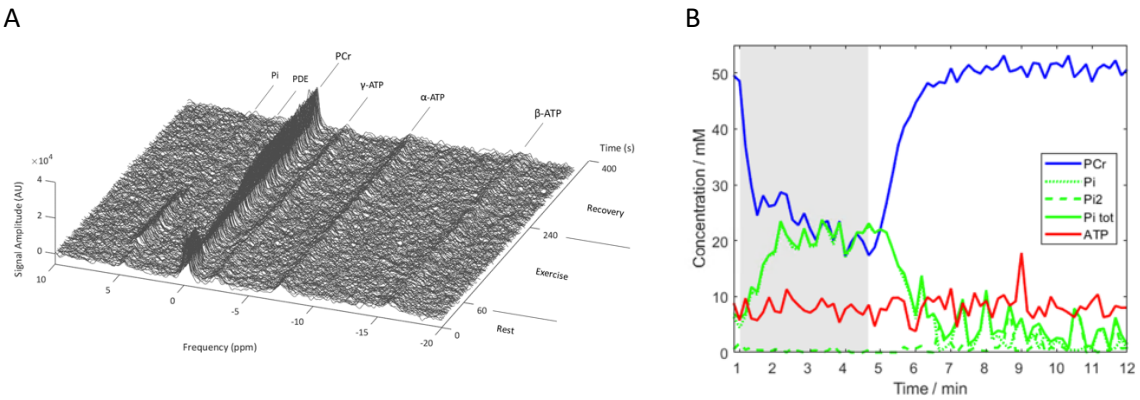

Figure 3.2 IRON HEART Representative skeletal muscle phosphorus spectral analysis

(A) dynamic spectra including inorganic phosphate (Pi), PDE, PCr, y-ATP, α- ATP, β-ATP, signals at rest, during exercise, and consecutive recovery; (B) Concentration time curve demonstrating drop in PCr (blue curve) with increase in Pi (green curve) during exercise (1-5 minutes, grey area) and recovery (5-12 minutes, white area) to facilitate stable ATP concentrations (red curve).

3.1.3 Arterial spin labelling to assess skeletal muscle perfusion and oxygenation

Arterial spin labelling (ASL) is a non-contrast imaging technique to measure tissue perfusion and oxygenation. [186] A flow-alternating inversion recovery pulsed ASL (PALS) [186] is used to magnetically label protons of inflowing blood and subtracting it from non-flowing protons in tissue. [177] It quantifies perfusion by subtracting one acquisition where the arterial/ inflowing protons are 'tagged/labelled' in the blood using a radiofrequency pulse, from a second acquisition which occurs without tagging. [187] In the limbs, ASL is most widely used in the assessment of peripheral artery disease. [188] In the IRON HEART study, ASL of the calf was performed at rest, during exercise, and recovery before and after i.v. FCM to assess whether iron replacement improves skeletal muscle perfusion due to its effects on vascular smooth muscle cells and oxygen utilisation of the skeletal muscle.

3.1.4 Impact of previous exercise on results of skeletal muscle ^{31}P-MRS and ASL

The time for full PCr recovery (tau) to its baseline/pre-exercise level depend on the extent of exercise and muscle fibre composition (type I and II fibres). [189] Submaximal voluntary contraction may lead to a significant decrease/ complete depletion of PCr, to facilitate the increased rate of ATP requirement. The effect of previous exercise on the PCr recovery time is poorly understood. It has been shown that the complete recovery time of PCr in Type I fibres of healthy volunteers may be as short as 4 mins, however this time is not sufficient for recovery in type II fibres. [189] Another study has shown that PCr kinetics are altered even after 6 minutes of exercise with no change seen at 15 minutes. [190] However, little is known about the potential prolongation of the PCr recovery time in chronic disease states like HF. This is further complicated by the fact that there is a change in skeletal muscle composition in patients with HF to predominantly type II fibres [191], with prolonged recovery time [189].

The effect of heart failure on skeletal muscle perfusion has not been studied, however endothelial function and vascular distensibility [192] are likely affected by a chronic disease state like heart failure. However, as rest perfusion is low, exercise stress perfusion has been used in studies of patients with peripheral artery disease to assess perfusion reserve. [193] Due to the unknown effects of exercise on the measurements of skeletal muscle energetics and perfusion, a sub-study was performed. This sub-study aimed to examine the impact of exercise immediately preceding the assessment of tau (^{31}P-MRS) and perfusion (ASL) with blocks of 4 minutes exercise separated by 15-minute recovery. In the first study ^{31}P-MRS was performed first followed by ASL. In the second study ASL was performed first followed by ^{31}P-MRS. (See 3.2.6.)

3.1.5 Impact of exercise on phosphocreatine kinetics and muscle perfusion

To maximise the scope of the study, some data for this sub-study was collected collaboratively with Mehrsa Jafarpour. A small proportion of the skeletal muscle spectroscopy and perfusion protocol

was jointly acquired as part of a shared experimental design. The data analysis occurred independently based on our respective research objectives and hypotheses, while benefiting from shared data collection.

3.1.6 Aims of the IRON HEART Study

The **IRON HEART** study aimed to demonstrate the beneficial effects of i.v. FCM in patients with symptomatic non-ischaemic cardiomyopathy, reduced ejection fraction, and iron deficiency on cardiac and skeletal metabolism. Iron deficiency is common in patients with heart failure and associated with adverse prognosis. Large, randomised placebo-controlled trials have demonstrated that iron repletion results in improved exercise capacity and reduced symptom burden and may improve outcomes. The mechanistic understanding of those benefits and how cardiac and skeletal muscle metabolism and function are linked is less well understood. In the first of its kind, the **IRON HEART** study aimed of to assess the impact of i.v. FCM on:

1. Cardiac energetics at rest and stress
2. Skeletal muscle mitochondrial capacity
3. Skeletal muscle perfusion and oxygenation
4. Repeatability of skeletal muscle spectroscopy and perfusion assessment.

The study aimed to assess each of the four parts individually and in addition intended to aid understanding of the likely bidirectional link between cardiac and skeletal muscle performance on patients' symptoms and exercise capacity.

3.2 Methods

3.2.1 Ethical consideration

This chapter encompasses research that was favourable reviewed and received approval by a national research ethics committee (REC reference 13/SC/0376, IRAS ID: 128163). Additionally, authorization was granted by the Healthcare Research Authority and the Oxford University Hospitals NHS Foundation Trust (OUH) to conduct the investigations. Adherence to institutional guidelines and the principles laid out in the Declaration of Helsinki was maintained throughout the research process. Written informed consent was obtained from all research participants prior to their inclusion. Data collection occurred anonymously, and was safeguarded on a secure, compliant server. Confidential written materials were stored securely within locked filling cabinets at the research site.

3.2.2 Study Participants

IRON HEART was a single centre observational study investigating the effects of one dose of FCM on cardiac and skeletal muscle metabolism in symptomatic, non-ischaemic cardiomyopathy with LV EF less than 45%, and ID as defined by the European Society of Cardiology (serum ferritin <100 mg/L or serum ferritin 100–299 mg/L and Tsat <20%). Eligible patients were recruited from outpatient HF clinics in OUH. The administration of i.v. FCM was performed by the clinical team on the cardiology day ward in OUH.

3.2.3 Inclusion criteria

- Age 18-85
- Non-ischaemic cardiomyopathy
- LVEF ≤45%
- Chronic HF with NYHA II-III

- Ferritin <100 mg/dL OR, Ferritin 100-299 mg/dl + Tsat <20%
- Established on optimal medical therapy (OMT) over the preceding 4 weeks*

*OMT was defined as stable, guideline directed HF treatment appropriate for their clinical status, where both the clinician and the patients agreed that no further titration or adjustments were necessary.

3.2.4 Exclusion criteria

- Heart failure hospitalisation over preceding 3 months
- Flow limiting coronary artery disease or ischaemia
- Hypersensitivity to intravenous iron
- Sign and symptoms of infection including elevated inflammatory markers
- Evidence of bleeding or history of bleeding disorder
- Active malignancy or haematological disorder
- Inability to perform leg exercise
- General contraindication to MRI
- Pacemaker, CRT, or implantable loop recorder

3.2.5 Endpoints

The co-primary end points were improvement in cardiac PCr/ATP ratio and skeletal muscle mitochondrial capacity (Qmax) as surrogate markers of improved energy metabolism of the cardiac and skeletal muscle. Secondary endpoints included improvement in left ventricular ejection fraction (%), muscle perfusion (M, ml/g/min), 6-minute walk distance (m), and symptoms assessed by KCCQ.

3.2.6 Study Protocol

Participants who were eligible were invited for the two study visits prior to intravenous administration of FCM. The study visit flow is highlighted in **Figure 3.3** including clinical assessment, patient reported outcomes, cardiac and skeletal magnetic resonance imaging and spectroscopy. Cardiac MRI to assess cardiac volume and function was performed at rest only, both before and six weeks after i.v. FCM. Cardiac MRS was performed at rest and during dobutamine stress (targeting 65% of maximal heart rate) at the same two time points. Importantly, no exercise testing was performed during cardiac assessment, and dobutamine stress was not used during skeletal muscle assessment.

The skeletal muscle assessment was divided into skeletal muscle ^{31}P-MRS and skeletal muscle arterial spin labelling (ASL) and they are referred to as 'Leg 1' protocol (see **Figure 3.6**) where skeletal muscle spectroscopy was performed first followed by ASL and 'Leg 2' protocol (see **Figure 3.7**) where ASL was performed first followed by skeletal muscle spectroscopy. A follow up visit was performed six weeks after i.v. iron which was identical to the "Leg 1" protocol. (See **Figure 3.6**)

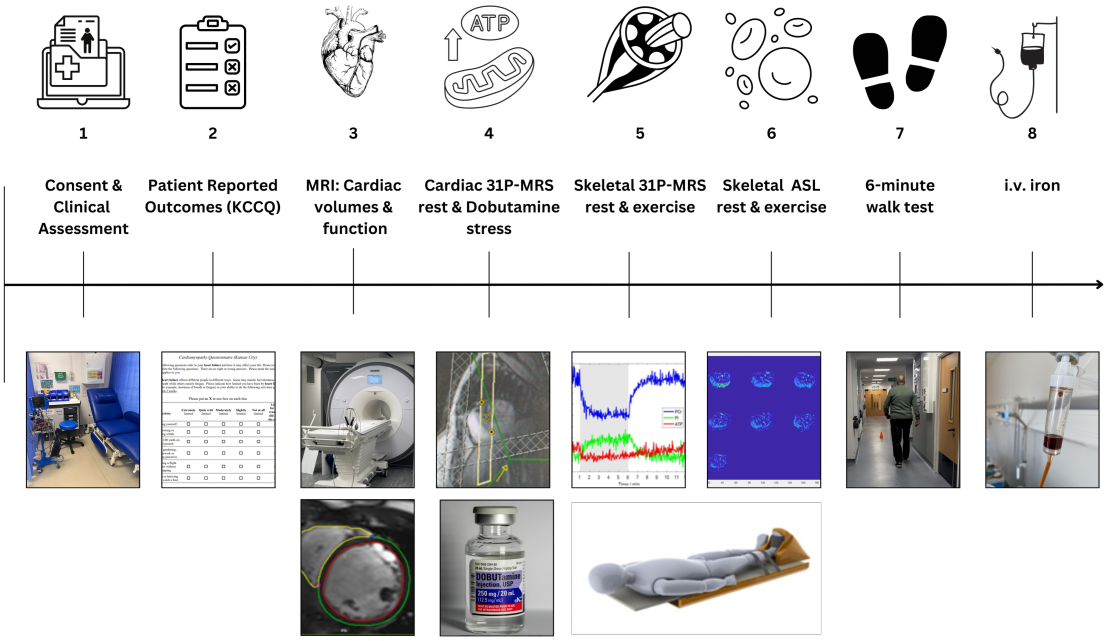

Figure 3.3 IRON HEART Study visit flow

(1) Consent and clinical assessment including height, weight, ECG, observations; (2) assessment of patient reported outcomes via Kansas City Cardiomyopathy Questionnaire (KCCQ); (3) cardiac Magnetic Resonance Imaging (MRI) to assess cardiac volumes and function; (4) cardiac phosphorus Magnetic Resonance Spectroscopy (^{31}P-MRS) at rest and Dobutamine stress; (5) skeletal muscle ^{31}P-MRS at rest and moderate exercise; (6) skeletal muscle arterial spin labelling (ASL) at rest and moderate exercise); (7) assessment of exercise capacity with 6-minute walk test (6-MWT); (8) administration of intravenous iron (i.v.) at the end of the study visit.

3.2.7 Magnetic Resonance Protocols

CMR studies were performed at 3 Tesla (Magnetom PRISMA, Siemens Healthineers, Erlangen, Germany) with a spine and 18-channel surface receive coils for proton imaging. A wide range of cardiac magnetic resonance imaging and spectroscopy methods were applied across the study (see **Figure 3.4**) which are as follows:

1. Cardiac volumes and function at rest
2. Cardiac ^{31}P-MRS at rest and dobutamine stress
3. Skeletal muscle ^{31}P-MRS at rest, exercise, and recovery
4. Skeletal muscle MRI with ASL

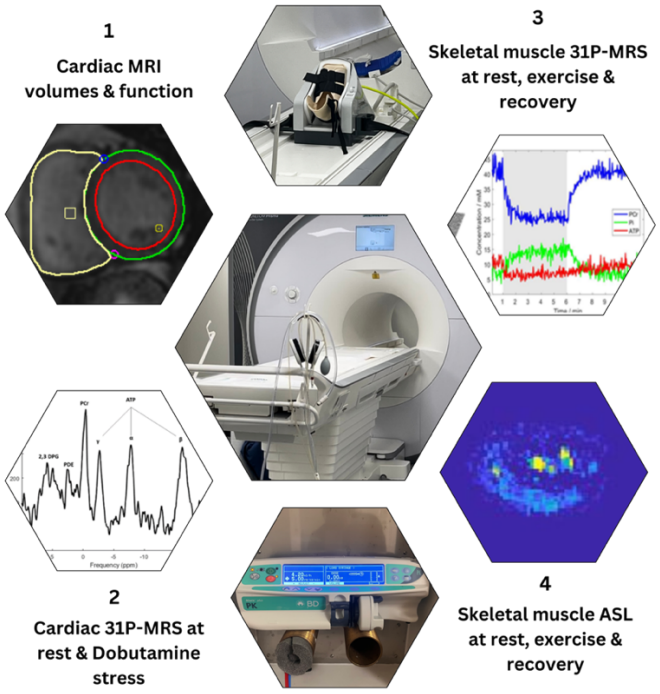

Figure 3.4 IRON HEART Study MR protocol overview

(1) Cardiac magnetic resonance imaging (MRI) to assess cardiac volumes and function; (2) Cardiac ^{31}P-magnetic resonance spectroscopy (^{31}P-MRS) at rest and Dobutamine stress; (3) ^{31}P-MRS of the skeletal muscle at rest, exercise and recovery; (4) Skeletal muscle arterial spin labelling (ASL) at rest, exercise and recovery.

3.2.7.1 Cardiac Magnetic Resonance Assessment

Please see Chapter 2 Methods for full details on cardiac magnetic resonance spectroscopy (2.8.1) and imaging (2.8.4)

3.2.7.2 Skeletal Muscle Magnetic Resonance Assessment

Skeletal spectroscopy ($^{1}H/^{31}P$ -MRS) and Arterial Spin Labelling (ASL) was performed using a Surface $^{1}H/^{31}P$ flex coil (Rapid Biomedical) secured under the right medial gastrocnemius muscle. Participants were placed in supine position with their right foot secured in an MR-conditional plantar flexion ergometer (Trispect, Ergospect, Innsbruck, Austria) facilitating exercise inside the MRI scanner bore. Prior to the start of the experiment, the Maximum Voluntary Contraction (MVC) was assessed. [194] This was achieved by fixing the ergometer pedal and participants were asked to push with maximal force for 2-3seconds. The measured maximal force was translated to pressure and 25% of the maximum voluntary contraction was used to perform exercise for 4 minutes. The DRESS selection slab (width 20mm) was centred over the gastrocnemius. (see **Figure 3.5**)

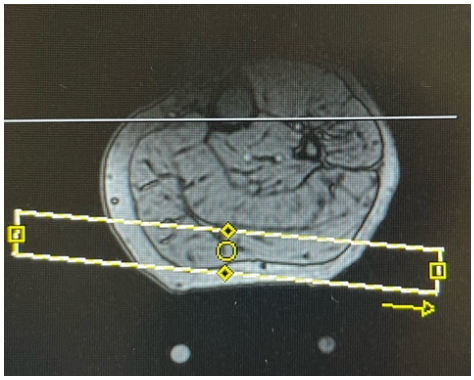

Figure 3.5 IRON HEART DRESS Selection slab over right medial gastrocnemius muscle

Selection voxel (yellow) centred over gastrocnemius muscle parallel to the coil (two white dots)

All participants underwent skeletal muscle magnetic resonance assessment at two different time points, ideally on the same day otherwise within a week of each other. First, referred to as 'Leg 1-protocol' (see **Figure 3.6**), a DRESS acquisition performed at rest (1 minute), exercise (4 minutes) and recovery (7 minutes) followed by a 2-minute break and subsequent ASL at rest (6 minutes), exercise (4 minutes) and recovery (7 minutes).

The second assessment, referred to as 'Leg 2-protocol' (see **Figure 3.7**), had the reverse order starting with ASL at rest (6 minutes), exercise (4 minutes) and recovery (7 minutes), followed by a 7-minute break and subsequent DRESS acquisition performed at rest (1 minute), exercise (4 minutes) and recovery (7 minutes).

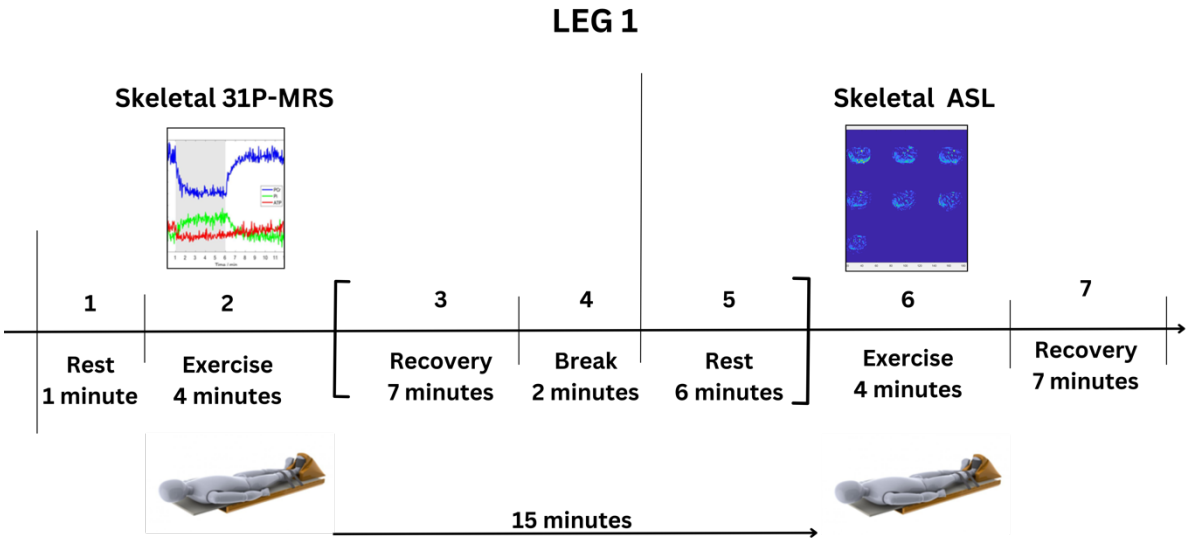

Figure 3.6 IRON HEART 'Leg 1' protocol.

Skeletal muscle 31P-MRS preformed for (1) one minute at rest, (2) four minutes exercise, (3) seven minutes recovery, followed by a (4) 2-minute break prior to start of the (5) ASL acquisition at rest (6) four minutes of exercise, and (7) seven minutes of recovery. The time between end of exercise block number one (2) and the start of exercise block number two (6) was 15 minutes.

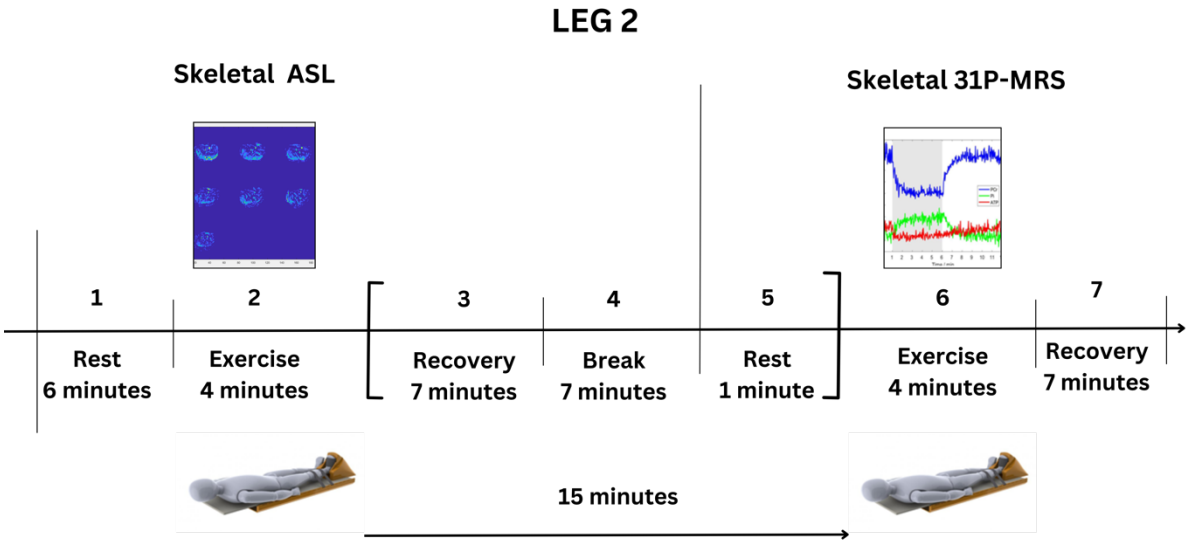

Figure 3.7 IRON HEART 'Leg 2' protocol.

Skeletal muscle ASL (1) at rest for 6 minutes, (2) four minutes of exercise, and (3) seven minutes of recovery, followed by (4) a seven-minute break prior to the start of skeletal muscle 31P-MRS preformed for (1) one minute at rest, (2) four minutes exercise, (3) seven minutes recovery. The time between end of exercise block number one (3) and the start of exercise block number two (6) was 15 minutes.

3.2.8 Spectral Analysis

Offline spectral analysis was performed using the OXSA toolbox in MATLAB [137], applying the AMARES algorithm with prior knowledge to allow the dynamic quantification of PCr and ATP/ADP. The absolute metabolite concentrations are quantified using an internal concentration reference, i.e. γ-ATP, assuming ATP concentration of 8.2 mM. [195] The following parameters were calculated from the fitted spectra: [195]

- skeletal muscle PCr at baseline (PCr_rest) in mM per litre (mM/L) cell water
- pH at baseline (pH_rest)
- ADP at baseline (ADP_rest) in micro Mol (μM)
- PCr at the end of exercise (PCr_ee) in mmol/L cell water
- PCr at the end of recovery (PCr_recovery) in mmol/L cell water
- drop of PCr during exercise (PCr_drop) in percent (%)
- PCr recovery rate time constant (tau, τ) in seconds (s)
- pH at the end of exercise (pH_ee)
- ADP at the end of exercise (ADP_ee) in μM
- rate of PCr resynthesis equivalent to rate of ATP synthesis (V_{PCr}) in mmol/L/s
- maximum rate of oxidative capacity (Q_{max}) in mM/s

Subsequently, the interpretation of the results was focused on the skeletal muscle PCr recovery rate time constant (t_{PCr}), rate of ATP synthesis (V_{PCr}) and rate of oxidative capacity (Q_{max}) under the condition that pH remains stable above 6.8 which was calculated by using the frequency difference (chemical shift) of Pi and PCr. [196] PCr recovery rate describes the concentration of PCr at the end of exercise (PCr_ee) plus the difference between PCr at the beginning and end of exercise. [173] The PCr recovery rate is dependent on oxygen availability and reflects the mitochondrial oxidative capacity in the skeletal muscle and therefor is higher in athletes and lower in patients with HF. [182] The oxidative capacity (Q_{max}) i.e. the “maximum rate of mitochondrial ATP synthesis” [196] was

calculated using the 'ADP-based model'. [196] The initial rate of ATP synthesis (V_{PCr}) relies on oxidative phosphorylation in the inner mitochondrial membrane [197] and was calculated from the PCr recovery time curve. [173] The predetermined data quality criteria were as follows: PCr-Rest 30-40 mM, PCr-drop >15% and matched between individuals, and Tau <300. If the data did not meet those criteria the study visit was excluded from the final analysis.

3.2.9 Analysis of Perfusion and Oxygenation

The offline post processing of Pulsed Arterial Spin Labelling (PASL) images (see 3.1.3) occurs in two stages. Firstly, the subtraction of the two images resulting in a perfusion weighted image, solely displaying signal from microvascular perfusion [192] without static tissue (see **Figure 3.8**). [198] In addition, oxygenation maps are produces by a subtraction between the current untagged image with the first untagged images acquired at baseline, which provides a blood oxygenation level dependent (BOLD) contrast image of the muscle.

Secondly, the offline post processing and analysis of the axial stack of subtracted images of the calf muscle in MATLAB, where firstly 7 slices are selected by drawing a region of interest around them (see **Figure 3.8A**), which eliminates movement artifacts. Subsequently a second ROI is manually drawn around the medial and lateral gastrocnemius muscle. (See **Figure 3.8B**)

The quantification of the signal within the muscle in MATLAB is derived from a formula described by Detre et al [198] considering longitudinal magnetization of water, arterial and venous blood and the relaxation time of tissue. [192] Three Perfusion maps (see **Figure 3.9 top row**) and three oxygenation maps (see **Figure 3.9 bottom row**) are generated at rest, after 4 minutes of exercise and at the end of recovery (7 minutes).

MATLAB generates a time course of the perfusion changes summed over 7 slices to determine the time to max (TTM) perfusion, which is displayed in **Figure 3.10A**. Perfusion was assessed during 6 minutes of rest (time points 0-100), during 4 minutes of plantar flexion (grey area 100-150), and 7 minutes of recovery (time points 150-300). This allows the calculation of the peak perfusion (M, ml/g/min) and time to maximal perfusion immediately after the exercise. The peak perfusion was defined as the highest perfusion signal after exercise, which is showcased in **Figure 3.10B**, where the recovery starts at 150, and the peak perfusion is assessed at time point x=154 and calculated as Y=1.014 ml/g/min.

A ROI 1

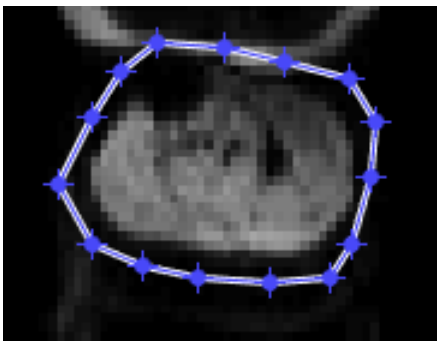

B ROI 2

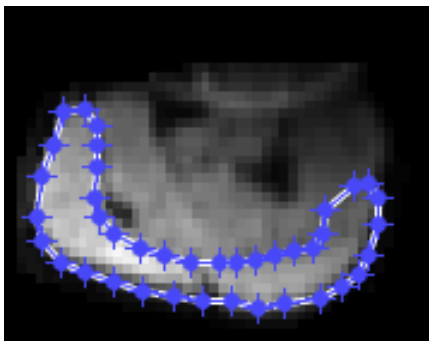

Figure 3.8 IRON HEART Axial proton images for ASL analysis

(A) Region of interest 1 (ROI 1) to identify calf circumference, (B) Region of interest 2 (ROI 2) to identify gastrocnemius muscle.

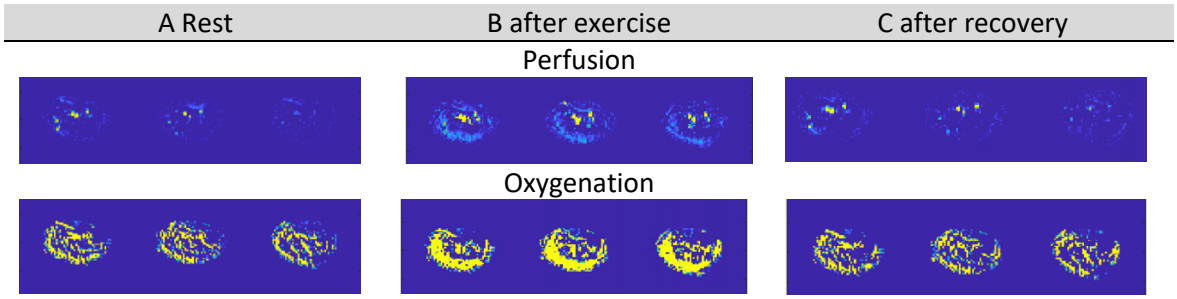

Figure 3.9 IRON HEART Perfusion maps and Oxygenation maps

Perfusion map (top row) and Oxygenation maps (bottom row) at of three axial slices (A) rest, (B) after 4 minutes of exercise, (C) after 7 minutes of recovery

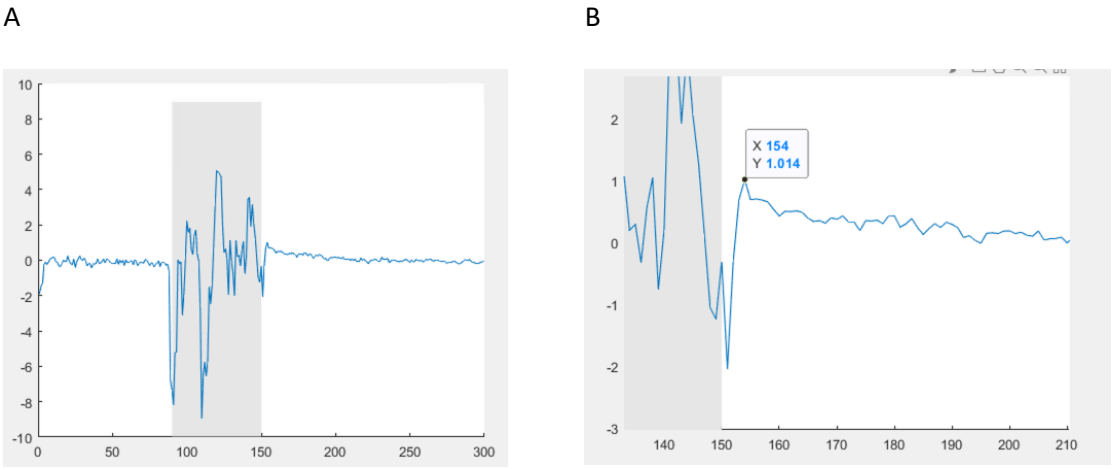

Figure 3.10 IRON HEART Summed perfusion graph

(A) perfusion at rest (time points 0-100), during exercise (grey area 100-150) and recovery (150-300); (B) Magnified from (A) to showcase Time to max (TTM) perfusion immediately after exercise at time point x=154 highlighting net perfusion of Y=1.014 ml/g/min.

3.2.10 Statistics

The **IRON HEART** study was designed and funded as a pilot study examining 4 parts:

(1) Cardiac muscle: Assessment of cardiac PCr/ATP before and after iron administration at rest and dobutamine stress,

(2) Skeletal muscle energetics ('Leg 1' protocol): Assessment of skeletal muscle energetics (Q_{max}) before and after iron administration

(3) Skeletal muscle perfusion ('Leg 1' protocol): Assessment of skeletal muscle perfusion before and after i.v. FCM

(4) Comparison of skeletal muscle energetics and perfusion prior to iron administration between 'Leg 1' and 'Leg 2' protocol

A further aim of this pilot study was to identify the effect size of intravenous iron administration in patients with HF and the effect on cardiac and skeletal muscle energetics. This will provide insights into a larger study design.

The endpoint analysis included participants with: (1) cardiac muscle PCr/ATP pre and post FCM administration, (2) Q_{max} measurement (skeletal muscle) pre and post FCM, and (3) paired data from both legs before i.v. FCM.

Normality of distribution was assessed using the Shapiro–Wilks test. For normally distributed data, parametric tests including paired t-test (to compare means between two groups) was used. For data, which was not normally distributed, a non-parametric test including the Wilcoxon signed rank test, instead of the paired t-test was performed.

Continuous variables were summarised using descriptive statistics for example mean and standard deviation for normally distributed data and median and interquartile range (IQR) for non-normally distributed data. Categorical variables were summarised using frequencies and percentages, presented as mean ± standard deviation (SD) or frequencies (%).

3.3 Results

3.3.1 Study Population and Baseline Characteristics

Between September 2022 and May 2024, approximately 3000 cardiology patients were screened at clinics in Oxford University Hospitals NHS Foundation Trust. (See **Figure 3.11**) Of 100 eligible patients with symptomatic non-ischaemic cardiomyopathy (DCM) without contraindications to MRI, 45 with ID were invited, and 21 consented. One participant withdrew due to claustrophobia. Three participants attended the initial MRI assessment and received i.v. FCM but did not consent to a follow up visit, leaving 17 participants who were included in the data analysis. Five did not receive Dobutamine infusion for ^{31}P-MRS at stress, two had contraindications to Dobutamine, three did not consent to Dobutamine.

Skeletal muscle MRS was performed in 17 participants; in four participants the skeletal muscle MRS assessment (Leg 1 pre/post) were excluded due to predetermined quality criteria (see **3.2.8**). In the second part of the study assessment (Leg 1 versus Leg 2), one set was excluded. There were no significant changes to any pre-existing medications throughout the study.

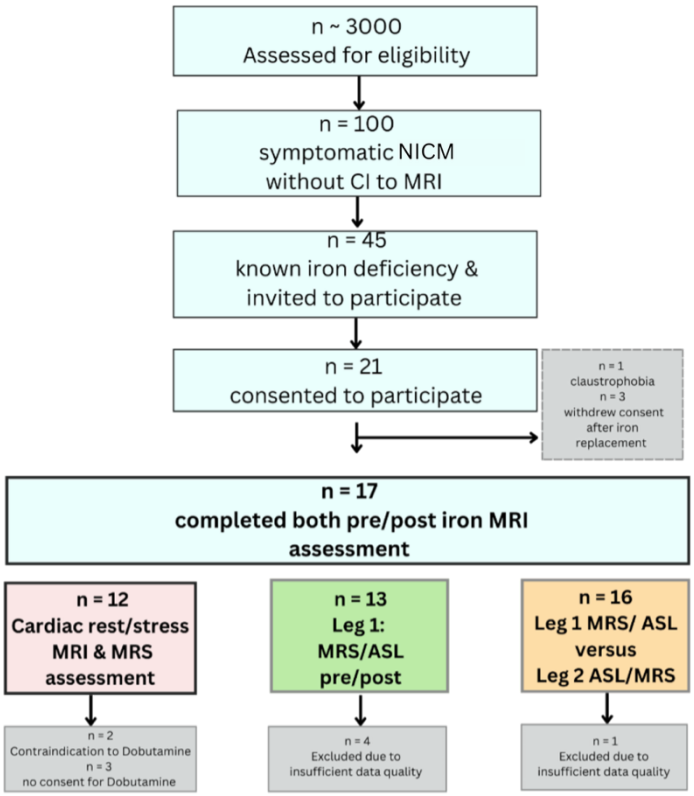

Figure 3.11 IRON HEART Flowchart Recruitment

NICM= non-ischaemic cardiomyopathy, CI=contraindication, MRI=magnetic resonance imaging, MRS=magnetic resonance spectroscopy, ASL=arterial spin labelling

The average age was 63±16 years of age, 9 participants were female (53%). (See **Table 3.1)** LVEF measured with echocardiography prior to enrolment was 32±8%. Absolute ID (ferritin <100mcg/L) was present in 12, functional ID (ferritin 100-299 mcg/L and Tsats <20%) was present in 5 patients with a mean ferritin level of 101±74 mcg/L and mean Tsats 17±8%. Baseline or follow up blood test were included in the study protocol, consequently, baseline NTproBNP- which was not taken as part of routine NHS care- and iron studies were not assessed after i.v. FCM administration.

In 4 patients iron deficiency and anaemia (defined as haemoglobin (Hb) levels less than 13.5 mg/dl in men, less than 12.0 mg/dl in women) was detected with an average Hb of 135 ± 16 mg/dL. The

mean BMI was 28.5kg/m^2. Mean baseline blood pressure was 118±20/67±12 mmHg with a mean resting heart rate of 66±9 bpm at enrolment.

Baseline Characteristic	Pre-Iron n = 17	Post-Iron n = 17	p-value
Anthropometrics: % or mean ±SD			
Age (years)	63±16		
Female n (% of total)	9 (53%)		
White n (% of total)	14 (82%)		
Black n (% of total)	3 (18%)		
NYHA classification	II-III		
BMI (kg/m^2)	28±5		
Ferritin (mcg/L)	101±74		
Transferrin Saturation (%)	17±8		
eGFR (mL/min/m^2)	71±20		
Systolic blood pressure (mmHg)	118±20	115±16	0.6748
Diastolic blood pressure (mmHg)	67±12	65±8	0.3609
Resting heart rate (bpm)	66±9	70±12	0.1239
LV EF on Echo	32±8		

Table 3.1 IRON HEART Baseline characteristics.

NYHA=New York Heart Association; eGFR=Estimated glomerular filtration rate; BMI=Body mass index

Six participants had atrial fibrillation (AF), four had chronic kidney disease (CKD), other conditions like hypertension, diabetes, and osteoarthritis were less common. (See **Table 3.2**) Four participants had a past medical history of malignancy. Most participants were on guideline-directed HF therapy: 88% on β-blocker, 88% on Angiotensin Converting Enzyme Inhibitors (ACE-I), Angiotensin II Receptor Blockers (ARB) or Angiotensin Receptor Neprilysin Inhibitors (ARNI), 76% on Mineralocorticoid Receptor Antagonists (MRA), and 82% on Sodium/Glucose Co-Transporter 2 inhibitors (SGLT2i). On average 428±947 days passed from HF diagnosis (referral from general

practitioner) to full up titration. The average time between full up-titration and enrolment in the study was 167±233 days, between enrolment and i.v. FCM was 6±8 days, and between i.v. FCM and follow up MRI were 45±13 days.

Comorbidities (n)	**Baseline n (%)**
Atrial Fibrillation	6 (35)
Hypertension	2 (12)
Diabetes	2 (12)
Chronic kidney disease (eGFR<60 mL/min/m^2)	4 (24)
Osteoarthritis	5 (24)
Obstructive sleep apnoea	2 (9)
History of malignancy of any kind	4 (24)
Concomitant medications, (n)	
β-blocker	15 (88)
ACE-I/ ARB	8 (47)
ARNI	7 (41)
MRA	13 (76)
SGLT2i	14 (82)
Furosemide	7 (41)
Oral ferrous fumarate	1 (6)

Table 3.2 IRON HEART Comorbidities and concomitant medication

ACE-I Angiotensin Converting Enzyme Inhibitor; ARB Angiotensin II Receptor Blocker; ARNI Angiotensin Receptor Neprilysin Inhibitor; MRA Mineralocorticoid Receptor Antagonist, SGLT2i Sodium/Glucose Co-Transporter 2 inhibitor

3.3.2 Cardiac ^{31}P-MRS at Rest and Dobutamine Stress Pre/Post

Paired data of Cardiac ^{31}P-MRS at rest was available in 16 participants and stress in 12 participants. Normality of distribution was assessed using the Shapiro–Wilks test: Cardiac PCr/ATP was normally distributed.

There was no significant change in the PCr/ATP at rest (see **Figure 3.12A**) and stress (see **Figure 3.12B**) before versus 6-weeks after the administration of i.v. FCM (rest pre PCr/ATP 1.5±0.35, post PCr/ATP 1.64±0.1, p=0.8126; stress pre PCr/ATP 1.41±0.4, post PCr/ATP 1.42±0.8, p=0.7769), however there was a large variation between participants (SD of differences 0.37)

Intravenous FCM did not alter the rest/stress ratio of PCr/ATP (delta +0.02, p= 0.3238, see **Figure 3.12C**).

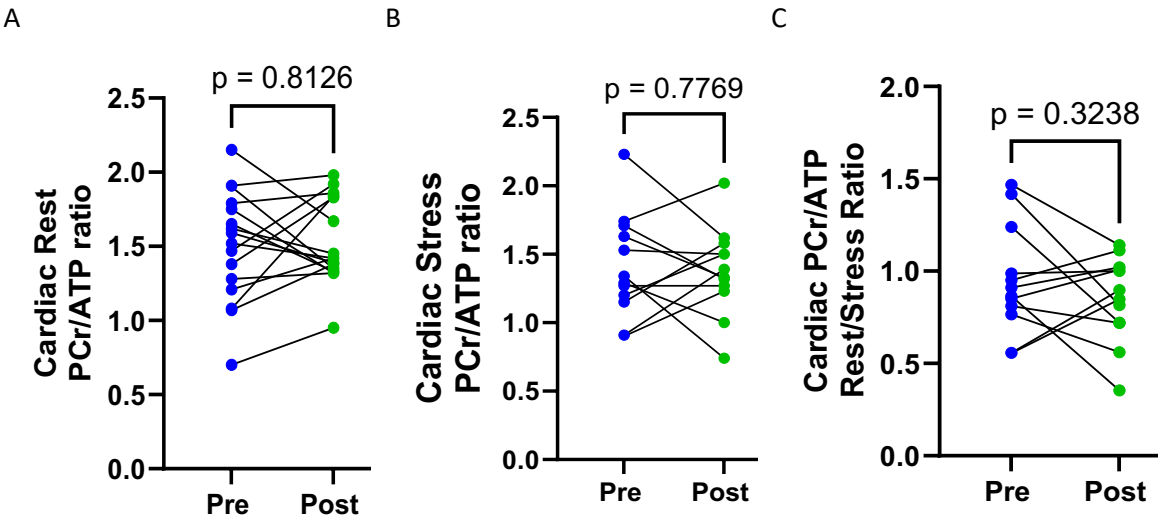

Figure 3.12 IRON HEART Primary Endpoint: PCr/ATP ratio.

PCr/ATP pre/post and the rest/stress difference in PCr/ATP: (A) No difference in PCR/ATP after intravenous (i.v.) Ferric carboxymaltose (FCM); (B) no difference in stress augmentation in PCr/ATP ratio after i.v. iron

3.3.3 Cardiac Volumes and Function at Rest

Paired cardiac volumes and function at rest were available in 17 participants (see **Table 3.3**). Administration of i.v. iron was associated with a significant decrease in LVESV (p=0.006) with a mean decrease of 15±20ml (see **Figure 3.13A**) and significant increase in LVEF (p=0.018) with a mean increase of 4.5% (see **Figure 3.13B**). There was no significant difference in heart rate (mean difference 5 bpm, p=0.124).

(means ±SD)	**Pre**	**Post**	**P-value**
Left Ventricle			
LVEDV (ml)	196±62	187±69	0.161
LVESV (ml)	125±53	110±57	0.006*
LVSV (ml)	72±20	75±24	0.393
LVEF (%)	38±9	42±10	0.018*
LV mass (g)	116±39	107±32	0.344
LVCO (ml/min)	4694±1368	5228±1669	0.095
Right Ventricle			
RVEDV	128±32	130±41	0.722
RVESV (ml)	68±24	63±26	0.268
RVSV (ml)	67±20	67±24	0.895
RVEF (%)	50±9	52±11	0.437

Table 3.3 IRON HEART resting cardiac volumes and function

Significant (*) decrease in LVESV and significant increase in LVEF, otherwise no changes in cardiac volumes; LVEDV=left ventricular end-diastolic volumes; LVEF=left ventricular ejection fraction; LVESV=left ventricular end-systolic volume; LVSV=left ventricular stroke volume; RVEDV=right ventricular end-diastolic

A

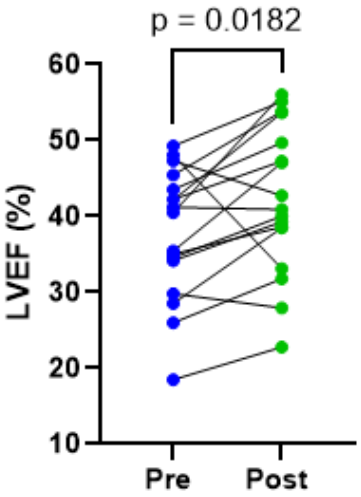

B

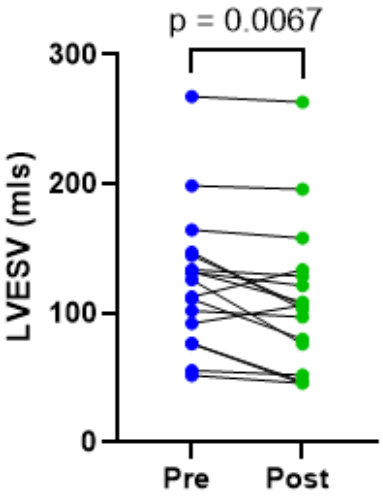

Figure 3.13 IRON HEART Left ventricular function and volume

Significant decrease in (A) Left Ventricular Ejection Fraction (LVEF) and significant decrease in Left Ventricular End-Systolic Volumes (LVESV)

3.3.4 Clinical Outcomes: 6-minute Walk Test

6-minute walk distance (6-MWD) at 6 weeks after i.v. FCM showed a statistically and clinically meaningful increase (pre mean 378±101m to post 410±104m) with a mean increase in walk distance of 33±34m; p = 0.0028). (see **Figure 3.14**)

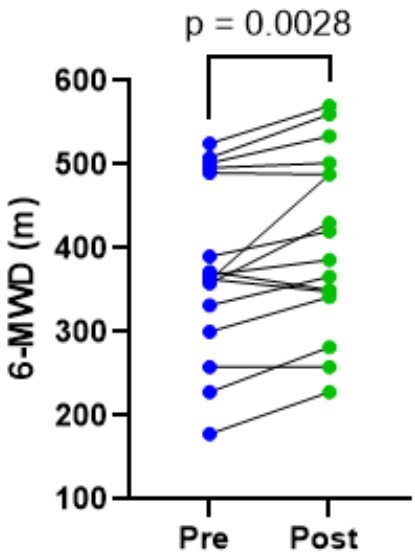

Figure 3.14 IRON HEART 6-minute walk distance

3.3.5 Clinical Outcomes: 12-item Kansas City Cardiomyopathy Questionnaire

FCM resulted in a numerical and clinically meaningful but borderline statistically significant increase in 12-item KCCQ (pre mean 49±12 to post 53±10) with a mean increase of 4 points (p=0.0532) reflecting a reduction in symptom burden. (see **Figure 3.15**)

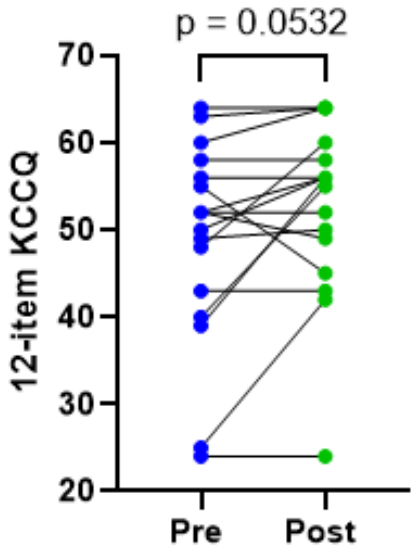

Figure 3.15 IRON HEART 12-item Kansas City Cardiomyopathy Questionnaire

KCCQ= Kansas City Cardiomyopathy Questionary

3.3.6 Skeletal Muscle Magnetic Resonance ^{31}P-MRS

Following 4 minutes of repeated plantar flexion (same resistance on all study visits), there was a significant increase in the skeletal muscle mitochondrial oxidative capacity with i.v. FCM (Q_{max}, pre 0.44±0.2 vs post 0.56±0.3, p=0.0322, n=14). (See **Figure 3.16)**

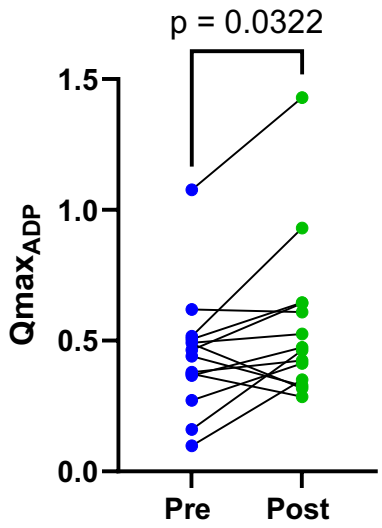

Figure 3.16 IRON HEART Skeletal muscle mitochondrial oxidative capacity

Significant improvement in skeletal muscle mitochondrial oxidative capacity (Qmax) with intravenous Ferric carboxymaltose (FCM).

Using the same resistance at all study visits, there was no significant difference in skeletal muscle PCr at baseline (PCr_rest), PCr drop at the end of exercise (PCr_drop), pH at the end of exercise (pH_ee), and PCr recovery rate time constant (tau). (see **Table 3.4**)

	Pre (mean±SD)	**Post (mean±SD)**	**p-value**
V_{PCr}	0.30±0.2	0.38±0.2	0.159
PCr_drop (%)	53.4±25.0	63.0±17.2	0.304
pH_ee	6.8±0.2	6.81±0.1	0.779
t_{PCr}	94.4±71.7	67.7±28.2	0.081
Q_{max}	0.44±0.2	0.56±0.3	0.032*

Table 3.4 IRON HEART Skeletal Muscle spectroscopy results overview.

Significant (*) improvement in maximum rate of oxidative capacity (Q_{max}); no significant improvement in initial rate of PCr resynthesis equivalent to the rate of ATP synthesis (V_{PCr}), PCr during exercise (PCr_drop) measured in percentage (%), pH at the end of exercise (pH_ee)

3.3.7 Skeletal Muscle Perfusion

Following repeated plantar flexion at 25% MVC (n=15) for 4 minutes, there was a significant increase in the net perfusion measured (ml/g/min) after administration of iron (pre 1.8±1.2 vs post 2.6±1.6 ml/min/g, p=0.0285). (See **Figure 3.17**) with a mean difference in perfusion of 1.2±1.9 ml/min/g.

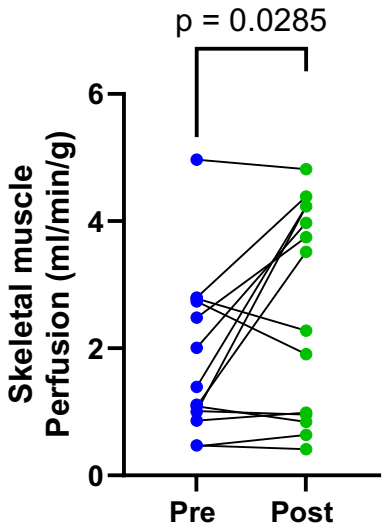

Figure 3.17 IRON HEART Skeletal muscle perfusion

(A) paired perfusion measures pre/post iron administration; (B) the increase in mean rank may indicate increase post iron (C) Mann-Whitney U test demonstrated that there is no significant difference in net perfusion between the groups.

3.3.8 Impact of Exercise on Muscle Energetics and Perfusion (Leg 1 vs Leg 2 protocol)

To assess repeatability prior to i.v. FCM, 'Leg 1-protocol' (^{31}P-MRS followed by ASL) was compared to 'Leg 2-protocol' ASL followed by ^{31}P-MRS). While all participants began with 'Leg 1-protocol', half of the participants completed the 'Leg 2-protocol' on the same day (ID*) and the other half completed the 'Leg 2-protocol' on a separate day (ID, within one week). (See **Table 3.5 and 3.6**) Irrespective of timing of ^{31}P-MRS and ASL measurements ('Leg 1 and Leg 2-protocol'), no significant differences were found between protocols, supporting the repeatability of the results independent of prior exercise.

ID	PCr_drop (%)		pH_ee		tau		Q_{max}		V_{PCr}	
	Leg 1	Leg 2	Leg 1	Leg 2	Leg 1	Leg 2	Leg 1	Leg 2	Leg 1	Leg 2
1*	79.5	75.7	6.8	6.8	60.4	105.9	0.51	0.29	0.42	0.24
2*	49.0	14.8	6.9	6.9	64.4	9.4	0.16	0.43	0.10	0.14
3	52.1	73.0	7.0	6.9	50.6	56.4	0.46	0.47	0.32	0.38
4*	46.7	32.7	7.1	7.0	23.2	35.5	1.08	0.59	0.75	0.34
5	60.4	92.9	6.8	6.7	62.4	127.7	0.49	0.41	0.32	0.38
6	88.5	88.2	6.5	6.8	92.9	61.1	0.62	0.65	0.51	0.59
7	68.7	95.7	6.7	6.7	242.9	101.3	0.27	0.55	0.25	0.52
8	88.3	77.0	6.6	6.7	114.5	115.6	0.49	0.41	0.42	0.32
9	67.9	57.7	6.9	6.9	52.0	69.6	0.67	0.39		0.27
10*	95.0	92.9	6.5	6.7	151.5	111.2	0.37	0.38	0.34	0.36
11*	18.2	89.4	6.8	6.7	59.4	189.6	0.38	0.21	0.12	0.19
12	39.6	62.6	7.0	7.0	45.6	44.2	0.52	0.93	0.32	0.74
13*	30.6	20.8	7.0	7.0	54.1	77.5	0.44	0.19	0.23	0.08
14*	75.2	91.0	6.8	6.5	70.0	116.8	0.13	0.34	0.11	0.29
Mean	61.4	68.9	6.8	6.8	81.7	87.3	0.5	0.4	0.3	0.3
SD	22.27	26.72	0.18	0.14	54.22	44.34	0.22	0.18	0.17	0.17
p-value^{all}	0.31		0.49		0.75		0.71		0.63	
p-value*	0.89		0.37		0.86		0.36		0.36	

Table 3.5 IRON HEART Skeletal muscle energetics 'Leg 1-protocol' and 'Leg 2-protocol'.

No significant difference between any of the measured parameters even in those participants who had 'Leg 1-protocol' on the same day as 'Leg 2-protocol' (ID) PCr_drop=PCr drop during exercise; pH_ee=pH at the end of exercise; tau=PCr recovery rate; Q_{max}=maximum rate of oxidative capacity; VPCr=PCr resynthesis; p-value^{all}=all participants; p-value*=participants who completed the protocol on the same day.*

M (perfusion) ml/g/min

ID	Leg 1	Leg 2
1*	2.48	2.44
2	0.86	0.91
3*	4.97	7.33
4	8.57	4.63
5	0.47	0.82
6*	0.46	0.64
7*	2.78	1.33
8	2.01	4.10
9	2.74	8.56
10*	1.11	2.16
11	1.39	7.54
12	6.13	2.83
13	2.84	1.84
16*	2.80	3.44
17*	1.09	3.52
18	1.00	1.06
19*	1.09	1.79
21*	1.01	1.61
Mean	2.43	3.14
SD	2.10	2.37
p-value^{all}	0.26	
p-value*	0.33	

Table 3.6 IRON HEART Skeletal muscle perfusion 'Leg 1-protocol' and 'Leg 2-protocol'.

No significant difference in perfusion even in those participants who had 'Leg 1-protocol' on the same day as 'Leg 2-protocol' (ID)*

3.4 Discussion

This exploratory single centre pilot study examined the short-term effects of intra venous administration of FCM in patients with non-ischaemic cardiomyopathy, reduced ejection fraction and iron deficiency. In this study, the effect of iron on PCr/ATP ratio as a marker of energy reserve in the cardiomyocyte, and Q_{max} as a marker of mitochondrial oxidative capacity in the skeletal muscle was examined. A variety of exploratory outcomes including cardiac function, symptomatic assessment with KCCQ, change in exercise capacity (6MWT) and skeletal muscle perfusion were also assessed. The aim of the study was to explore the mechanism behind the well-established clinical improvement associated with iron repletion in patients with heart failure and iron deficiency to help understand whether it is mainly driven by improvement in cardiac muscle function or skeletal muscle function.

The key positive findings of the study are that administration of i.v. FCM in this cohort of patients with non-ischaemic DCM with ejection fraction 45% or less and iron deficiency resulted in:

- A significant increase of LV ejection fraction.
- Significant increase in functional capacity measured by 6-minute walk distance.
- A significant increase in skeletal muscle mitochondrial oxidative capacity.

3.4.1 Participant Recruitment and Baseline Characteristics

The study cohort was broadly representative of the local HF population, with diversity in both sex and ethnicity. It reflects one of the most contemporary cohorts in which the effects of i.v. FCM in HF were evaluated alongside widespread use of guideline directed medical therapy. Notably, 82% of participants were receiving a sodium-glucose cotransporter-2 inhibitors (SGLT2i). SGTL2i are increasingly recognised to influence haemoglobin, erythropoiesis, and iron metabolism. [199] [200] Angerman et al. [201] could demonstrate an improvement of myocardial iron content with SGLT2i

Empagliflozin and that lower myocardial iron content, measured by higher myocardial T2* values, correlates with lower peak oxygen consumption, the iron regulator hepcidin, and higher LV volumes.

3.4.2 Cardiac Function and Energetics

Previous studies [202] have demonstrated that iron deficiency has an negative impact on myocardial PCr/ATP independent of the presence of anaemia and the degree of systolic function. However, to date no study has been conducted to assess the impact of iron repletion in HF and ID on myocardial PCr/ATP. Baseline PCr/ATP values were consistent with previously published values of patient with HF both with and without ID. [202] In our pilot study, myocardial PCr/ATP at rest and during Dobutamine stress showed no significant change after iron administration. This might be either because there is no effect of intravenous iron on PCr/ATP, or the effect could not be detected due to the relatively small sample size. In addition, the effect of iron may not directly influence myocardial high-energy phosphate metabolism as measured in this study but might exert beneficial effects on cardiac energetics via increased efficiency in the creatine kinase system. [203]

In addition, participants in this study demonstrated an improvement in cardiac volumes (LVESV -15ml) and function (LVEF +5%). Iron deficiency [204] and low myocardial iron content [201] has a negative effect on LV function, and the results of this study supports previous findings [205] that iron improves ejection fraction. However, the clinically meaningful impact of the mild improvement in ejection fraction is questionable and might be a result of measurement variability [206] due to image quality, endocardial border tracing and biological variation between the two timepoints. Furthermore, serum iron studies a myocardial iron content assessed by T2*, were not assessed therefore no causal inference can be drawn.

Previous studies suggest an association between reduced ejection fraction and lower PCr/ATP [28], however, given the small sample size and absence of control group this association could not be

confirmed in the **IRON HEART** study. However, the increase in exercise capacity might have resulted in a relative increase in ATP demand. Therefore, a stable PCr/ATP during increased energy demands might still reflect a beneficial effect of iron repletion on cardiac energetics, as previously suggested.[202]

However, in this study the beneficial effect on LV volumes and function may not solely be contributed to iron repletion. Although the enrolled patients were established on stable optimal medical therapy for at least 3 months, improvement in LVEF following established optimal medical therapy are known to continue beyond three months for up to 24 months [207, 208], therefore the increase in LVEF observed in this study may reflect the ongoing effect of medical therapy rather than a direct effect of i.v. FCM. In addition, iron repletion was not confirmed prior to follow up study visit.

3.4.3 Changes in Skeletal Muscle Metabolism and Perfusion

Skeletal muscle oxidative capacity (Q_{max}) improved significantly (+27%) post-iron therapy, suggesting enhanced skeletal muscle mitochondrial function and oxidative metabolism. In contrast to previous studies [67], no significant changes were observed in other parameters such as PCr recovery rate time constant (τ) or PCr drop during exercise. Even though the study was under-powered, overall, these findings support the hypothesis that iron repletion may improve exercise capacity in this cohort through improved skeletal muscle energetics. These results shine the spotlight on the importance of the skeletal muscle and its contribution to the symptom burden of patients with heart failure and iron deficiency. [209] Skeletal muscle dysfunction plays a key role in exercise intolerance in heart failure and may be responsible for worsening physical activity and deconditioning. [210]

In addition, HF is associated with impairment in peripheral muscle perfusion [211, 212] and function [213]. Iron is critical in oxygen transport and utilization, as it is an essential component of haemoglobin and myoglobin. [51] In the first of its kind, the **IRON HEART** study found a significant increase in skeletal muscle perfusion after i.v. FCM. This raises the hypothesis that iron replacement may not just affect oxygen delivery but also intracellular energy metabolism. Iron is a key element in the signalling pathways of the vascular endothelium [214], which might have contributed to the augmentation of skeletal muscle perfusion seen in this study. Furthermore, the improvement of skeletal muscle function may be directly linked to improvement in heart function and subsequent improvement in skeletal muscle perfusion which is linked to oxidative metabolism. [215]

These findings support the rationale for larger trials to evaluate the link between skeletal muscle metabolism, perfusion and symptoms in patients with heart failure.

3.4.4 Changes in Clinical Data

Iron deficiency in HF is associated with worse symptoms, poorer quality of life, hospitalisation and death. [216] The observed improvement in clinical outcomes as measured objectively by the 6-MWT and subjectively by the KCCQ, aligns with findings of previous large international trials.[64, 65] In the **IRON HEART** study the degree of improvement after 6-weeks was more pronounced than in previous trials, despite the shorter follow up of six weeks. [58, 65] However, it has been shown that improvement within the first 4 months is often sustained long-term. In addition, a training effect which is recognised as a limitation of the 6-MWT might have contributed to the improvement. [217]

In contrast to the previously published trials in iron deficiency and heart failure, in this study, the short 12-item KCCQ was used to assess the clinical change experienced and reported by patients. [123] However, only a small improvement in KCCQ by a mean of 4 points could be shown, whereas

a change of 5 points is commonly assumed to be clinically significant. [120] However, a more recent analysis of the FAIR-HF trial [121] suggested that an even smaller change in KCCQ might reflect a meaningful improvement for patients. Therefore, a mean improvement of 4 points, as seen in this study, may reflect a clinical meaningful although not statistically significant result.

3.4.5 Limitation

This was the first study to combine the assessment of cardiac and skeletal muscle energetics and skeletal muscle perfusion with the aim to understand the link between exercise intolerance and ID in HF. As an exploratory pilot study, it was designed to establish the effect size of iron replacement on cardiac and skeletal muscle energetics and inform a power calculation for larger studies.

The study's final sample size was lower than expected and some data sets were retrospectively excluded as they did not meet the predefined quality criteria, which was partly due to noise contamination, partly due to movement artifacts. As a result, the study's sample size and statistical power limits the conclusion from the study. However, to detect a difference in skeletal muscle energetics (Qmax) and skeletal muscle net perfusion (M) approximately 22 paired measurements were required. The available 14 paired dataset achieve a power for the paired t-test of approximately 64%.

In contrast to the larger randomized trials, sufficient iron repletion was not confirmed, which prohibited re-dosing and therefore the full extent of reversal of ID, particularly on myocardial energetics and skeletal muscle perfusion could not be shown.

Although this study included a demographically diverse patient population of non-ischaemic DCM, in a sample size less than 20, this might have resulted in considerable variability in baseline cardiac and skeletal muscle physiology dependant on age (range from 35-85 years) and training status. In

addition, the severity of HF, ID (functional versus absolute ID) and presence of anaemia may have influenced the results further. The duration of stable optimal medical therapy was short and its effect on left ventricular function may have persisted throughout the study duration. [207]

3.4.6 Clinical Implications and Future Directions

If my results can be reproduced in larger studies, the aim should be to better understand the relationship between cardiac and skeletal muscle function in patients with iron deficiency and heart failure. This would provide answers to three key remaining concerns; firstly, the stratification of different patient groups based on severity of ID (functional versus absolute iron deficiency). Secondly, the effect of anaemia in patients with HF and ID and subsequent changes in skeletal and cardiac MRS and perfusion. And thirdly, the undertaking of a sub-group analysis to characterise so call 'super responders to iron' to facilitate more precise phenotyping of patients living with HF with individualized treatment.

3.5 Conclusion

In conclusion, this study underscores the potential benefits of iron supplementation on cardiac volumes and function, exercise capacity and skeletal muscle oxidative capacity. It adds to the existing evidence highlighting that iron is an intrinsic part of HF treatment. The results emphasized the importance of the interaction between skeletal muscle function and exercise capacity and its impact on the day-to-day symptom burden experienced by patients with HF. Addressing the methodological challenges highlighted in this study will further enhance our understanding of the role of iron in modulating cardiac and skeletal muscle dysfunction.

4 IMPROVE-Diabetic Cardiac Energetics 2 Study 'DICE'

Obesity, insulin resistance, T2DM and metabolic HFpEF, all of which are commonly linked, are characterised by an increase in myocardial FFA uptake and metabolism and a reduction in myocardial energetics. [71] To counteract this, Ninerafaxstat was designed to limit FAO, increase glucose oxidation, restore metabolic flexibility and improve cardiac energetics. [75] It was initially studied in patients at risk of HFpEF with obesity and diabetes (IMPROVE-DiCE) and was shown to improve myocardial energetics, reduce myocardial steatosis and improve LV diastolic filling. [74] In this chapter the results of the follow up trial IMPROVE-DiCE-2, are presented, aiming to confirm the mechanistic effect in obesity, diabetes and established HFpEF.

4.1 Background

4.1.1 Diagnosis of Heart Failure with Preserved Ejection Fraction

Diagnosing HFpEF involves assessing structural abnormalities on echocardiography, biomarkers, and risk factors (age, obesity, atrial fibrillation (AF), HTN). [218] (See **Figure 4.1**) Definitions of HFpEF vary [218] and there is no consensus which HF score should be use in clinical practise [219, 220]. The Heart Failure Association (HFA) of the European Society of Cardiology (ESC) 'Pretest assessment, echocardiography and natriuretic peptide, functional testing and final aetiology' (HFA-PEFF) score [219] (see **Figure 4.1A**) includes functional and morphological changes alongside biomarkers. The H2FPEF Score [220] (see **Figure 4.1B**) focuses on cardiometabolic risk factors including body mass index (BMI) >30 kg/m^2, HTN, presence of AF, age, alongside structural changes like pulmonary artery systolic pressure (PASP) >35 mm Hg and elevated filling pressures (E/e' >9). A score higher than 5.5. is associated with worse outcomes. [221]

A HFA-PEFF

	Functional	Morphological	Biomarker (SR)	Biomarker (AF)
Major	septal e' < 7 cm/s or lateral e' < 10 cm/s or Average E/e' ≥ 15 or TR velocity > 2.8 m/s (PASP > 35 mmHg)	LAVI > 34 ml/m² or LVMI ≥ 149/122 g/m² (m/w) and RWT > 0,42 #	NT-proBNP > 220 pg/ml or BNP > 80 pg/ml	NT-proBNP > 660 pg/ml or BNP > 240 pg/ml
Minor	Average E/e' 9 -14 or GLS < 16 %	LAVI 29-34 ml/m² or LVMI > 115/95 g/m² (m/w) or RWT > 0,42 or LV wall thickness ≥ 12 mm	NT-proBNP 125-220 pg/ml or BNP 35-80 pg/ml	NT-proBNP 365-660 pg/ml or BNP 105-240 pg/ml

Major Criteria: 2 points — ≥ 5 points: HFpEF

Minor Criteria: 1 point — 2-4 points: Diastolic Stress Test or Invasive Haemodynamic Measurements

B H_2FPEF Score

	Clinical Variable	Values	Points
H_2	Heavy	Body mass index > 30 kg/m²	2
	Hypertensive	2 or more antihypertensive medicines	1
F	Atrial Fibrillation	Paroxysmal or Persistent	3
P	Pulmonary Hypertension	Doppler Echocardiographic estimated Pulmonary Artery Systolic Pressure > 35 mmHg	1
E	Elder	Age > 60 years	1
F	Filling Pressure	Doppler Echocardiographic E/e' > 9	1
	H_2FPEF score		Sum (0-9)

Total Points 0 1 2 3 4 5 6 7 8 9

Probability of HFpEF 0.2 0.3 0.4 0.5 0.6 0.7 0.8 0.9 0.95

Figure 4.1 DICE Heart failure with preserved ejection fraction scores

(A) HFA-PEFF score and (B) H_2FPEF score

4.1.1.1 Assessment of diastolic dysfunction at rest and exercise

Diastole, the phase between aortic valve (AV) and mitral valve (MV) closure, consists of four physiological phases (**Table 4.1A**) assessed by echocardiographic measurement (**Table 4.1B**) including Tissue Doppler Imaging (TDI), mitral valve E-wave velocity, E/A ratio, and deceleration time, which reflect HFpEF-related changes (**Table 4.1C**). [222] The mitral E-wave, indicating the atrial-ventricular pressure gradient, reflects LV compliance. Diastolic dysfunction in HFpEF is characterized by impairment of LV relaxation and reduced compliance, leading to limited LV filling capacity, elevated left ventricular end-diastolic pressure (LVEDP), and increased left atrial (LA) diastolic pressure causing pulmonary congestion. [223] Clinically, this presents as dyspnoea and exercise intolerance, hallmark symptoms of HFpEF. [224] Early diastolic dysfunction appears as reduced E-wave (abnormal relaxation), which normalises as LA pressure rises. Progressive diastolic dysfunction reduces late diastolic filling (A-wave), increasing the E/A ratio. [223] Tissue doppler imaging (TDI) derived e' assesses LV longitudinal relaxation, which declines with age and progressive diastolic dysfunction. In early HFpEF, elevated LV filling pressures (increased E/e' ratio), may occur only during exercise, emphasising the value exercise stress testing. [224]

A Physiology	B Echocardiographic measurement	C Pathophysiology
Isovolumetric relaxation (AV & MV closed)	IVRT	Impaired relaxation with normal LA pressure and longer IVRT Elevated LA pressure and shorter IVRT
Early rapid filling	Transmitral E wave	Peak E velocity reflects LA-LV pressure difference and left atrial pressure. Falls as LV relaxation becomes impaired.
	DT	Marker of LV diastolic stiffness Lengthens with age & diastolic dysfunction.
Diastasis (no filling)	none	No pressure difference between LA & LV. Depending on heart rate and rhythm.
Atrial contraction in SR	A velocity	Decreases with increased LV diastolic pressure.

Table 4.1 DICE Four stages of diastole

(A) Four physiological stages of diastole and (B) the echocardiographic assessment; (C) pathophysiological features; IVTR= Isovolumetric Relaxation Time; AV= aortic valve; MV= mitral valve; SR= Sinus rhythm; DT= deceleration time; LA= left atrial; LV= left ventricle

4.1.1.2 HFpEF Haemodynamics, Exercise Intolerance and Lung Water

Under normal conditions LV end-diastolic volume (LVEDV), heart rate (HR) and EF increase enhancing LV peak filling rate. In HFpEF, LVH and myocardial stiffness lead to elevated LV and RV end-diastolic pressure, limiting LV filling during exercise and reducing LV peak filling rate, a key determinant of haemodynamic response during exercise. [225] Elevated LV filling pressure increases LA volume, a known poor prognostic marker. [226] Advanced MRI techniques, such as the Ultrashort Echo Time (UTE) lung water sequence, can quantify exercise-induces pulmonary congestion, indicating increased LV pressures and worse outcomes. [227]

4.1.2 Metabolic Alteration in Obesity, T2DM and HFpEF

The WHO states that around 60% of people living in Europe are either overweight or obese. [228] Obesity is defined as a BMI of $\geq$30 kg/m^2 and is a risk factor for cardiometabolic diseases such as fatty liver disease, T2DM and HF. Obesity is a key driver for HTN [229, 230], leading to pressure overload, LVH, and diastolic dysfunction [231], increased myocardial energy demands [232], and HF [233]. Obesity is associated with insulin resistance and hyperinsulinemia resulting in a downregulation of insulin-stimulated glucose transporter (GLUT4) promoting hyperglycaemia. [234] In parallel, in obesity, free fatty acid (FFA) levels in the blood [235] are elevated promoting increased myocardial fatty acid uptake [236], utilisation and oxidation [237].

In T2DM the incidence of HF is increased, independent of the presence of obesity or hypertension. [238] Diabetic cardiomyopathy may lead to HFpEF [239] and is characterized by structural, metabolic and haemodynamic changes in the heart which are not associated with coronary artery disease, valvular heart disease, and hypertension [240] and may be referred to as metabolic HFpEF. Structurally, metabolic HFpEF is characterised by pathological cardiac remodelling such as interstitial fibrosis, LVH, microvascular dysfunction [241], increased cardiac pressure and up-regulation of the RAAS system [242]. Hyperglycaemia and an increased concentration of FFA contribute to microvascular dysfunction and production of Reactive Oxygen Species (ROS) and advanced glycation end-products (AGE). [243] Additionally, autonomic dysfunction, frequently arising from diabetic neuropathy, impairs heart rate variability and baroreceptor- heart rate reflex sensitivity, further contributing to heart failure progression in T2DM.[244]

In animal models of HFpEF have highlighted that altered signalling pathways affect disease progression offering potential therapeutic targets influencing inflammation, cardiac energetics, mitochondrial respiration, and oxidative stress [245], interstitial fibrosis, endothelial dysfunction and microcirculation [4]. Excess fatty acid metabolism, oxygen consumption and myocardial

triglyceride accumulation are key contributors, supporting the hypothesis that promoting glucose oxidation could reduce oxygen consumption [246], improve diastolic function [247], and improve exercise capacity [248] in HFpEF.

In humans, the precise adaptations of cardiac metabolism associated with metabolic HFpEF are less well understood, partially due to the complicating contribution of insulin resistance diabetes which commonly coexist in patients with HF. Increased insulin resistance and subsequent T2DM results in a reduction of insulin-stimulated glucose transport (GLUT4) and an increased expression of fatty acid translocase (FAT/CD36) [249] facilitating increase fatty acid uptake and metabolism for ATP generation. [250] [247, 251] Progressive insulin resistance activates peroxisome proliferator activated receptor-α (PPARα) [68] which lead to suppression of the pyruvate dehydrogenase (PDH) activity resulting in increased lactate production by uncoupling of glycolysis from glucose oxidation. [70] The shift away from glucose oxidation towards increased FAO [69] leads to increased oxygen consumption [252] and the increased fatty acid uptake results in conversion of FFA to triglycerides (TAG) which are stored inside the cardiomyocyte [249].

4.1.3 Modulating myocardial substrate utilisation as a therapeutic target

Modulating myocardial substrate utilisation is an emerging treatment approach in ischaemic cardiomyopathy [253], hypertrophic cardiomyopathy [254] and heart failure [255, 256], though large randomized trials are lacking [257]. Based on the glucose-fatty acid oxidation interplay described by Randle et al. (1963) [39], shifting myocardial metabolism from fatty acid oxidation to more oxygen-efficient glucose oxidation is hypothesised to improve cardiac function and symptoms. [258] Various drugs have been assessed for their ability to improve cardiac energetics, including Perhexaline [259], ß-Blocker [256], and Sodium-glucose Cotransporter-2 Inhibitors (SGLT2i) [260] and Trimetazidine [261]. While Perhexaline inhibits the carnitine palmitoyltransferase-1 and -2 enzymes required for ß-oxidation, small trials have shown that it

increases ATP via glycolysis, improves symptoms and cardiac function. [262] In contrast, ß -blockers improve PCr/ATP [256] and clinical outcomes in HFrEF [263], whereas SGLT2i improve clinical outcomes [264, 265] without any change in cardiac energetics [260].

4.1.3.1 Trimetazidine

Trimetazidine was first described 50 years ago [266], and its effects on cardiac metabolism have since been studied across various cardiovascular diseases. It was initially studied in the context of ischaemic heart disease [261], where it improved exercise tolerance [267]. In 2003, a randomized controlled trial [253] showed improved LVEF and lower glucose levels in patients with diabetes and ischaemic cardiomyopathy, findings replicated in a larger study in 2017 [268]. Trimetazidine has also been studied in patients with ischaemic [267] and non-ischaemic heart failure [269], improving exercise tolerance [267, 270, 271], ejection fraction [269, 270], insulin sensitivity [269], and PCr/ATP ratio [271]. However, assessment of tolerability (trimetazidine-induced parkinsonism) [272], mechanistic clarity [273] and beneficial effects on clinical outcomes in large randomized controlled trials are lacking. It may currently only be considered in the treatment of angina in selected cases, for example in the presence of diabetes [274].

4.1.3.2 Ninerafaxstat

In this context, Ninerafaxstat ($C_{22}H_{29}N_3O_5$) was designed by Dr. Andrew Levin and marketed through IMBRIA Pharmaceuticals Inc (US) from 2017 with the aim to partially inhibit fatty acid metabolism, counteract the undesirable consequences of increased myocardial fatty acid uptake and metabolism and to increase cardiac metabolic efficiency. [72]

Ninerafaxstat (IMB-1018972) is a pro-drug which undergoes hydrolysis to release nicotinic acid [73] and the active substance IMB-102 which is metabolised to either Trimetazidine (TMZ) [72] or carboxy-8814, a structural analogue to TMZ. (See **Figure 4.2**) Unpublished data in animal models

suggests that Ninerafaxstat is predominantly metabolised into carboxy-8814, which has superior efficacy to TMZ in the competitive inhibition of the mitochondrial Long-Chain 3-Ketoacyl Coenzyme A Thiolase (3-KAT) [275, 276], the last of the four enzymes of the β-oxidation pathway in the mitochondria [34]. The aim of the carboxy-8814 component of Ninerafaxstat is to shift cardiac substrate metabolism towards glucose oxidation and therefore increase ATP production per unit of oxygen consumed. [277]

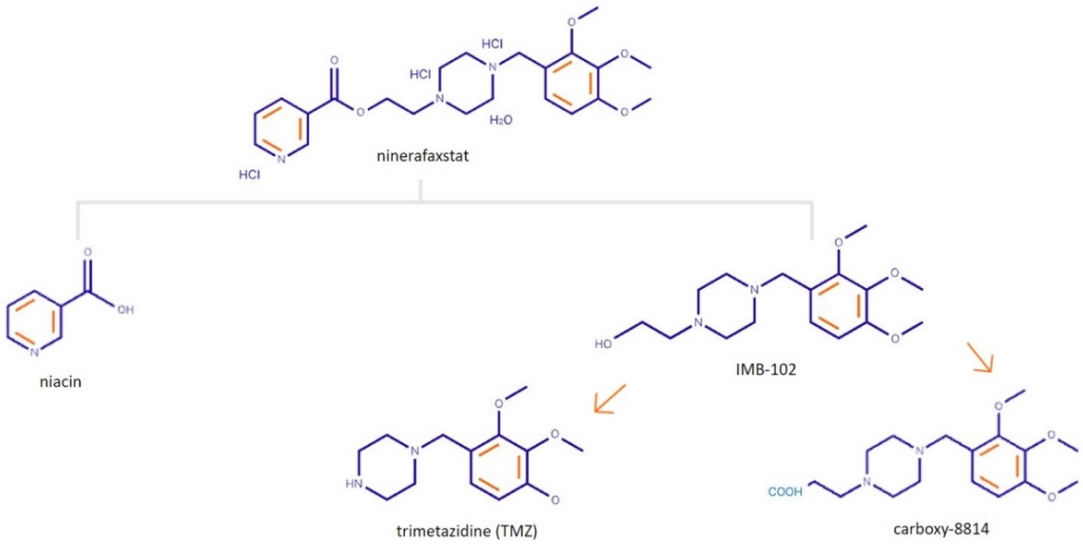

Figure 4.2 Chemical structure of Ninerafaxstat (provided by IMBRIA)

The second component of Ninerafaxstat is the systemically available, cell permeant NAD^+ precursor nicotinic acid/niacin. NAD^+ precursors are absorbed through diet and are converted into NAD^+ via three different pathways in the cytosol, nucleus and/or mitochondria. [278] NAD^+ is an essential molecule in mitochondrial health, energy production [279] [280], regulation of metabolic and aging pathways (via sirtuin enzymes) [281], and DNA repair via poly(ADP-ribose)polymerase (PARP) [282]. (See **Figure 4.3**) The pool of NAD^+ reduces with age, obesity and cardiovascular disease [283] and as, in contrast to other organs, in the heart the enzymes required for the de novo synthesis of NAD^+

are absent from the heart [284], NAD^+ supplementation is therefore a potential therapeutic target to modulate cardiac metabolism.

Animal models have shown that increasing the availability of nicotinic acid in the myocardium and therefore the pool of NAD^+, which is reduced in heart failure [75], may improve mitochondrial function, enhance glucose metabolism, reduced cardiac fibrosis [285], and may improve exercise tolerance [286]. In three different mouse models of HFpEF, supplementation with the NAD^+ precursor, nicotinamide, improved diastolic function, hypertension and cardiometabolic syndrome. [287]

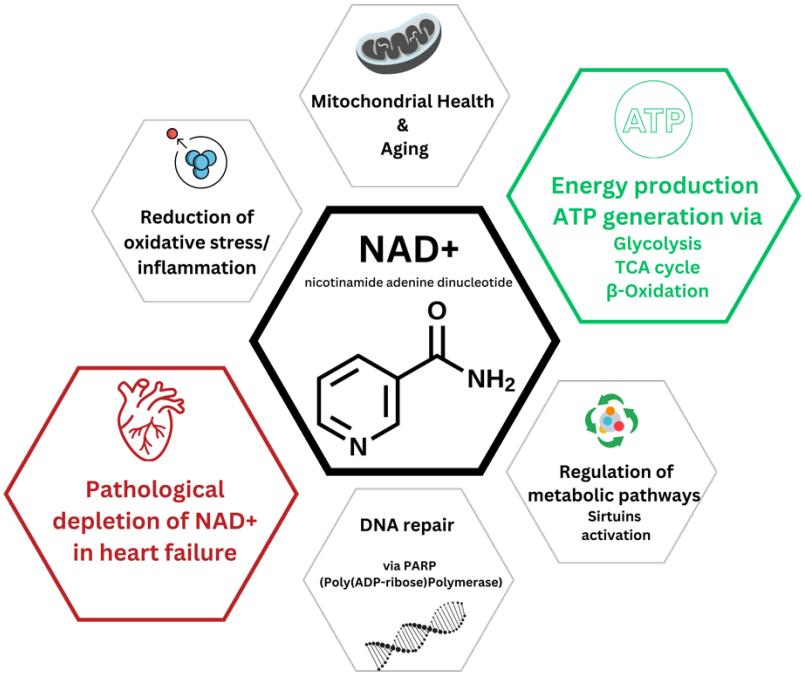

Figure 4.3 Graphical Overview of NAD^+ in Metabolism

In humans supplementation of NAD^+ precursors was found to reduce levels of FFA with subsequent beneficial effects on the cholesterol profile and also increased blood glucose levels [288], which is likely enhanced glucose oxidation. [289] In addition, niacin has been shown to increase expression of GLUT4, further increasing glucose uptake [290] resulting in improved insulin sensitivity in

overweight and obesity [291]. In a prospective population-based study assessing those with a food intake associated with an average intake of 27-29 mg of NAD^+ precursors, were seen to have a reduction in blood pressure, a lower risk of all cause death predominantly due to a reduction in cardiac mortality. [287] A small placebo controlled randomised trial of 1000 mg twice daily of the NAD^+ precursor nicotinamide ribose, showed improvement in NAD^+ levels and mitochondrial function which did not relate to changes in physical and cardiac function in HFrEF. [292]

Ninerafaxstat (200mg MR orally twice daily), contains approximately 30% of niacin, equating to around 60 mg of niacin. Due to its greater bio-availability of the two compounds carboxy-8814 and TMZ versus TMZ alone [293] and the addition of NAD^+ precursors as described above it is expected to be superior to TMZ alone in enhancing glucose oxidation and improve energy production through the replenishment of the cellular NAD^+ pool.

Ninerafaxstat has been studied in patients with angina [294], non-obstructive hypertrophic cardiomyopathy (HCM) [254], and diabetic cardiomyopathy [295]. While it showed no clinical benefit in patients with angina, it did demonstrate the mechanistic effect of increased glucose utilisation in this cohort. [294] In patients with non-obstructed HCM, it significantly improved ventilatory efficiency and symptoms. [254]

To evaluate the safety and efficacy of Ninerafaxstat in cardiometabolic HFpEF, it was initially studied in obesity and diabetes (IMPROVE DiCE) [74] with the aim to modulate substrate metabolism towards glucose metabolism (TMZ) and increase cardiac metabolic efficiency by increasing the synthesis of NAD^+ to improve mitochondrial function [75]. In this mechanistic trial [74] it highlighted its potential to improve myocardial energetics by modulation of substrate utilisation and augmentation of PDH flux resulting in improved diastolic function. In addition, plasma metabolomic analysis in this study showed a significant increase in downstream

metabolites of niacin, an active moiety of Ninerafaxstat, linking the results to the mechanistic action of Ninerafaxstat.

The “IMPROVE-DiCE-2 Study” described in this chapter explores the effect of Ninerafaxstat on cardiac energetics in obesity, T2DM and HFpEF aiming to confirm the mechanistic effect seen previously in patients with obesity, diabetes and HFpEF.

4.1.4 Aims of the DICE Study

Obesity and T2DM are linked with structural, functional and metabolic myocardial alteration which may progress to HF. Despite the global increase in obesity, T2DM and subsequent HFpEF, limited treatment options are available and knowledge about effective treatments targeting cardiometabolic alterations are limited. After the mechanistic effects of Ninerafaxstat in obesity and T2DM have been assessed, IMPROVE-DICE-2 aimed to assess the impact of Ninerafaxstat in obesity, T2DM and HFpEF. MRS and MRI techniques, alongside clinical parameters, were used to assess:

1. Myocardial energetics (PCr/ATP)
2. Cardiac structure and systolic and diastolic function
3. Clinical outcomes including exercise capacity and symptoms

By partially inhibiting FAO with the aim to increase glucose oxidation, the study aimed to showcase the ability of Ninerafaxstat to modulate substrate utilisation and downstream metabolism to improve function and exercise capacity in obesity, diabetes and HFpEF.

4.2 Methods

4.2.1 Ethical Considerations

The IMPROVE-DiCE-2 Study "DICE" was a single-centre, open-label, mechanistic phase 2a, pharmacodynamic study designed to assess the effects of 200mg Ninerafaxstat twice a day (BID) on myocardial energetics, metabolism and function in patients with HFpEF, obesity and T2DM. This thesis encompasses research that was reviewed and received favourable approval by the London – Hampstead Research Ethics Committee (REC reference: 20/LO/1120, EudraCT No.: 2020-003280-26, IRAS ID: 287405). Complementary regulatory endorsement was received by the Medicines and Healthcare products Regulatory Agency for the research involving the Investigational Medicinal Products (IMP) for DICE. Additionally, authorization was granted by the Healthcare Research Authority and OUH to conduct the investigations. Adherence to institutional guidelines and the principles laid out in the Declaration of Helsinki was maintained throughout the research process. Written informed consent was obtained from all research participants prior to inclusion. Data collection occurred anonymously, and was safeguarded on a secure, compliant server. Confidential written materials were stored securely within locked filling cabinets at the research site.

4.2.2 Study Participants

Patients with HFpEF (EF ≥ 50%), overweight or obese (BMI ≥ 27.5 kg/m2) with pre-diabetes or T2DM (HbA1c ≥ 6,0%) were recruited from cardiology clinics in 3 trusts: Oxford University Hospitals NHS Foundation Trust, Buckinghamshire Healthcare NHS trust in Wycombe, and The Great Western Hospital in Swindon between January 2023 and March 2024. Patients who met eligibility criteria were sent an invitation to participate alongside an information leaflet.

4.2.3 Inclusion Criteria

- Provision of written informed consent before any screening procedures
- Male or female aged between 18 and 80 years at screening
- Agreement to adequate contraception requirements as follows:
    - Women of childbearing potential (WOCBP) must have a negative serum pregnancy test at screening and a negative pregnancy test (serum or urine) on the day of baseline pre-dosing;
    - WOCBP must agree to use dual methods of contraception, including 1 highly effective and 1 effective method of contraception, from the day of first dosing until 3 months after the last administration of test product; and
    - Male patients must use an effective barrier method of contraception if sexually active with a WOCBP, from the day of first dosing until 3 months after the last administration of test product
    - Must agree not to donate sperm or ova from the day of first dosing until 3 months after last dosing.
    - Women not of childbearing potential must be either surgically sterile (hysterectomy, bilateral tubal ligation, salpingectomy, and/or bilateral oophorectomy at least 26 weeks before screening) or postmenopausal, defined as spontaneous amenorrhea for at least 2 years with follicle-stimulating hormone (FSH) in the postmenopausal range at screening.
- Must be able and willing to comply with all study procedures and requirements.
- Diagnosis of pre-diabetes or T2DM (HbA1c ≥6.0%, 43 mmol/mol)
- Elevated BMI defined as ≥27.5 kg/m^2
- Preserved LVEF defined as EF ≥50%
- If on oral hypoglycaemic (anti-diabetic) therapy, no change in therapy over the past 3 months.

- Be ambulant and have clinically stable symptomatic (NYHA functional class II to III) HF.
- Diagnosis of HFpEF by the Heart Failure Association HFA-PEFF diagnostic algorithm or by obtaining a score of ≥6 in the H_2FPEF scoring system.

4.2.4 Exclusion criteria

- BMI >45 kg/m^2
- Uncontrolled hypertension (resting blood pressure >180/90 mmHg) at screening
- Standard contraindication(s) to MR scanning
- More than moderate valvular heart disease (patients with severe tricuspid regurgitation due to HFpEF were potentially eligible)
- History of sustained ventricular tachycardia or cardiac arrest
- Arrhythmia with an uncontrolled ventricular response >110 bpm
- Active exertional angina or intermittent claudication
- Significant obstructive coronary artery disease
- Any of the following within 6 months before screening: History of stroke, transient ischaemic attack, acute coronary syndrome, myocardial infarction, peripheral vascular disease, hospitalisation for HF, or any arterial revascularisation procedure (including coronary artery bypass grafting)
- Presence of indwelling cardiac device (pacemaker, cardiac resynchronisation therapy, and/or implantable cardioverter defibrillator)
- Inability to exercise
- Known significant primary lung disease or primary pulmonary hypertension, or uncontrolled obstructive sleep apnoea
- Significant hepatic impairment defined as total bilirubin and/or ALT and/or aspartate aminotransferase (AST) >2 upper limit of normal (ULN)

- Moderate or severe renal impairment defined as estimated glomerular filtration rate (eGFR) <30 mL/min/1.73 m^2

4.2.5 Study Protocol

Patients expressing interest were invited for a screening visit (Visit 1) at the Oxford Centre for Clinical Magnetic Resonance Research, following informed consent. (See **Table 4.2**) The screening visit included eligibility assessment (see **4.2.3.,4.2.4**.), demographics, medical history, medications, 12-lead electrocardiogram (ECG), vital signs, height, weight, physical examination, and laboratory testing (see **Table 4.3**). Eligible participants proceeded to Visit 2 (imaging visit pre-treatment) for enrolment to 12 weeks treatment with Ninerafaxstat 200 mg twice daily (BD). Mid-treatment, symptom assessment occurred at Visit 3, followed by post-treatment imaging Visit 4, and a final safety follow up at Visit 5 four weeks later. (See **Table 4.2**.)

Open-Label Dosing: All Patients Treated with Ninerafaxstat at 200 mg BD for 12 Weeks.					
	Screening	**Enrolment**		**End of Treatment (EOT)**	**End of Study (EOS)**
	Visit 1	**Visit 2** Imaging visit pre-treatment	**Visit 3** Non-imaging visit	**Visit 4** Imaging visit post-treatment	**Visit 5** Non-imaging visit
Pre-diabetes or T2DM (HbA1c ≥ 43 mmol/mol) **Overweight/ obesity** (≥27.5 kg/m^2) **HFpEF** (LVEF >50%) **NYHA II-III**	• Consent • Clinical Assessment • Laboratory Tests • Echo	• ^{31}P-MRS at Rest • Hepatic Steatosis • Visceral Fat • Aortic Distensibility • Cardiac ^{1}H-MRS • RT CINE at Rest/Exercise • Lung Water at Rest/Exercise • Blood Sampling • Body Composition • 6-MWT • KCCQ, PGI-C, PGI-S	Assessment of Symptoms & Adverse Events	• ^{31}P-MRS at Rest • Hepatic Steatosis • Visceral Fat • Aortic Distensibility • Cardiac ^{1}H-MRS • RT CINE at Rest/Exercise • Lung Water at Rest/Exercise • Blood Sampling • Body Composition • 6-MWT • KCCQ, PGI-C, PGI-S	• Biomarkers • KCCQ, PGI-C, PGI-S

Table 4.2 DICE Study visit flow

T2DM= Type 2 Diabetes; BMI= Body Mass Index: LVEF= Left ventricular ejection fraction; HFpEF= Heart failure with preserved ejection fraction; Echo= Echocardiogram; ^{31}P-MRS= ^{31}Phosphorus Magnetic Resonance Spectroscopy, ^{1}H-MRS= Proton Magnetic Resonance Spectroscopy; RT= real time; 6-MWT= 6-minute walk test; KCCQ= Kansas City Cardiomyopathy Questionary; PGI-C= patient global impression score of change; PGI-S= patient global impression score of symptoms

The following sections will describe the elements of the study visits which have not been described in detail in **Chapter 2** in the general methods section and are specific to this study which includes blood sampling, bioimpedance analysis, dosage and administration of Ninerafaxstat. For an overview of the study protocol for the imaging visit see **Figure 4.4**.

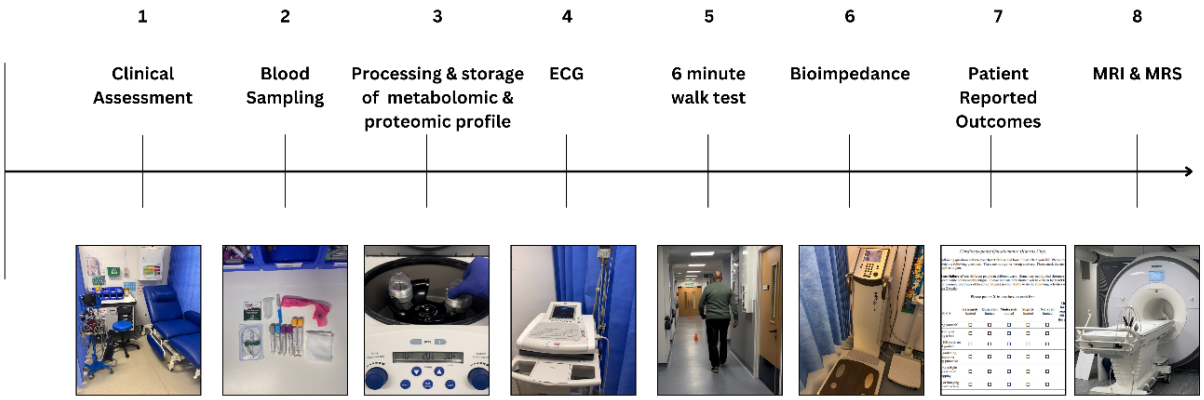

Figure 4.4 DICE Imaging visit timeline

A DICE imaging visit starts with (1) clinical assessment which includes (2) blood sampling, (3) metabolomic & proteomic profiling, and (4) an Electrocardiogram (ECG). Exercise capacity is assessment with a (5) 6-minute walk test (6-MWT); body composition is measured by (6) Bioimpedance scales; patient's symptoms are evaluated by health questionary; the visit is concluded with a comprehensive (8) Magnetic Resonance Imaging and Spectroscopy assessment.

4.2.6 Primary Endpoint

The primary efficacy endpoint was:

- Change in cardiac PCr/ATP ratio at rest measured by ^{31}P-MRS at baseline and at End of Treatment (EoT).

4.2.7 Secondary Efficacy Endpoints

Secondary efficacy endpoints, measured as absolute (±relative) change from baseline to EOT where appropriate, include the following measurements with 200 mg BD of Ninerafaxstat for 12 weeks.

CMR-derived cardiac structural and functional measures:

- exercise stress-inducible change derived from LV volume-time curves, including, peak LV diastolic filling rate normalised to cavity size (end-diastolic volume, EDV)
- Left atrial (LA) / right atrial (RA) size and function
- LV and RV responses to exercise (stress and change/augmentation with exercise stress) assessed by LV/RV stroke volume (LVSV/RVSV, mls), ejection fraction (EF, %) and cardiac output (CO, L/min).
- LV mechanics by CMR, including global longitudinal
- Myocardial steatosis by ^{1}H-MRS

TTE-derived cardiac functional measures:

- Diastolic function evaluated by medial, lateral e' velocity, E-wave and A-wave velocity, E/A ratio, E/e' ratio using mitral inflow Doppler and Tissue Doppler Imaging (TDI).
- Peak tricuspid regurgitation velocity (where jet present)

4.2.8 Explorative Efficacy Endpoints

Exploratory efficacy endpoints, measured as absolute (±relative) change from baseline to EOT including

- Body weight
- Peripheral blood biomarkers:

    - Fasting plasma insulin, fasting blood glucose, HbA1c, lipid profile (total cholesterol, high density lipoprotein cholesterol, low density lipoprotein cholesterol, and triglycerides) and free fatty acids
    - Plasma metabolomic profile, including analysis of acylcarnitines as a proxy for fatty acid ß-oxidation
    - Cardiometabolic biomarkers including, high sensitivity Troponin (hs-cTn), NT-proBNP, UACR, high sensitivity C-reactive protein, circulating uric acid/urate, ketone bodies
- Exploratory proteomic analysis
- Correlation analysis of PK measures (plasma concentration of Ninerafaxstat and its major metabolites, IMB-1028814, and trimetazidine) and study endpoints
- Exercise stress-inducible pulmonary congestion (both absolute and stress-inducible change from rest) measured by pulmonary proton density (lung water) imaging
- Additional MRI/MRS-derived measures:
    - Hepatic steatosis
    - Abdominal visceral fat volume
    - Aortic distensibility (at the ascending aorta and the abdominal aorta)
- PROs
    - Kansas City Cardiomyopathy Questionary (KCCQ-23); including total symptom score (KCCQ-TSS), clinical summary score (KCCQ-CSS), and overall summary score (KCCQ-OSS)
    - Patient Global Impression of change (PGI-C) and severity (PGI-S) scores
    - New York Heart Association (NYHA) functional class assessment
- 6-minute walk distance (6-MWD) assessed by 6-minute walk test (6-MWT)
    - Borg effort and dyspnoea scores during 6MWT
- Body composition by bioimpedance analysis

4.2.9 Safety Endpoints

The safety of Ninerafaxstat was assessed from the time of informed consent until the end of the safety follow-up period. All safety endpoints have been summarised descriptively. The safety endpoints were secondary endpoints and include adverse events (AEs), serious AEs, vital signs, clinical laboratory tests, physical examinations, and 12-lead ECGs.

4.2.10 Blood Sampling

Venous blood samples were collected at the screening visit, with clinical chemistry and haematology assessed at all visits, and coagulation tests conducted at screening, EOT, and EOS. In addition to blood sampling detailed in Chapter 2, the metabolomic and proteomic profile was analysed, and a pharmacokinetics sample was taken at EOT. The blood samples were pre-processed in OCMR by centrifugation (3,000rpm, 10 mins, room temperature) and stored at -80 °C. At study completion, frozen samples were shipped to Pharmaceutical Research Associates Group B.V., ICON Bioanalytical Laboratory, Assen, Netherlands for analysis. For an overview of laboratory samples analysed in the DICE study. (see **Table 4.3**)

Haematology

- Haemoglobin, Haematocrit
- Reticulocyte count, Red blood cell count (RBC)
- White Blood cells and differential
- Platelet count

Clinical chemistry

- Electrolytes (Sodium, Potassium, Chloride, Calcium, Inorganic phosphate)
- Creatinine (estimated glomerular filtration rate, eGFR), Bicarbonate, Uric acid, Albumin
- , Amylase, GGT (gamma-glutamyl transferase)
- Alkaline phosphatase
- ALT (alanine transaminase)
- AST (aspartate transaminase)
- Total bilirubin, Total Protein
- FSH (Follicle-stimulating hormone)

Cardiometabolic biomarkers

- Hs Troponin I, NTproBNP, Ketone bodies
- Creatine kinase (CK), C-reactive protein (CRP)
- Glycated haemoglobin A_{1c} (HBA_{1c})
- Fasting blood glucose and insulin

Lipids

- Fasting lipid profile: Total Cholesterol, high density lipoprotein (HDL) cholesterol, Calculated LDL cholesterol, Triglycerides), Free-fatty acids

Coagulation

- aPTT (activated partial thromboplastin time)
- PT (Prothrombin time)
- INR (International normalised ratio)

Urine

- Urinary albumin-creatinine ratio

Serum proteomic analysis

- Exploratory analysis by multiplex assay

Serum metabolomic analysis

- 2,3-phosphoglycerate, Aconitate, Adenosine
- Fructose1,6-bisphosphate
- Adenosine monophosphate (AMP)
- α-ketobutyrate, α-ketoglutarate
- Dimethylglycine (DMG)
- g-amino butyric acid (GABA) Glucose, Isocitrate, Inosine, Bisphosphoglycerate
- Lactate, Malate, Succinate, Pyruvate, Citrate, S-Adenosylhomocystein (SAH)

Table 4.3 DICE List of Laboratory tests performed

4.2.11 Bioimpedance Analysis

Body composition was assessed noninvasively using bioimpedance analysis at enrolment (V2) and at end of treatment (EOT, V4). Specific bioimpedance scales (see **Figure 4.5**) applied a low-level electrical current and measured resistance (impedance) to estimate fat mass (FM) and fat-free mass (FFM). FM represents water-free body components, while FFM includes skeletal muscle, internal organs. [296, 297]

Figure 4.5 DICE Bioimpedance scale

4.2.12 Cardiac MR Protocols and Analysis

In addition to the CMR studies described in **Chapter 2,** the following MRI assessments were performed: (see **Figure 4.6**)

- Pulmonary proton density imaging at rest and submaximal physiological exercise
- Hepatic steatosis
- Abdominal adiposity to assess fat volume
- Aortic distensibility

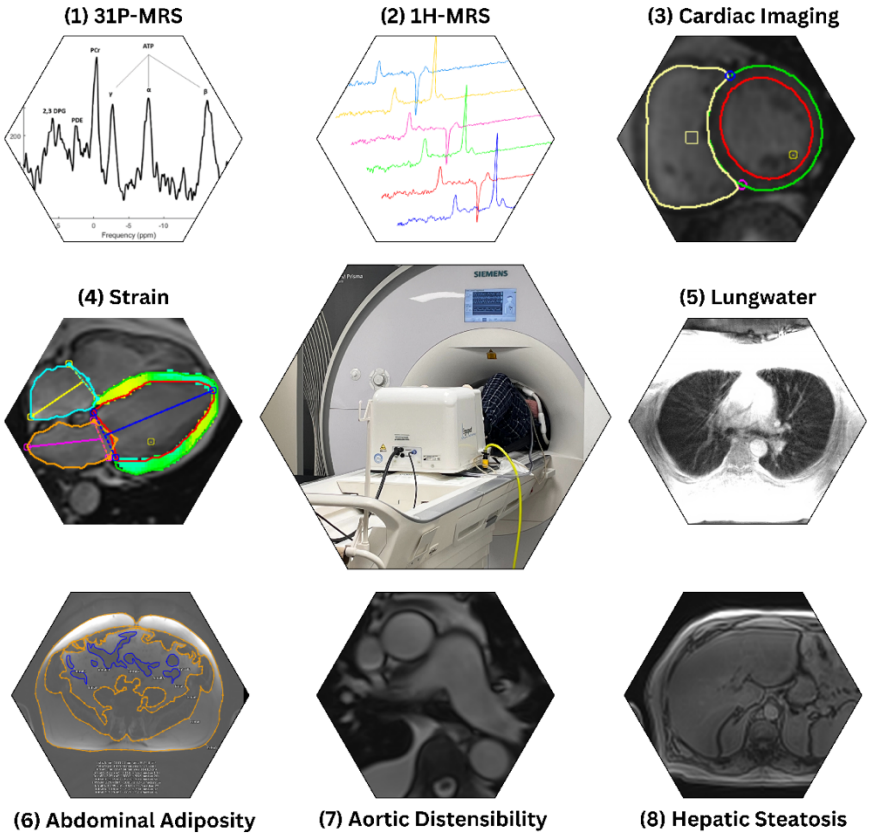

Figure 4.6 DICE Study MR protocol overview

As part of a DICE imaging visit the following magnetic resonance assessments were performed: (1) ^{31}P-MRS (31-phophorus magnetic resonance spectroscopy); (2) ^{1}H-MRS (proton magnetic resonance spectroscopy); (3) Cardiac Imaging to assess cardiac volumes and function; (4) Myocardial Strain; (5) Pulmonary Proton Density Imaging to assess lung water; (6) Abdominal Adiposity assessment; (7) Aortic Distensibility; (8) Hepatic Steatosis.

4.2.12.1 Cardiac Volumes and Function During Exercise Stress

Exercise stress CMR was performed with a CMR-compatible stepping ergometer (see **Figure 4.7A**) in the supine position (see **Figure 4.7B**) (Cardio Step Module, Ergospect GmbH, Innsbruck, Austria).

A Cardio Step Module, Ergospect

B MRI Exercise assessment

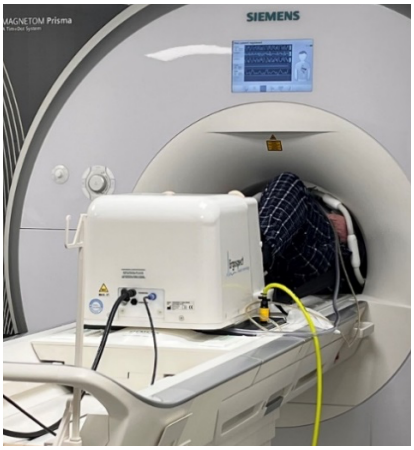

Figure 4.7 DICE Cardio Step Module

(A) Cardio Step Module; (B) Magnetic Resonance Imaging (MRI) assessment during exercise

The exercise protocol comprised a stepwise increase in workload from 1 min without resistance followed by 5 mins at a workload of 30 Watts (W). (See **Figure 4.8**) Whole-heart RT cine imaging was acquired at 5 mins of exercise. Proton density imaging for lung water assessment was performed after 6 minutes of exercise at rest.

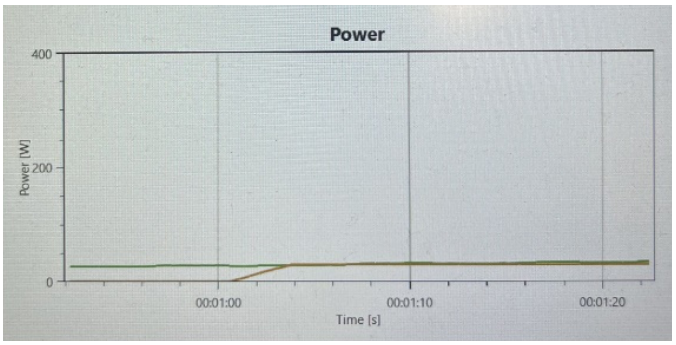

Figure 4.8 DICE Ergometer power output over time

After one minute of exercise without resistance (green line), the Cardio Step power was increased to 30 Watts (orange line).

4.2.12.2 Hepatic Steatosis with Proton Density Fat Fraction

Image acquisition was performed with a 30-channel surface coil (Siemens Healthineers, Erlangen, Germany) with the participant in the supine position. A multi-echo Dixon technique [298] was used to assess hepatic proton density fat fraction (PDFF). Six different echo times (TE) were used to separate fat and water signals. [299] This generated a non-fat suppressed image (see **Figure 4.9A**) and a fat-supressed image (see **Figure 4.9B**), which was analysed with MicroDicom Viewer 2024.2(64-bit).

Proton density fat fraction (PDFF) was calculated by the ratio of density of mobile protons from fat and the total density of protons from mobile fat and water, [300] displayed as percentage of fat within tissue. Three regions of interest (ROI) were drawn in the non-fat suppressed (see **Figure 4.9A**) and in the fat suppressed images (see **Figure 4.9B**) at the level of the main portal vein in a homogenous part of the liver (right anterior, right posterior, and left medial), to derive mean and standard deviation of fat fraction. [301]

The average fat fraction in % and the standard deviation was documented. Histological studies define the upper limit of normal liver fat content as 5% which equates to 6-6.4% assessed with PDFF. [302] The difference occurs due to the fact that not all tissue can be identified [300] with PDFF and is therefore not considered in the analysis.

A Non-fat suppressed image

B Fat Suppressed Image

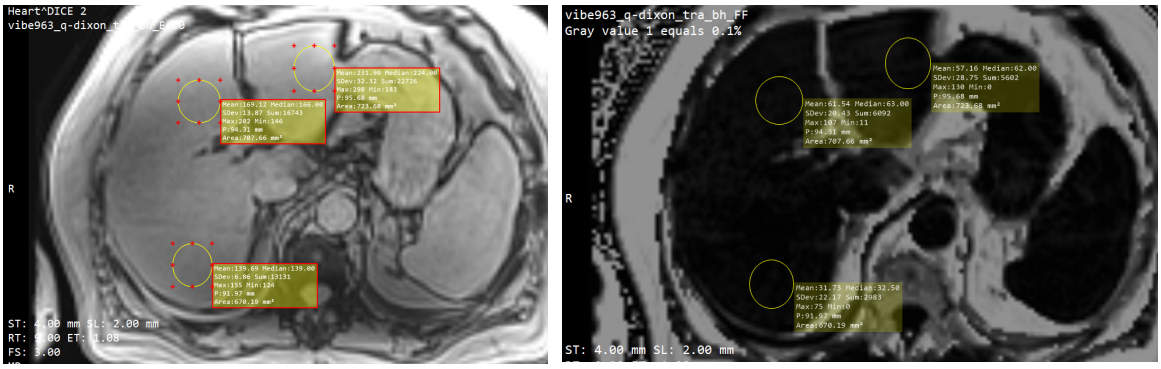

Figure 4.9 DICE Multi-Echo Dixon Image to assess hepatic steatosis

Fat and water signals in each voxel are separated to generate (A) non-fat suppressed and (B) fat suppressed image. In MicroDicom Viewer three regions of interest (yellow circles) are drawn at the level of the main portal vein to establish average fat fraction in % and the standard deviation (yellow box)

4.2.12.3 Quantification of the Visceral and Subcutaneous Fat

Five 8 mm axial T_1-weighted slices (see **Figure 4.10A**) were acquired at the level of Lumbar disc 4 and 5 (see **Figure 4.10B**) to quantify subcutaneous and visceral fat (see **Figure 4.10D**).[303] Image analysis was performed at the level of L4/L5 [304] using CVI42 (see **Figure 4.10C**) with a line drawn along the abdominal wall to separate intra and extra abdominal compartments. Visceral and subcutaneous fat areas were documented in cm^2. Adipose tissue was categorized into the following categories:

(1) Intra-abdominal content

(2) Visceral adiposity (VA)

(3) Abdominal circumference

(4) Inner margin of subcutaneous fat

(5) Subcutaneous adiposity (SA)

(6) Total fat area (VA + SA)

A Coronal view

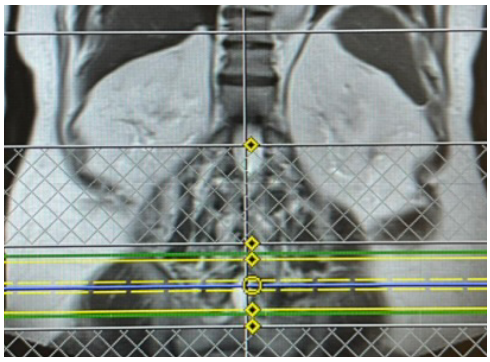

B Sagittal view

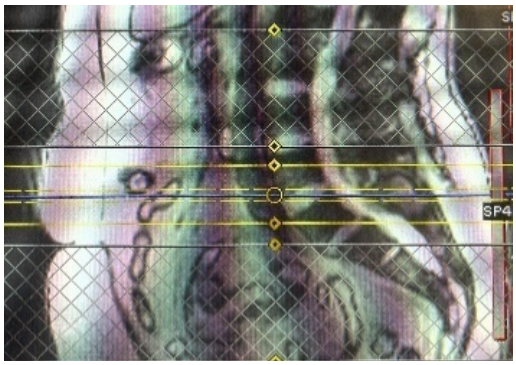

C Axial view

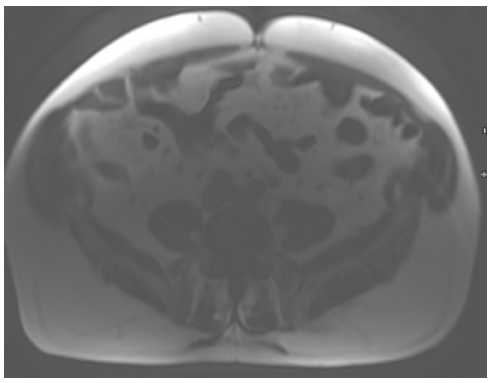

D Categorisation of adipose tissue

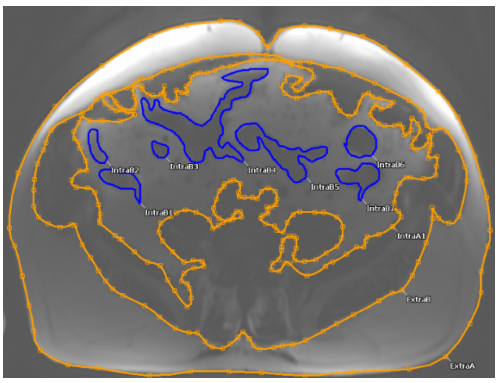

Figure 4.10 DICE T1-weighted abdominal MRI for the quantification of adiposity

(A) Five horizontal slices were acquired at (B) the level of Lumbar disc 4 and 5 to generate (C) an axial image to quantification subcutaneous and visceral fat by (D) drawing regions of interest in CVI42.

4.2.12.4 Aortic Distensibility

Age [305], hypertension, T2DM and HFpEF [306] result in increased vascular stiffness [307] which can be assessed non-invasively with pulse wave velocity (PWV) [308], the distance between two measurement points divided by the time required for blood to travel this distance. [309] Aortic distensibility refers to the relative change in the cross-sectional area of the aorta during systole divided by the pulse pressure. [309] An axial SSFP sequence was performed at the level of the pulmonary trunk to plan the assessment of the proximal ascending (see **Figure 4.11A**) and distal ascending aorta (15 cm distal to the ascending aortic measurement) (see **Figure 4.11B**). In parallel,

PWV analysis was performed via a blood pressure cuff connected to a Vicorder to assess systolic (P_{Max}) and diastolic blood (P_{Min}) pressure, pulse wave form to generate aortic pressure graph reflective of central blood pressure. (see **Figure 4.11D**)

Image analysis was performed via semi-automated segmentation of aortic cine images as previously prescribed [310] using a locally modified Matlab code ('Segment_vessel') (see **Figure 4.11C**). Minimal aortic area (A_{Min}) and maximal aortic area (A_{Max}) were defined for the proximal ascending (see **Figure 4.11A**) and descending aorta (see **Figure 4.11B**) to generated aortic area-time curves (see **Figure 4.11D**). Ascending and descending aortic distensibility was calculated by the following formula: [311] Aortic distensibility ($10^{-3}mmHg^{-1}$= (A_{Max} - A_{Min})/((P_{Max} - P_{Min})x A_{Min})x10^{-3}. Normal values vary with age and gender between 8.9±3.6 $10^{-3}mmHg^{-1}$at the level of the ascending aorta and 8.3±3 $10^{-3}mmHg^{-1}$at the level of descending aorta. [311]

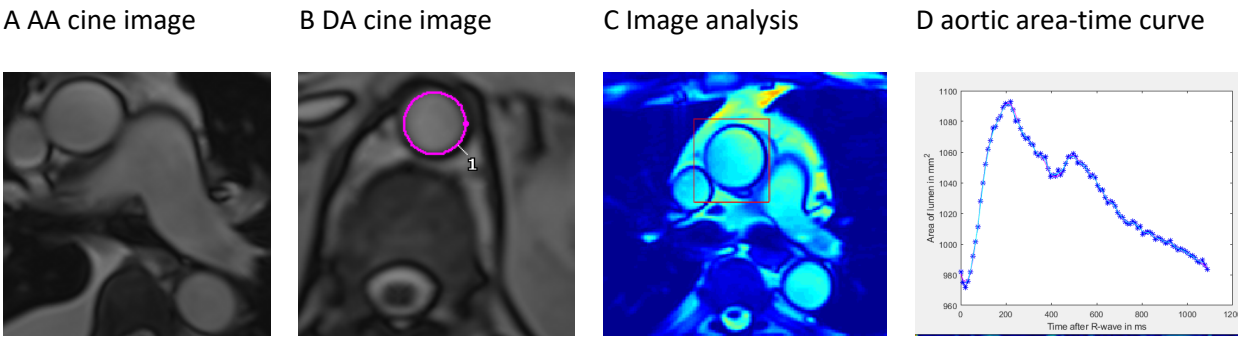

Figure 4.11 DICE Aortic distensibility acquisition and analysis

Cine imaging of the (A) ascending aorta (AA) was performed at the level of the pulmonary trunk and the (B) descending aorta (DA) 15 cm below the AA measurement. (C) Semi-automated Image analysis was performed with MATLAB to (D) generate an aortic area-time curve.

4.2.12.5 Pulmonary Proton Density Imaging at Rest and Exercise

Shortness of breath during exercise and decreased exercise tolerance are the hallmark signs of HFpEF, often termed subclinical pulmonary oedema. [312] A previous study linked increased lung water and filling pressure to patients symptoms. [313] This study used pulmonary proton density

imaging at rest and after 6-minutes of sub-maximal (30W) exercise with an MRI-compatible cardio stepper (Cardio Step, Ergospect GmbH, Innsbruck, Austria. (See **Figure 4.12**) Five axial slices were acquired: one at the pulmonary artery (PA) level, with two slices above and two below to account for movement. Images were post processed by Prof. Jack Miller. (See **Figure 4.12A**) The Fiji Image processing package was used to define the analysis threshold differentiating lung tissue from surrounding tissue, at the level of the right atrium. (See **Figure 4.12B**) Grey values histograms defined the lung tissue threshold (usually between 5000-20000). (See **Figure 4.12C**) A semi-automated analysis by 3DSlicer was used to trace the borders of the lungs (see **Figure 4.12D**) to providing an arbitrary unit (AU) of lung water within the selected area. (See **Figure 4.12E**)

A Post processed image

B Threshold analysis in Fiji

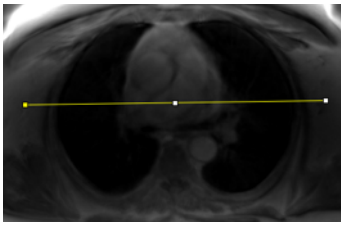

C Histogram of grey values

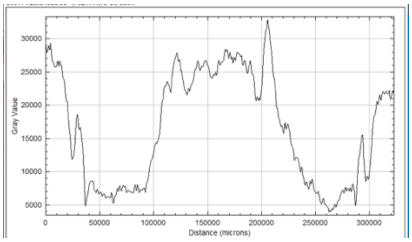

D Lung Segmentation

E Lung tissue above the threshold

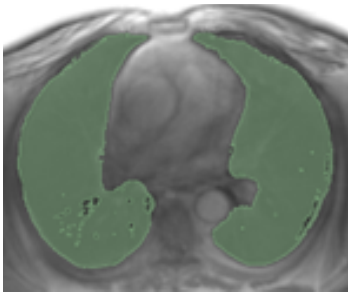

Figure 4.12 DICE Lung water analysis

(A) Post-processed axial proton density image; (B) Threshold analysis of along cross section of lung (yellow line); (C) Histogram of grey values to assess threshold for analysis; (D) Lung segmentation to define area of interest (yellow line); (E) threshold for tissue included in the lung water analysis (green area)

4.2.13 Dosage and Administration of Ninerafaxstat

Ninerafaxstat (200mg modified-release tablet) was designed to release the active ingredient over a period of 8 hours. It was self-administered twice daily with food or water, starting on Day 1 after baseline MRI (Visit 2) Participants were given a Dosing Diary to record the date, time, amount of test product taken, and any further information (such as missed doses, etc.). Compliance was assessed by the study team by pill counting. Pharmacokinetic samples were taken at the follow up visit after approximately 83 days of dosing.

4.2.14 Statistics

Specific data describing the impact of Ninerafaxstat on measures of energy metabolism in patients with HFpEF, T2DM, obesity, are limited. However, based on the IMPROVE-DiCE 1 study [295] Ninerafaxstat in our centre we anticipated the effect size to be small (absolute change of around 0.2 in PCr/ATP). A power calculation defined the need for 25 participants to enable the observation of an absolute change of 0.2 in PCr/ATP with a power of 80% and an alpha of 0.05. Therefore, we aimed to recruit a maximum possible number of 25 participants. Considering the dropout rate, two additional participants were enrolled.

The completers population comprised all participants who fully completed Ninerafaxstat administration and all study assessments without premature discontinuation or with medication compliance <80%. The primary endpoint analysis was performed in patients with a valid PCr/ATP result available before and after intervention. Protocol violations were reviewed before the database lock.

Statistical analysis was performed with GraphPad Prism 10 and IBM SPSS Statistics 29.0.2.0. Normality of distribution was assessed using the Shapiro-Wilks test. For normally distributed data, parametric tests including the paired t-test were used, such as PCr/ATP pre-/post Ninerafaxstat. For data, which was not normally distributed a non-parametric test including the Wilcoxon signed rank test, instead of the paired t-test was performed. Values of $p < 0.05$ were considered statistically significant.

4.3 Results

4.3.1 Study Population and Baseline Characteristics

Approximately 6000 patients were assessed for eligibility, mostly at Oxford University Hospitals NHS Foundation Trust. Two Participant Identification Centres (PICs) contributed: Great Western Hospital (Swindon) led by Dr. Marco Spartera (4 participants); and Buckinghamshire Healthcare NHS Trust (Wycombe) led by Dr. Mayooran Shanmuganathan (2 participants). Of 53 patients screened, 26 were enrolled after Visit 2. (see **Figure 4.13**) One withdrew at Visit 2 due to claustrophobia. Three female participants (age 73-76 years) experienced gastrointestinal side effects and did not complete Visit 4 and 5, leaving 23 who completed Visit 5. Two were excluded after the imaging visit due to medication non-compliance (<80%): one due to a rash, one due to missed doses. One had a severe adverse event unrelated to the study drug but continued treatment. No significant medication changes occurred during the study.

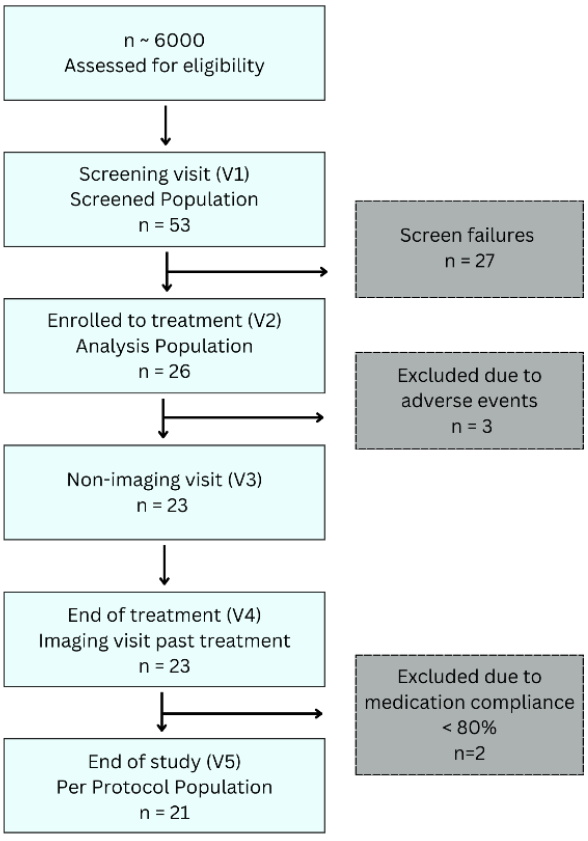

Figure 4.13 DICE Recruitment Flowchart

Baseline characteristics are shown in **Table 4.4** for the 21 participants in the per protocol set. The median age for participants was 71 years (60-79), 29% being female and 100% white. The mean weight was 104kg, mean BMI 35.2 kg/m^2. Mean baseline blood pressure was 137/77 mmHg with a resting heart rate of 70 bpm. For eligibility a H_2FPEF score >5 or an HFA-PEFF score ≥6 was required. Mean scores were 7±1.8 (H_2FPEF) and 5±1.3 (HFA-PEFF) indicating that not all participants met the diagnostic threshold in both scores.

Characteristic	Pre-Treatment (V2) N=21	Post-Treatment (V4) N=21	p-value
Anthropometrics, mean ±SD			
Age (years)	71±6		
Female n (% of total)	6 (29)		
White Race n (% of total)	21 (100)		
Weight (kg)	104	103	0.082
BMI (kg/m^2)	35.2	34.8	0.040
Systolic BP (mmHg)	137	138	0.719
Diastolic blood pressure (mmHg)	77	75	0.208
Resting HR (bpm)	70	69	0.787
NYHA classification	2±0.3	2±0.4	
NT-proBNP (ng/ml, [IQR])	538 [246,1222]	679 [211,1147]	0.56
Heart failure scores			
H2PEF score	7±1.8		
HFA-PEFF score	5±1.3		

Table 4.4 DICE Anthropometrics

BMI= Body mass index; BP=blood pressure; HR= heart rate; NYHA= New York Heart Association; NT-proBNP= N-terminal pro-B-type-natriuretic peptide, IQR= interquartile range,HFA-PEFF score= Heart Failure Association Pre-test assessment, Echocardiography and natriuretic peptide, Functional testing, and Final aetiology); SD= standard deviation; V2= Visit 2; V4= Visit 4

Diagnosis of diabetes was present in 16 participants, 12 of whom received glycaemic medication, with a mean HbA1c measured at screening of 52 (42-88). (see **Table 4.5**) In line with the risk factors of HFpEF, most patients were treated for hypertension (91%) and received statin therapy (91%). Atrial fibrillation (paroxysmal or permanent) was present in the majority (67%) and in all cases treated with anticoagulation. Sinus rhythm was present in 9 participants at enrolment.

Comorbidities (n)	**Baseline**
Pre-diabetes	5
Diabetes	16
- Mean HBA1c (mmol/L) at V1	52 (42-88)
Hypertension	19
Paroxysmal Atrial Fibrillation	4
Permanent Atrial Fibrillation	10
Ischaemic heart disease	4
Diagnosis of Chronic kidney disease	4
Osteoarthritis	5
Lung disease (sleep apnoea, pleural effusion,bronchitis)	4
Concomitant medications, (n)	
Glycaemic medication	12
- Metformin	9
- SGLT2i	3
- Insulin	3*
- Gliclazide	1
β-blocker	18
ACE-I, ARB	17
MRA	6
Ca^{2+}- Channel Blocker	5
Statin	19
Loop diuretic	14*
Anti-coagulation	15

Table 4.5 DICE Comorbidities and concomitant medication

HBA1c= Haemoglobin A1c; V1= Visit 1; SGLT2i= Sodium-Glucose cotransporter 2 inhibitor, ACE-I= Angiotensin-converting-enzyme inhibitor; ARB= Angiotensin II receptor blocker; MRA= Mineralocorticoid receptor antagonist

**Average daily dose 35 mg, one participant had a reduction from 40 to 20 mg furosemide, and a reduction in insulin*

4.3.2 Primary Outcome

4.3.2.1 PCr/ATP ratio

Administration of Ninerafaxstat led to a statistically significantly increased PCr/ATP (baseline mean 1.24±0.3 to EOT 1.39±0.24) with a mean increase of PCr/ATP of 0.15±0.25 (p = 0.02). (See **Figure 4.14**) Out of the 21 participants who were included in the analysis, one case was excluded due to insufficient data quality. Representative phosphorus spectra acquired before (see **Figure 4.15A**) and after (see **Figure 4.15B**) treatment are displayed in **Figure 4.15**.

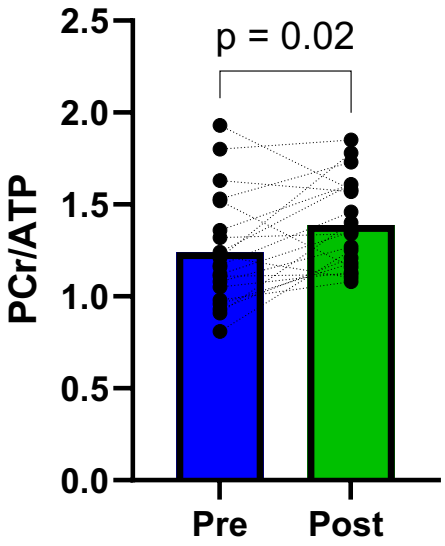

Figure 4.14 DICE PCr/ATP before and after treatment

A

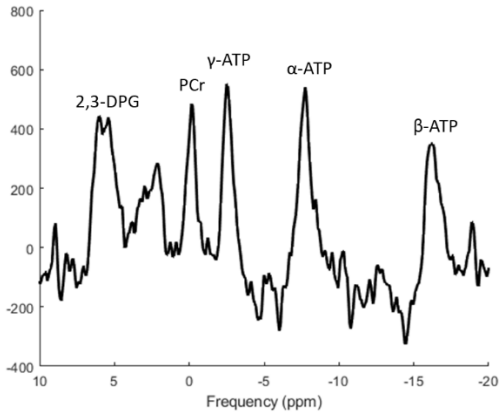

B

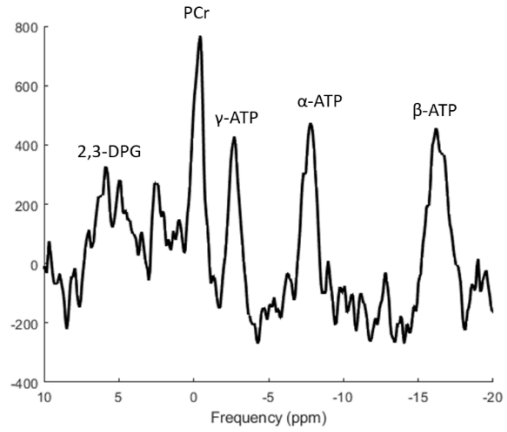

Figure 4.15 DICE Representative PCr/ATP spectrum before (A) and after (B) treatment

2,3-DPG= 2,3-diphosphoglycerate; PCr= Phosphocreatine; ATP= adenosine triphosphate; ppm= parts per million

4.3.3 Secondary Efficacy Endpoints

4.3.3.1 Cardiac Volumes and Function at Rest and Stress

Ninerafaxstat was not associated with any significant changes in LV volumes, LV function, LV mass. (See **Table 4.6, Figure 4.16**). There was no change in markers of systolic strain, or exercise stress-inducible change in peak LV diastolic filling rate. However, there was a significant improvement in LVSV augmentation and cardiac output during exercise after treatment. (See **Figure 4.17**) Treatment with Ninerafaxstat was associated with significant changes in RV morphology at rest versus stress pre and post treatment (see **Table 4.6, Figure 4.18**). There was a significant reduction in RVEDV at rest, RVSV at rest and stress, and a significant increase of RVEF post treatment. There was significant improvement in RVSV augmentation and cardiac output during exercise after treatment (see **Figure 4.19**).

	Rest			30W Exercise Stress		
Means	**Pre**	**Post**	**p-value**	**Pre**	**Post**	**p-value**
LVEDV (ml)	152±29	148±38	0.11	157±26	157±37	0.82
LVESV (ml)	62±17	58±21	0.08	61±18	57±20	0.22
LVSV (ml)	92±18	89±±20	0.18	96±17	101±24	0.56
LVEF (%)	61±7	61±7	0.87	61±8	64±8	0.24
LV mass (g)	128±24	131±29	0.64	122±29	126±24	0.48
LVCO (ml/min)	6309±1340	5886±1237	0.06	9431±3303	1047±4226	0.18
RVEDV	171±46	160±36	0.02*	185±41	182±41	0.41
RVESV (ml)	80±29	71±23	0.03*	88±29	77±26	0.02*
RVSV (ml)	92±19	89±20	0.21	97±18	105±26	0.31
RVEF (%)	55±7	56±8	0.42	53±8	59±8	0.03*
RVCO (ml/min)	6304±1333	5864±1259	0.14	9419±3064	10979±4634	0.10

Table 4.6 DICE Changes in cardiac volumes and function at resting and stress

LVEDV=left ventricular end-diastolic volumes; LVEF=left ventricular ejection fraction; LVESV=left ventricular end-systolic volume; LVSV=left ventricular stroke volume; RVEDV=right ventricular end-diastolic volume; RVEF=right ventricular ejection fraction; RVESV= right ventricular end-systolic volume; RVSV=right ventricular stroke volume; W= Watt

4.3.3.1.1 Left Ventricular Volume and Function

There was no change in LV volumes or function. Baseline mean rest LVEDV (see **Figure 4.16 column A**) was 152±46 ml and 148±38 ml post treatment (p= 0.11) and stress LVEDV was 157±26 ml pre and 157±37 ml post treatment. Baseline mean rest LVESV (see **Figure 4.16 column B**) was 62±17 ml and 58±21 ml post treatment (p= 0.08) and stress LVESV 61±18 ml pre and 57±20 ml post treatment (p=0.22). Baseline mean rest LVSV (see **Figure 4.16 column C**) was 92±18 ml and 89±20 ml post treatment (p=0.18). Baseline mean stress LVSV was 96±17 ml pre and 101±24 ml post treatment (p=0.56). There was no change in resting LVEF (see **Figure 4.16 column D**).

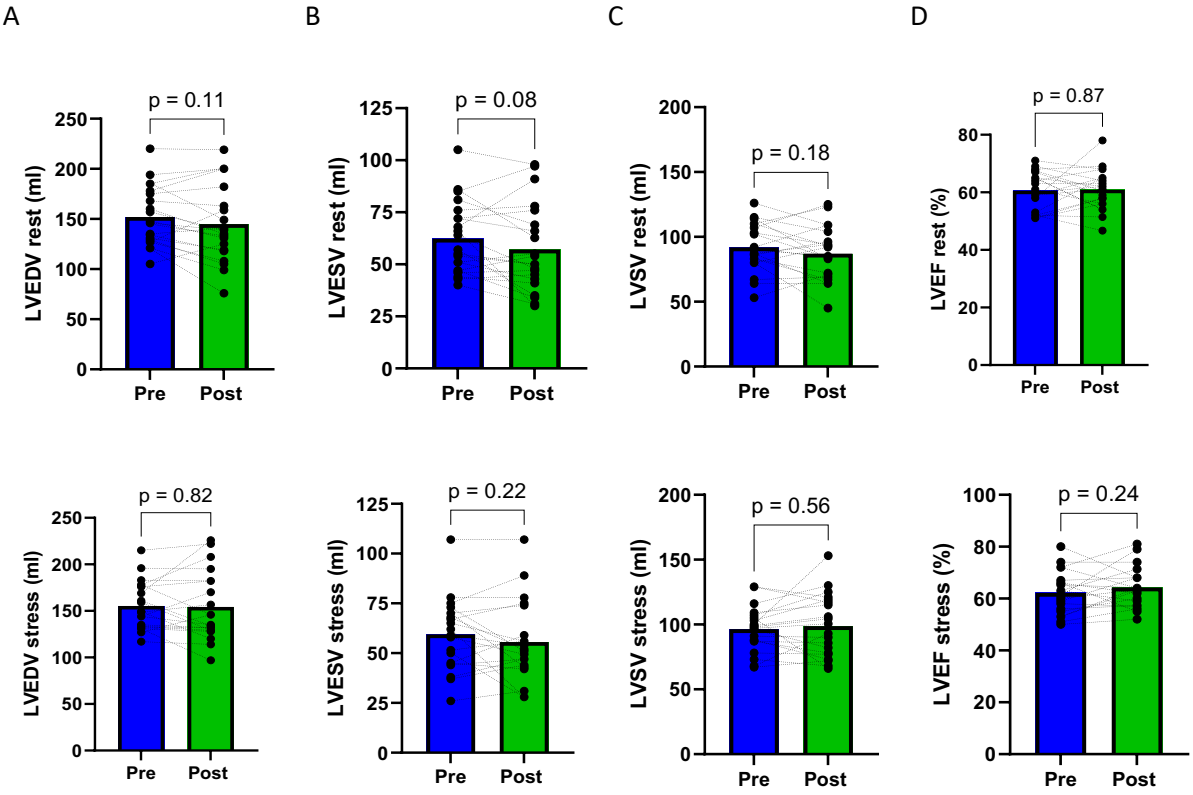

Figure 4.16 DICE Left ventricular volumes and function at rest and stress

There were no significant changes in left ventricular (LV) parameters at rest versus stress pre and post treatment. LVEDV=left ventricular end-diastolic volumes; LVESV=left ventricular end-systolic volume; LVSV=left ventricular stroke volume; LVEF=left ventricular ejection fraction.

4.3.3.1.2 Left Ventricular Exercise Induced Changes in Volume and Function

There was a statistically significant increase in LVSV augmentation with stress after treatment with a mean difference of 8 ml (p=0.03) (See **Figure 4.17A**) There was a borderline significant augmentation of cardiac output after treatment with a mean difference of 1474±3168 ml (p=0.05). (See **Figure 4.17B**) There was no significant difference in heart rate pre (average heart rate 105 beats per minute) and post (110 beats per minute).

A

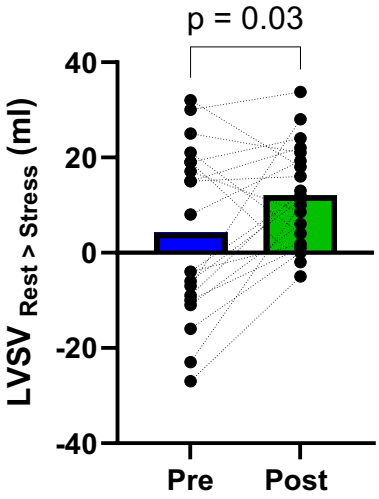

B

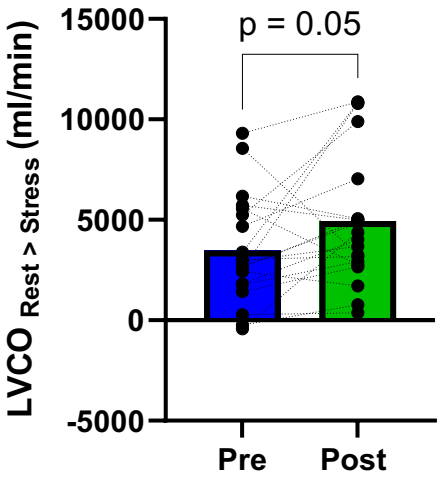

Figure 4.17 DICE Changes in LV stroke volume and cardiac output with stress

LVSV=left ventricular stroke volume, LVCO=left ventricular cardiac output

4.3.3.1.3 Right Ventricular Volume and Function

Treatment with Ninerafaxstat was associated with a significant change in RVEDV, RVESV and RVEF. (See Table 4.6 and Figure 4.18) There was a significant reduction in RVEDV (see **Figure 4.18 column A**) at rest (171±29 ml at pre to 160±36 ml post, p=0.02) but no change in RVEDV at stress (185±42 ml to 182±37 ml, p=0.41). A significant reduction in RVESV (see **Figure 4.18 column B**) at rest (80±29 ml at pre to 71±23 ml post, p= 0.03) and at stress (88±29ml at pre to 77±26 ml post, p= 0.02) was observed. However, no change in RVSV (see **Figure 4.18 column C**) at rest (92±19ml versus 97±18ml, p=0.21) or stress (97±18ml versus 105±26 ml, p=0.31) was observed. There was no change in resting RVEF (see **Figure 4.18 column D**) (55±7% to 56±8%, p=0.42). However, there was a significant increase in RVEF post treatment during exercise (53±8% to 59±26%, p=0.03).

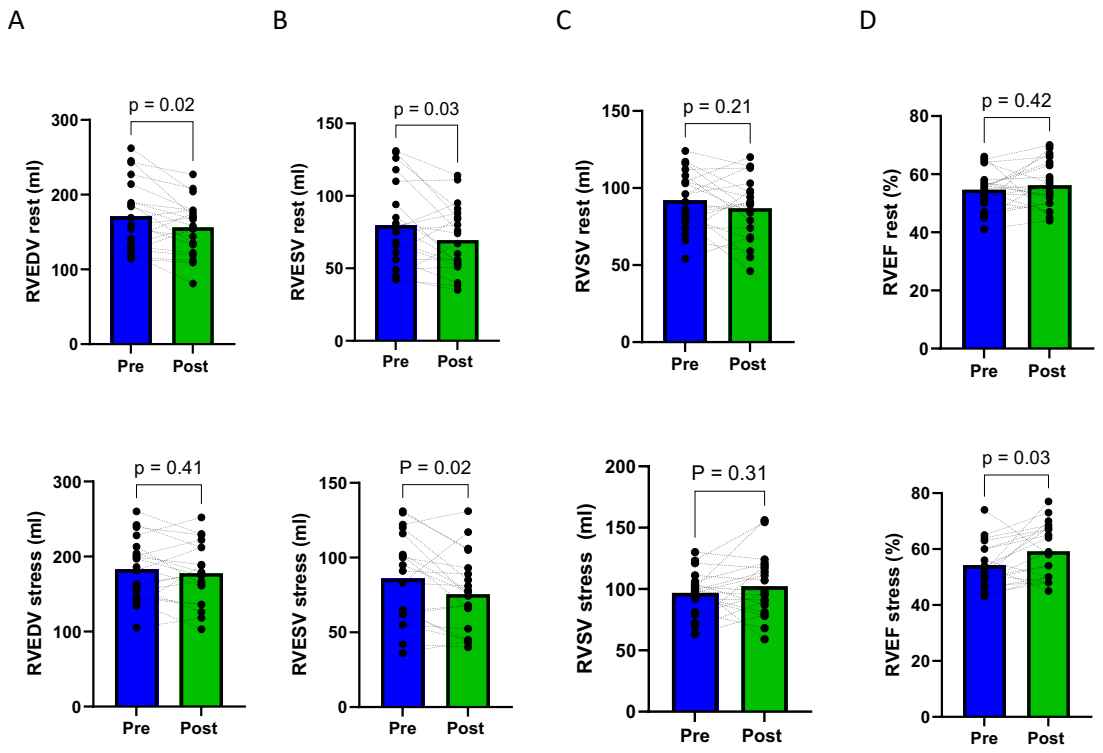

Figure 4.18 DICE Right ventricular volumes and function at rest and stress

RVEDV=right ventricular end-diastolic volumes; RVESV=right ventricular end-systolic volume; RVSV=right ventricular stroke volume; RVEF=right ventricular ejection fraction

4.3.3.1.4 Right Ventricular Exercise Induced Changes in Volume and Function

There was a statistically significant increase in RVSV augmentation with stress after treatment (4.7 ml before and 16 ml after treatment) with a mean difference of 8 ml (p=0.03). (See **Figure 4.19A**) There was a statistically significant increase in augmentation of cardiac output after treatment (mean difference of 1474±3168 ml, p=0.05). (See **Figure 4.19B**)

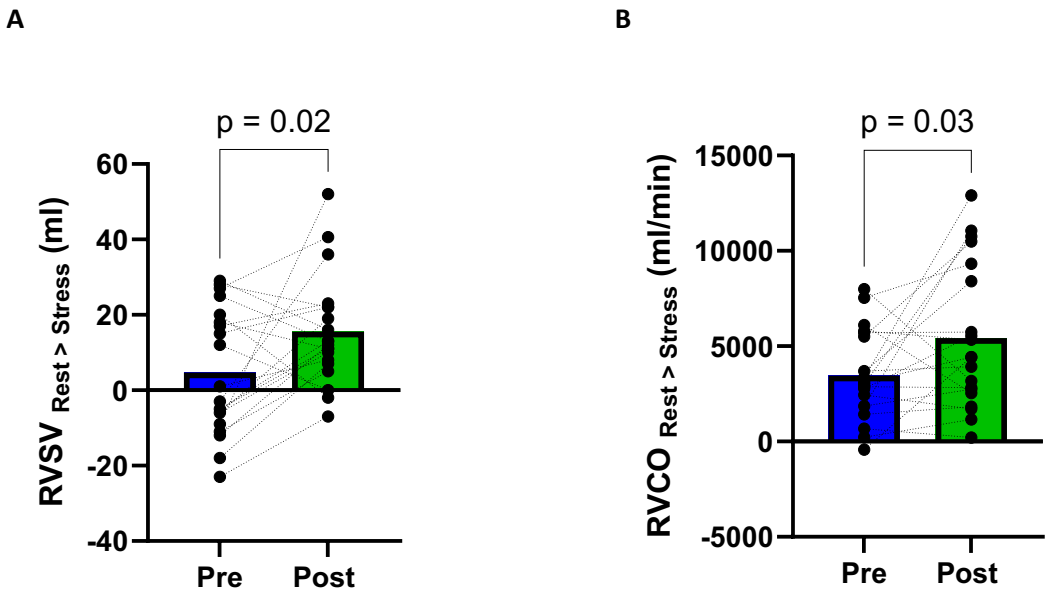

Figure 4.19 DICE Changes in right ventricular volume and function with stress

RVSV=left ventricular stroke volume, RVCO=left ventricular cardiac output

4.3.3.1.5 Correlation between Cardiac Energetics and Cardiac Stroke volumes

There was a moderate positive correlation between the change in PCr/ATP and the change in LVSV (see **Figure 4.20A**) with a Spearman's rank correlation coefficient rho (ρ)=0.57 (p=0.009) and Pearson's correlation coefficient r=0.56 demonstrating a significant positive association between PCr/ATP and LVSV. There was a weak positive correlation between the change in PCr/ATP and the change in RVSV (see **Figure 4.20B**) with Spearman's rank correlation coefficient rho (ρ)=0.46 (p=0.039) and Pearson's correlation coefficient r=0.30.

A

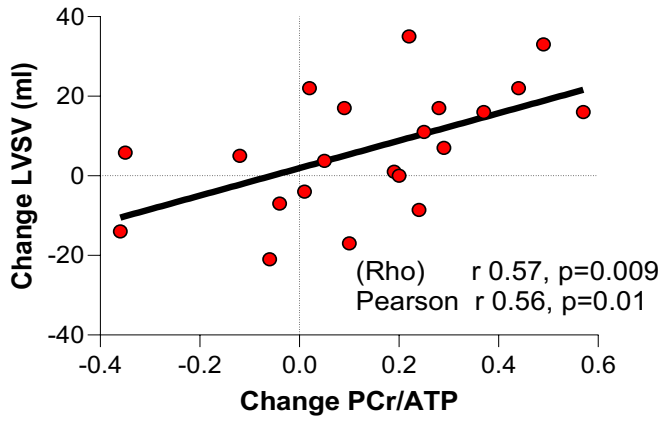

B

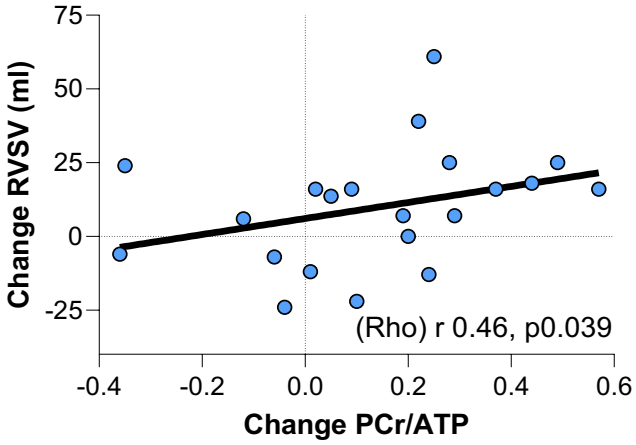

Figure 4.20 DICE Correlation between cardiac energetics and cardiac volumes

LVSV= left ventricular stroke volume; RVSV= Right ventricular stroke volume; PCr/ATP= phosphocreatine/adenosine triphosphate; Rho= Spearman Correlation Coefficient; Pearson r=Pearson Correlation Coefficient

4.3.3.2 Clinical outcomes: 6-Minute Walk Test

6-minute walk distance after 3 months of treatment (baseline mean 385.3 meters (SD±83) to EOT 402.3 meters (SD±89) with a mean statistically significant increase in walk distance of 17 meters (SD±30; p = 0.02) after treatment. (See **Figure 4.21**)

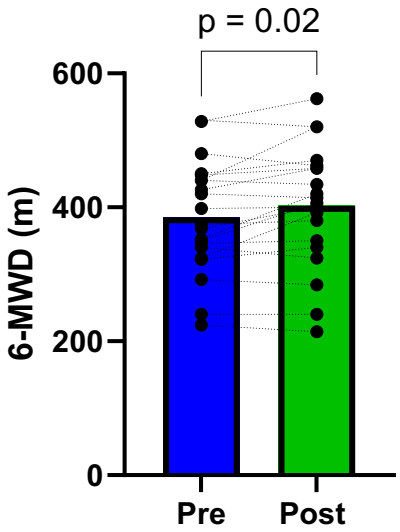

Figure 4.21 DICE 6-minute walk distance

4.3.3.3 Patient Reported Outcomes: NYHA and KCCQ

4.3.3.3.1 Kansas City Cardiomyopathy Questionnaire

Administration of Ninerafaxstat led to non-significantly increased KCCQ overall summary score (OSS) with a mean increase of 5.7 (SD±17, p=0.14) points. There was a significant improvement in the KCCQ clinical summary score (CCS), including the physical and symptomatic aspects of HF, in participants with a KCCQ CCS <80 points at enrolment (n=17) with a mean improvement of 8.3±17 points (p=0.04). (See **Figure 4.22**)

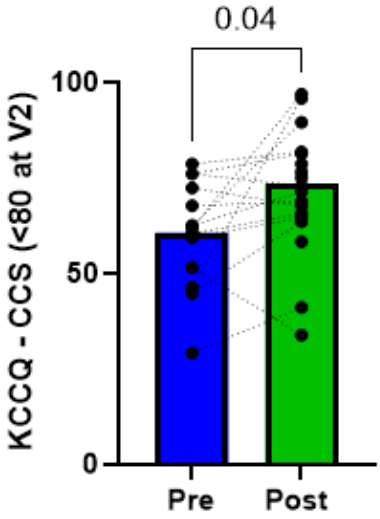

Figure 4.22 DICE Kansas City Cardiomyopathy Questionnaire Clinical Summary Score

4.3.3.3.2 New York Heart Association classification

Administration of Ninerafaxstat led to a non-significant and not clinically meaningful improvement in NYHA classification from a mean of 2.1±0.35 at baseline to 1.86±0.43 at EOT (p=0.0566). (See **Figure 4.23**) Patients with a NYHA class I and IV were not included.

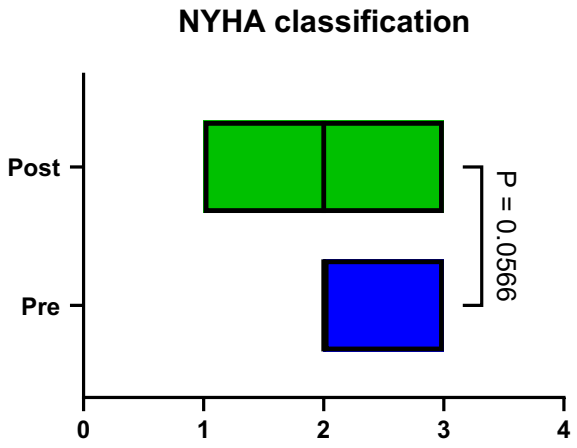

Figure 4.23 DICE New York Heart Association classification

4.3.3.3.3 Patient Global Impression of Severity and Change score

There was a significant improvement in symptom severity reported by the participants after 3 months of treatment with the mean PGI-S score of 1.23±0.62 at baseline and 0.76±0.8 (p=0.0143) at the end of treatment. (See **Figure 4.24**) There was no participant who reported severe or very severe symptoms. Considering the Patient Global Impression of Change (PGI-C) score, a total of 9 participants (42%) reported no change in symptoms. (See **Table 4.7**)

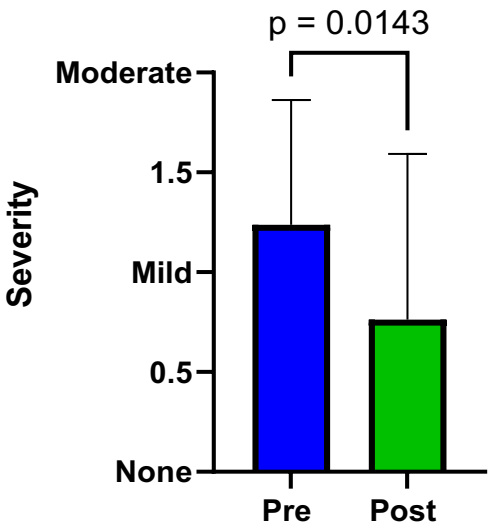

Figure 4.24 DICE Patient Global Impression Severity Score

	PGI-S Change						
PGI-C	**2-point worsening**	**1-point worsening**	**0 no change**	**1-point improvement**	**2-point improvement**	**3-point improvement**	**Total**
	0	0	0	0	0	0	0
A little worse	0	1	0	0	0	0	3
No change	0	3	6	0	0	0	9
A little better	0	1	1	3	0	0	5
Much better	0	0	0	2	2	0	4

Table 4.7 DICE Cross-tabulation of Patient Global Impression of Severity and Change

4.3.3.4 Echo-Derived Diastolic Functional Measures

There was no significant change in any of the echo-derived diastolic function parameters. Diastolic function was assessed in 21 participants at rest and in 19 participants during stress. Two participants felt unable to perform stress testing at the time of EOT. There was no change in average E/e' at rest (baseline mean 9.2±2.9 to EOT 9.4±3.5, mean difference -0.72±3.2 (p = 0.87) (see **Figure 4.25A**) or average E/e' at stress (baseline mean 9.2±5.3 to EOT 8.5±3.5, mean difference -0.33±3.4 (see **Figure 4.25B**) after 3 months treatment.

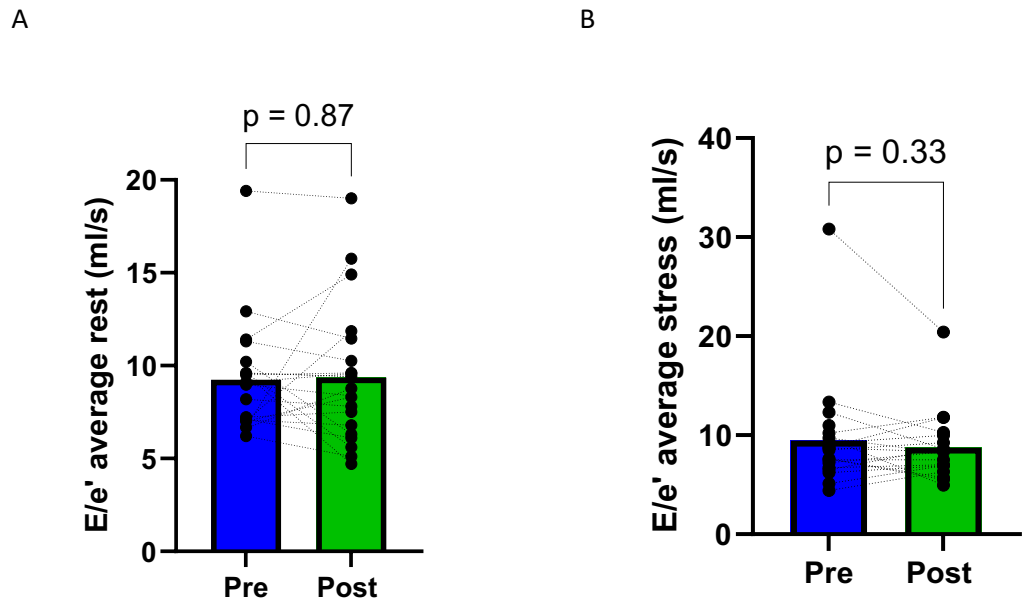

Figure 4.25 DICE Echo derived diastolic function at rest and stress

4.3.3.6 Lung Water

Lung water analysis was performed in 16 participants who had two paired data sets with sufficient image quality (histogram allows clear demarcation of lung tissue). There was no significant change in lung water measured in arbitrary units (AU) at rest (baseline 11418±2328 AU and EOT 10192±2154, p= 0.266) (see **Figure 4.26A**) or stress (baseline 11475±2024 AU and EOT 10420±2062, p= 0.271) (see **Figure 4.26B**). No significant change in transudation was detected with treatment (p=0.6808) (see **Figure 4.26C**).

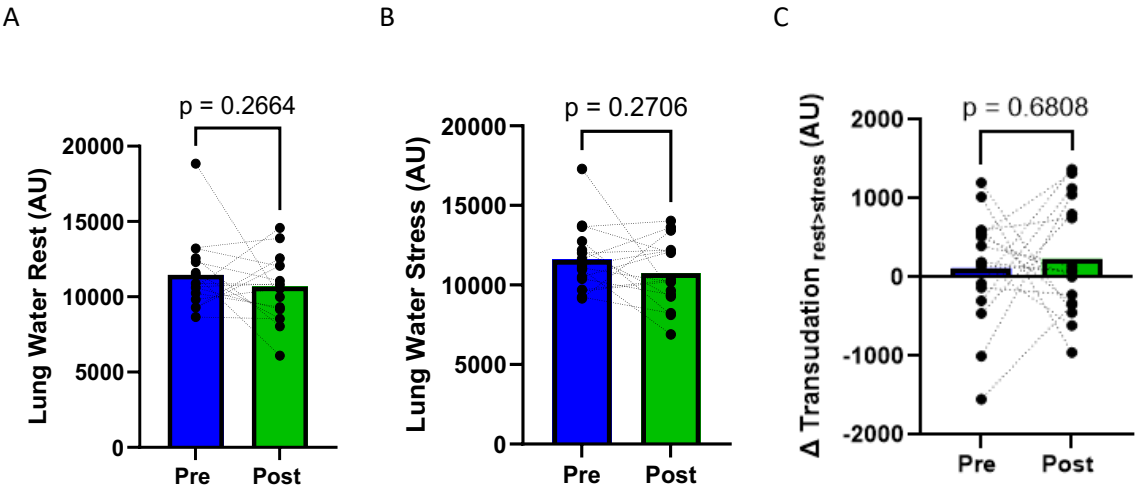

Figure 4.26 DICE Lung Water Analysis at rest and stress

4.3.3.7 Myocardial and Liver Steatosis

Administration of Ninerafaxstat led to a significantly increased myocardial lipid content per % water (baseline 1.2±1.1% to EOT 1.6±1.2%) with a mean increase of 0.47±0.7% (p=0.0148). (See **Figure 4.27A**) There was a non-significant reduction in hepatic steatosis measured as fat fraction (%) (baseline mean 8.03±5.5% to EOT 7.21±5.5%), mean decrease -0.82±2.1% (p=0.102). (See **Figure 4.27B**)

A B

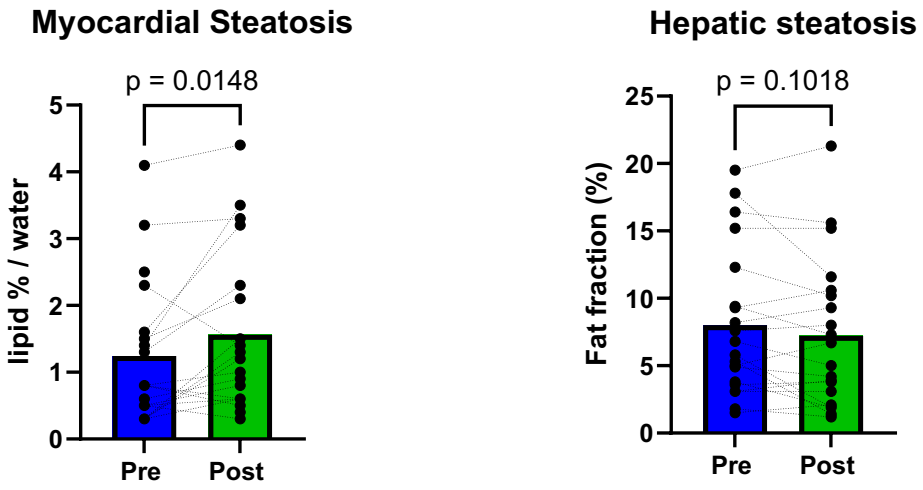

Figure 4.27 DICE Myocardial and Liver Steatosis

4.3.3.8 Abdominal Visceral Adiposity

Administration of Ninerafaxstat led to a significant decrease in subcutaneous adiposity with a mean decrease of -20±42 cm^2 (p=0.045). (See **Figure 4.28A**) There was a significant reduction in BMI with a mean reduction of -0.42±0.87 kg/m^2 (p= 0.0399). (see **Figure 4.28B**)

A

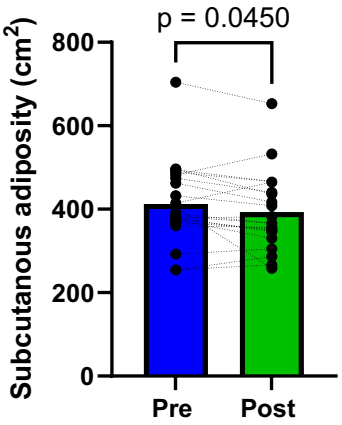

B

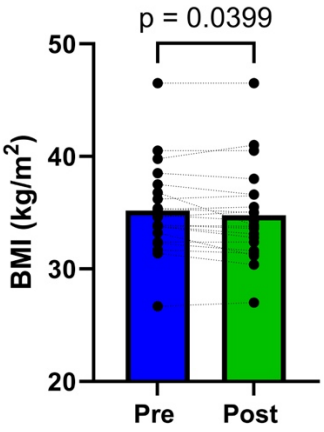

Figure 4.28 DICE Abdominal adiposity

4.3.3.9 Bioimpedance Analysis

Administration of Ninerafaxstat led to no significant changes in any of the additional parameter measures by bioimpedance analysis. (See **Table 4.8**)

Bioimpedance, mean	V2	V4	p-value
Total Body water (litres)	45.3	44.8	0.2801
Body fat mass (g)	42.6	42.3	0.5325
Weight (kg)	104.0	103.1	0.0824
Body Mass Index (kg/m^2)	35.2	34.7	0.0399
Skeletal muscle mass (kg)	33.8	33.4	0.2464
Body fat mass (g)	42.6	42.3	0.5325
Percentage body fat (%)	40.8	40.8	No difference
Extracellular water ratio	0.4	0.4	No difference
Intracellular water (litres)	27.5	27.2	0.2579
Extracellular water (litres)	17.8	17.7	0.3314
Visceral fat area (cm^2)	176.6	173.9	0.2018
Waist-hip ratio	1.1	1.1	0.1647
Bone mineral content (kg)	3.5	3.5	0.7754
Body cell mass (kg)	39.2	38.9	0.2425

Table 4.8 DICE Bioimpedance Analysis

4.3.3.10 Cardiovascular and Metabolic Biomarkers

Administration of Ninerafaxstat led to no significant change in biomarkers. (see **Table 4.9**)

Mean ±SD	Pre-Treatment (V2) N=21	Post-Treatment (V4) N=21	p-value
Total cholesterol	4.0±1.0	3.9±0.9	0.49
LDL cholesterol	2.2±0.8	2.1±0.7	0.24
HDL cholesterol	1.2±0.3	1.2±0.3	0.87
Triglycerides	1.6±1.0	1.5±1.2	0.53
Fasting Glucose	6.7±1.3	7.0±1.9	0.25
Fasting Insulin	116.3±101.2	110.6±68.3	0.77
FFA	0.6±0.3	0.6±0.3	0.72
β-hydroxybutyrate	0.2±0.2	0.1±0.1	0.45
γ- GT	93.2	93.5	0.95
NT-proBNP	538 (246,1222)	679 (211,1147)	0.46
Hs-c-Troponin	8.3±10.1	6.3±6.4	0.15
CRP	4.8±5.2	6.5±8.8	0.15
Uric Acid/Urate	409.3±87.3	412.3±74.6	0.69
CK	94.0±48.3	92.4±48.1	0.80
Creatinine	94.5±19.7	96.7±23.4	0.28
eGFR	66.4±15.8	65.0±17.9	0.34
BUN	3.6±0.9	3.7±1.2	0.72
uACR	20.8±55.5	16.9±38.2	0.25

Table 4.9 DICE Cardiovascular and Metabolic Biomarkers

Ttl cholesterol= Total Cholesterol in mmol/l; LDL = Low-Density Lipoprotein in mmol/l; HDL = High-Density Lipoprotein in mmol/l; Triglycerides in mmol/l; Fasting Glucose in mmol/; Fasting Insulin (in picomol per litre=pmol/l); FFA= Free Fatty Acids in mmol/l); β-hydroxybutyrate in mmol/l; γ-GT= γ-Glutamyl Transferase in mmol/l; NT-proBNP= N-Terminal pro-B-type natriuretic peptide in in nanogram per millilitre (ng/ml); Hs-c-Troponin= high sensitivity cardiac troponin in nanogram per litre (ng/L); CRP= C-reactive protein in milligram/litre (mg/l);); Uric Acid/Urate in micromole/litre (µmol/L); CK= Creatine Kinase in International Units per litre (IU/l);); Creatinine in mg/DL; eGFR= estimated Glomerular Filtration Rate in mL/min/m2;BUN= Blood Urea Nitrogen in mmol/l; uACR= urinary Albumin-Creatinine Ratio in mg/mmol

4.3.3.11 Adverse Events

There were 39 adverse events reported by 13 participants (48%) during the study period. One serious adverse event (SAE) was reported by one patient who was admitted to hospital during the study which was unrelated to the study drug or any study intervention and did not result in a discontinuation of the study drug. In 15 cases the reported side effect was attributed to the study drug. Interruption or withdrawal of the study drug was reported on 16 occasions, which occurred in 5 participants. The severity was reported as mild in 12 cases, moderate in 4 events, and severe in 1 case (SAE). Due to adverse events, 3 participants withdrew from the study events prior to the end of treatment. Gastrointestinal side effects including diarrhoea, nausea and vomiting, constipation was reported in 6 participants. One participant experienced a rash, which resulted in premature discontinuation of the study drug, and this participant was subsequently excluded due to medication compliance <80%.

4.4 Discussion

DICE was one of three phase 2a clinical trials assessing the effect of a novel cardiac mitotrope Ninerafaxstat. This study assessed the impact of Ninerafaxstat on myocardial energetics in patients with obesity, T2DM and HFpEF, as well as its safety and tolerability. Furthermore, its effect on cardiac function, exercise capacity, cardiovascular biomarkers and patient reported symptoms were evaluated. The DICE study met its primary endpoint of improving cardiac energetics (PCr/ATP) after 3 months of treatment with Ninerafaxstat. It also demonstrated an improvement in patient reported outcomes, exercise capacity and an improved exercise adaptation shown by a significant increase in stroke volume difference with exercise. These finding suggest that Ninerafaxstat positively affects cardiac energetics resulting in improvements in HF symptoms and exercise capacity in patients with HFpEF. Overall, Ninerafaxstat was safe and well tolerated.

4.4.1 Changes in Myocardial Energy Metabolism

In this cohort of patients with obesity, T2DM and HFpEF, PCr/ATP ratio was substantially lower (PCr/ATP= 1.24 at baseline) than in previous studies performed locally [23] including patients with either T2DM (PCr/ATP= 1.6) [295] or HFpEF (PCr/ATP= 1.44) [23]. This suggests a negative additive effect of T2DM and HFpEF as increased insulin resistance reduces intracellular glucose uptake and availability for mitochondrial oxidation. [314] As a result, cardiac metabolism shifts towards fatty acid metabolism [237], reducing the metabolic flexibility of the heart [25] and increasing oxygen requirements to maintain ATP production. [315] This leads to energetic impairment measured by a reduced PCr/ATP, which is seen in obesity [31, 71] and diabetes [295] and progressively worsens [31] in HF [23], findings supported by this study.

In obesity, the increase in fatty acid metabolism leads to accumulation of fatty acids in the cardiomyocyte which correlates with adverse remodelling and reduced cardiac function. [316, 317] In the IMPROVE-DiCE study [295] up to eight weeks of Ninerafaxstat treatment led to a significant

improvement in resting myocardial PCr/ATP in patients at risk of HF with obesity and T2DM up to a physiologically normal range. This mechanistic study confirmed the three-pronged approach of Ninerafaxstat; firstly, inhibition of FAO leads to increase in glucose metabolism, secondly, increase in PDH flux augments glucose oxidation, thirdly, repletion of NAD^+ improves mitochondrial function. These findings support the hypothesis that Ninerafaxstat positively influences cardiac energetics.

In contrast to a single published study of TMZ in 25 patients with HFpEF (DoPING-HFpEF trial) [318] where treatment did not result in modulation of cardiac energetics, the currently presented IMPROVE-DiCE-2 study in patients with obesity, T2DM and HFpEF showed that three months of Ninerafaxstat led to a 12% improvement in PCr/ATP. The reasons for that may be multi-fold:

1. TMZ has shown benefits in ischaemic cardiomyopathy in particularly when associated with diabetes [253], which considering the beneficial effects of Ninerafaxstat in both cohorts of diabetes without (IMPROVE-DiCE) [295] and with HFpEF (IMPROVE-DiCE-2) may contribute to the difference seen.
2. Ninerafaxstat is metabolised to the TMZ analogue IMB-1028814 which has a higher bioavailability than conventional TMZ.
3. The addition of the NAD^+ precursor niacin in Ninerafaxstat offers additional benefits to TMZ alone. NAD^+ works in synergy with the partial fatty acid inhibitor TMZ/ IMB-1028814 resulting in greater coupling of increased glucose uptake (NAD^+)[319] with increased PDH flux (TMZ)[320], to enhance glucose oxidation. Furthermore, it may be superior due to the potential increase in cellular bioenergetics by replenishing the cellular NAD^+ pool.

Modulation of cardiac energetics offers a new approach to heart failure treatment [321], which is particularly exciting in HFpEF where very few treatment options have shown benefit [6]. Ninerafaxstat is the first drug treatment to demonstrate an improvement of cardiac energetics in

obesity, T2DM with and without HFpEF. [295] Whilst this was statistically significant, to what degree this increase in PCr/ATP correlates with clinical outcomes such as seen with ß-blockers in HFrEF [322] requires further studies. In addition to metabolic modulation, it has been shown to have benefits on cardiac structure, function and symptoms as discussed below. [295]

4.4.2 Cardiac Structure and Function

In the IMPROVE-DiCE study [295], with its focus on diabetic cardiomyopathy, where the key imaging features consist of LVH and diastolic dysfunction [323], Ninerafaxstat significantly improved diastolic function. With the progression into HFpEF, assessed in IMPROVE-DiCE-2, the beneficial effects of Ninerafaxstat on diastolic function could not be replicated.

However, treatment with Ninerafaxstat did result in a statistically significant increase in LVSV augmentation at stress, improvement in exercise tolerance and patient reported symptoms. A positive correlation between LVSV augmentation and cardiac energetics measured by PCr/ATP supports previously published findings [23] that impaired exercise tolerance may be linked to impaired cardiac energetics. As exercise intolerance is often the first sign of HFpEF and can be caused by limited heart rate variability and stroke volume augmentation (contractile reserve) [324] resulting in elevated LV filling pressures [325], the change in PCr/ATP ratio correlated with an improvement in LVSV difference during physical exercise links the effect of Ninerafaxstat to meaningful improvement in patient symptoms.

Elevated LV filling pressure in HFpEF may lead to transient increased pulmonary pressures [324], which can be evaluated by MRI based quantification of lung water [23, 227] Although Ninerafaxstat improved LVSV augmentation and exercise capacity, these changes did not correlate with lung water assessment on imaging .

4.4.3 Changes in Myocardial Steatosis

In healthy subjects, the myocardial triglyceride (MTG) content can vary with fasting, exercise or during hyperinsulinaemia and/or hyperglycaemia with normal values between 0.5 and 1%lipid/water. [111, 326] In healthy subjects, cardiac steatosis positively correlates with increasing visceral fat [327] and is associated with increased myocardial mass [328]. In contrast to that, in patients with T2DM, MTG are elevated which is associated with diastolic dysfunction, regardless of body fat. [329] However, in our cohort of patients with an average BMI of 35 kg/m^2 and normal myocardial mass, the average MTG content at baseline was only mildly elevated (1.2% lipid/water). Contrary to the anticipated increase in MTG through inhibition of FAO, previous studies [295] have shown a reduction in myocardial triglyceride (MTG) concentration after up to eight weeks of Ninerafaxstat. This study showed an opposite effect with a statistically significant mean increase of MTG of 0.47±0.7% (p=0.0148). Considering the low baseline MTG, no change in circulating FFA levels and no change in diastolic function, this unlikely represents a clinically meaningful increase in MTG.

4.4.4 Limitation

Study recruitment took part across three sites in Oxfordshire aiming to enrol a representative cohort of patients with HFpEF. Although the study cohort was reflective of the local demographics, ethnic minorities were not represented. Under representation of ethnic minorities is a common concern in cardiovascular trials [330], however in HFpEF this might be exacerbated by current diagnostic criteria which likely underdiagnose black patients [331]. Furthermore, there was an underrepresentation of female participants who completed the trial, however considering those who withdrew from the study, 48% of the enrolled patients were female.

This was a prospective, observational, non-blinded, non-randomised study which was exposed to multiple areas of bias which may have influenced the result. Firstly, selection bias, only patients

who were able to exercise were included, representing those at a milder spectrum of disease without significant frailty. Secondly, the lack of blinding resulted in performance bias which may have particularly affected the patient reported outcomes and the 6-minute walk test. Thirdly, attrition bias, as the patients who withdrew from the study prior to the end of study visit were not included in the final analysis, the results might be more favourable.

The use of SGLT2i in this cohort was low, and while SGLT2i are not believed to significantly alter cardiac metabolism [260], broader uptake might still influence clinical outcomes and therefore future trial results. Similarly, GLP-1 receptor agonist use was minimal, and with emerging evidence of their benefit and subsequent increased utilisation may interact with the observed therapeutic effect.

Additionally, the small sample size in this study impairs generalisability. With a sample size of 21 participants and the study is underpowered for the primary endpoint of PCr/ATP. A larger, phase III, randomized, multi-centre study might support the beneficial findings of Ninerafaxstat in HFpEF. Finally, we note the presence of multiple testing where the number of endpoints increases the likelihood of false-positive findings. Even though the endpoints were exploratory, the results should be interpreted with caution and should be confirmed in adequately powered studies.

4.4.5 Future Directions in Heart Failure with preserved Ejection Fraction

HFpEF is a heterogenous condition with multiple aetiologies including metabolic syndrome, arrhythmia (atrial fibrillation), coronary artery disease, pulmonary hypertension and right ventricular failure, infiltrative and hypertrophic cardiomyopathies. [332] Unsurprisingly only SGLT2i have a Class I indication for the treatment of HFpEF regardless of aetiology to improve symptoms and outcomes beyond the management of comorbidities. [6] To characterise the different

phenotypes of HFpEF, a UK wide registry is underway which will facilitate the understanding of HFpEF pathology and subsequent research into therapeutics. [333] The understanding of sub-types of HFpEF will promote individualised care mirroring the progress made in oncology. Ninerafaxstat is the first molecule to demonstrate energetic, structural and symptomatic benefit in a metabolic phenotype of HFpEF. This should encourage further research not only into the inhibition of fatty acid metabolism with Ninerafaxstat in larger randomised trials but also other substrate regulators like Peroxisome proliferator-activated receptor α (PPAR-α) ligands. [334]

4.4.6 Conclusion

In this trial, participants with obesity, T2DM, and HFpEF were enrolled. Participants fulfilled the diagnostic criteria for symptomatic HFpEF, experienced exercise intolerance and reduced quality of life. Their heart was characterised by reduced PCr/ATP, diastolic impairment, and failure of systolic augmentation to exercise. This Phase 2a clinical trial showed that three months of treatment with Ninerafaxstat increased PCr/ATP, improved biventricular systolic augmentation to exercise and improved HF symptoms resulting in enhanced exercise capacity. Ninerafaxstat was safely tolerated in a patient cohort with multiple comorbidities including T2DM and may improve cardiac energetics, function and symptoms in the cardiometabolic phenotype of HFpEF.

5 HYPER-HEART

Aortic stenosis (AS) is the most common valve disease in the UK [335] with a rising incidence [336] due to aging, obesity, HTN, T2DM, smoking, and renal disease. [337] Aortic stenosis and associated pressure loading leads to LV remodelling, LVH [76] and changes in metabolism [77]. However the association between LVH in AS and metabolic modulation is less well understood. [79] The **HYPER HEART** study was the first study which assessed LV remodelling and cardiac metabolism with and without LV pressure load, and the long-term effects of transcatheter aortic valve implantation (TAVI) on LVH regression and energetic recovery by quantifying cardiac energetic state (PCr/ATP) during and after removal of pressure load and, in selected cases, in-vivo changes in Pyruvate Dehydrogenase (PDH) flux.

5.1 Background

Progressive AS lead to LVH negatively impacting cardiac function, outcomes [338], and cardiac metabolism [339]. Inconclusive results arose from animal models studying the impact of LVH on substrate utilisation with hyperpolarised MRI/ MRS (see **5.4**). In humans, progressive changes in metabolism due to AS have been shown [77], however the understanding of the effects of pressure load and its subsequent removal and the reversibility of metabolic alterations is limited.

5.1.1 Impact of Pressure Overload on Cardiac Metabolism

Animal studies of pressure loaded hearts show a shift from predominant FAO to an increase in glucose uptake, with uncoupling of glycolysis from glucose oxidation via PDH, resulting in a reduction in energy production. [79, 262, 340] This may lead to a shift of myocardial metabolism away from oxidative metabolism and fatty acid oxidation towards glycolysis [77] and increased myocardial uptake of ketone bodies [78]. The degree of metabolic derangement and utilisation of different metabolic pathways may vary dependent on the degree of pressure overload LVH [341]

and on the type of LVH (pressure or volume overload) [342]. However, depending on the pre-clinical model of pressure load, different metabolic alterations have been described. Three models of hypertrophy were used in animal studies (see **Figure 5.1**); spontaneous hypertensive rats [85], hyperthyroidism induced hypertrophy [343], and abdominal aortic banding model [87], which have shown variable changes in metabolism depending on the model used. To assess different metabolic pathways in those models, hyperpolarised MRI/ MRS techniques were utilised (see **5.4**).

Flux through PDH was found to be increased in spontaneously hypertensive rats [344], and this was linked to reduced expression of the fatty acid transporter, CD36, in this model. In contrast, a reduction in PDH flux was seen in hyperthyroidism-induced hypertrophy, explained by elevated pyruvate dehydrogenase kinase (PDK) expression and activity leading to PDH inhibition and reduced glucose oxidation. [340] Subsequent treatment with dichloroacetic acid, a PDK inhibitor, was shown to improve metabolic flexibility via substrate selection [345], reduce hypertrophy [86], and restore cardiac function [345, 346]. No change in PDH flux was seen in the abdominal aortic banding model [87], which seems clinically most relevant. In this aortic banding model, an increased production of [1-^{13}C]lactate was observed, suggesting increased anaerobic metabolism, supporting the hypothesis of uncoupling between glycolysis and glucose oxidation [347].

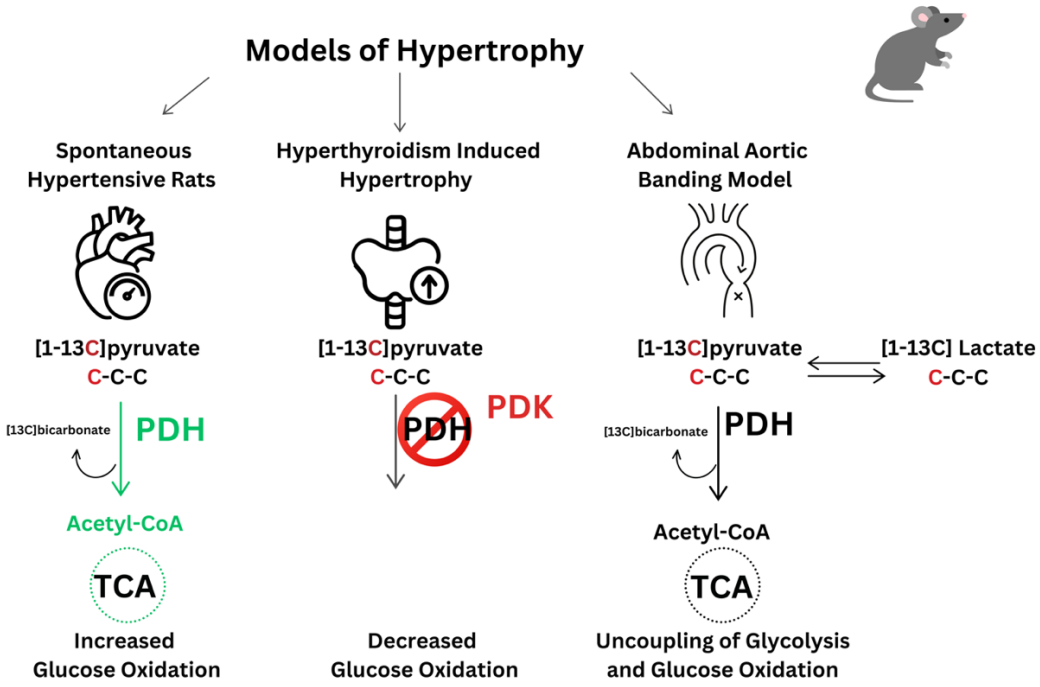

Figure 5.1 Animal Models of Hypertrophy

In the spontaneous hypertensive rat model Pyruvate Dehydrogenase (PDH) flux was increased suggestive increased glucose oxidation; in the hyperthyroidism induced hypertrophy model increased pyruvate dehydrogenase kinase expression led to PDH inhibition and decreased glucose oxidation; in the abdominal aortic banding model PDH flux did not change and increased lactate production suggest uncoupling of glycolysis and glucose oxidation.

Human studies have demonstrated that the increased diastolic pressures seen in AS [80] and LVH [79] are linked to decreased PCr/ATP and systolic function [81]. With the progression of AS, substrate utilisation shifts from FAO towards glucose metabolism with increased glucose update and glycolysis but no increase in glucose oxidation overall resulting in a reduction in PCr/ATP. [79] However, regardless of the LV remodelling in AS, energy reserve measured by total PCr [41], PCr/ATP [81], and CK flux [81] is reduced even in moderate AS. Regardless of the regression of LVH, PCr/ATP significantly increased 12 months after aortic valve replacement. [84]

AS leads to significant pressure load in the LV, resulting in complex metabolic and structural adaptations. However, the effects of relieving this pressure both immediate (within 24 hours) and long-term effects (within 6 months) remain incompletely understood. Understanding these pathways is key to developing targeted treatment [348] and lays the foundation for the **HYPER HEART** study presented in this chapter.

5.1.2 Imaging in Aortic Stenosis

Echocardiography is the predominant tool for the diagnosis of AS [349], allowing grading based on the effective orifice area (EOA <1cm^2 in severe AS), mean pressure gradient (ΔPm >40 mmHg in severe AS), and peak flow velocity (Vmax >4 m/s in severe AS). [350] However, cardiac MRI is increasingly recognised for its value in assessing myocardial changes in AS. [351] Cardiac MRI allows accurate measurement of EF [352], LVH [353], replacement fibrosis demonstrated by late gadolinium enhancement (LGE) and T_1 mapping [354]. Aortic stenosis may lead to three LVH patterns [355]: eccentric hypertrophy (increased LV mass and diameter due to volume overload), concentric hypertrophy (increased mass with normal dimension), concentric remodelling (normal mass and increased dimensions). [356] Asymmetrical hypertrophy in the septum, associated with poorer outcomes [357], often regresses within months of aortic valve replacement [358]. Even though the presence of LVH is associated with adverse outcomes [355], its presence is not considered in the timing of aortic valve intervention. Late gadolinium imaging is a prognostic tool [359] to characterise focal septal [360] and RV insertion point fibrosis or diffuse fibrosis [361]. In addition native T_1 mapping values might indicate fibrosis or amyloid deposition [362], which often coexist. [363] Post-contrast T_1 mapping techniques are used to allow calculation of the Extracellular Volume (ECV) which is commonly increased with myocardial fibrosis. [362]

5.1.3 Transcatheter Aortic Valve Implantation

Management of AS varies based on the severity and symptoms experienced by patients, with options including surveillance or aortic valve replacement via surgical (SAVR) or transcatheter approaches (TAVI). The first TAVI was performed in 2002 in France [364] and has since transformed the care of patients with AS [365]. It is now the first-line treatment for patients aged 75 years or older [349]. After the initial indication for TAVI, Computer Tomography (CT) assessment [366] is performed to assess suitability and discussion in a multidisciplinary 'Heart Team' [367] takes place. The Edwards Sapien valve is the most commonly used [368] TAVI valve (see **Figure 5.2**), which is made of cow tissue attached to a metal (cobalt-chromium) frame for support (see **Figure 5.2A**). It is folded and placed into a balloon catheter (see **Figure 5.2B**) which is inserted via (most commonly) the right femoral artery (see **Figure 5.2C**) to reach the aortic valve (see **Figure 5.2D**) where it is expanded with a balloon during fast ventricular pacing (see **Figure 5.2E**).

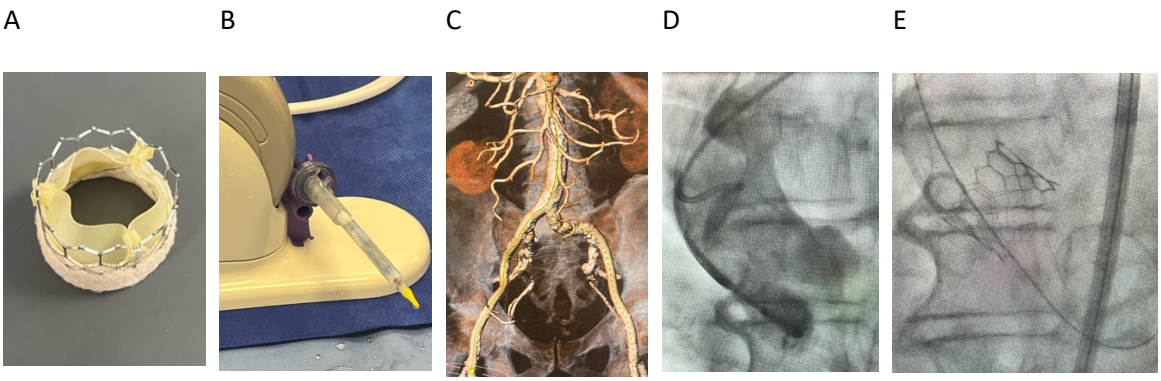

Figure 5.2 Edwards Sapien 3 Transcatheter Heart Valve System

(A) Sapien 3 Valve prior to insertion into (B) catheter in which it is advanced via (C) femoral access to (D) the aortic valve where it is (E) expanded with a balloon

5.1.4 Aims of the HYPER HEART study

AS leads to LVH, alterations in cardiac metabolism and impairment of cardiac function resulting in adverse outcomes. Over the last two decades, TAVI has transformed the treatment approach of patients with severe AS and has allowed more sophisticated research questions to be considered regarding structural myocardial changes like LVH and the impact of timing of valve intervention on outcomes. However, the effect of pressure load and removal on myocardial metabolism is less well understood. Understanding the impact of LVH and its regression on substrate utilisation and cardiac energetics may aid a more precise personalised approach, in particularly on the timing of TAVI but potentially also in future drug development.

The **HYPER HEART** study aimed to assess the impact of LV pressure load and the immediate (within 24 hours) and long-term (6 months) impact of TAVI on cardiac metabolism and LV remodelling. To facilitate this multinuclear (^{1}H, ^{31}P) MRS, MRI techniques and clinical parameters were used to assess:

1. Assessment of cardiac PCr/ATP during pressure load (severe AS) and the short- and longer-term effects of removal of pressure (within a day and six months post TAVI).
2. Characterisation of cardiac muscle during pressure load and its recovery from pressure load over time with diastology, LV mass, and fibrosis (T_1 mapping, LGE, ECV).
3. Comparison of values with age matched healthy volunteers.

5.2 Methods

5.2.1 Ethical Consideration

HYPER-HEART was a single-centre, observational study designed to assess the effects of TAVI on myocardial energetics, metabolism and function in severe AS when compared to sedentary control participants without cardiovascular disease referred to as healthy volunteers (HV). This British Heart Foundation (BHF) funded research study was reviewed and received approval from the Yorkshire and the Humber – Sheffield Research Ethics Committee (REC reference: 23/YH/0092, IRAS ID: 313523) on 13th November 2023. Additionally, on 1st December 2023, authorization was granted by OUH to conduct the study and enrol the first participants by 13th January 2024. Adherence to institutional guidelines and the principles laid out in the Declaration of Helsinki were maintained throughout the research process. Written informed consent was obtained prior to inclusion in the research study. Data collection occurred anonymously and was safeguarded on a secure, compliant server. Confidential written material was stored securely within locked filling cabinets at the research sites.

5.2.2 Sedentary Control Participants Without Cardiovascular Disease

Healthy volunteers were recruited from lists of people who had taken part in previous studies at the OCMR unit in Oxford and had given consent to being contacted to discuss future studies or through a volunteer poster approved by the ethics committee and placed within the Oxford University Hospitals NHS trust sites or through emails, social media and word of mouth. Eligible participants were considered if they reported to be in good health, without symptoms, treatment, or past medical history of cardiovascular disease, metabolic disease like diabetes, blood disorders, or cancer.

5.2.3 Study Participants with Severe Aortic Stenosis

Patients with symptomatic severe AS (referred to as AS) and preserved ejection fraction (EF ≥50%) undergoing TAVI were recruited from the TAVI MDT and TAVI clinics at OUH between January 2024 and December 2024. Eligible patients were referred to the study team by the responsible clinician. Indication, timing and performance of the TAVI procedure was in the sole responsibility of the structural interventional team and performed as part of standard NHS care in the catheter laboratory of OUH.

5.2.3.1 Participants with Severe AS

5.2.3.1.1 Inclusion Criteria for Participants with Severe AS

- Participant is willing and able to give informed consent for participation in the study.
- Adults aged 18 years or above
- Symptomatic severe AS with indication for TAVI
- LVEF ≥50%

5.2.3.1.2 Exclusion Criteria for participant with severe AS

- Metabolic disease like T2DM
- Flow limiting coronary artery disease or ischaemia
- General contraindications to MRI
- Pacemaker, Cardiac Resynchronisation Therapy (CRT), loop recorder
- Acute decompensated heart failure
- Previous valve replacement or significant other valve disease

5.2.3.2 Participants Without Cardiovascular Disease

5.2.3.2.1 Inclusion Criteria for Participants without Cardiovascular Disease

- Participant willing and able to give informed consent for participation in the study.
- Adults aged 18 years or above
- Participant reports to be in good health

- No known cardiovascular disease or symptoms suggestive of cardiovascular disease

5.2.3.2.2 Exclusion Criteria for Participants without Cardiovascular Disease

- Any significant past medical history including but not limited to active treatment for cardiovascular disease, metabolic disease like diabetes, blood disorders, cancer.
- Any significant family history including but not limited to genetic heart conditions, blood disorders, syndromes.
- General contraindications to MRI
- Pregnant or lactating participants

5.2.4 Endpoints

The primary end point was regression of LVH with associated improvement in cardiac PCr/ATP ratio at six months post TAVI. Secondary endpoints included improvement in cardiac PCr/ATP at Day 1 post TAVI, improvement in qualitative markers of left ventricular pressure overload (including diastology, T_1 mapping values and burden of LGE) over the two time points.

5.2.5 Study Protocol

For participants with severe aortic stenosis undergoing TAVI, the study consisted of three visits, baseline visit (V1) prior to their scheduled TAVI procedure, one day post TAVI (V2), and six months post TAVI (V3). For sedentary control participants without cardiovascular disease participants underwent the baseline visit (V1) only. (See **Figure 5.3**)

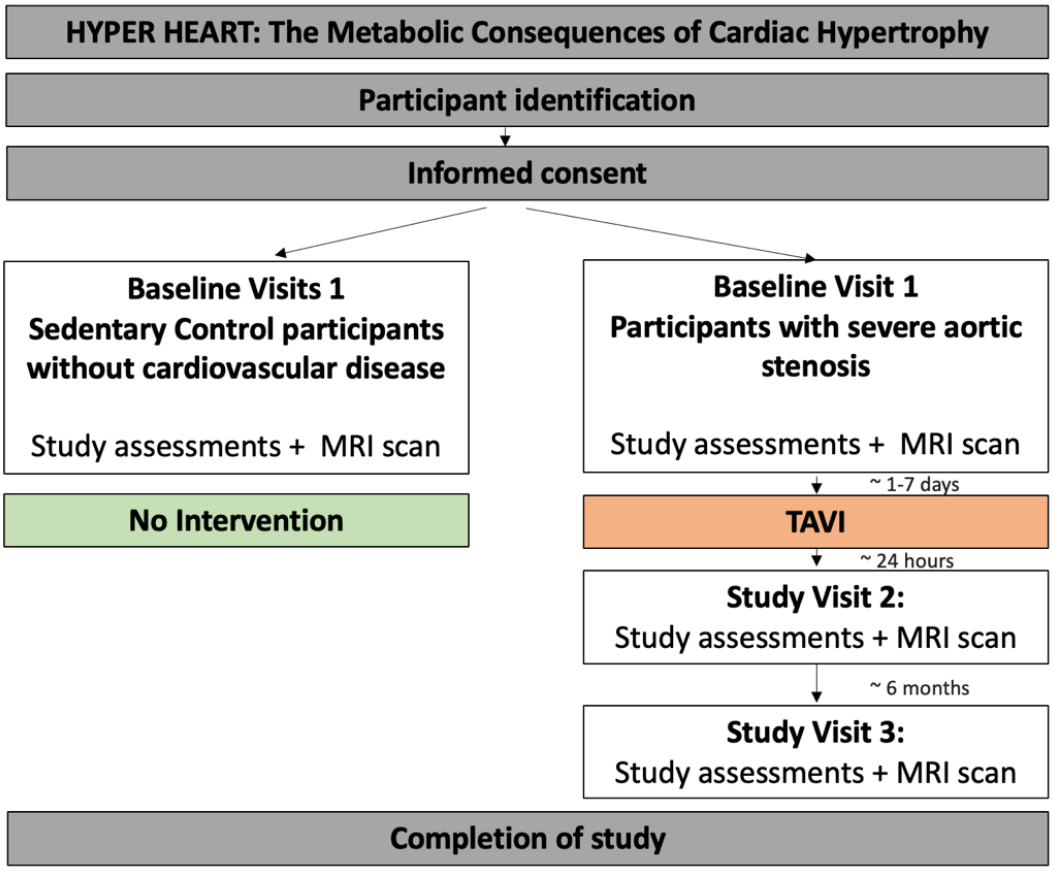

Figure 5.3 HYPER HEART Study flow Overview

After informed consent, participants are divided into two groups: sedentary controls without cardiovascular disease who undergo baseline assessment with no intervention and participants with severe aortic stenosis, who undergo baseline assessment, followed by TAVI within 1-7 days. Follow up assessments were performed within 24 hours post TAVI (Study Visit 2) and 6 months after TAVI (Study Visit 3).

Patients who were interested to join the study were invited for a baseline MRI study visit at the Oxford Centre for Clinical Magnetic Resonance Research (OCMR) within a week of their scheduled TAVI procedure. Prior to the start of the study, informed consent was obtained. All three study visits were identical and included the following procedures (see **Figure 5.4**): assessment of inclusion and exclusion criteria (see **5.2.3.1.1**, **5.2.3.1.2**), demographics, medical history, prior/concomitant medications, 12-lead electrocardiogram (ECG), vital signs, height, weight, physical examination, clinical laboratory tests including biochemistry, haematology, cardiac biomarkers, quality of life questionaries, 6-MWT, echocardiogram, magnetic resonance spectroscopy and imaging.

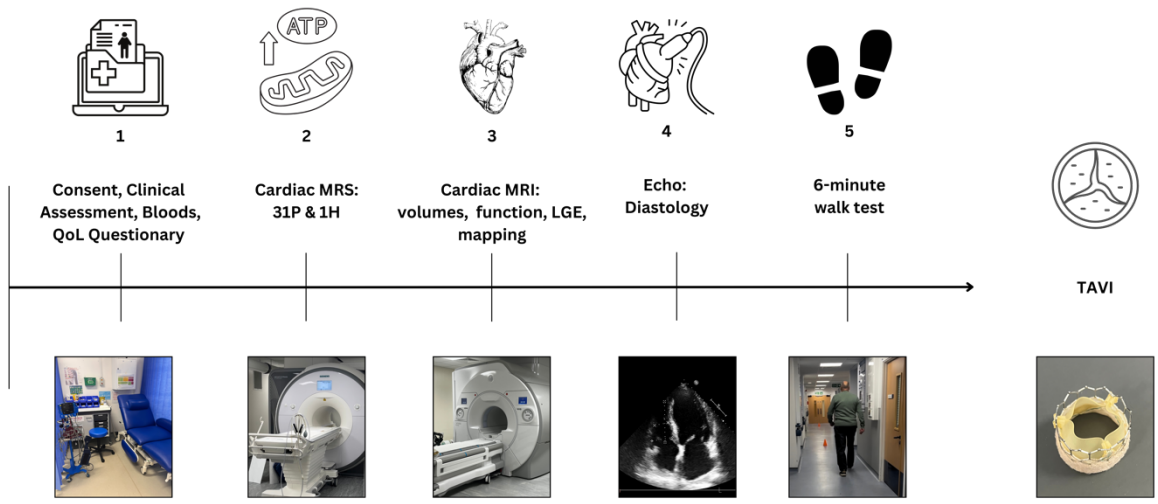

Figure 5.4 HYPER HEART Study visit flow

(1) Consent and clinical assessment including height, weight, ECG, observations, bloods, Quality of Life (QoL) questionary; (2) cardiac phosphorus Magnetic Resonance Spectroscopy (31P-MRS) and cardiac proton MRS (1H-MRS); (3) Cardiac MRI assessment including cardiac volumes, function, late gadolinium enhancement (LGE), and mapping; (4) echocardiography (echo) for the assessment of diastology; (5) assessment of exercise capacity with 6-minute walk test (6-MWT); followed by TAVI procedure.

5.2.6 Magnetic Resonance Protocol

CMR studies were performed using two different MRI scanners. (See **Figure 5.5**) A 3 Tesla Magnetom PRISMA MRI scanner (Siemens Healthineers, Erlangen, Germany) was used for spectroscopy assessments. Phosphorus spectroscopy (^{31}P-MRS) was performed using a home-built prototype multi-layer coil (four conductor layers of 2 oz copper [0.07mm], separated by dielectric insulator layers of 0.127mm Kapton; 82mm to 125mm in diameter). [129] Participants were positioned supine with the centre of the coil over the left ventricular septum. A non-gated 3D acquisition-weighted ultra-short echo time (UTE) ^{31}P-MRSI sequence was used. Proton spectroscopy (^{1}H-MRS) was performed with a spine and 18-channel surface receive coil. All spectroscopic assessments were performed after 6 hours of fasting. Participants were moved headfirst into the scanner until their heart was at isocentre.

A 3 Tesla Premier MRI Scanner (GE) equipped with a GE cardiac AIR^{TM} coil was used to assess cardiac function, volume, aortic valve function, T_1 mapping before and after administration of contrast (Dotarem), and late gadolinium imaging.

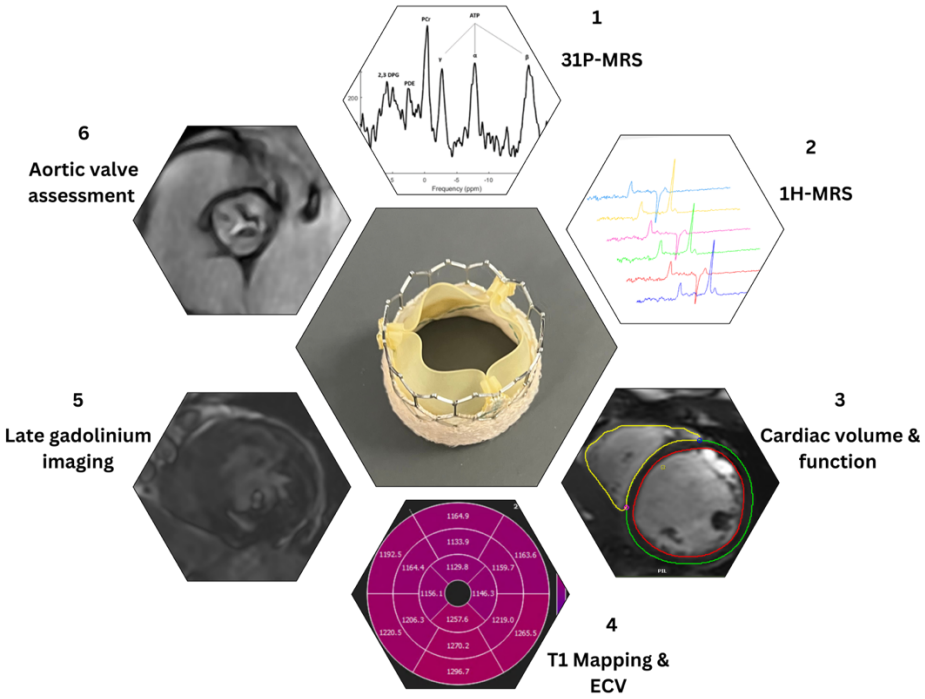

Figure 5.5 HYPER HEART MR study protocol overview

Cardiac phosphorus (^{31}P-MRS) and proton (^{1}H-MRS) magnetic resonance spectroscopy; Cardiac magnetic resonance imaging (MRI) to assess cardiac volumes and function; T1 mapping and Extra-cellular volume (ECV) assessment (T1 mapping 15 minutes post contrast); Late gadolinium imaging; aortic valve assessment

5.2.6.1 Cardiac Magnetic Resonance spectroscopy

Please see Chapter 2 Methods for details on cardiac magnetic resonance spectroscopy (2.8.1).

5.2.6.2 Cardiac Magnetic Resonance Imaging

Please see Chapter 2 Methods for details on cardiac volume and function (2.8.4).

5.2.6.2.1 Native T_1 Mapping

The T_1 time, which refers to the time constant of longitudinal "spin-lattice" relaxation of hydrogen nuclei after excitation with a radiofrequency pulse is measured in milliseconds. [369] T_1- weighted images are used to differentiate different tissue types for example fat (short T_1, high signal intensity) from water (longer T_1, low signal intensity) [370] Alternatively, T_1 mapping can be undertaken to quantitatively measure the T_1 relaxation time (see **Figure 5.6**), both before ("native T_1 mapping" [371] [372]) and after administration of contrast ("post contrast T_1 mapping"). In this study, a MOdified Look-Locker Inversion recovery (MOLLI 5(3)3) sequence over nine heart beats [373] was used, where the number in parenthesis indicates the heart beats required for magnetization recovery, and the other numbers represent the images acquired during different heart beats following a single inversion recovery (IR) pulse [374]. Imaging was performed across three left ventricular slices (basal, mid, apical) (See **Figure 5.6A**) and analysed in CVI42 (see **Figure 5.6B**) to generate a segmental polar map with a 16-segment model (see **Figure 5.6C**). Normal T_1-values vary across different MRI scanners and depend on field strength and sequence used. [311] As normal T_1 values have not yet been established for the scanner used in this study, T_1 values of participants were compared to healthy volunteers and follow up values were compared to the baseline value of each participant.

A Slice selection in LVOT view	B Endo- and epicardial contours.	C T1 segmental polar map in CVI42

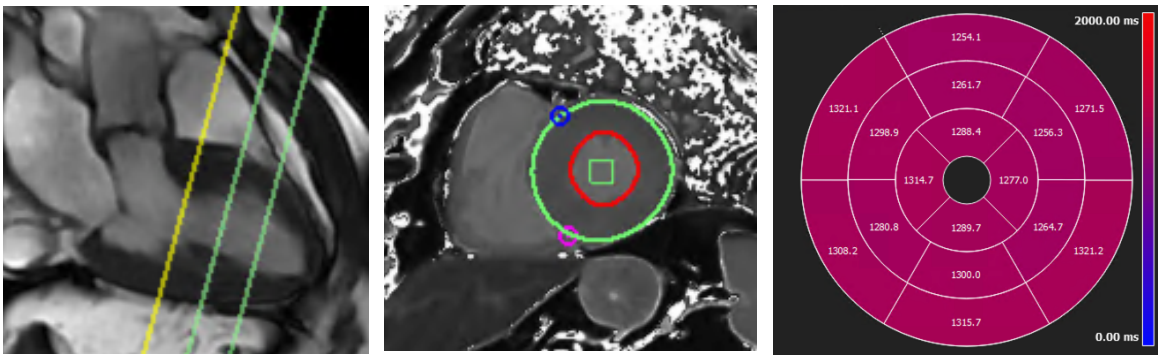

Figure 5.6 T1 mapping acquisition and analysis

(A) Selection of three slices (basal, mid, apical) in left ventricular outflow track view (LVOT); (B) analysis in CVI42 requires drawing of endocardial and epicardial contours to generate a (3) T1 segmental polar map.

5.2.6.2.2 Late Gadolinium Imaging

Gadolinium based contrast agents (GBCA) like Dotarem (gadoterate meglumine) are utilised to enhance image contrast by shortening T_1 and T_2 times. [373] GBCA remains extracellular [375] allowing quick wash out from the healthy myocardium. [376] In LVH, myocardial cells are replaced with fibroblasts increasing the extracellular volume (ECV), leading to gadolinium retention and increased signal intensity referred to as late gadolinium enhancement (LGE). [377] The pattern and distribution of LGE aids diagnosis and prognosis. [378]

In this study, LGE imaging was performed (if eGFR $\geq$ 30ml/1.73m2) to exclude significant myocardial infarction, quantify LGE, and assess ECV. An inversion scout (TI scout) (see **Figure 5.7A**) [379] was followed by a phase sensitive myocardial delayed enhancement (PSMDE) SA stack (see **Figure 5.7B**) 5-10 minutes after administration of 0.5 ml/kg Dotarem.

For the quantification of LGE in CVI42 endocardial (red circle) and epicardial (green circle) contours were drawn on all five short axis LGE images. (See **Figure 5.7C**) Normal myocardium was referenced (blue circle) and pixels with a signal intensity (SI) greater than 5 standard deviations (SA) above the average signal in the myocardium of the reference area were identified (yellow area). [380]

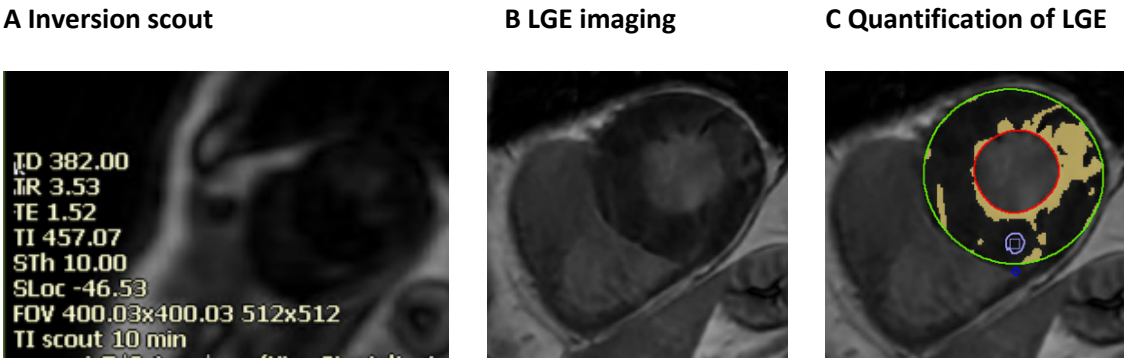

Figure 5.7 Late gadolinium imaging and analysis.

An inversion scout (A) is performed to define the inversion time of the myocardium prior to (B) Late gadolinium enhancement (LGE) imaging. (C) Automated LGE quantification (yellow area) is performed in CVI42 by defining the myocardial reference (blue circle) in between endocardial and epicardial (red and green circle).

5.2.6.2.3 Extracellular Volume

Post contrast T_1 mapping was used to quantify ECV (see **Figure 5.8**) which increases with diffuse fibrosis, commonly seen in LVH. [362] Following the native T_1 MOLLI sequence described above (5.2.7.2.11), post contrast T_1 mapping was performed of the same three slices at 15 minutes post contrast. In CVI42, in each of the three pre- and post- contrast T_1-maps, endocardial and epicardial contours and as well as a region of interest in the blood pool were drawn to assess the T_1 value of myocardium and blood. An automated calculation of the change in relaxation rate of the myocardium (ΔR1myo) and blood (ΔR1blood) before and after contrast administration was performed by CVI42 using the following formula: [381]

$$\mathbf{\Delta R1} = \frac{\mathbf{1}}{\mathbf{T1post - contrast}} - \frac{\mathbf{1}}{\mathbf{T1pre - contrast}}$$

Lambda (λ) is referred to as the partition coefficient of gadolinium [382] and is the ratio of the relative change in T_1 relaxation times between blood and myocardium after contrast administration.

$$\boldsymbol{\lambda} = \frac{\mathbf{\Delta R1\ myocardium}}{\mathbf{\Delta R1\ blood}}$$

Extracellular volume (ECV, %) which consists of interstitial and extracellular matrix [362], can be derived from the combination of pre-contrast and post-contrast T_1 mapping and the patient's haematocrit, which is entered into CVI42. [382]

$$\boldsymbol{ECV}\ (\%) = \boldsymbol{\lambda\, x}\ (\mathbf{100} - \boldsymbol{HCT})$$

A Native T1 Map

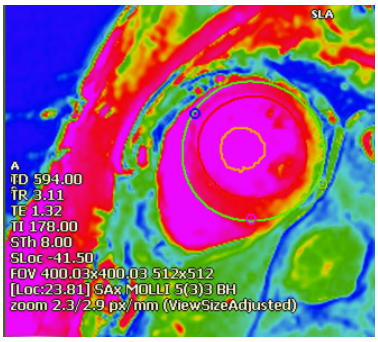

B ECV Map

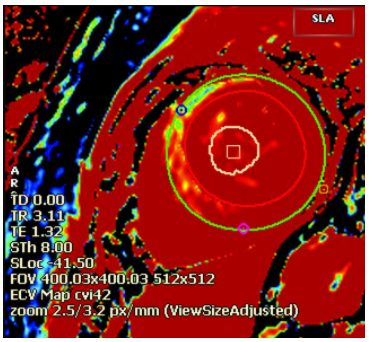

E T1 Map analysis

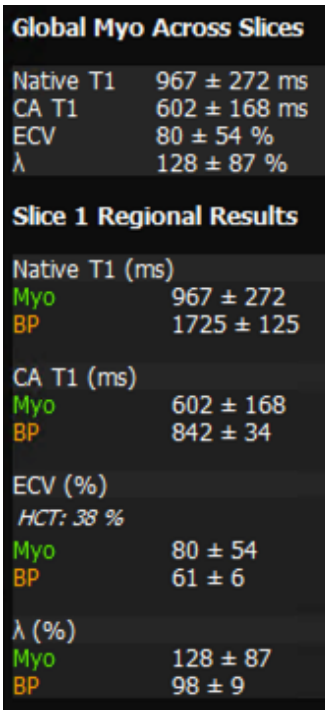

C Post contrast T1 Map

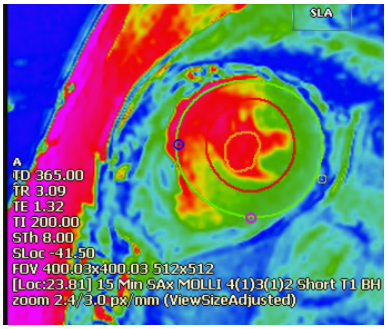

D LGE

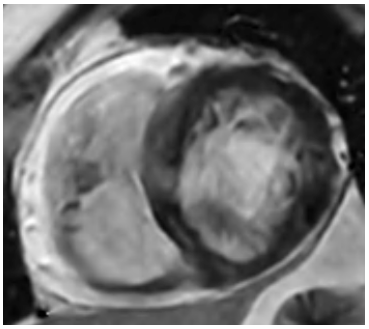

Figure 5.8 Extracellular Volume acquisition and analysis

(A) Native T_1 values and (C) post contrast T_1 values of the myocardium (epicardial contour in green, endocardial contour in red) and blood (yellow circle in the left ventricular cavity) are used by CVI42 for automated creation of (B) Extracellular volume Map (ECV). (D) Demonstration of a late gadolinium (LGE) imaging of the same patient in the same position highlight the area of enhancement matching the associated increased ECV in (B). (E) T_1 Map analysis performed by CVI4; Lambda (λ) partition coefficient of gadolinium.

5.2.6.2.4 Aortic Valve Assessment

Aortic valve structure and function was assessed with radial aortic valve cine imaging (balanced steady-state free precession (bSSFP) sequence) (see **Figure 5.9A, B, C**) to assesses valve anatomy and aortic valve area (ARA). [383] Through-plane phase-contrast MRI (see **Figure 5.9D, E, F**) allowed quantification of the peak flow velocity (see **Figure 5.9J, K, L**), pressure gradient and valve area. In-plane phase-contrast MRI images were acquired to demonstrate the flow pattern (see **Figure 5.9G, H, I**). To assess these dynamic aortic valve parameters, a velocity encoding (VENC) value [384], of approximately 400 cm/s in AS and 180 cm/s post TAVI [383] was used.

Radial Aortic Valve Cine

A Healthy volunteer

B Severe AS

C Post TAVI

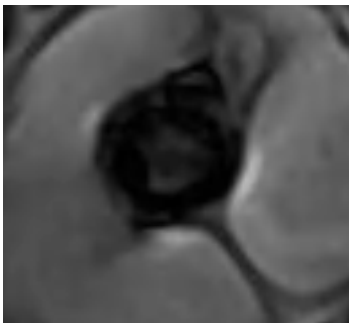

Through-plane Phase-Contrast MRI

D Healthy Volunteer

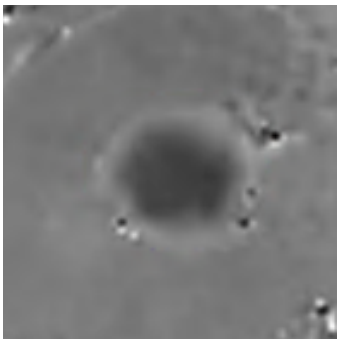

E Severe AS

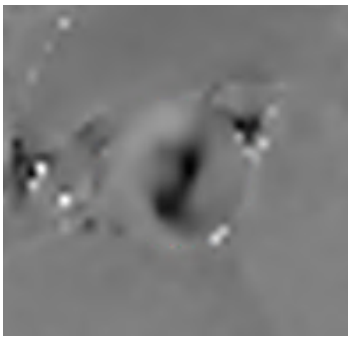

F Post TAVI

In-plane Phase-contrast MRI

G Healthy Volunteer

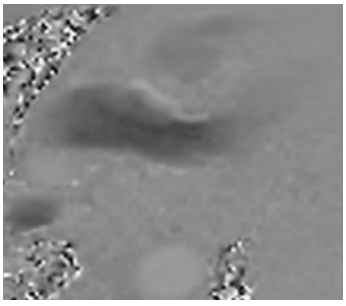

H Severe AS

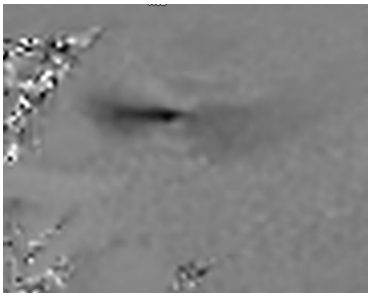

I Post TAVI

Flow (ml/s) assessment in CVI42

J Healthy Volunteer

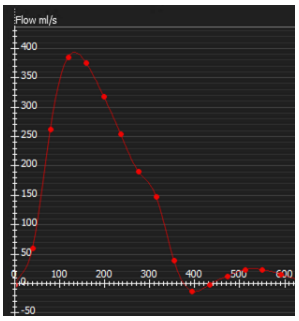

K Severe AS

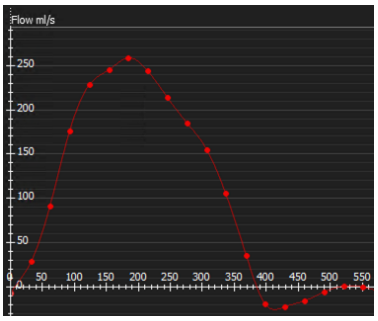

L Post TAVI

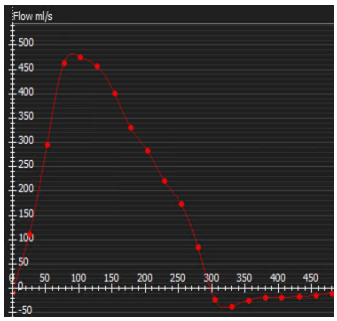

Figure 5.9 Aortic Valve Assessment with CMR

Four staged aortic valve assessment: radial aortic valve cine in (A) Healthy volunteer (HV), (2) participants with severe Aortic stenosis (AS), (3) post transcatheter aortic valve implantation (TAVI); through-plane phase contrast MR in (D) HV, (E) severe AS, (F) post TAVI; In-plane phase contrast MRI (G) HV, (H) Severe AS, (I) post TAVI; flow assessment in CVI42 in (J) HV, (K) severe AS, (L) post TAVI.

5.2.6.2.5 Myocardial Strain

Strain measures how cardiomyocytes change shape during contraction and is assessed in three directions: global longitudinal strain (GLS), global radial thickening strain (GRS) and global circumferential shortening strain (GCS). [385] (See **Figure 5.10**) GLS reflect the longitudinal shortening from base to apex. [386] A value of less negative than -16% is considered abnormal. [385] GRS describes the radially directed shortening of myocardial fibres towards the center of the LV cavity and is expressed in positive values. GCS reflects the circumferential shortening of muscle fibres and is measured as positive strain without a consensus on normal values. [387] Cardiac MR strain measurements can be obtained either by specific acquisition methods, for example CMR tagging, or through post -processing with feature tracking [386], which was used in this study, as it provides an early sign of functional impairment [388], and appears to be associated with prognosis in HFpEF. [388, 389]

A HLA view

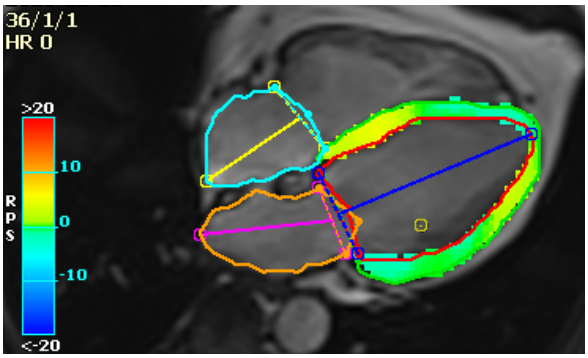

B Global LV longitudinal strain (%)

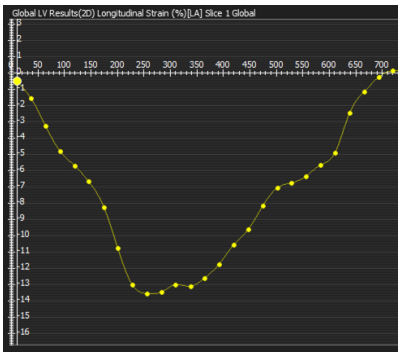

Figure 5.10 Global longitudinal strain acquisition and analysis

Assessment of global longitudinal strain by (A) feature tracking in Horizontal Long Axis (HLA) view resulting in (B) automated output of global left ventricular (LV) longitudinal strain assessment in % in CVI42

5.2.7 Statistics

The **HYPER HEART** study was designed and funded as a pilot study examining three main parts:

(1) Assessment of cardiac PCr/ATP during pressure load (severe AS) and the short- and longer-term effects of removal of pressure (within a day and six months post TAVI).

(2) Characterisation of cardiac muscle during pressure load and its recovery from pressure load over time with diastology, LV mass, and fibrosis (T_1 mapping, LGE, ECV).

(3) Comparison of values with age matched healthy volunteers.

A further aim of this pilot study was to identify the effect size of TAVI on cardiac muscle energetics and changes in tissue characterisation. This will provide insights into a larger study design. The presentation of the current results of 12 paired data sets provides a statistical power of 68% which may increase to 80% if a further four paired data sets are enrolled.

The endpoint analysis was performed on participants with a matching value before and after TAVI. Statistical analysis was performed with GraphPad Prism 10 and IBM SPSS Statistics 29.0.2.0. Normality of distribution was assessed using the Shapiro-Wilks test. For normal distributed data, parametric tests including the paired t-tests were used, such as PCr/ATP pre-/post TAVI. Repeated measures Analysis of Variance (ANOVA) was used to compare the data of the participants with aortic stenosis at three different time points; V1= severe AS pre-TAVI, V2= 24 hours post TAVI, V3= 6 months follow up. To compare HV to participants with AS (AS-V1) an unpaired t-test was performed.

For data, which was not normally distributed, a non-parametric test including the Wilcoxon signed rank test, instead of the paired t-test were performed.

5.3 Results

5.3.1 Study Population and Baseline Characteristics

All patients who were referred to the TAVI team at OUH were considered for participation in the study. Four structural consultant cardiologists perform between 8-10 TAVI procedures per week leading to approximately 450-500 procedures per year, all of which were screened and considered for participation in the study. (See **Figure 5.11**) Nine participants without cardiovascular disease, were enrolled and completed the baseline visit. Out of 13 participants with AS who were enrolled, one participant received a pacemaker and was therefore excluded from continuing with visit 2 and 3. One participant attended visit 1 and 2 but withdrew from the study at the 6 months follow up and one participant was not medically stable enough post TAVI to attend visit 2, but returned for visit 3. Study visit 3 was completed by 11 participants. In this result section data is presented from 12 participants with AS who have at least two paired data sets. There were no adverse events related to the study.

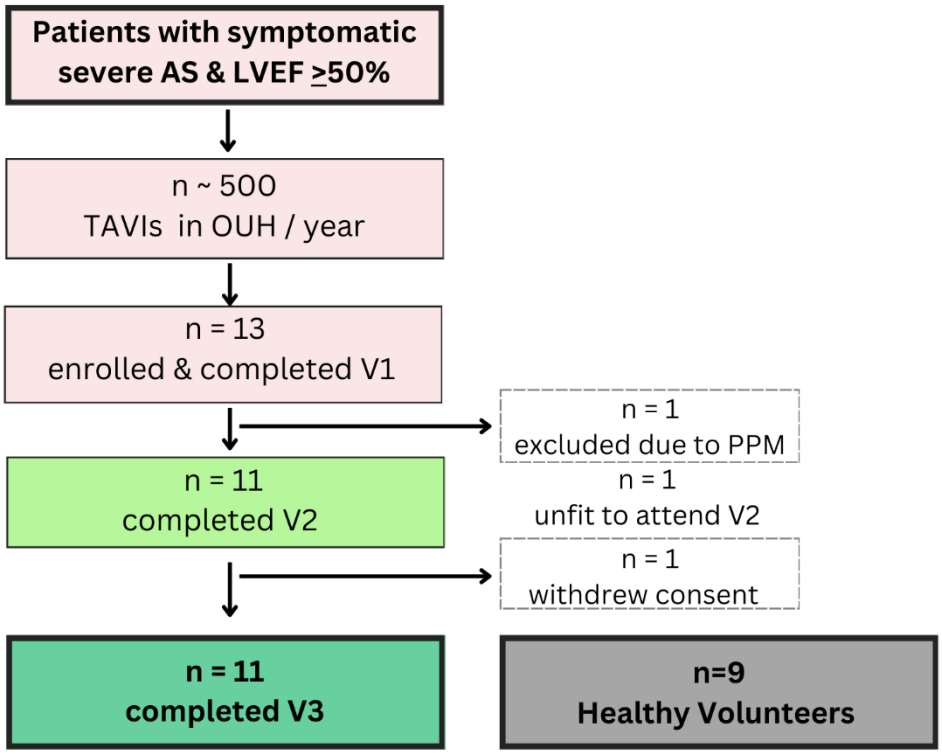

Figure 5.11 HYPER HEART Patient flow

Baseline characteristics are shown in **Table 5.1** for the 9 participants in the control group and 13 participants with AS who attended at least one study visit. The median age in the control group was 72±10 years versus 80±7 in the AS group (p=0.027). Only 2 participants were female in the control group versus 54% of the participants in the AS group. All participants were from a White British background. There was no significant difference in weight (72±11 vs 70±15, p=0.735) or BMI (25±27 vs 26±6, p=0.670) between the groups. Blood pressure was significantly higher in the control group (160±15/81±8 mmHg) vs AS group (136±23/71±12 mmHg, p=0.020/0.049).

Characteristic mean (SD)	**Healthy Controls (n=9)**	**AS patients (n=13)**	**p-value**
Age	72±10	80±7	0.027
Female n (%)	2 (22)	7 (54)	
White Race n (%)	9 (100)	13 (100)	
Weight (kg)	72±11	70±15	0.735
BMI (kg/m^2)	25±2	26±6	0.670
sBP (mmHg)	160±15	136±23	0.020
dBP (mmHg)	81±8	71±12	0.049
HR (bpm)	63±16	79±12	0.023

Table 5.1 HYPER HEART Anthropometrics

Age in years, weight in kg, BMI= Body mass index (kg/m2); sBP= systolic blood pressure in mmHg, dBP= diastolic blood pressure in mmHg, HR= heart rate in beats per minute (bpm)

The most common comorbidities in the group undergoing TAVI were hypercholesterinaemia (n=9), and hypertension (n=7), followed by chronic kidney disease (n=6), and the presence of atrial fibrillation (n=3). All patients with hypercholesterinaemia were treated with a statin, hypertension was commonly treated with Ca^{2+}-channel blocker or ACEi/ARB. All cases with atrial fibrillation were anti-coagulated. None of the participants were on SGLT2i. (See **Table 5.2**) Participants enrolled in the control group (healthy volunteers) had no documented cardiovascular disease, comorbidities or concomitant medication use.

Comorbidities	n (%)	Concomitant medications	n (%)
Hypercholesterolaemia	9 (75)	Statin	9 (75)
Hypertension	7 (58)	Ca^{2+}- Channel Blocker	6 (50)
Chronic kidney disease	6 (50)	ACE-I/ARB	5 (42)
Atrial Fibrillation	3 (25)	Diuretic	4 (33)
		Anti-coagulation	3 (25)
		$SGLT2_i$	0

Table 5.2 HYPER HEART Comorbidities and concomitant medications in patients with AS

Angiotensin Converting Enzyme Inhibitors (ACE-I), Angiotensin receptor blocker (ARB), Sodium-Glucose Cotransporter-2 inhibitor (SGLT2i)

5.3.2 Cardiac Volumes and Function

There was no significant difference in LV volumes or function between healthy volunteers (HV) and participants with AS (AS-V1) and between at all the three timepoints of patients with severe AS (AS-V1 vs AS- V2, AS-V1 vs AS-V3). (See **Table 5.3 row 1, 2, 3, 4**)

The RVEDV (130±27ml) and RVESV (55±18ml) in AS at V1 was significantly (*) smaller than in HV (RVEDV 169±47ml, p=0.0485 and RVESV 75±22 p=0.0439). In the cohort with AS, there was no

significant difference in RV volumes or function between the different time points (V1, V2, V3). (See **Table 5.3 row 7, 8, 9, 10**).

Means	**HV**	**AS-V1**	p HV vs AS-V1	**AS-V2**	p AS-V1 vs AS-V2	**AS-V3**	p AS-V1 vs AS-V3
LVEDV (ml)	**160±39**	**135±35**	0.1979	**131±28**	0.9922	**129±19**	0.9860
LVESV (ml)	**64±15**	**58±19**	0.1979	**55±21**	0.9691	**57±14**	0.9185
LVSV (ml)	**97±28**	**77±19**	0.1257	**75±16**	0.9702	**72±12**	0.8028
LVEF (%)	**60±6**	**57±6**	0.3991	**58±10**	0.8725	**56±7**	0.8153
LVCO (l/min)	**5.6±2.2**	**5.3±1.4**	0.6925	**5.4±1**	0.6480	**4.6±0.6**	0.6945
RVEDV (ml)	**169±47**	**130±27**	0.0485*	**126±33**	0.9807	**126±22**	0.9004
RVESV (ml)	**75±22**	**55±18**	0.0439*	**52±20**	0.9972	**55±15**	0.9978
RVSV (ml)	**95±30**	**75±16**	0.1447	**74±18**	0.8012	**71±12**	0.7075
RVEF (%)	**56±7**	**58±9**	0.4002	**60±9**	0.8856	**57±8**	0.9546

Table 5.3 HYPER HEART Cardiac Volumes and Function

HV= Healthy volunteer, AS= aortic stenosis, V1=Visit 1, V2=Visit 2, V3=Visit 3; LVEDV=left ventricular end-diastolic volumes; LVESV=left ventricular end-systolic volume; LVSV=left ventricular stroke volume; LVEF=left ventricular ejection fraction; LV mass= left ventricular mass; LVCO= left ventricular cardiac output; RVEDV=right ventricular end-diastolic volume; RVESV= right ventricular end-systolic volume; RVSV=right ventricular stroke volume; RVEF=right ventricular ejection fraction.

5.3.3 Left Ventricular Mass

There was a significant (*) reduction in LV mass at 6 months follow up (AS-V3) in participants with AS between V1 and V3 (p= 0.0335) but no significant different between HV (108±18g) and AS-V1 (122±27g, p=0.1322). (See **Figure 5.12A**) A mixed-effect model analysis demonstrated a significant difference in LV mass across the three time points (overall fixed-effects results p=0.0158). This was driven by the significant reduction in LV mass at 6 months follow up (mean LV mass V3 102±14g) in comparison to V1 (mean LV mass 122±27g, p=0.035). (See **Figure 5.12B**)

A

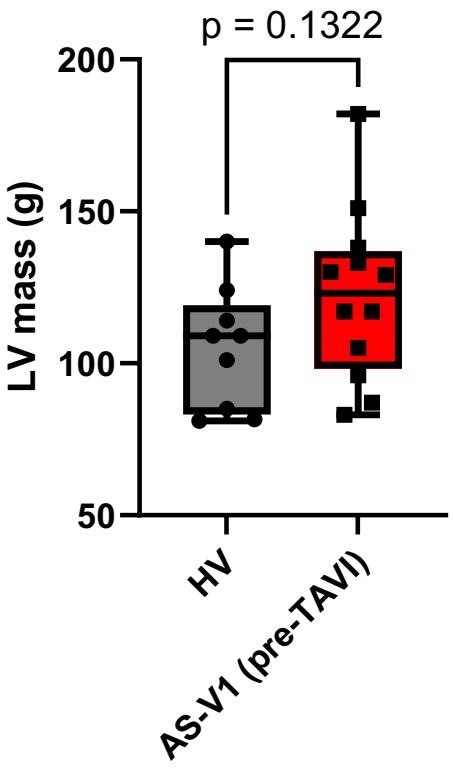

B

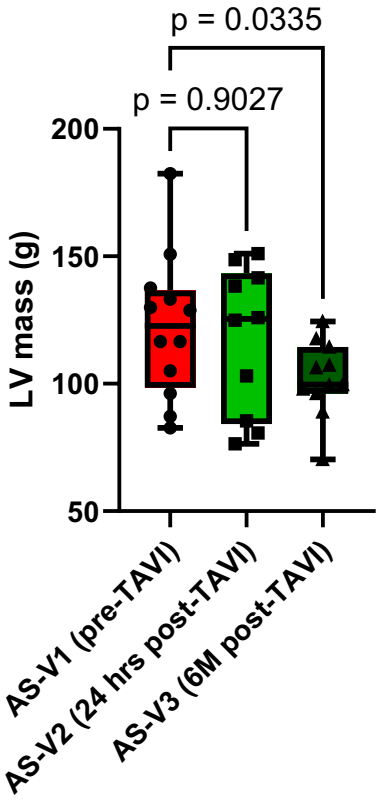

Figure 5.12 HYPER HEART Left ventricular (LV) mass

AS-V1 (pre-TAVI)= Visit 1 at baseline; AS-V2 (24 hours post-TAVI)= Visit 2 within 24 hours of TAVI; AS-V3 (6M post-TAVI)= Visit 3 six months post TAVI.

5.3.4 Echocardiographic Assessment of Diastolic Function

Reference ranges of diastolic function dependent on the presence of sinus rhythm (SR) or atrial fibrillation (AF) and age. [223] Participants without cardiovascular disease (HV) with an average age of 72 years showed normal average E/e' values (6.7±4) indicative of normal diastolic function. (See **Table 5.3**) When compared to the HV, participants with severe AS and a significantly higher age (mean 80 years, p=0.027) had significantly (*) worse diastolic function (average E/e' 14.5±5.3, p=0.0002).

	Normal values BSE > 60 years of age	**HV**	**AS V1**	**p-value (HV – AS V1)**
E/A	0.96±0.18	1.3±0.29	0.7±0.15	0.0017*
Septal e'	10.4±2.1	8.1±2.6	4.8±1.4	0.045*
Lateral e'	12.9±3.5	10.1±3.8	8.4±2.7	0.2846
Average E/e'	AF<11, SR<14	6.7±4	14.5±3	0.0002*

Table 5.3 HYPER HEART Echocardiographic assessment of diastolic function at baseline

BSE= British Society of Echocardiography; HV=healthy volunteers/ participants without cardiovascular disease; AS= severe aortic stenosis; V1= visit 1 pre-TAVI; E/A= Mitral E to A velocity in meters per second; Septal and lateral e' in centimetre per second (cm/s), Atrial fibrillation (AF), Sinus rhythm (SR), ±SD= standard deviation

There was no significant difference of diastolic markers in participants with AS at the three different time points (AS-V1 pre-TAVI, AS-V2 24 hrs post-TAVI, 6M post-TAVI). (See **Table 5.4**)

Multiple comparison	AS-V1	AS-V2	p value (AS-V1 vs. AS-V2)	AS-V3	p value (AS-V1 vs. AS-V3)
E/A	0.7±0.15	0.8±0.18	0.2947	0.68±0.17	0.9929
Septal e'	4.8±1.4	5.2±1.7	0.8924	4.6±1.7	0.8733
Lateral e'	8.4±2.7	6.5±2.0	0.2172	8.1±2.8	0.8422
Average E/e'	18.2±5.0	17.3±5.5	0.4085	17.9±4.3	0.8293

Table 5.4 HYPER HEART Echocardiographic assessment of diastolic function over time

E/A= Mitral E to A velocity; V1= visit 1/baseline; V2= visit 2: V3= Visit 3; SD= standard deviation

5.3.5 Late Gadolinium Enhancement

The percentage (%) of LGE per gram (g) of LV mass (% LGE/g LV mass) was significantly lower in HV (mean 11±6%) in comparison to AS (mean 38±15%, p=0.0009). There was a significant regression of enhancement between V1 (38±15%) and V3 (15±11%, P=0.001). (See **Figure 5.13**)

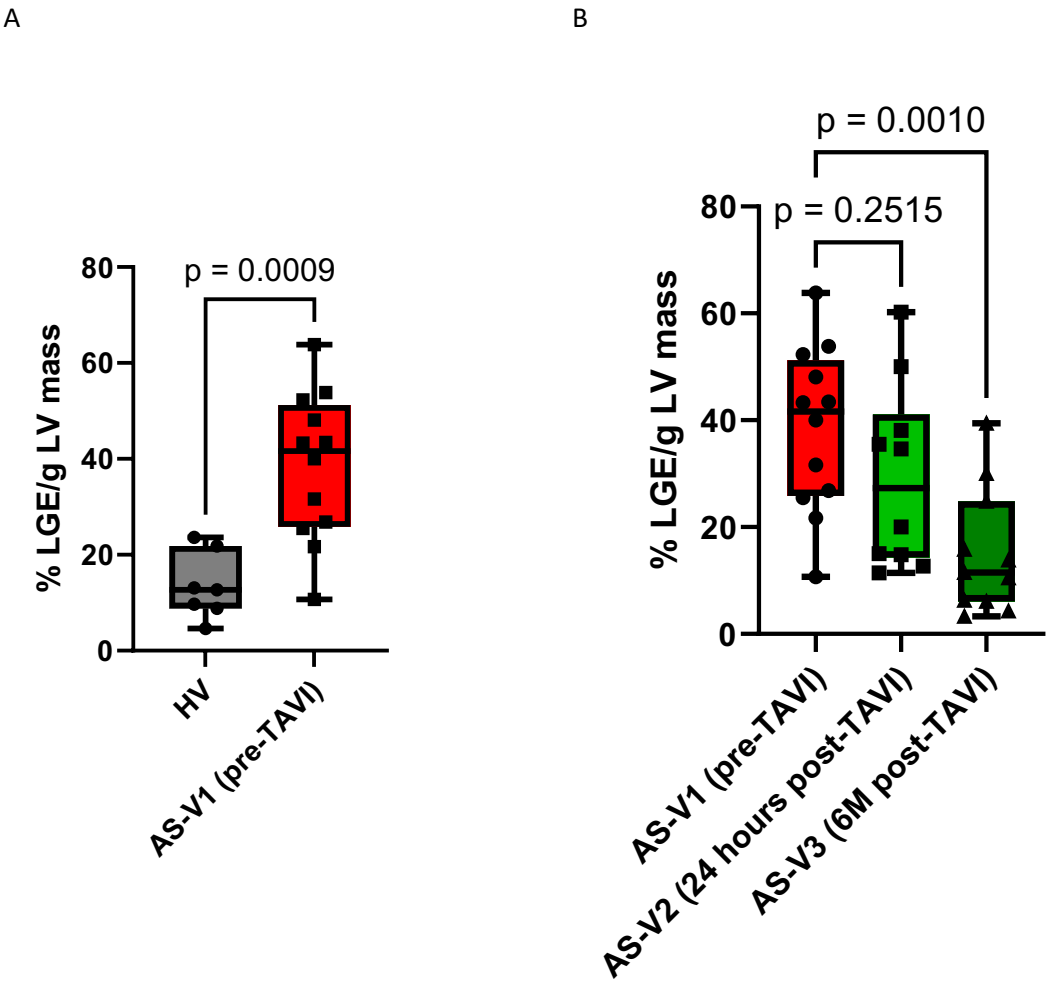

Figure 5.13 HYPER HEART Late gadolinium enhancement

AS-V1 (pre-TAVI)= Visit 1 at baseline; AS-V2 (24 hours post-TAVI)= Visit 2 within 24 hours of TAVI; AS-V3 (6M post-TAVI)= Visit 3 six months post TAVI.

5.3.6 Cardiovascular and Metabolic Biomarkers

Apart from Haemoglobin (Hb) and estimated Glomerular Filtration Rate (eGFR) there were no significant changes between HV and those with AS. (see * in **Table 5.5 column 1, 2, 3**)

There were significant changes (see * in **Table 5.5**) in Hb, White Blood Cell (WBC) count, platelet count, troponin (Hs-c-Trop), C-reactive protein (CRP), triglycerides, glucose levels pre (AS-V1) and immediately after TAVI (AS-V2) all of which recovered to near baseline at six months (AS-V3). Apart from a statistically and clinically significant increase in Hs-c-Trop after the procedure, all other significant changes were not clinically significant. The baseline level of NT-proBNP was high (1412±1984 ng/L) with 5 participants over 1000ng/L at V1. There was no significant improvement in NT-proBNP within 24 hours post TAVI (1380±1175 ng/L, p=0.756) or after 6 months (1176±995 ng/L, p=0.372). The NT-proBNP level of four participants remained above 1200 ng/L at V3.

	HV	ASV1	p-value HV- ASV1	ASV2	p-value ASV1-V2	ASV3	p-value ASV1-V3
Hb	146±9.1	129±19	0.0347*	118±23.2	0.0538	129±16	0.3242
WBC	5.6±1.2	6.6±1.4	0.1490	12.1±4.2	<0.0001*	7.0±1.3	0.9804
PLT	240±52	231±60	0.7571	190±54	<0.0106*	239±64	0.9924
Creatinine	78±16	89±27	0.9307	92±26	0.5744	85±26	0.3139
eGFR	83±8	65±18	0.0242*	63±17	0.6163	66±17	0.2188
Hs-c-Trop	5±4.6	28±37	0.2678	738±480	<0.0001*	19±22	0.9705
NT-proBNP	127±53	1412±1984	0.2947	1380±1175	0.9527	1176±995	0.3178
CRP	1±0.2	2.4±3.0	0.2075	11.1±14.2	0.0337*	5.0±5.2	0.7105
Urate	290±37	315±115	0.6932	307±110	0.7806	314±86	0.9963
Triglycerides	0.7±0.4	1.2±0.4	0.0572	0.9±0.3	0.002*	1.4±0.5	0.3031
Glucose	4.7±0.2	5.3±1.1	0.3494	7.4±2.8	0.019*	5.1±0.6	0.8652

Table 5.5 HYPER HEART blood results

HV= healthy volunteers; AS= aortic stenosis; V1= visit 1; V2= visit 2; V3= visit 3; Hb= Haemoglobin in gram per litre (g/L); WBC= white blood cells in x109 g/L); PLT= platelet count in × 10^9/L. eGFR= estimated Glomerular Filtration Rate in mL/min/m2; Hs-c-Trop = high sensitivity cardiac troponin in nanogram per litre (ng/L); N-terminal pro-B-Type natriuretic peptide (NT-proBNP) in nanogram per millilitre (ng/ml); CRP= C-reactive protein in milligram/litre (mg/l); Uric Acid/Urate in micromole/litre (µmol/L); Triglycerides and fasting Glucose in millimole per litre (mmol/L);

**Significant change*

5.3.7 Primary Endpoint: PCr/ATP Ratio all Three Timepoints

A total of 12 participants who had at least one paired data set were included in the analysis. Cardiac PCr/ATP was normally distributed: Test statistics (*W*) 0.921, p-value 0.292.

An unpaired t-test was performed to compare HV with AS-V1 (pre-TAVI). There was a significant difference in mean PCr/ATP between HV (1.64±0.28) and participants with AS pre- TAVI (1.33±0.18, p=0.0097). (See **Figure 5.14A**)

A mixed-effects model analysis (ANOVA) was performed to assess the difference over time in participants with AS (AS-V1, AS-V2, AS-V3). The median PCr/ATP ratio was 1.36 [1.15,1.5] (V1), 1.26 [0.98,1.37] (V2), 1.33 [1.17,1.43] (V3). (See **Figure 5.14B**) There was no significant difference in participants with AS between the three timepoints (p=0.1974).

A

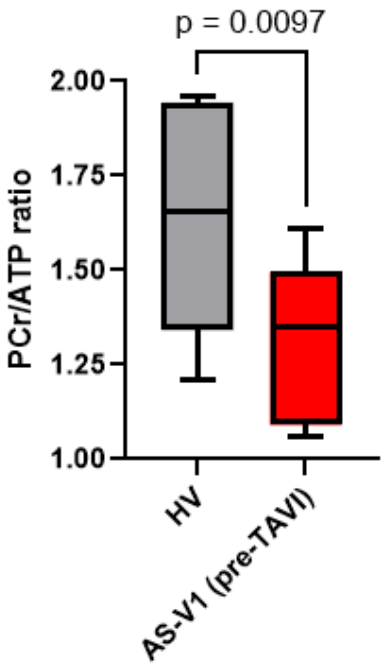

B

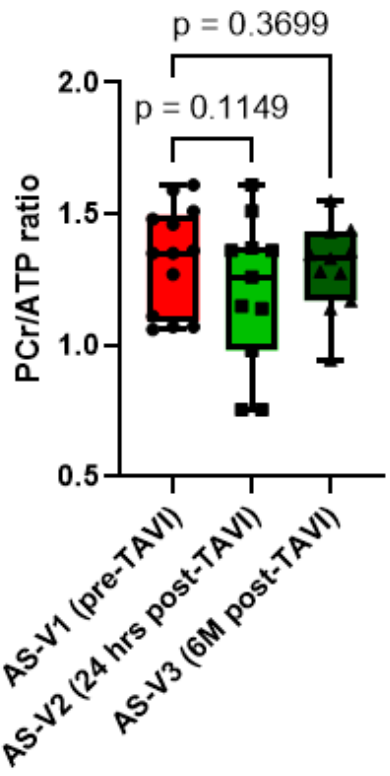

Figure 5.14 HYPER HEART PCr/ATP ratio

AS-V1 (pre-TAVI)= Visit 1 at baseline; AS-V2 (24 hours post-TAVI)= Visit 2 within 24 hours of TAVI; AS-V3 (6M post-TAVI)= Visit 3 six months post TAVI.

5.3.8 Patient Reported Outcomes

5.3.8.1 Toronto Aortic Stenosis Quality of Life Questionnaire

The Toronto Aortic Stenosis Quality of Life Questionnaire was not collected in HV. In participant with AS, the maximum total score of the Toronto aortic stenosis quality of life questionnaire is 112 points. There was a significant improvement of the overall score between V1 (57±20 points) and V2 (86±21 points, p=0.00068) and further improvement at 6-months (V3 101±5 points, p=0.005). (See **Figure 5.15**)

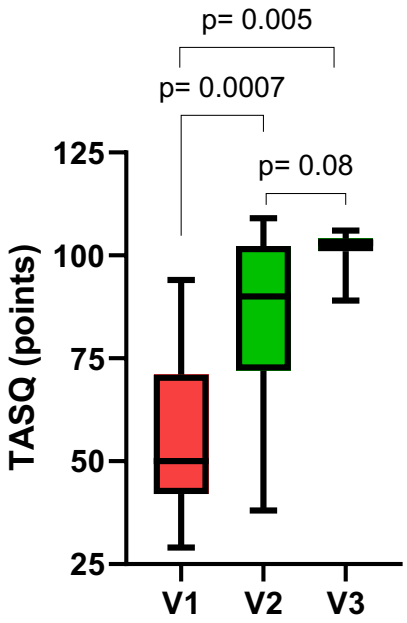

Figure 5.15 HYPER HEART Toronto aortic stenosis quality of life questionnaire (TASQ)

5.3.8.2 New York Heart Association Classification

TAVI led to a significant (p<0.001) improvement in NYHA classification from a mean of NYHA III at V1 to NYHA II at V2 (p=0.002) and NYHA I at V3 (p=0.003. (See **Figure 5.16**)

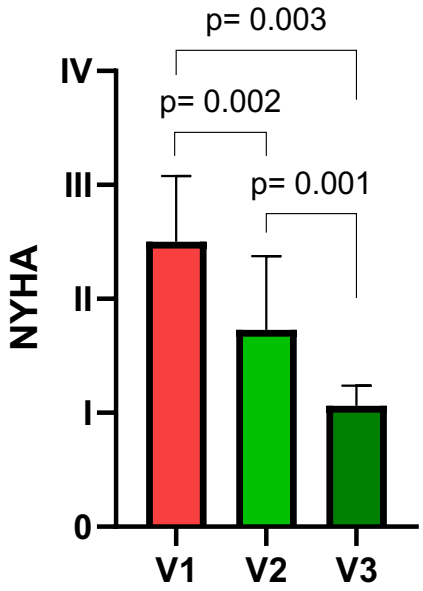

Figure 5.16 HYPER HEART New York Heart Association Classification

5.3.9 Six-Minute Walk Distance

The average 6-MWD in HV was with 553±63 m significantly higher than in AS-V1 (333±71 m, p<0.0001). (see **Figure 5.17A**) There was a significant improvement at 6 months follow up (AS-V3 355±30 m, p=0.0292). (See **Figure 5.17B**)

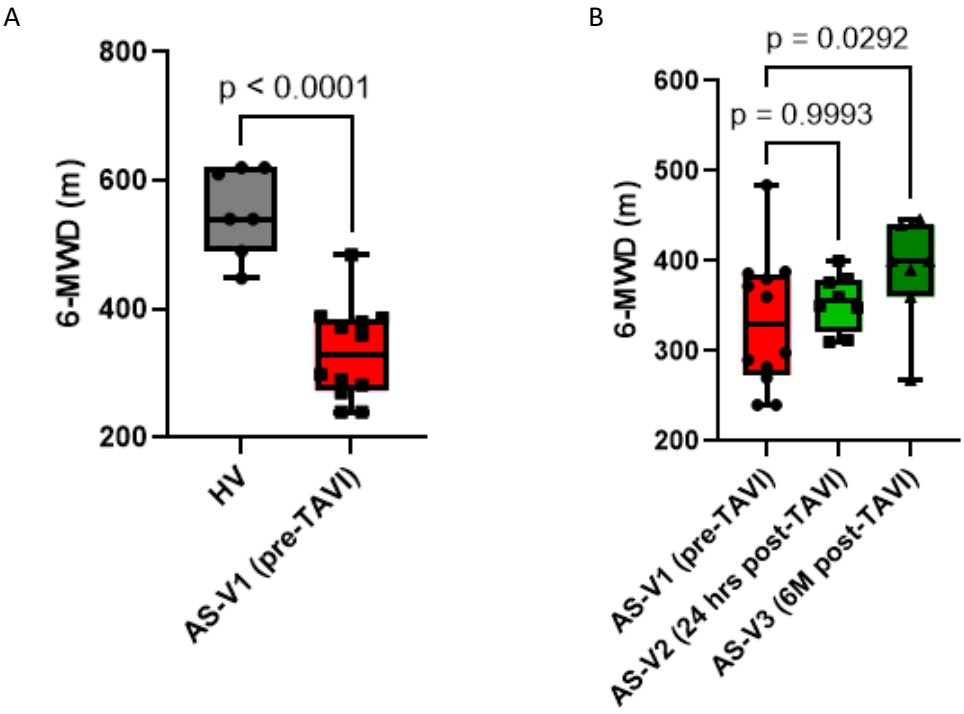

Figure 5.17 HYPER HEART 6-Minute Walk Distance

5.4 Hyperpolarised [1-^{13}C]Pyruvate Magnetic Resonance Spectroscopy

Hyperpolarised MRI/ MRS is a novel imaging technique which allows the visualisation of intricate metabolic pathways. The injection of hyperpolarised [1-^{13}C]pyruvate allows the assessment of intracellular metabolic processes via the quantification of metabolites like [1-^{13}C]pyruvate, [^{13}C]bicarbonate, [1-^{13}C]lactate, and [1-^{13}C]alanine via magnetic resonance spectroscopy. [116, 390].

Quantifying the ratios of Lactate:Pyruvate, Bicarbonate:Pyruvate, Alanine:Pyruvate allows estimation of the enzyme activity of three key enzymes: the pyruvate dehydrogenase complex (PDH), lactate dehydrogenase (LDH), and alanine transaminase (ALT). PDH reflects the uni-directional link between glycolysis and the TCA cycle, LDH converts pyruvate into lactate and vice versa, and ALT converts pyruvate into alanine. (See **Figure 5.18**). The Pyruvate:Bicarbonate ratio indicates PDH flux, and allows the extrapolation of the activity of mitochondrial oxidative metabolism. [391] A high Lactate:Pyruvate ratio may suggest increased anaerobic glycolysis activity [392], as seen in heart failure. [393]

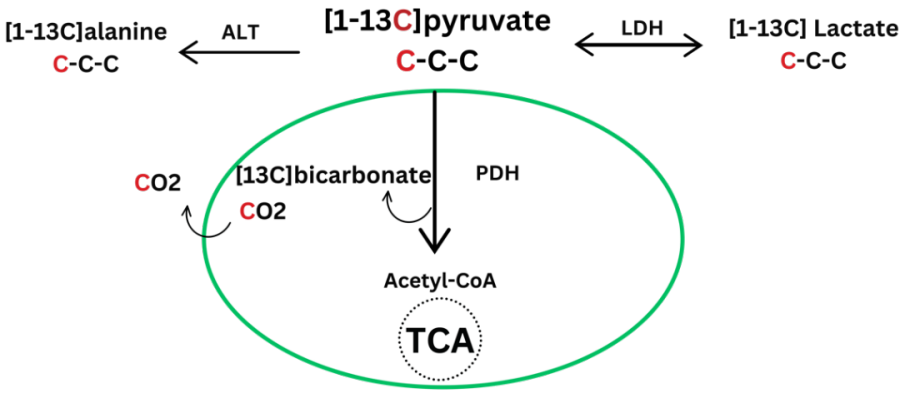

Figure 5.18 HYPER HEART Fate of Pyruvate

ALT= alanine aminotransferase; LDH= lactate dehydrogenase; PDH= pyruvate dehydrogenase; TCA= tricarboxylic acid cycle

5.4.1.1 Dynamic Nuclear Polarization

Compared to conventional MRI methods, hyperpolarised MRS is an advanced technique which offers a significantly better signal-to-noise ratio for molecules like carbon-13 (^{13}C) and allows assessment of cellular metabolism. [116] In this thesis, hyperpolarisation was achieved through a process called Dynamic Nuclear Polarization (DNP) [394], which temporarily increases the signal strength by approximately 10,000 times in comparison to conventional methods. This is achieved by transferring electron spins from an electron paramagnetic agent (EPA) to nuclear spins of a biological molecule like [1-^{13}C]pyruvate via microwave irradiation. [395]. To achieve this, the EPA is combine with [1-^{13}C]pyruvate in a single vial which is then frozen using liquid helium. [396] With the application of a strong magnetic field and irradiation with microwaves at a specific frequency the electrons in the EPA transfer their spin state to the [1-^{13}C]pyruvate. [390] To create an injectable solution, the polarised sample is thawed rapidly, quality checked and injected.

5.4.2 Methods

A hyperpolarised MR experiment can be divided into five parts [96]: (See **Figure 5.19**)

A. **Production of a Sterile Fluid Pathway (SFP)** production which contains 1.47 g of [1-13C]pyruvic acid (Sigma Aldrich, Gillingham, UK) and 15 mM AH111501 (Syncom, Groningen, Netherlands) as the electron paramagnetic agent (EPA), which is stored at -20 °C and thawed on the day of the experiment.

B. **Dynamic Nuclear Polarisation (DNP)** in a General Electric SpinLab system (GE Healthcare, Chicago, USA) is achieved by lowering the pyruvate containing vial into the SpinLab to cool it to very low temperatures (around 1K/-272°C) in the presence of a high magnetic field and irradiating it with microwaves at the correct frequency for approximately 3 hours.

C. **Dissolution** takes place when the hyperpolarised sample is being dissolved with water at 160 degrees and then neutralised with NaOH solution and therefore rapidly heated to physiological temperature for injection.

D. **Injection of Hyperpolarized [1-13C]pyruvate solution** through a venous cannula at a dose of 0.4 ml/kg, performed at a rate of 5 ml/sec, followed by a 25 ml 0.9 % normal saline flush using a MEDRAD power injector system (Bayer, Berlin, Germany).

E. **Spectral acquisition:** Patients were placed in a supine position on the GE Premier (General Electric Healthcare) scanner bed with a two channel transmit, 8 channel surface-receive array (Rapid Biomedical, Rimpar, Germany) place anteriorly and posteriorly on their chest. A 10mm mid-ventricular short axis single slice-selective hyperpolarised spectra were acquired during end expiration using an ECG- trigger at end-diastole. Data was acquired after every heartbeat for up to 4 minutes after the injection.

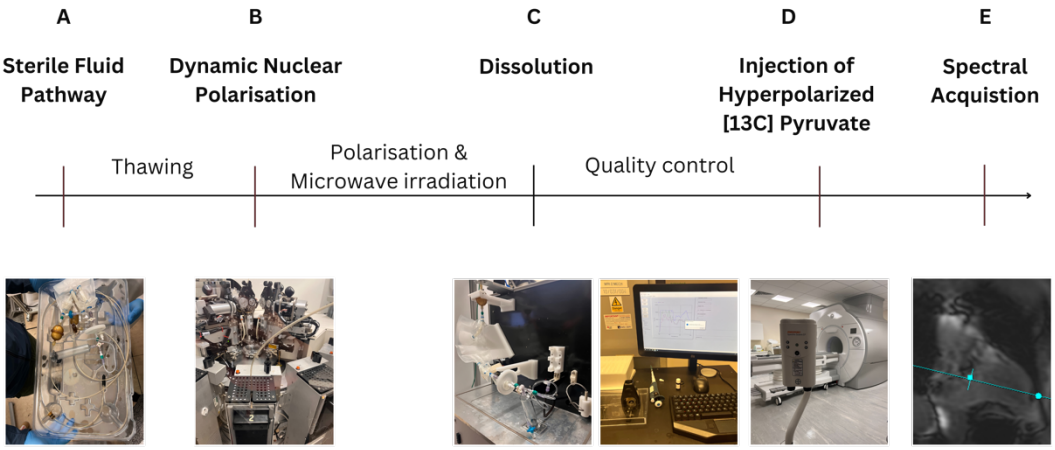

Figure 5.19 HYPER HEART Hyperpolarised Experiment

Spectral analysis was performed using MATLAB and jMRUI (Java-based Magnetic Resonance User Interface). AMARES (Advanced Method for Accurate, Robust, and Efficient Spectral fitting) was used to calculate metabolite-to-pyruvate ratios. (See **Figure 5.21**)

A Summed Spectra

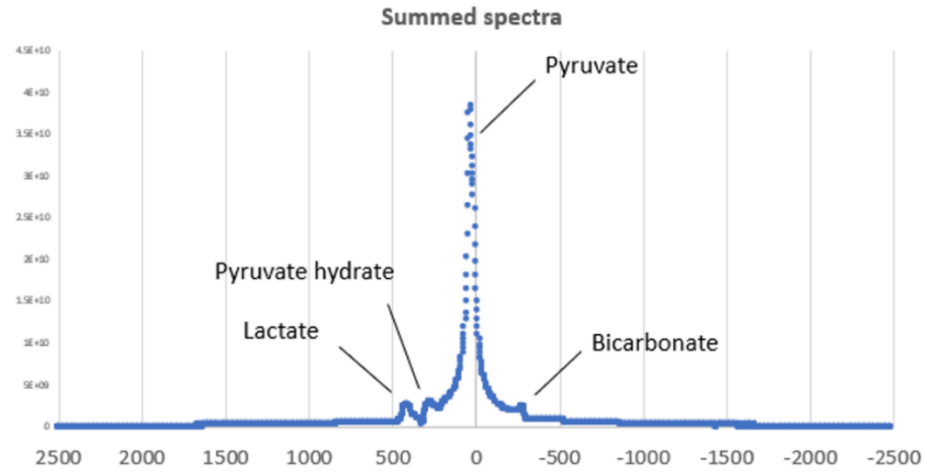

B Waterfall plot

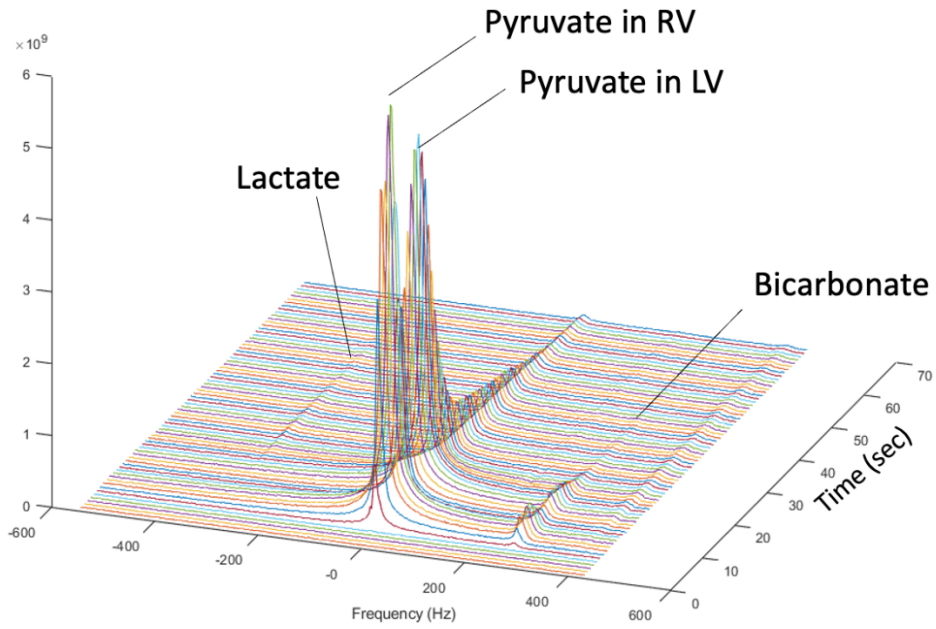

Figure 5.20 HYPER HEART Representative Hyperpolarised Spectra

Display of a representative Hyperpolarised spectrum (A) summed over time; Lactate at 400 Hertz (Hz)), Pyruvate hydrate at 290 Hz, Pyruvate at 0 Hz, Bicarbonate at -300 Hz, (B) displayed as a waterfall plot over time highlighting the two pyruvate speaks (entry of pyruvate into the right and left ventricle) and the metabolism of pyruvate into lactate and bicarbonate

5.4.3 Results

Due to limitation in the supply of the required buffer fluid, hyperpolarised [1-^{13}C]pyruvate MRS examination could only be performed in two patients and two healthy volunteers. Five hyperpolarised experiments were performed in two patients with AS (one pre and post TAVI) and two healthy volunteers. The enzymatic conversion of hyperpolarised [1-^{13}C]pyruvate into [1-^{13}C]lactate (see Lactate:Pyruvate ratio in **Figure 5.21A**) and [^{13}C]bicarbonate (see Bicarbonate:Pyruvate ratio in **Figure 5.21B**) was assessed.

AS1 was a participant with severe AS, heart failure with reduced ejection fraction (LVEF 45%) and increased LV mass (150g) assessed before (AS-V1) and after TAVI (AS1-V2) where ejection fraction remained reduced (LVEF 40%). The high Lactate:Pyruvate ratio (0.10) (See **Figure 5.21A**) normalises at V2 (0.05) to a level seen in the healthy volunteers (0.045). Whereas the Bicarbonate:Pyruvate ratio remained high (0.03) (See **Figure 5.21B**) at both time points and above the level seem in HV (0.015 & 0.023).

AS4 was a participant with severe AS and heart failure with preserved ejection fraction (LVEF 61%) and lower LV mass (129 g) who was assessed prior to TAVI only (AS4-V1). The Lactate:Pyruvate ratio prior to TAVI (0.03) was comparable of that in HV (0.045). (See **Figure 5.21A**) However, there was a marked difference in Bicarbonate:Pyruvate ratio (0.006) in comparison to both AS1 (0.034) and healthy volunteers (0.019). (See **Figure 5.21B**)

A

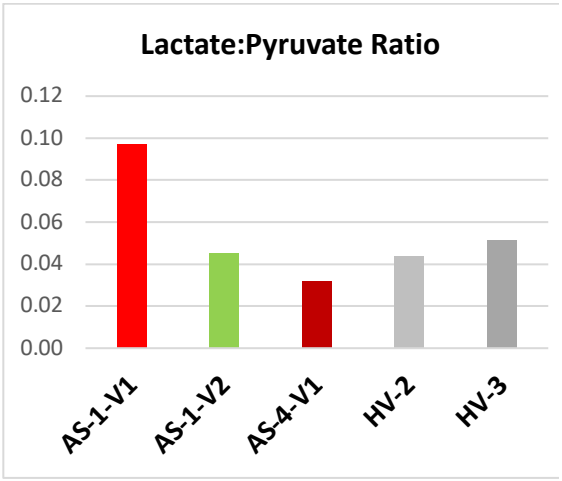

B

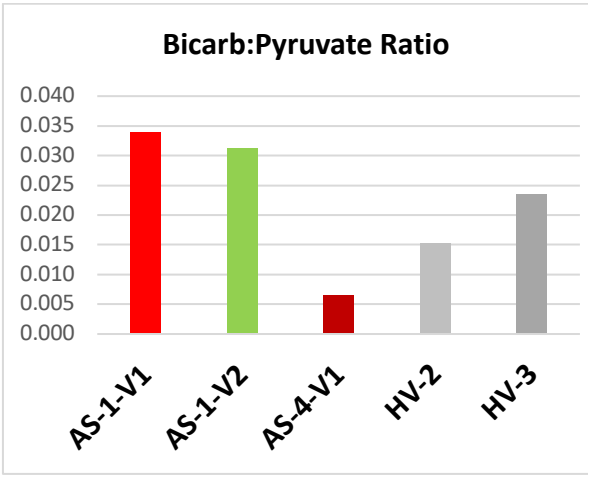

Figure 5.21 HYPER HEART Conversion of hyperpolarised [1-^{13}C]pyruvate

AS-1-V1= participant with aortic stenosis number 1 (AS1) at the baseline visit (V1); AS-1-V2= participant with aortic stenosis number 1 (AS1) at first follow up visit 24 hours post valve implantation (V2); AS-4-V1= Participant with aortic stenosis number 4 (AS4) at baseline visit (V1); HV-2= Healthy volunteer number 2; HV-3= Healthy volunteer number 3

5.5 Discussion

The **HYPER HEART** study demonstrated the detrimental effects of pressure load on both cardiac remodelling and cardiac energetics and attempted to examine the link between structural and metabolic recovery with pressure removal. As previously shown in animal [87] and humans studies [41, 81] [79], the pressure loaded heart displays energetic impairment. However, the association between structural [397] and metabolic modulation is less well understood [79]. As evidenced in earlier studies [359] fibrosis and LVH were significantly increased in severe AS and in this study gradual regression over the 6 months after TAVI was demonstrated. However, in contrast to previous studies [84], a positive association between LVH regression and PCr/ATP could not be shown. A significant improvement in clinical parameters and patient reported outcomes was seen over time confirming the link between regression of LVH with improved outcomes. [398] It has been proposed that the mechanism of energetic impairment in the pressure loaded heart is due to the uncoupling of glycolysis from glucose oxidation. [87] The **HYPER HEART** study was the first study attempting to examine this metabolic imbalance with the assessment of cardiac energy state (PCr/ATP) and PDH flux with and without pressure load. The results presented here support the need for larger studies to assess cardiac metabolism in the pressure overloaded heart and its association with LVH. This will facilitate phenotyping of patients with AS and aid prognostication in the future, which might be most relevant in moderate AS or asymptomatic severe AS.

5.5.1 Participant Recruitment and Baseline Characteristics

The study cohort was representative of the local population referred to the TAVI service, even though there was a lack of representation of ethnic minorities. In contrast to most studies [399], women and men were equality represented. In line with the guidelines for aortic valve replacement [349], the average age was well above 75, which is often the cut off between TAVI and surgical aortic valve replacement. The exclusion criteria limited the enrolment of participants with T2DM, therefore it is not surprising that the BMI was low in both groups and numbers of comorbidities

and concomitant medication were low. Despite the well-known pathophysiological connection between hypertension and AS [400] the participants without cardiovascular disease had significantly higher blood pressure than the AS group raising the suspicion of undiagnosed and undertreated hypertension in this cohort of participants.

5.5.2 Metabolic Adaptation in Severe AS and Left Ventricular Hypertrophy

Aortic stenosis results in cardiac remodelling (LVH), changes in cardiac metabolism (PCr/ATP), and ultimately HF. [77] In line with previous studies, we could confirm a significant reduction in PCr/ATP in participants with AS and LVH [81] in comparison to HV. The mechanism between pressure loading and impaired cardiac energetics measured by PCr/ATP is less well understood and is likely driven by a combination of structural and metabolic adaptations highlighted in the following section. Energy demand increased with increasing LVH [342] and in combination with myocardial fibrosis leads to reduced oxygen supply [401], which may explain the shift in myocardial metabolism away from glucose and fatty acid oxidation towards glycolysis [77] leading to PCr/ATP reduction in AS. In addition, LVH seen in this patient cohort may further contribute to lower mitochondrial density, disorganisation of mitochondria in myofibrils [402] in the hypertrophied muscle, which has been associated with impairment in mitochondrial function [401] contributing to energetic deficit. Furthermore, a reduction in creatine availability [403] and reduced CK flux [203, 342] may be a distinct contributor to energetic impairment and a marker of progression from healthy, to hypertrophied and failing heart [403]. Highlighting a reduction in PCr/ATP in participants with AS and LVH in comparison to HV represents only one marker of the cardiac energetic state and does not capture the totality of the complex metabolic remodelling in the pressure loaded hearts.

In contrast to previous studies [84], removal of pressure load with TAVI replacement did not lead to an overall change in PCr/ATP over time, despite significant regression of LVH and fibrosis. Despite

imaging evidence of early structural remodelling within 24 hours of valve implantation, in this study the adverse metabolic adaptations persisted over the 6 months of follow up. The short follow up period may be the key difference to previous studies which demonstrated metabolic recovery after valve replacement at between six [316], ten [88], and twelve [84] months. In the addition to the timing of follow up, the duration of pressure load prior to TAVI may have significantly impacted the ability of mitochondrial to recovery. [404] This recovery involves multiple factors including persistent structural and functional changes of the mitochondria [405], ongoing enzymatic changes limiting oxidative metabolism [406], and irreversible damage to the CK system [27] by chronically increased pressure load.

Regression of late gadolinium enhancement over the six months follow up was particularly notable, which reflects reversal of pressure loading, but also potential reversal of extracellular matrix expansion. Mechanistically, regression of late gadolinium enhancement may reflect a reduction in diffuse interstitial fibrosis rather than established replacement fibrosis. [407]

In this study, the profound immediate haemodynamic and clinical improvement was not replicated by short- or longer-term metabolic improvement. This highlights the complexity of linking symptom burden with structural and metabolic measures. PCr/ATP is influenced by creatine supply and Creatine Kinase (CK) activity and may therefore not be the best marker of metabolic performance in isolation. [401] In addition PCr/ATP levels might not correlate with symptoms similar to ejection fraction values, which often don't reflect patient's symptoms. [408] In addition, the significant reduction in symptom burden has likely impacted on exercise frequency and intensity, affecting not only energetic demand but also leading to repair and synthesis of mitochondria [409], which the simple PCr/ATP ratio does not sufficiently capture.

A more sophisticated method to assess metabolic modulation in pressure load is hyperpolarised MRS which, due to the complexity of the experiment, was only performed in selected cases. In the

participant with AS, LVH and reduced EF an elevated Lactate:Pyruvate ratio prior to TAVI indicated increased anaerobic glycolysis, consistent with the metabolic profile of hypertrophied and failing myocardium. [262] The normalisation of Lactate:Pyruvate ratio with the reduction of afterload (post TAVI) to levels seen in HV may suggests a possible normalisation of metabolism over time. In the second participant with severe AS, mild LVH and preserved ejection fraction, Lactate:Pyruvate ratio was comparable to HV. However, it cannot be concluded that this is solely due to reduced metabolic impairment. [410]

The Bicarbonate:Pyruvate ratio reflects PDH flux [116] and the degree of oxidative metabolism, which are often impaired in pathologies like heart failure or hypertrophy. [411] However, in the participant with reduced ejection fraction Bicarbonate:Pyruvate ratio was persistently high raising the possibility of compensatory upregulation to maintain energy supply. However, the contrary was seen in the participant with preserved EF limiting the ability to draw conclusion from this small data set.

In conclusion, pressure loading results in significant metabolic alterations including reduced PCr/ATP and changes in PDH flux in comparison to healthy volunteers. However, PCr/ATP may not be the most accurate marker to display the beneficial metabolic remodelling after valve implantation to reflect the significant haemodynamic, structural and clinical improvement.

5.5.3 Changes in Clinical Outcome

Severe AS is associated with a significant reduction in quality of life [412] and duration [413], with overall five-year survival for symptomatic severe aortic stenosis of less than 12% and a mean survival of less than two years. Despite the significant improvement in patient reported outcomes within 24 hours of TAVI, the objectively assessed exercise capacity did not follow to the same degree of improvement suggesting a large contribution from the emotional impact of TAVI. [124]

However, in line with other studies [412], there was a consistent improvement in the TASQ score at 6-months follow up with six participants scoring above 100/112 points. Participants in the HYPER-HEART study had better exercise capacity than those participants initially enrolled in the PARTNER trial [414] and, in contrast to the PARTNER trial, demonstrated a significant improvement in the 6-MWD at 6 months. However, in this study, patients with AS and subsequent TAVI did not return to an exercise capacity seen in HV of a similar age.

5.5.4 Limitations

This prospective, observational pilot study highlights the role of advanced cardiac MR imaging and spectroscopy in the assessment of AS severity and associated myocardial remodelling. It showcases the opportunities provided by metabolic phenotyping; however, it was limited by a small sample size and short duration of follow up, which might have impacted the ability to demonstrate metabolic recovery after valve replacement.

Study recruitment took place from the OUH TAVI clinic providing care across Oxfordshire and beyond. Despite this ethnic minorities were not represented, which is a common problem in cardiovascular trials [330] and clinical practise [415]. The study was exposed to selection bias as only patients without metabolic comorbidities were enrolled reflecting those at a milder spectrum of disease with limited frailty and results cannot be extrapolated to patients with diabetes.[89] PCr/ATP and PDH are two of many markers of energetic state and performance [100], however they might not capture the integrate interplay between mitochondrial structure, function and density and myocardial performance in the pressure loaded heart. [48]

Furthermore, the lack of significant improvement in NT-proBNP despite haemodynamic unloading suggest that a subset of patients may have coexisting myocardial pathology such as transthyretin amyloidosis, which has been reported around 8% of elderly TAVI recipients [416], and is known to blunt LV mass regression, limit biomarker improvement and affect outcomes [417].

5.5.5 Future Directions

Aortic valve replacement is an established treatment for severe symptomatic AS [349] and recent studies [418] even show a benefit in asymptomatic AS. CMR will become a cornerstone in the management of patients with AS to identify precise AS severity and the degree of myocardial remodelling [419] to risk stratify patients with asymptomatic AS and to inform management in patients with moderate to severe AS. Larger studies might be able to establish a link between reverse remodelling and associated changes in energy state, which might aid the phenotyping of asymptomatic patients with AS. Pressure overload induced alteration in metabolism proceed structural changes and detailed understanding of the shift in metabolic pathways for example by the assessment of PDH flux will inform potential targets for drug treatment to either prevent progression of cardiac remodelling or aid recovery post valve intervention.

5.5.6 Conclusion

In this trial, participants with severe AS, LVH and preserved EF with an indication for TAVI were enrolled. Participants experienced exercise intolerance and reduced QoL in comparison to HV of a similar age. The study highlighted the central role of CMR in the assessment of patients with AS, which allows detailed assessment of structural changes with prognostic significance. The hearts of patients with AS were characterised by profound haemodynamic, structural and metabolic changes. This study confirmed the beneficial effects of TAVI on clinical, haemodynamic and structural remodelling, however the link to metabolic remodelling was not established. Larger studies with prolonged follow up and focus on hyperpolarised MRI for the detailed assessment of metabolism are required to aid the understanding between structural and metabolic remodelling in the pressure loaded heart.

6 Conclusion

6.1 General Conclusion and Future Directions

In this thesis I have investigated skeletal and cardiac muscle metabolism in patients with HF across the spectrum of EF and various aetiologies testing three distinct interventions: i.v. FCM in reduced EF (**IRON HEART, Chapter 3**), Ninerafaxstat in preserved EF (**DICE, Chapter 4**), and TAVI in severe AS and preserved EF (**HYPER HEART, Chapter 5**). I performed two pilot studies and one phase 2a clinical trial where I demonstrated how state-of-the-art MR imaging and spectroscopy techniques can aid the diagnosis and monitoring of treatment response in patients with HF. I have showcased how advanced multi-nuclear (^{31}P-, ^{1}H-, ^{13}C-) magnetic resonance spectroscopy can seamlessly be integrated into diagnosis, management and most important aid drug development in these cohorts.

6.1.1 General Conclusion

In the following I summarise the key findings of each study:

In a prospective observational pilot study (**IRON HEART**, **Chapter 3**) I enrolled patients with non-ischaemic cardiomyopathy, and reduced EF and ID and assessed the potential benefits of i.v. FCM on skeletal and cardiac muscle function and metabolism. This study showed that i.v. FCM is intrinsically involved in cardiac and skeletal muscle function. It reinforces the role of iron in HF and its link to exercise ability and symptoms supporting its ongoing use in clinical practise and assessment in trials. Furthermore, this study highlighted the importance of linking skeletal muscle function to day-to day symptom burden experiences in patients with HF. This study contributes to an understudied topic raising awareness of the interplay between skeletal and cardiac muscle on metabolism and its potential target for treatment strategies in the future. Addressing the

methodological challenges highlighted in this study will further enhance our understanding of cardiac and skeletal muscle dysfunction in cardiovascular disease.

Heart failure with preserved ejection fraction is under-diagnosed, under-studied and under-treated and with the rise in obesity and diabetes will become an increasing burden to patients and health care providers. Beyond the treatment of comorbidities, patients with metabolic HFpEF have limited treatment options. The phase 2a clinical drug trial (**DICE**, **Chapter 4**), aimed to assess the effects of the partial fatty acid oxidation inhibitor, Ninerafaxstat, in patients with HFpEF, obesity and T2DM. After three months of treatment, there was a significant improvement in cardiac energetics which were accompanied by improvements in exercise capacity and reductions in symptoms. In addition, it demonstrated that Ninerafaxstat is safely tolerated in this cohort and might be beneficial in the treatment of cardiometabolic heart disease. Current treatment strategies in HFpEF don't target energy metabolism and cardiac mitotropes like Ninerafaxstat may be the first attempt at modulating substrate utilisation and cardiac performance in metabolic HFpEF.

Aortic stenosis has often been considered an isolated valve disease, however, with the advancement of imaging modalities and their use in clinical trials, the intricate relationship between pressure load, cardiac remodelling, and metabolism is increasingly recognised. In a third prospective, observational pilot study (**HYPER HEART**, **Chapter 5**), I aimed to demonstrate the link between different pressure loading conditions (severe AS versus TAVI) on cardiac function and metabolism. A comprehensive magnetic resonance imaging and multinuclear (^{31}P, ^{1}H, ^{13}C) spectroscopy protocol was performed before and after TAVI. While a direct link between structural recovery and metabolic adaptation remains to be established, the study highlighted the central role of CMR in the assessment of patients with AS. Examining the prognostic significance between metabolic and structural changes will be able to aid clinical decision making, particularly in patients with asymptomatic severe aortic stenosis who currently receive surveillance.

6.1.2 Future Directions

Cardio-metabolic research has been performed for decades but few clinical trials have utilised multi-nuclear spectroscopy of cardiac and skeletal muscle to aid drug development and utilisation. This might be partially driven by the expertise required to perform those trials but also by the associated cost of advanced imaging trials. However, the following three aspects might allude to the benefits of advanced cardiac MR imaging and spectroscopy in the diagnosis, monitoring and treatment of patients with cardiovascular disease and highlight its potential to lay the foundation for the development of cardiac mitotropes, drugs improving myocardial energetics. The combination of MR imaging and spectroscopy can lead the way in precision medicine, integrating genotyping into standard clinical care. It makes three key contributions to patient care.

Firstly, it facilitates mechanistic drug trials like DICE to further the development of cardiac mitotropes in cardiometabolic disease like HFpEF or in other disease areas with limited treatment options like hypertrophic cardiomyopathy.

Secondly, multi-nuclear MR has the potential to refine patients' characteristics offering a tool for risk stratification. In patients with iron deficiency, it may allow better classification of patients based on the severity of iron deficiency, the impact of anaemia on skeletal and cardiac muscle function and the characterisation of 'super responders' enabling more personalised treatment and improving outcomes. In patients with HFpEF comprehensive multi-nuclear CMR will aid differentiation of the metabolic phenotypes, their prognostic features and allow personalised drug development. In valve disease, it can be used to identify early metabolic remodelling before structural remodelling. This will inform risk stratification, time of intervention and treatment options to aid recovery post valve intervention.

Thirdly, hyperpolarised MR imaging and spectroscopy enables detailed assessment of dynamic metabolic pathways. It is a true bridge from bench to bedside providing a powerful tool to unravel the link between structural cardiac abnormality and metabolic alterations both in cardiac and skeletal muscle, which to date has been largely studied in preclinical models.

A compelling future direction is the application of multinuclear spectroscopy and advanced CMR to the population of patients with coexisting aortic stenosis and transthyretin amyloidosis. The increasing recognition of amyloid infiltration in patients with aortic stenosis undergoing TAVI raises the possibility that metabolic abnormalities in AS may be driven not only by pressure loading conditions but also by myocardial infiltration of amyloid fibrils. A future programme of studies could randomise patients with moderate to severe aortic stenosis and transthyretin amyloidosis cardiomyopathy to receive medical treatment with for example Tafamidis either pre-TAVI (during moderate aortic stenosis) versus post-TAVI, enabling mechanistic assessment of the interaction between amyloid stabilisation and pressure loading and removal. Such study would meaningfully advance the role of metabolic imaging in concomitant aortic stenosis and amyloidosis phenotyping, inform best-practice treatment algorithms in older TAVI candidates, and clarify whether metabolic recovery after valve replacement is limited by, and potentially modifiable through, the amyloid disease process.

This direction reflects the broader vision that advanced cardiac magnetic resonance imaging and spectroscopy techniques will transition from specialist research tools to integral components of personalised medicine in the future, informing prevention, diagnosis, treatment and drug development in the cardiology of the future.

References

1. Havranek, E.P., et al., *Social Determinants of Risk and Outcomes for Cardiovascular Disease.* Circulation, 2015. **132**(9): p. 873-898.
2. Chioncel, O., et al., *Acute heart failure and valvular heart disease: A scientific statement of the Heart Failure Association, the Association for Acute CardioVascular Care and the European Association of Percutaneous Cardiovascular Interventions of the European Society of Cardiology.* European Journal of Heart Failure, 2023. **25**(7): p. 1025-1048.
3. McDonagh, T.A., et al., *2021 ESC Guidelines for the diagnosis and treatment of acute and chronic heart failure: Developed by the Task Force for the diagnosis and treatment of acute and chronic heart failure of the European Society of Cardiology (ESC) With the special contribution of the Heart Failure Association (HFA) of the ESC.* European Heart Journal, 2021. **42**(36): p. 3599-3726.
4. Shah, S.J., et al., *Phenotype-Specific Treatment of Heart Failure With Preserved Ejection Fraction.* Circulation, 2016. **134**(1): p. 73-90.
5. Worster, A., et al., *Diagnostic accuracy of BNP and NT-proBNP in patients presenting to acute care settings with dyspnea: A systematic review.* Clinical Biochemistry, 2008. **41**(4): p. 250-259.
6. McDonagh, T.A., et al., *2023 Focused Update of the 2021 ESC Guidelines for the diagnosis and treatment of acute and chronic heart failure.* Eur Heart J, 2023. **44**(37): p. 3627-3639.
7. Schwinger, R.H.G., *Pathophysiology of heart failure.* Cardiovasc Diagn Ther, 2021. **11**(1): p. 263-276.
8. Ng, S.M., S. Neubauer, and O.J. Rider, *Myocardial Metabolism in Heart Failure.* Curr Heart Fail Rep, 2023. **20**(1): p. 63-75.
9. Judge, A. and M.S. Dodd, *Metabolism.* Essays Biochem, 2020. **64**(4): p. 607-647.
10. Al-Khami, A.A., P.C. Rodriguez, and A.C. Ochoa, *Energy metabolic pathways control the fate and function of myeloid immune cells.* J Leukoc Biol, 2017. **102**(2): p. 369-380.
11. Wilson, B.A., J.C. Schisler, and M.S. Willis, *Sir Hans Adolf Krebs: Architect of Metabolic Cycles.* Laboratory Medicine, 2010. **41**(6): p. 377-380.
12. Koppenol, W.H., P.L. Bounds, and C.V. Dang, *Otto Warburg's contributions to current concepts of cancer metabolism.* Nat Rev Cancer, 2011. **11**(5): p. 325-37.
13. <https://www.nobelprize.org/prizes/medicine/1953/lipmann/biographical/, F.L.B.N.o.N.P.O.F.O.
14. <https://www.nobelprize.org/prizes/medicine/1953/krebs/lecture/, H.K.N.L.N.o.N.P.O.F.O.
15. *Prof. A. von Szent-Györgyi: Nobel Prize for Medicine.* Nature, 1937. **140**(3549): p. 798-798.
16. Hütter, J.F., et al., *Inhibition of fatty acid oxidation and decrease of oxygen consumption of working rat heart by 4-bromocrotonic acid.* Journal of Molecular and Cellular Cardiology, 1984. **16**(1): p. 105-108.
17. Galis, P., et al., *Update on clinical and experimental management of diabetic cardiomyopathy: addressing current and future therapy.* Front Endocrinol (Lausanne), 2024. **15**: p. 1451100.
18. Lopaschuk, G.D., et al., *Beneficial effects of trimetazidine in ex vivo working ischemic hearts are due to a stimulation of glucose oxidation secondary to inhibition of long-chain 3-ketoacyl coenzyme a thiolase.* Circ Res, 2003. **93**(3): p. e33-7.
19. Read, A.D., et al., *Mitochondrial iron-sulfur clusters: Structure, function, and an emerging role in vascular biology.* Redox Biol, 2021. **47**: p. 102164.
20. Xian, H. and Y.-C. Liou, *Functions of outer mitochondrial membrane proteins: mediating the crosstalk between mitochondrial dynamics and mitophagy.* Cell Death & Differentiation, 2021. **28**(3): p. 827-842.

21. Gabr, R.E., et al., *High-energy phosphate transfer in human muscle: diffusion of phosphocreatine.* Am J Physiol Cell Physiol, 2011. **301**(1): p. C234-41.
22. Salin, K., et al., *Variation in the link between oxygen consumption and ATP production, and its relevance for animal performance.* Proc Biol Sci, 2015. **282**(1812): p. 20151028.
23. Burrage, M.K., et al., *Energetic Basis for Exercise-Induced Pulmonary Congestion in Heart Failure With Preserved Ejection Fraction.* Circulation, 2021. **144**(21): p. 1664-1678.
24. Bhatt, K.N. and J. Butler, *Myocardial Energetics and Heart Failure: a Review of Recent Therapeutic Trials.* Current Heart Failure Reports, 2018. **15**(3): p. 191-197.
25. S., N., *The failing heart—an engine out of fuel.* N Engl J Med, 2007. **356**(11): p. 1140-51.
26. Bonilla, D.A., et al., *Metabolic Basis of Creatine in Health and Disease: A Bioinformatics-Assisted Review.* Nutrients, 2021. **13**(4).
27. Neubauer, S., *The Failing Heart — An Engine Out of Fuel.* New England Journal of Medicine, 2007. **356**(11): p. 1140-1151.
28. Neubauer, S., et al., *Myocardial Phosphocreatine-to-ATP Ratio Is a Predictor of Mortality in Patients With Dilated Cardiomyopathy.* Circulation, 1997. **96**(7): p. 2190-2196.
29. Ranjbarvaziri, S., et al., *Altered Cardiac Energetics and Mitochondrial Dysfunction in Hypertrophic Cardiomyopathy.* Circulation, 2021. **144**(21): p. 1714-1731.
30. Henry, J.A., L.S. Couch, and O.J. Rider, *Myocardial Metabolism in Heart Failure with Preserved Ejection Fraction.* Journal of Clinical Medicine, 2024. **13**(5): p. 1195.
31. Henry, J.A., et al., *143 Measuring pcr/atp as a marker of myocardial energetics across the spectrum of metabolic cardiac disease.* Heart, 2022. **108**(Suppl 1): p. A109-A110.
32. Morrow, D.A. and M.M. Givertz, *Modulation of Myocardial Energetics.* Circulation, 2005. **112**(21): p. 3218-3221.
33. Ritterhoff, J. and R. Tian, *Metabolism in cardiomyopathy: every substrate matters.* Cardiovascular Research, 2017. **113**(4): p. 411-421.
34. Lopaschuk, G.D., et al., *Myocardial Fatty Acid Metabolism in Health and Disease.* Physiological Reviews, 2010. **90**(1): p. 207-258.
35. De Jong, K.A. and G.D. Lopaschuk, *Complex Energy Metabolic Changes in Heart Failure With Preserved Ejection Fraction and Heart Failure With Reduced Ejection Fraction.* Canadian Journal of Cardiology, 2017. **33**(7): p. 860-871.
36. Scott, W., J. Stevens, and S.A. Binder–Macleod, *Human Skeletal Muscle Fiber Type Classifications.* Physical Therapy, 2001. **81**(11): p. 1810-1816.
37. Argilés, J.M., et al., *Skeletal Muscle Regulates Metabolism via Interorgan Crosstalk: Roles in Health and Disease.* Journal of the American Medical Directors Association, 2016. **17**(9): p. 789-796.
38. Stephens, F.B., D. Constantin-Teodosiu, and P.L. Greenhaff, *New insights concerning the role of carnitine in the regulation of fuel metabolism in skeletal muscle.* J Physiol, 2007. **581**(Pt 2): p. 431-44.
39. Randle, P.J., et al., *THE GLUCOSE FATTY-ACID CYCLE ITS ROLE IN INSULIN SENSITIVITY AND THE METABOLIC DISTURBANCES OF DIABETES MELLITUS.* The Lancet, 1963. **281**(7285): p. 785-789.
40. Neubauer, S., et al., *Contributions of 31P-magnetic resonance spectroscopy to the understanding of dilated heart muscle disease.* Eur Heart J, 1995. **16 Suppl O**: p. 115-8.
41. Beer, M., et al., *Absolute concentrations of high-energy phosphate metabolites in normal, hypertrophied, and failing human myocardium measured noninvasively with 31P-SLOOP magnetic resonance spectroscopy.* Journal of the American College of Cardiology, 2002. **40**(7): p. 1267-1274.
42. Rosano, G.M. and C. Vitale, *Metabolic Modulation of Cardiac Metabolism in Heart Failure.* Card Fail Rev, 2018. **4**(2): p. 99-103.

43. Taylor, M., et al., *An evaluation of myocardial fatty acid and glucose uptake using PET with [18F]fluoro-6-thia-heptadecanoic acid and [18F]FDG in Patients with Congestive Heart Failure.* J Nucl Med, 2001. **42**(1): p. 55-62.
44. Zhu, N., et al., *Plasma levels of free fatty acid differ in patients with left ventricular preserved, mid-range, and reduced ejection fraction.* BMC Cardiovasc Disord, 2018. **18**(1): p. 104.
45. Flam, E., et al., *Integrated landscape of cardiac metabolism in end-stage human nonischemic dilated cardiomyopathy.* Nature Cardiovascular Research, 2022. **1**(9): p. 817-829.
46. Warren, J.S., et al., *Metabolic reprogramming via PPARα signaling in cardiac hypertrophy and failure: From metabolomics to epigenetics.* Am J Physiol Heart Circ Physiol, 2017. **313**(3): p. H584-h596.
47. Ramaccini, D., et al., *Mitochondrial Function and Dysfunction in Dilated Cardiomyopathy.* Front Cell Dev Biol, 2020. **8**: p. 624216.
48. Hinton, A., Jr., et al., *Mitochondrial Structure and Function in Human Heart Failure.* Circ Res, 2024. **135**(2): p. 372-396.
49. Bornstein, M.R., R. Tian, and Z. Arany, *Human cardiac metabolism.* Cell Metabolism, 2024. **36**(7): p. 1456-1481.
50. Hinton, A., et al., *Mitochondrial Structure and Function in Human Heart Failure.* Circulation Research, 2024. **135**(2): p. 372-396.
51. Alnuwaysir RI, H.M., van Veldhuisen DJ, van der Meer P, et al. , *Iron deficiency in heart failure: mechanisms and pathophysiology. .* Journal of Clinical Medicine, 2021. **11**(1): p. 125.
52. Oexle H, G.E., Weiss G. , *Iron-dependent changes in cellular energy metabolism: influence on citric acid cycle and oxidative phosphorylation. .* Biochimica et Biophysica Acta (BBA)-Bioenergetics., 1999. **1413**(3): p. 99-107.
53. Melenovsky, V., et al., *Myocardial iron content and mitochondrial function in human heart failure: a direct tissue analysis.* Eur J Heart Fail, 2017. **19**(4): p. 522-530.
54. Oexle, H., E. Gnaiger, and G. Weiss, *Iron-dependent changes in cellular energy metabolism: influence on citric acid cycle and oxidative phosphorylation.* Biochimica et Biophysica Acta (BBA) - Bioenergetics, 1999. **1413**(3): p. 99-107.
55. Papalia, F., et al., *Cardiac energetics in patients with chronic heart failure and iron deficiency: an in-vivo (31) P magnetic resonance spectroscopy study.* Eur J Heart Fail, 2022. **24**(4): p. 716-723.
56. Menon, R.G., et al., *Dynamic 31P-MRI and 31P-MRS of lower leg muscles in heart failure patients.* Scientific Reports, 2021. **11**(1): p. 7412.
57. Bolger, A.P., et al., *Intravenous iron alone for the treatment of anemia in patients with chronic heart failure.* J Am Coll Cardiol, 2006. **48**(6): p. 1225-7.
58. Anker, S.D., et al., *Ferric carboxymaltose in patients with heart failure and iron deficiency.* N Engl J Med, 2009. **361**(25): p. 2436-48.
59. Klip, I.T., et al., *Iron deficiency in chronic heart failure: an international pooled analysis.* American heart journal, 2013. **165**(4): p. 575-582. e3.
60. Ponikowski, P., et al., *Beneficial effects of long-term intravenous iron therapy with ferric carboxymaltose in patients with symptomatic heart failure and iron deficiency†.* Eur Heart J, 2015. **36**(11): p. 657-68.
61. Piotr Ponikowski, A.A.V., Stefan D Anker, Héctor Bueno, John G F Cleland, Andrew J S Coats, Volkmar Falk, José Ramón González-Juanatey, Veli-Pekka Harjola, Ewa A Jankowska, Mariell Jessup, Cecilia Linde, Petros Nihoyannopoulos, John T Parissis, Burkert Pieske, Jillian P Riley, Giuseppe M C Rosano, Luis M Ruilope, Frank Ruschitzka, Frans H Rutten, Peter van der Meer, ESC Scientific Document Group, 2016 ESC Guidelines for the diagnosis and treatment of acute and chronic heart failure: The Task Force for the diagnosis and treatment of acute

and chronic heart failure of the European Society of Cardiology (ESC), *2016 ESC Guidelines for the diagnosis and treatment of acute and chronic heart failure: The Task Force for the diagnosis and treatment of acute and chronic heart failure of the European Society of Cardiology (ESC)*

Developed with the special contribution of the Heart Failure Association (HFA) of the ESC. European Heart Journal, 2016. **37**(27): p. 2129-2200.

62. van Veldhuisen, D.J., et al., *Effect of Ferric Carboxymaltose on Exercise Capacity in Patients With Chronic Heart Failure and Iron Deficiency.* Circulation, 2017. **136**(15): p. 1374-1383.
63. Ponikowski P, K.B., Anker SD, McDonagh T, Dorobantu M, et. al., *Ferric carboxymaltose for iron deficiency at discharge after acute heart failure: a multicentre, double-blind, randomised, controlled trial. .* The Lancet, 2020. **396**(10266): p. 1895-904.
64. Kalra PR, C.J., Petrie MC, Thomson EA, Kalra PA, et. al. and p. Intravenous ferric derisomaltose in patients with heart failure and iron deficiency in the UK (IRONMAN): an investigator-initiated, randomised, open-label, blinded-endpoint trial. The Lancet. 2022 Nov 5., *Intravenous ferric derisomaltose in patients with heart failure and iron deficiency in the UK (IRONMAN): an investigator-initiated, prospective, randomised, open-label, blinded-endpoint trial.* The Lancet, 2022.
65. Mentz, R.J., et al., *Ferric Carboxymaltose in Heart Failure with Iron Deficiency.* New England Journal of Medicine, 2023. **389**(11): p. 975-986.
66. Drozd, M.D., et al., *Intravenous iron supplementation improves energy metabolism of exercising skeletal muscles without effect on either oxidative stress or inflammation in male patients with heart failure with reduced ejection fraction.* Cardiol J, 2024. **31**(2): p. 300-308.
67. Charles-Edwards G, A.N., Sleigh A, Ayis S, Catibog N, et al. , *Effect of iron isomaltoside on skeletal muscle energetics in patients with chronic heart failure and iron deficiency: FERRIC-HF II randomized mechanistic trial. .* Circulation, 2019. **139**(21): p. 2386-98.
68. Chance, B., et al., *Control of oxidative metabolism and oxygen delivery in human skeletal muscle: a steady-state analysis of the work/energy cost transfer function.* Proc Natl Acad Sci U S A, 1985. **82**(24): p. 8384-8.
69. Chong, C.R., K. Clarke, and E. Levelt, *Metabolic Remodeling in Diabetic Cardiomyopathy.* Cardiovasc Res, 2017. **113**(4): p. 422-430.
70. Finck, B.N., et al., *The cardiac phenotype induced by PPARalpha overexpression mimics that caused by diabetes mellitus.* J Clin Invest, 2002. **109**(1): p. 121-30.
71. Rider, O.J., et al., *Effects of Catecholamine Stress on Diastolic Function and Myocardial Energetics in Obesity.* Circulation, 2012. **125**(12): p. 1511-1519.
72. PubChem [Internet]. Bethesda (MD): National Library of Medicine (US), N.C.f.B.I.-P.C.S.f.C., Trimetazidine; [cited 2025 Jan. 2]. Available from: https://pubchem.ncbi.nlm.nih.gov/compound/Trimetazidine.
73. Gonçalves, E.M., et al., *Energetics and structure of nicotinic acid (niacin).* J Phys Chem B, 2010. **114**(16): p. 5475-85.
74. Hundertmark, M., et al., *Ninerafaxstat Modulates Cardiac Energy Metabolism in Cardio-metabolic Syndromes: A Mechanistic, Hyperpolarized MR Trial.* Journal of Cardiovascular Magnetic Resonance, 2024. **26**.
75. Horton, J.L., et al., *Mitochondrial protein hyperacetylation in the failing heart.* JCI Insight, 2016. **2**(1).
76. Sasayama, S., et al., *Adaptations of the left ventricle to chronic pressure overload.* Circ Res, 1976. **38**(3): p. 172-8.
77. Monga, S., et al., *Insights Into the Metabolic Aspects of Aortic Stenosis With the Use of Magnetic Resonance Imaging.* JACC Cardiovasc Imaging, 2022. **15**(12): p. 2112-2126.
78. Voros, G., et al., *Increased Cardiac Uptake of Ketone Bodies and Free Fatty Acids in Human Heart Failure and Hypertrophic Left Ventricular Remodeling.* Circulation: Heart Failure, 2018. **11**(12): p. e004953.

79. Monga, S., et al., *Role of Cardiac Energetics in Aortic Stenosis Disease Progression: Identifying the High-risk Metabolic Phenotype.* Circulation: Cardiovascular Imaging, 2023. **16**(10): p. e014863.
80. Neubauer, S., et al., *Cardiac high-energy phosphate metabolism in patients with aortic valve disease assessed by 31P-magnetic resonance spectroscopy.* J Investig Med, 1997. **45**(8): p. 453-62.
81. Peterzan, M.A., et al., *Cardiac Energetics in Patients With Aortic Stenosis and Preserved Versus Reduced Ejection Fraction.* Circulation, 2020. **141**(24): p. 1971-1985.
82. Lewis, A.J.M., D.J. Tyler, and O. Rider, *Clinical Cardiovascular Applications of Hyperpolarized Magnetic Resonance.* Cardiovasc Drugs Ther, 2020. **34**(2): p. 231-240.
83. Wang, Z.J., et al., *Hyperpolarized (13)C MRI: State of the Art and Future Directions.* Radiology, 2019. **291**(2): p. 273-284.
84. Mannacio, V., et al., *Myocardial metabolism and diastolic function after aortic valve replacement for aortic stenosis: influence of patient-prosthesis mismatch.* Eur J Cardiothorac Surg, 2012. **41**(2): p. 316-21.
85. Dodd MS, B.D., Schroeder MA, Le Page LM, el al., *In vivo alterations in cardiac metabolism and function in the spontaneously hypertensive rat heart.* Cardiovascular research., 2012. **95**(1): p. 69-76.
86. Atherton, H.J., et al., *The role of PDH inhibition in the development of hypertrophy in the hyperthyroid rat heart: a combined MRI and hyperpolarized MRS study.* Circulation, 2011. **123**(22): p. 2552.
87. Seymour AM, G.L., Ball V, Miller JJ, el al. , *In vivo assessment of cardiac metabolism and function in the abdominal aortic banding model of compensated cardiac hypertrophy.* Cardiovascular research., 2015. **106**(2): p. 249-60.
88. Beyerbacht, H.P., et al., *Aortic Valve Replacement in Patients with Aortic Valve Stenosis Improves Myocardial Metabolism and Diastolic Function.* Radiology, 2001. **219**(3): p. 637-643.
89. Jex, N., et al., *Association Between Type 2 Diabetes and Changes in Myocardial Structure, Contractile Function, Energetics, and Blood Flow Before and After Aortic Valve Replacement in Patients With Severe Aortic Stenosis.* Circulation, 2023. **148**(15): p. 1138-1153.
90. Tognarelli, J.M., et al., *Magnetic Resonance Spectroscopy: Principles and Techniques: Lessons for Clinicians.* J Clin Exp Hepatol, 2015. **5**(4): p. 320-8.
91. Slavkovsky, P. and R. Uhliar, *The Nobel Prize in Physiology or Medicine in 2003 to Paul C. Lauterbur, Peter Mansfield for magnetic resonance imaging.* Bratisl Lek Listy, 2004. **105**(7-8): p. 245-9.
92. Lauterbur, P.C., *Magnetic resonance zeugmatography.* Pure and Applied Chemistry, 1974. **40**(1-2): p. 149-157.
93. Mansfield, P. and A.A. Maudsley, *Medical imaging by NMR.* Br J Radiol, 1977. **50**(591): p. 188-94.
94. Meyerspeer, M., et al., *(31) P magnetic resonance spectroscopy in skeletal muscle: Experts' consensus recommendations.* NMR Biomed, 2020. **34**(5): p. e4246.
95. Gillinder, L., et al., *Quantification of Intramyocardial Metabolites by Proton Magnetic Resonance Spectroscopy.* Front Cardiovasc Med, 2015. **2**: p. 24.
96. Cunningham, C.H., et al., *Hyperpolarized 13C Metabolic MRI of the Human Heart: Initial Experience.* Circ Res, 2016. **119**(11): p. 1177-1182.
97. Jacobus, W.E., et al., *Phosphorus nuclear magnetic resonance of perfused working rat hearts.* Nature, 1977. **265**(5596): p. 756-8.
98. Neubauer, S., et al., *31P magnetic resonance spectroscopy in dilated cardiomyopathy and coronary artery disease. Altered cardiac high-energy phosphate metabolism in heart failure.* Circulation, 1992. **86**(6): p. 1810-8.

99. Valkovič, L., M. Chmelík, and M. Krššák, *In-vivo(31)P-MRS of skeletal muscle and liver: A way for non-invasive assessment of their metabolism.* Anal Biochem, 2017. **529**: p. 193-215.
100. Watson, W.D., et al., *Use of cardiac magnetic resonance to detect changes in metabolism in heart failure.* Cardiovascular Diagnosis and Therapy, 2020. **10**(3): p. 583-597.
101. Santos-Díaz, A. and M.D. Noseworthy, *Phosphorus magnetic resonance spectroscopy and imaging (31P-MRS/MRSI) as a window to brain and muscle metabolism: A review of the methods.* Biomedical Signal Processing and Control, 2020. **60**: p. 101967.
102. Layec, G., et al., *Accuracy and precision of quantitative 31P-MRS measurements of human skeletal muscle mitochondrial function.* Am J Physiol Endocrinol Metab, 2016. **311**(2): p. E358-66.
103. Valkovič, L., et al., *Measuring inorganic phosphate and intracellular pH in the healthy and hypertrophic cardiomyopathy hearts by in vivo 7T (31)P-cardiovascular magnetic resonance spectroscopy.* J Cardiovasc Magn Reson, 2019. **21**(1): p. 19.
104. Valkovič, L., et al., *Depth-resolved surface coil MRS (DRESS)-localized dynamic (31) P-MRS of the exercising human gastrocnemius muscle at 7 T.* NMR Biomed, 2014. **27**(11): p. 1346-52.
105. Tyler, D.J., et al., *Reproducibility of 31P cardiac magnetic resonance spectroscopy at 3 T.* NMR in Biomedicine, 2009. **22**(4): p. 405-413.
106. Lamb, H.J., et al., *Reproducibility of human cardiac 31P-NMR spectroscopy.* NMR Biomed, 1996. **9**(5): p. 217-27.
107. Tkáč, I. and G. Öz, *Single voxel magnetic resonance spectroscopy: principles and applications*, in *Advances in Magnetic Resonance Technology and Applications*. 2021, Elsevier. p. 503-518.
108. Rial, B., et al., *Rapid quantification of myocardial lipid content in humans using single breath-hold 1H MRS at 3 Tesla.* Magnetic resonance in medicine, 2011. **66**(3): p. 619-624.
109. Faller, K.M., et al., *(1)H-MR spectroscopy for analysis of cardiac lipid and creatine metabolism.* Heart Fail Rev, 2013. **18**(5): p. 657-68.
110. Soghomonian, A., et al., *Is increased myocardial triglyceride content associated with early changes in left ventricular function? A (1)H-MRS and MRI strain study.* Front Endocrinol (Lausanne), 2023. **14**: p. 1181452.
111. Oneglia, A.P., et al., *Myocardial steatosis across the spectrum of human health and disease.* Experimental Physiology, 2024. **109**(2): p. 202-213.
112. Stanley, W.C. and F.A. Recchia, *Lipotoxicity and the Development of Heart Failure: Moving from Mouse to Man.* Cell Metabolism, 2010. **12**(6): p. 555-556.
113. Bakermans, A.J., et al., *Quantification of Myocardial Creatine and Triglyceride Content in the Human Heart: Precision and Accuracy of in vivo Proton Magnetic Resonance Spectroscopy.* J Magn Reson Imaging, 2021. **54**(2): p. 411-420.
114. Egerton, A., *The potential of (1)H-MRS in CNS drug development.* Psychopharmacology (Berl), 2021. **238**(5): p. 1241-1254.
115. Bakermans, A.J., et al., *Fasting-Induced Myocardial Lipid Accumulation in Long-Chain Acyl-CoA Dehydrogenase Knockout Mice Is Accompanied by Impaired Left Ventricular Function.* Circulation: Cardiovascular Imaging, 2011. **4**(5): p. 558-565.
116. Rider, O.J., et al., *Noninvasive In Vivo Assessment of Cardiac Metabolism in the Healthy and Diabetic Human Heart Using Hyperpolarized (13)C MRI.* Circ Res, 2020. **126**(6): p. 725-736.
117. Woitek, R. and F.A. Gallagher, *The use of hyperpolarised (13)C-MRI in clinical body imaging to probe cancer metabolism.* Br J Cancer, 2021. **124**(7): p. 1187-1198.
118. Committee, N.Y.H.A.C., *Nomenclature and criteria for diagnosis of diseases of the heart and great vessels*. 1979: Little, Brown Medical Division.
119. Green, C.P., et al., *Development and evaluation of the Kansas City Cardiomyopathy Questionnaire: a new health status measure for heart failure.* Journal of the American College of Cardiology, 2000. **35**(5): p. 1245-1255.

120. Spertus, J., et al., *Monitoring clinical changes in patients with heart failure: a comparison of methods.* American heart journal, 2005. **150**(4): p. 707-715.
121. Butler, J., et al., *Minimal clinically important difference in quality of life scores for patients with heart failure and reduced ejection fraction.* European Journal of Heart Failure, 2020. **22**(6): p. 999-1005.
122. Gopal, D.P., et al., *Implicit bias in healthcare: clinical practice, research and decision making.* Future Healthc J, 2021. **8**(1): p. 40-48.
123. Spertus, J.A. and P.G. Jones, *Development and Validation of a Short Version of the Kansas City Cardiomyopathy Questionnaire.* Circulation: Cardiovascular Quality and Outcomes, 2015. **8**(5): p. 469-476.
124. Frank, D., et al., *Aortic valve replacement: validation of the Toronto Aortic Stenosis Quality of Life Questionnaire.* ESC Heart Fail, 2021. **8**(1): p. 270-279.
125. Styra, R., et al., *Toronto aortic stenosis quality of life questionnaire (TASQ): validation in TAVI patients.* BMC Cardiovasc Disord, 2020. **20**(1): p. 209.
126. Guy, W., *ECDEU assessment manual for psychopharmacology*. 1976: US Department of Health, Education, and Welfare, Public Health Service ….
127. Society, A.T., *ATS statement: Guidelines for the sixmin walk test.* Am J Respir Crit Care Med, 2002. **166**: p. 111-117.
128. Borg, G. and H. Dahlstrom, *A pilot study of perceived exertion and physical working capacity.* Acta Societatis Medicorum Upsaliensis, 1962. **67**: p. 21-27.
129. Zhou, T., et al., *Multilayer Radiofrequency Coils: A Novel Surface Coil Design for Improved B1+ Efficiency and Signal-to-Noise.*
130. Valkovič, L., et al., *Effects of contrast agents on relaxation properties of 31P metabolites.* Magnetic Resonance in Medicine, 2021. **85**(4): p. 1805-1813.
131. Bottomley, P.A., T.B. Foster, and R.D. Darrow, *Depth-resolved surface-coil spectroscopy (DRESS) for in vivo 1H, 31P, and 13C NMR.* Journal of Magnetic Resonance (1969), 1984. **59**(2): p. 338-342.
132. Bottomley, P.A., C.J. Hardy, and P.B. Roemer, *Phosphate metabolite imaging and concentration measurements in human heart by nuclear magnetic resonance.* Magn Reson Med, 1990. **14**(3): p. 425-34.
133. Tyler, D.J., et al., *Reproducibility of 31P cardiac magnetic resonance spectroscopy at 3 T.* NMR Biomed, 2009. **22**(4): p. 405-13.
134. Strach, K., et al., *Cardiac stress MR imaging with dobutamine.* European Radiology, 2006. **16**(12): p. 2728-2738.
135. Ruffolo, R.R., *Review: The Pharmacology of Dobutamine.* The American Journal of the Medical Sciences, 1987. **294**(4): p. 244-248.
136. Kramer, C.M., et al., *Standardized cardiovascular magnetic resonance imaging (CMR) protocols: 2020 update.* Journal of Cardiovascular Magnetic Resonance, 2020. **22**(1): p. 17.
137. Purvis, L.A.B., et al., *OXSA: An open-source magnetic resonance spectroscopy analysis toolbox in MATLAB.* PLoS One, 2017. **12**(9): p. e0185356.
138. Vanhamme, L., A. van den Boogaart, and S. Van Huffel, *Improved Method for Accurate and Efficient Quantification of MRS Data with Use of Prior Knowledge.* Journal of Magnetic Resonance, 1997. **129**(1): p. 35-43.
139. Tyler, D., et al. *Measurement of the longitudinal relaxation time (T1) of cardiac phosphorus metabolites at 3T*. in *Proc ISMRM*. 2006.
140. Cavassila, S., et al., *Cramér-Rao Bound Expressions for Parametric Estimation of Overlapping Peaks: Influence of Prior Knowledge.* Journal of Magnetic Resonance, 2000. **143**(2): p. 311-320.
141. Ding, B., et al., *Water-suppression cycling 3-T cardiac 1H-MRS detects altered creatine and choline in patients with aortic or mitral stenosis.* NMR in Biomedicine, 2021. **34**(7): p. e4513.

142. Rial, B., et al., *Rapid quantification of myocardial lipid content in humans using single breath-hold 1H MRS at 3 Tesla.* Magn Reson Med, 2011. **66**(3): p. 619-24.
143. Nakae, I., et al., *Clinical features of myocardial triglyceride in different types of cardiomyopathy assessed by proton magnetic resonance spectroscopy: comparison with myocardial creatine.* J Card Fail, 2010. **16**(10): p. 812-22.
144. Nakae, I., et al., *Proton magnetic resonance spectroscopy can detect creatine depletion associated with the progression of heart failure in cardiomyopathy.* J Am Coll Cardiol, 2003. **42**(9): p. 1587-93.
145. Myerson, S.G., N.G. Bellenger, and D.J. Pennell, *Assessment of Left Ventricular Mass by Cardiovascular Magnetic Resonance.* Hypertension, 2002. **39**(3): p. 750-755.
146. Dhaliwal, S. and A.P. Kalogeropoulos, *Markers of Iron Metabolism and Outcomes in Patients with Heart Failure: A Systematic Review.* Int J Mol Sci, 2023. **24**(6).
147. Ponikowski, P., et al., *Efficacy of ferric carboxymaltose in heart failure with iron deficiency: an individual patient data meta-analysis.* European Heart Journal, 2023. **44**(48): p. 5077-5091.
148. Ganz, T., *Erythropoietic regulators of iron metabolism.* Free Radic Biol Med, 2019. **133**: p. 69-74.
149. Pias, S.C., *How does oxygen diffuse from capillaries to tissue mitochondria? Barriers and pathways.* The Journal of Physiology, 2021. **599**(6): p. 1769-1782.
150. Intaglietta, M., P.C. Johnson, and R.M. Winslow, *Microvascular and tissue oxygen distribution.* Cardiovascular research, 1996. **32**(4): p. 632-643.
151. RN., P., *Regulation of Tissue Oxygenation.* . Chapter 9, Exercise and Hemorrhage. . 2011, https://www.ncbi.nlm.nih.gov/books/NBK54105/: San Rafael (CA): Morgan & Claypool Life Sciences.
152. Zhang, S., et al., *Double-edge sword roles of iron in driving energy production versus instigating ferroptosis.* Cell Death Dis, 2022. **13**(1): p. 40.
153. Abbaspour, N., R. Hurrell, and R. Kelishadi, *Review on iron and its importance for human health.* J Res Med Sci, 2014. **19**(2): p. 164-74.
154. Fang, X., et al., *The molecular and metabolic landscape of iron and ferroptosis in cardiovascular disease.* Nat Rev Cardiol, 2023. **20**(1): p. 7-23.
155. Lavine, K.J. and O.L. Sierra, *Skeletal muscle inflammation and atrophy in heart failure.* Heart Fail Rev, 2017. **22**(2): p. 179-189.
156. Pandey, A., et al., *Exercise Intolerance in Older Adults With Heart Failure With Preserved Ejection Fraction: JACC State-of-the-Art Review.* J Am Coll Cardiol, 2021. **78**(11): p. 1166-1187.
157. Pasricha, S.-R., et al., *Iron deficiency.* The Lancet, 2021. **397**(10270): p. 233-248.
158. Rosenblum, S.L., *Inflammation, dysregulated iron metabolism, and cardiovascular disease.* Front Aging, 2023. **4**: p. 1124178.
159. Rizzo, C., et al., *Iron Deficiency: A New Target for Patients With Heart Failure.* Front Cardiovasc Med, 2021. **8**: p. 709872.
160. Cohen-Solal, A., et al., *High prevalence of iron deficiency in patients with acute decompensated heart failure.* Eur J Heart Fail, 2014. **16**(9): p. 984-91.
161. Kocyigit D., G.K. *Iron deficiency and its treatment in heart failure: indications and effect on prognosis*. 2016 [cited 2023 03OCT2023].
162. Lakhal-Littleton, S. and J.G.F. Cleland, *Iron deficiency and supplementation in heart failure.* Nature Reviews Cardiology, 2024. **21**(7): p. 463-486.
163. Piotr Ponikowski, A.A.V., Stefan D Anker, Héctor Bueno, John G F Cleland, Andrew J S Coats, Volkmar Falk, José Ramón González-Juanatey, Veli-Pekka Harjola, Ewa A Jankowska, Mariell Jessup, Cecilia Linde, Petros Nihoyannopoulos, John T Parissis, Burkert Pieske, Jillian P Riley, Giuseppe M C Rosano, Luis M Ruilope, Frank Ruschitzka, Frans H Rutten, Peter van der Meer, ESC Scientific Document Group; 2016 ESC Guidelines for the diagnosis and treatment

of acute and chronic heart failure: The Task Force for the diagnosis and treatment of acute and chronic heart failure of the European Society of Cardiology (ESC), *2016 ESC Guidelines for the diagnosis and treatment of acute and chronic heart failureThe Task Force for the diagnosis and treatment of acute and chronic heart failure of the European Society of Cardiology (ESC)Developed with the special contribution of the Heart Failure Association (HFA) of the ESC.* European Heart Journal, 2016. **37**(27): p. 2129-2200.

164. Thyfault, J.P. and A. Bergouignan, *Exercise and metabolic health: beyond skeletal muscle.* Diabetologia, 2020. **63**(8): p. 1464-1474.
165. Janssen, I., et al., *Skeletal muscle mass and distribution in 468 men and women aged 18–88 yr.* Journal of applied physiology, 2000.
166. Zurlo, F., et al., *Skeletal muscle metabolism is a major determinant of resting energy expenditure.* The Journal of clinical investigation, 1990. **86**(5): p. 1423-1427.
167. Hargreaves, M. and L.L. Spriet, *Skeletal muscle energy metabolism during exercise.* Nature metabolism, 2020. **2**(9): p. 817-828.
168. Plotkin, D.L., et al., *Muscle Fiber Type Transitions with Exercise Training: Shifting Perspectives.* Sports (Basel), 2021. **9**(9).
169. Staron, R.S. and R.S. Hikida, *Histochemical, biochemical, and ultrastructural analyses of single human muscle fibers, with special reference to the C-fiber population.* Journal of Histochemistry & Cytochemistry, 1992. **40**(4): p. 563-568.
170. Bottinelli, R. and C. Reggiani, *Human skeletal muscle fibres: molecular and functional diversity.* Progress in Biophysics and Molecular Biology, 2000. **73**(2): p. 195-262.
171. Ohlendieck, K., *Proteomics of skeletal muscle glycolysis.* Biochimica et Biophysica Acta (BBA) - Proteins and Proteomics, 2010. **1804**(11): p. 2089-2101.
172. Baker, J.S., M.C. McCormick, and R.A. Robergs, *Interaction among Skeletal Muscle Metabolic Energy Systems during Intense Exercise.* J Nutr Metab, 2010. **2010**: p. 905612.
173. Valkovič, L., M. Chmelík, and M. Krššák, *In-vivo 31P-MRS of skeletal muscle and liver: A way for non-invasive assessment of their metabolism.* Analytical Biochemistry, 2017. **529**: p. 193-215.
174. Wells, G.D., H. Selvadurai, and I. Tein, *Bioenergetic provision of energy for muscular activity.* Paediatric Respiratory Reviews, 2009. **10**(3): p. 83-90.
175. Sahlin, K., *Muscle energetics during explosive activities and potential effects of nutrition and training.* Sports Med, 2014. **44 Suppl 2**(Suppl 2): p. S167-73.
176. Fiedler, G.B., et al., *Skeletal muscle ATP synthesis and cellular H+ handling measured by localized 31P-MRS during exercise and recovery.* Scientific Reports, 2016. **6**(1): p. 32037.
177. Prompers, J.J., et al., *Dynamic MRS and MRI of skeletal muscle function and biomechanics.* NMR in Biomedicine, 2006. **19**(7): p. 927-953.
178. Overmyer, K.A., et al., *Maximal oxidative capacity during exercise is associated with skeletal muscle fuel selection and dynamic changes in mitochondrial protein acetylation.* Cell Metab, 2015. **21**(3): p. 468-78.
179. Seiler, M., et al., *Skeletal Muscle Alterations Are Exacerbated in Heart Failure With Reduced Compared With Preserved Ejection Fraction.* Circulation: Heart Failure, 2016. **9**(9): p. e003027.
180. Glaister, M., *Multiple sprint work : physiological responses, mechanisms of fatigue and the influence of aerobic fitness.* Sports Med, 2005. **35**(9): p. 757-77.
181. HUG, F., et al., *Recovery Kinetics throughout Successive Bouts of Various Exercises in Elite Cyclists.* Medicine & Science in Sports & Exercise, 2006. **38**(12): p. 2151-2158.
182. Haseler, L.J., M.C. Hogan, and R.S. Richardson, *Skeletal muscle phosphocreatine recovery in exercise-trained humans is dependent on O2availability.* Journal of Applied Physiology, 1999. **86**(6): p. 2013-2018.

183. Wanigatunga, A.A., et al., *Relationship between skeletal mitochondrial function and digital markers of free-living physical activity in older adults.* Geroscience, 2024. **46**(6): p. 6173-6182.
184. Cahalin, L.P., et al., *A meta-analysis of the prognostic significance of cardiopulmonary exercise testing in patients with heart failure.* Heart Fail Rev, 2013. **18**(1): p. 79-94.
185. Dominelli, P.B., et al., *The Oxygen Cascade During Exercise in Health and Disease.* Mayo Clin Proc, 2021. **96**(4): p. 1017-1032.
186. Raynaud, J.S., et al., *Determination of skeletal muscle perfusion using arterial spin labeling NMRI: Validation by comparison with venous occlusion plethysmography.* Magnetic Resonance in Medicine, 2001. **46**(2): p. 305-311.
187. Pohmann, R., et al., *Fast perfusion measurements in rat skeletal muscle at rest and during exercise with single-voxel FAIR (flow-sensitive alternating inversion recovery).* Magnetic Resonance in Medicine, 2006. **55**(1): p. 108-115.
188. Lopez, D., et al., *Arterial spin labeling perfusion cardiovascular magnetic resonance of the calf in peripheral arterial disease: cuff occlusion hyperemia vs exercise.* J Cardiovasc Magn Reson, 2015. **17**(1): p. 23.
189. Casey, A., et al., *Metabolic response of type I and II muscle fibers during repeated bouts of maximal exercise in humans.* Am J Physiol, 1996. **271**(1 Pt 1): p. E38-43.
190. Forbes, S.C., et al., *Effects of recovery time on phosphocreatine kinetics during repeated bouts of heavy-intensity exercise.* European Journal of Applied Physiology, 2008. **103**(6): p. 665-675.
191. Larsen, A.I., et al., *Effect of exercise training on skeletal muscle fibre characteristics in men with chronic heart failure. Correlation between skeletal muscle alterations, cytokines and exercise capacity.* Int J Cardiol, 2002. **83**(1): p. 25-32.
192. Englund, E.K., et al., *Measurement of skeletal muscle perfusion dynamics with pseudo-continuous arterial spin labeling (pCASL): Assessment of relative labeling efficiency at rest and during hyperemia, and comparison to pulsed arterial spin labeling (PASL).* J Magn Reson Imaging, 2016. **44**(4): p. 929-39.
193. Jiji, R.S., et al., *Reproducibility of rest and exercise stress contrast-enhanced calf perfusion magnetic resonance imaging in peripheral arterial disease.* J Cardiovasc Magn Reson, 2013. **15**(1): p. 14.
194. Stephenson, M.C., et al., *Evidence for inefficient contraction and abnormal mitochondrial activity in sarcopenia using magnetic resonance spectroscopy.* J Cachexia Sarcopenia Muscle, 2023. **14**(3): p. 1482-1494.
195. Kemp, G.J., M. Meyerspeer, and E. Moser, *Absolute quantification of phosphorus metabolite concentrations in human muscle in vivo by 31P MRS: a quantitative review.* NMR Biomed, 2007. **20**(6): p. 555-65.
196. Kemp, G.J., et al., *Quantification of skeletal muscle mitochondrial function by 31P magnetic resonance spectroscopy techniques: a quantitative review.* Acta Physiol (Oxf), 2015. **213**(1): p. 107-44.
197. Heine, K.B., H.A. Parry, and W.R. Hood, *How does density of the inner mitochondrial membrane influence mitochondrial performance?* Am J Physiol Regul Integr Comp Physiol, 2023. **324**(2): p. R242-r248.
198. Detre, J.A., et al., *Perfusion imaging.* Magnetic resonance in medicine, 1992. **23**(1): p. 37-45.
199. Docherty, K.F., et al., *Intravenous iron and SGLT2 inhibitors in iron-deficient patients with heart failure and reduced ejection fraction.* ESC Heart Fail, 2024. **11**(4): p. 1875-1879.
200. Cases, A., et al., *Effect of SGLT2 inhibitors on anemia and their possible clinical implications.* Nefrología (English Edition), 2024. **44**(2): p. 165-172.

201. Angermann, C.E., et al., *Anaemia predicts iron homoeostasis dysregulation and modulates the response to empagliflozin in heart failure with reduced ejection fraction: the EMPATROPISM-FE trial.* European Heart Journal, 2025. **46**(16): p. 1507-1523.
202. Papalia, F., et al., *Cardiac energetics in patients with chronic heart failure and iron deficiency: an in-vivo 31P magnetic resonance spectroscopy study.* European Journal of Heart Failure, 2022. **24**(4): p. 716-723.
203. Rayner, J.J., et al., *Myocardial Energetics in Obesity: Enhanced ATP Delivery Through Creatine Kinase With Blunted Stress Response.* Circulation, 2020. **141**(14): p. 1152-1163.
204. Kobak, K.A., et al., *Structural and functional abnormalities in iron-depleted heart.* Heart Fail Rev, 2019. **24**(2): p. 269-277.
205. Awad, A.K., et al., *Intravenous iron for acute and chronic heart failure with reduced ejection fraction (HFrEF) patients with iron deficiency: An updated systematic review and meta-analysis.* Clinical Medicine, 2024: p. 100211.
206. Cole, G.D., et al., *Defining the real-world reproducibility of visual grading of left ventricular function and visual estimation of left ventricular ejection fraction: impact of image quality, experience and accreditation.* Int J Cardiovasc Imaging, 2015. **31**(7): p. 1303-14.
207. Veltmann, C., et al., *Therapy duration and improvement of ventricular function in de novo heart failure: the Heart Failure Optimization study.* Eur Heart J, 2024. **45**(30): p. 2771-2781.
208. DeVore, A.D., et al., *Improvement in Left Ventricular Ejection Fraction in Outpatients With Heart Failure With Reduced Ejection Fraction.* Circulation: Heart Failure, 2020. **13**(7): p. e006833.
209. Sullivan, M.J., H.J. Green, and F.R. Cobb, *Skeletal muscle biochemistry and histology in ambulatory patients with long-term heart failure.* Circulation, 1990. **81**(2): p. 518-27.
210. Gallagher, H., et al., *Skeletal muscle atrophy, regeneration, and dysfunction in heart failure: Impact of exercise training.* J Sport Health Sci, 2023. **12**(5): p. 557-567.
211. Piña, I.L., et al., *Exercise and Heart Failure.* Circulation, 2003. **107**(8): p. 1210-1225.
212. Wilson, J.R., et al., *Noninvasive detection of skeletal muscle underperfusion with near-infrared spectroscopy in patients with heart failure.* Circulation, 1989. **80**(6): p. 1668-74.
213. Stugiewicz, M., et al., *The influence of iron deficiency on the functioning of skeletal muscles: experimental evidence and clinical implications.* European Journal of Heart Failure, 2016. **18**(7): p. 762-773.
214. Bosseboeuf, E. and C. Raimondi, *Signalling, Metabolic Pathways and Iron Homeostasis in Endothelial Cells in Health, Atherosclerosis and Alzheimer's Disease.* Cells, 2020. **9**(9).
215. Toussaint, J.F., et al., *Local relation between oxidative metabolism and perfusion in leg muscles of patients with heart failure studied by magnetic resonance imaging and spectroscopy.* J Heart Lung Transplant, 1998. **17**(9): p. 892-900.
216. Graham, F.J., et al., *Treating iron deficiency in patients with heart failure: what, why, when, how, where and who.* Heart, 2024. **110**(20): p. 1201-1207.
217. Gibbons, W.J., et al., *Reference values for a multiple repetition 6-minute walk test in healthy adults older than 20 years.* J Cardiopulm Rehabil, 2001. **21**(2): p. 87-93.
218. Formiga, F., et al., *Diagnosis of heart failure with preserved ejection fraction: a systematic narrative review of the evidence.* Heart Fail Rev, 2024. **29**(1): p. 179-189.
219. Pieske, B., et al., *How to diagnose heart failure with preserved ejection fraction: the HFA-PEFF diagnostic algorithm: a consensus recommendation from the Heart Failure Association (HFA) of the European Society of Cardiology (ESC).* Eur Heart J, 2019. **40**(40): p. 3297-3317.
220. Paulus, W.J., *H(2)FPEF Score: At Last, a Properly Validated Diagnostic Algorithm for Heart Failure With Preserved Ejection Fraction.* Circulation, 2018. **138**(9): p. 871-873.
221. Sun, Y., et al., *Predictive value of H2FPEF score in patients with heart failure with preserved ejection fraction.* ESC heart failure, 2021. **8**(2): p. 1244-1252.

222. Kim, H., et al., *Usefulness of tissue Doppler imaging-myocardial performance index in the evaluation of diastolic dysfunction and heart failure with preserved ejection fraction.* Clin Cardiol, 2011. **34**(8): p. 494-9.
223. Robinson, S., et al., *The assessment of left ventricular diastolic function: guidance and recommendations from the British Society of Echocardiography.* Echo Research & Practice, 2024. **11**(1): p. 16.
224. Guazzi, M., et al., *Exercise testing in heart failure with preserved ejection fraction: an appraisal through diagnosis, pathophysiology and therapy - A clinical consensus statement of the Heart Failure Association and European Association of Preventive Cardiology of the European Society of Cardiology.* Eur J Heart Fail, 2022. **24**(8): p. 1327-1345.
225. Hieda, M., et al., *Left Ventricular Volume-Time Relation in Patients With Heart Failure With Preserved Ejection Fraction.* Am J Cardiol, 2018. **121**(5): p. 609-614.
226. Santos, A.B., et al., *Prognostic Relevance of Left Atrial Dysfunction in Heart Failure With Preserved Ejection Fraction.* Circ Heart Fail, 2016. **9**(4): p. e002763.
227. Thompson, R.B., et al., *Quantification of lung water in heart failure using cardiovascular magnetic resonance imaging.* Journal of Cardiovascular Magnetic Resonance, 2019. **21**(1): p. 58.
228. Boutari, C. and C.S. Mantzoros, *A 2022 update on the epidemiology of obesity and a call to action: as its twin COVID-19 pandemic appears to be receding, the obesity and dysmetabolism pandemic continues to rage on.* Metabolism, 2022. **133**: p. 155217.
229. Shariq, O.A. and T.J. McKenzie, *Obesity-related hypertension: a review of pathophysiology, management, and the role of metabolic surgery.* Gland Surg, 2020. **9**(1): p. 80-93.
230. McEvoy, J.W., et al., *2024 ESC Guidelines for the management of elevated blood pressure and hypertension: Developed by the task force on the management of elevated blood pressure and hypertension of the European Society of Cardiology (ESC) and endorsed by the European Society of Endocrinology (ESE) and the European Stroke Organisation (ESO).* European Heart Journal, 2024: p. ehae178.
231. Nemtsova, V., T. Burkard, and A.S. Vischer, *Hypertensive Heart Disease: A Narrative Review Series-Part 2: Macrostructural and Functional Abnormalities.* J Clin Med, 2023. **12**(17).
232. Rayner, J.J., et al., *Myocardial Energetics in Obesity.* Circulation, 2020. **141**(14): p. 1152-1163.
233. Boonman-de Winter, L.J., et al., *High prevalence of previously unknown heart failure and left ventricular dysfunction in patients with type 2 diabetes.* Diabetologia, 2012. **55**(8): p. 2154-62.
234. Singla, P., A. Bardoloi, and A.A. Parkash, *Metabolic effects of obesity: A review.* World J Diabetes, 2010. **1**(3): p. 76-88.
235. Ormazabal, V., et al., *Association between insulin resistance and the development of cardiovascular disease.* Cardiovascular Diabetology, 2018. **17**(1): p. 122.
236. Actis Dato, V., S. Lange, and Y. Cho, *Metabolic Flexibility of the Heart: The Role of Fatty Acid Metabolism in Health, Heart Failure, and Cardiometabolic Diseases.* Int J Mol Sci, 2024. **25**(2).
237. Peterson, L.R., et al., *Effect of Obesity and Insulin Resistance on Myocardial Substrate Metabolism and Efficiency in Young Women.* Circulation, 2004. **109**(18): p. 2191-2196.
238. Kannel, W.B., M. Hjortland, and W.P. Castelli, *Role of diabetes in congestive heart failure: The Framingham study.* American Journal of Cardiology, 1974. **34**(1): p. 29-34.
239. Seferović, P.M. and W.J. Paulus, *Clinical diabetic cardiomyopathy: a two-faced disease with restrictive and dilated phenotypes.* Eur Heart J, 2015. **36**(27): p. 1718-27, 1727a-1727c.
240. Jia, G., M.A. Hill, and J.R. Sowers, *Diabetic Cardiomyopathy.* Circulation Research, 2018. **122**(4): p. 624-638.
241. Savji, N., et al., *The Association of Obesity and Cardiometabolic Traits With Incident HFpEF and HFrEF.* JACC Heart Fail, 2018. **6**(8): p. 701-709.

242. Weber, K.T. and C.G. Brilla, *Pathological hypertrophy and cardiac interstitium. Fibrosis and renin-angiotensin-aldosterone system.* Circulation, 1991. **83**(6): p. 1849-65.
243. Horton, W.B. and E.J. Barrett, *Microvascular Dysfunction in Diabetes Mellitus and Cardiometabolic Disease.* Endocr Rev, 2021. **42**(1): p. 29-55.
244. Kaze, A.D., et al., *Cardiac autonomic neuropathy and risk of incident heart failure among adults with type 2 diabetes.* Eur J Heart Fail, 2022. **24**(4): p. 634-641.
245. Smith, A.N., et al., *Genomic, Proteomic, and Metabolic Comparisons of Small Animal Models of Heart Failure With Preserved Ejection Fraction: A Tale of Mice, Rats, and Cats.* J Am Heart Assoc, 2022. **11**(15): p. e026071.
246. Korvald, C., O.P. Elvenes, and T. Myrmel, *Myocardial substrate metabolism influences left ventricular energetics in vivo.* Am J Physiol Heart Circ Physiol, 2000. **278**(4): p. H1345-51.
247. Fukushima, A. and G.D. Lopaschuk, *Cardiac fatty acid oxidation in heart failure associated with obesity and diabetes.* Biochimica et Biophysica Acta (BBA) - Molecular and Cell Biology of Lipids, 2016. **1861**(10): p. 1525-1534.
248. Mahmod, M., et al., *The interplay between metabolic alterations, diastolic strain rate and exercise capacity in mild heart failure with preserved ejection fraction: a cardiovascular magnetic resonance study.* J Cardiovasc Magn Reson, 2018. **20**(1): p. 88.
249. Bayeva, M., K.T. Sawicki, and H. Ardehali, *Taking diabetes to heart--deregulation of myocardial lipid metabolism in diabetic cardiomyopathy.* J Am Heart Assoc, 2013. **2**(6): p. e000433.
250. Jia, G., V.G. DeMarco, and J.R. Sowers, *Insulin resistance and hyperinsulinaemia in diabetic cardiomyopathy.* Nat Rev Endocrinol, 2016. **12**(3): p. 144-53.
251. Lopaschuk, G.D., et al., *Cardiac Energy Metabolism in Heart Failure.* Circulation Research, 2021. **128**(10): p. 1487-1513.
252. Falcão-Pires, I. and A.F. Leite-Moreira, *Diabetic cardiomyopathy: understanding the molecular and cellular basis to progress in diagnosis and treatment.* Heart Failure Reviews, 2012. **17**(3): p. 325-344.
253. Fragasso, G., et al., *Short- and long-term beneficial effects of trimetazidine in patients with diabetes and ischemic cardiomyopathy.* Am Heart J, 2003. **146**(5): p. E18.
254. Maron, M.S., et al., *Safety and Efficacy of Metabolic Modulation With Ninerafaxstat in Patients With Nonobstructive Hypertrophic Cardiomyopathy.* Journal of the American College of Cardiology, 2024. **83**(21): p. 2037-2048.
255. Beadle, R.M., et al., *Improvement in cardiac energetics by perhexiline in heart failure due to dilated cardiomyopathy.* JACC: Heart Failure, 2015. **3**(3): p. 202-211.
256. Spoladore, R., et al., *Beneficial effects of beta-blockers on left ventricular function and cellular energy reserve in patients with heart failure.* Fundamental & Clinical Pharmacology, 2013. **27**(4): p. 455-464.
257. Lim, G.B., *Benefits of ninerafaxstat in non-obstructive hypertrophic cardiomyopathy.* Nature Reviews Cardiology, 2024. **21**(6): p. 357-357.
258. Jaswal, J.S., et al., *Targeting fatty acid and carbohydrate oxidation — A novel therapeutic intervention in the ischemic and failing heart.* Biochimica et Biophysica Acta (BBA) - Molecular Cell Research, 2011. **1813**(7): p. 1333-1350.
259. Ashrafian, H., J.D. Horowitz, and M.P. Frenneaux, *Perhexiline.* Cardiovascular Drug Reviews, 2007. **25**(1): p. 76-97.
260. Hundertmark, M.J., et al., *Assessment of Cardiac Energy Metabolism, Function, and Physiology in Patients With Heart Failure Taking Empagliflozin: The Randomized, Controlled EMPA-VISION Trial.* Circulation, 2023. **147**(22): p. 1654-1669.
261. Chierchia, S.L. and G. Fragasso, *Metabolic management of ischaemic heart disease.* Eur Heart J, 1993. **14 Suppl G**: p. 2-5.
262. Lionetti, V., W.C. Stanley, and F.A. Recchia, *Modulating fatty acid oxidation in heart failure.* Cardiovasc Res, 2011. **90**(2): p. 202-9.

263. McDonagh T, M.M., Adamo M, Gardner R et al. , *ESC Guidelines for the diagnosis and treatment of acute and chronic heart failure: Developed by the Task Force for the diagnosis and treatment of acute and chronic heart failure of the European Society of Cardiology (ESC) With the special contribution of the Heart Failure Association (HFA) of the ESC.* European Heart Journal, 2021. **42**(36): p. 3599–3726.
264. Anker, S.D., et al., *Empagliflozin in heart failure with a preserved ejection fraction.* New England Journal of Medicine, 2021. **385**(16): p. 1451-1461.
265. Solomon, S.D., et al., *Dapagliflozin in heart failure with preserved and mildly reduced ejection fraction: rationale and design of the DELIVER trial.* European journal of heart failure, 2021. **23**(7): p. 1217-1225.
266. Brodbin, P. and C.A. O'Connor, *Trimetazidine in the treatment of angina pectoris.* Br J Clin Pract, 1968. **22**(9): p. 395-6.
267. Di Napoli, P., et al., *Beneficial effects of trimetazidine treatment on exercise tolerance and B-type natriuretic peptide and troponin T plasma levels in patients with stable ischemic cardiomyopathy.* Am Heart J, 2007. **154**(3): p. 602.e1-5.
268. Li, R., et al., *The effect of trimetazidine treatment in patients with type 2 diabetes undergoing percutaneous coronary intervention for AMI.* Am J Emerg Med, 2017. **35**(11): p. 1657-1661.
269. Tuunanen, H., et al., *Trimetazidine, a metabolic modulator, has cardiac and extracardiac benefits in idiopathic dilated cardiomyopathy.* Circulation, 2008. **118**(12): p. 1250-8.
270. Fragasso, G., et al., *A randomized clinical trial of trimetazidine, a partial free fatty acid oxidation inhibitor, in patients with heart failure.* J Am Coll Cardiol, 2006. **48**(5): p. 992-8.
271. Fragasso, G., et al., *Effects of metabolic modulation by trimetazidine on left ventricular function and phosphocreatine/adenosine triphosphate ratio in patients with heart failure.* Eur Heart J, 2006. **27**(8): p. 942-8.
272. Dy, A.M.B., L.L.G. Limjoco, and R.D.G. Jamora, *Trimetazidine-Induced Parkinsonism: A Systematic Review.* Front Neurol, 2020. **11**: p. 44.
273. Chrusciel, P., J. Rysz, and M. Banach, *Defining the role of trimetazidine in the treatment of cardiovascular disorders: some insights on its role in heart failure and peripheral artery disease.* Drugs, 2014. **74**(9): p. 971-80.
274. Kallistratos, M.S., L.E. Poulimenos, and A.J. Manolis, *Stable angina pectoris: which drugs or combinations to use in which patients.* E-Journal of Cardiology Practice, 2017. **15**(8).
275. Kantor, P.F., et al., *The antianginal drug trimetazidine shifts cardiac energy metabolism from fatty acid oxidation to glucose oxidation by inhibiting mitochondrial long-chain 3-ketoacyl coenzyme A thiolase.* Circulation research, 2000. **86**(5): p. 580-588.
276. Fantini, E., et al., *Some biochemical aspects of the protective effect of trimetazidine on rat cardiomyocytes during hypoxia and reoxygenation.* J Mol Cell Cardiol, 1994. **26**(8): p. 949-58.
277. Chamberlin, P., et al., *PHASE 1 SAFETY AND TOLERABILITY STUDY OF IMB-1018972, A NOVEL ORAL MODULATOR OF MYOCARDIAL SUBSTRATE UTILIZATION DESIGNED TO IMPROVE CARDIAC METABOLIC EFFICIENCY AND BIOENERGETICS.* Journal of the American College of Cardiology, 2021. **77**(18_Supplement_1): p. 180-180.
278. Amjad, S., et al., *Role of NAD+ in regulating cellular and metabolic signaling pathways.* Molecular metabolism, 2021. **49**: p. 101195.
279. Weidele, K., S. Beneke, and A. Bürkle, *The NAD+ precursor nicotinic acid improves genomic integrity in human peripheral blood mononuclear cells after X-irradiation.* DNA repair, 2017. **52**: p. 12-23.
280. Lin, Q., et al., *NAD+ and cardiovascular diseases.* Clinica Chimica Acta, 2021. **515**: p. 104-110.

281. Lombard, D.B., D.X. Tishkoff, and J. Bao, *Mitochondrial sirtuins in the regulation of mitochondrial activity and metabolic adaptation.* Handb Exp Pharmacol, 2011. **206**: p. 163-88.
282. Yaku, K., et al., *NAD Metabolism in Cancer Therapeutics.* Frontiers in Oncology, 2018. **Volume 8 - 2018**.
283. Xie, N., et al., *NAD+ metabolism: pathophysiologic mechanisms and therapeutic potential.* Signal Transduction and Targeted Therapy, 2020. **5**(1): p. 227.
284. Abdellatif, M., S. Sedej, and G. Kroemer, *NAD⁺ Metabolism in Cardiac Health, Aging, and Disease.* Circulation, 2021. **144**(22): p. 1795-1817.
285. Shi, C., et al., *NAD+ metabolism and therapeutic strategies in cardiovascular diseases.* Atheroscler Plus, 2024. **57**: p. 1-12.
286. Chiang, S.H., et al., *Genetic Ablation of CD38 Protects against Western Diet-Induced Exercise Intolerance and Metabolic Inflexibility.* PLoS One, 2015. **10**(8): p. e0134927.
287. Abdellatif, M., et al., *Nicotinamide for the treatment of heart failure with preserved ejection fraction.* Sci Transl Med, 2021. **13**(580).
288. Zhong, O., et al., *Effects of NAD+ precursor supplementation on glucose and lipid metabolism in humans: a meta-analysis.* Nutrition & Metabolism, 2022. **19**(1): p. 20.
289. Vitale, G.D., et al., *Myocardial glucose utilization and optimization of (18)F-FDG PET imaging in patients with non-insulin-dependent diabetes mellitus, coronary artery disease, and left ventricular dysfunction.* J Nucl Med, 2001. **42**(12): p. 1730-6.
290. Penumathsa, S.V., et al., *Niacin bound chromium treatment induces myocardial Glut-4 translocation and caveolar interaction via Akt, AMPK and eNOS phosphorylation in streptozotocin induced diabetic rats after ischemia-reperfusion injury.* Biochim Biophys Acta, 2009. **1792**(1): p. 39-48.
291. Yoshino, M., et al., *Nicotinamide mononucleotide increases muscle insulin sensitivity in prediabetic women.* Science, 2021. **372**(6547): p. 1224-1229.
292. Wang, D.D., et al., *Safety and Tolerability of Nicotinamide Riboside in Heart Failure With Reduced Ejection Fraction.* JACC Basic Transl Sci, 2022. **7**(12): p. 1183-1196.
293. Dézsi, C.A., *Trimetazidine in Practice: Review of the Clinical and Experimental Evidence.* Am J Ther, 2016. **23**(3): p. e871-9.
294. Knuuti, J., et al., *A randomized, double-blind, placebo-controlled, mechanistic trial on the safety, tolerability and pharmacodynamics of ninerafaxstat in patients with angina and chronic coronary syndrome.* European Heart Journal, 2024. **45**(Supplement_1).
295. Hundertmark, M., et al., *A phase 2a trial investigating ninerafaxstat – a novel cardiac mitotrope for the treatment of diabetic cardiomyopathy (IMPROVE-DiCE).* European Heart Journal, 2022. **43**(Supplement_2).
296. Kyle, U.G., et al., *Bioelectrical impedance analysis—part I: review of principles and methods.* Clinical nutrition, 2004. **23**(5): p. 1226-1243.
297. Schols, A. and C. Pichard, *ESPEN Working Group: Bioelectrical impedance analysis-part II: utilization in clinical practice.* Clinical nutrition, 2004. **23**: p. 1430-1453.
298. Kellman, P., et al., *Multiecho dixon fat and water separation method for detecting fibrofatty infiltration in the myocardium.* Magn Reson Med, 2009. **61**(1): p. 215-21.
299. Lins, C.F., C.E.G. Salmon, and M.H. Nogueira-Barbosa, *Applications of the Dixon technique in the evaluation of the musculoskeletal system.* Radiol Bras, 2021. **54**(1): p. 33-42.
300. Reeder, S.B., H.H. Hu, and C.B. Sirlin, *Proton density fat-fraction: a standardized MR-based biomarker of tissue fat concentration.* J Magn Reson Imaging, 2012. **36**(5): p. 1011-4.
301. Hu, F., et al., *3D Multi-Echo Dixon technique for simultaneous assessment of liver steatosis and iron overload in patients with chronic liver diseases: a feasibility study.* Quant Imaging Med Surg, 2019. **9**(6): p. 1014-1024.

302. Petäjä, E.M. and H. Yki-Järvinen, *Definitions of Normal Liver Fat and the Association of Insulin Sensitivity with Acquired and Genetic NAFLD-A Systematic Review.* Int J Mol Sci, 2016. **17**(5).
303. Shen, W., et al., *Total body skeletal muscle and adipose tissue volumes: estimation from a single abdominal cross-sectional image.* J Appl Physiol (1985), 2004. **97**(6): p. 2333-8.
304. Sottier, D., et al., *Quantification of the visceral and subcutaneous fat by computed tomography: interobserver correlation of a single slice technique.* Diagn Interv Imaging, 2013. **94**(9): p. 879-84.
305. Rider, O.J., et al., *Investigating a Liver Fat: Arterial Stiffening Pathway in Adult and Childhood Obesity.* Arterioscler Thromb Vasc Biol, 2016. **36**(1): p. 198-203.
306. Hundley, W.G., et al., *Cardiac cycle-dependent changes in aortic area and distensibility are reduced in older patients with isolated diastolic heart failure and correlate with exercise intolerance.* Journal of the American College of Cardiology, 2001. **38**(3): p. 796-802.
307. Assar, M.E., J. Angulo, and L. Rodríguez-Mañas, *Diabetes and ageing-induced vascular inflammation.* The Journal of Physiology, 2016. **594**(8): p. 2125-2146.
308. Biernacka, A. and N.G. Frangogiannis, *Aging and Cardiac Fibrosis.* Aging Dis, 2011. **2**(2): p. 158-173.
309. Dogui, A., et al., *Consistency of aortic distensibility and pulse wave velocity estimates with respect to the Bramwell-Hill theoretical model: a cardiovascular magnetic resonance study.* Journal of Cardiovascular Magnetic Resonance, 2011. **13**(1): p. 11.
310. Cecelja, M., et al., *Aortic Distensibility Measured by Automated Analysis of Magnetic Resonance Imaging Predicts Adverse Cardiovascular Events in UK Biobank.* J Am Heart Assoc, 2022. **11**(23): p. e026361.
311. Voges, I., et al., *Normal values of aortic dimensions, distensibility, and pulse wave velocity in children and young adults: a cross-sectional study.* J Cardiovasc Magn Reson, 2012. **14**(1): p. 77.
312. Thompson, R.B., et al., *Subclinical Pulmonary Edema Is Associated With Reduced Exercise Capacity in HFpEF and HFrEF.* Journal of the American College of Cardiology, 2017. **70**(14): p. 1827-1828.
313. Thompson, R.B., et al., *Quantification of pulmonary edema in heart failure using MRI: invasive validation and evaluation in HFpEF and HFrEF patients.* Journal of Cardiovascular Magnetic Resonance, 2016. **18**: p. O49.
314. Kim, J.A., Y. Wei, and J.R. Sowers, *Role of mitochondrial dysfunction in insulin resistance.* Circ Res, 2008. **102**(4): p. 401-14.
315. Rider, O.J., et al., *Myocardial substrate metabolism in obesity.* Int J Obes (Lond), 2013. **37**(7): p. 972-9.
316. Levelt, E., et al., *Relationship Between Left Ventricular Structural and Metabolic Remodeling in Type 2 Diabetes.* Diabetes, 2016. **65**(1): p. 44-52.
317. Karwi, Q.G., Q. Sun, and G.D. Lopaschuk, *The Contribution of Cardiac Fatty Acid Oxidation to Diabetic Cardiomyopathy Severity.* Cells, 2021. **10**(11).
318. van de Bovenkamp, A.A., et al., *Trimetazidine in heart failure with preserved ejection fraction: a randomized controlled cross-over trial.* ESC Heart Fail, 2023. **10**(5): p. 2998-3010.
319. Hopp, A.K., P. Grüter, and M.O. Hottiger, *Regulation of Glucose Metabolism by NAD(+) and ADP-Ribosylation.* Cells, 2019. **8**(8).
320. Guarini, G., et al., *Trimetazidine and Other Metabolic Modifiers.* Eur Cardiol, 2018. **13**(2): p. 104-111.
321. Dalal, J.J. and S. Mishra, *Modulation of myocardial energetics: An important category of agents in the multimodal treatment of coronary artery disease and heart failure.* Indian Heart Journal, 2017. **69**(3): p. 393-401.

322. Spoladore, R., et al., *Beneficial effects of beta-blockers on left ventricular function and cellular energy reserve in patients with heart failure.* Fundamental & clinical pharmacology, 2013. **27**(4): p. 455-464.
323. Negishi, K., *Echocardiographic feature of diabetic cardiomyopathy: where are we now?* Cardiovasc Diagn Ther, 2018. **8**(1): p. 47-56.
324. LaMonte, M.J. and C.B. Eaton, *Physical Activity in the Treatment and Prevention of Heart Failure: An Update.* Curr Sports Med Rep, 2021. **20**(8): p. 410-417.
325. Kitzman, D.W., et al., *Exercise intolerance in patients with heart failure and preserved left ventricular systolic function: failure of the Frank-Starling mechanism.* J Am Coll Cardiol, 1991. **17**(5): p. 1065-72.
326. Wu, C.-K., et al., *Myocardial adipose deposition and the development of heart failure with preserved ejection fraction.* European Journal of Heart Failure, 2020. **22**(3): p. 445-454.
327. Liu, C.Y., et al., *Myocardial steatosis and its association with obesity and regional ventricular dysfunction: evaluated by magnetic resonance tagging and 1H spectroscopy in healthy African Americans.* Int J Cardiol, 2014. **172**(2): p. 381-387.
328. Szczepaniak, L.S., et al., *Myocardial triglycerides and systolic function in humans: In vivo evaluation by localized proton spectroscopy and cardiac imaging.* Magnetic Resonance in Medicine, 2003. **49**(3): p. 417-423.
329. Rijzewijk, L.J., et al., *Myocardial steatosis is an independent predictor of diastolic dysfunction in type 2 diabetes mellitus.* J Am Coll Cardiol, 2008. **52**(22): p. 1793-9.
330. Michos, E.D., et al., *Improving the enrollment of women and racially/ethnically diverse populations in cardiovascular clinical trials: An ASPC practice statement.* Am J Prev Cardiol, 2021. **8**: p. 100250.
331. Brown, S., et al., *Race- and Ethnicity-Related Differences in Heart Failure With Preserved Ejection Fraction Using Natural Language Processing.* JACC Adv, 2024. **3**(8): p. 101064.
332. Shah, S.J., D.H. Katz, and R.C. Deo, *Phenotypic spectrum of heart failure with preserved ejection fraction.* Heart Fail Clin, 2014. **10**(3): p. 407-18.
333. Group, U.H.C., *Rationale and design of the United Kingdom Heart Failure with Preserved Ejection Fraction Registry.* Heart, 2024. **110**(5): p. 359-365.
334. Kaimoto, S., et al., *Activation of PPAR-α in the early stage of heart failure maintained myocardial function and energetics in pressure-overload heart failure.* Am J Physiol Heart Circ Physiol, 2017. **312**(2): p. H305-h313.
335. Geoffrey, A.S., et al., *Uncovering the treatable burden of severe aortic stenosis in the UK.* Open Heart, 2022. **9**(1): p. e001783.
336. d'Arcy, J.L., et al., *Large-scale community echocardiographic screening reveals a major burden of undiagnosed valvular heart disease in older people: the OxVALVE Population Cohort Study.* Eur Heart J, 2016. **37**(47): p. 3515-3522.
337. Eveborn, G.W., et al., *Assessment of risk factors for developing incident aortic stenosis: the Tromsø Study.* European Journal of Epidemiology, 2014. **29**(8): p. 567-575.
338. Saheera, S. and P. Krishnamurthy, *Cardiovascular Changes Associated with Hypertensive Heart Disease and Aging.* Cell Transplant, 2020. **29**: p. 963689720920830.
339. Ritterhoff, J., et al., *Metabolic Remodeling Promotes Cardiac Hypertrophy by Directing Glucose to Aspartate Biosynthesis.* Circulation Research, 2020. **126**(2): p. 182-196.
340. Atherton, H.J., et al., *Role of pyruvate dehydrogenase inhibition in the development of hypertrophy in the hyperthyroid rat heart: a combined magnetic resonance imaging and hyperpolarized magnetic resonance spectroscopy study.* Circulation, 2011. **123**(22): p. 2552-61.
341. Zhang, J., et al., *Bioenergetic abnormalities associated with severe left ventricular hypertrophy.* J Clin Invest, 1993. **92**(2): p. 993-1003.
342. Jameel, M.N. and J. Zhang, *Myocardial energetics in left ventricular hypertrophy.* Curr Cardiol Rev, 2009. **5**(3): p. 243-50.

343. *About Heart Failure*. 14/07/22].
344. Dodd, M.S., et al., *In vivo alterations in cardiac metabolism and function in the spontaneously hypertensive rat heart.* Cardiovascular Research, 2012. **95**(1): p. 69-76.
345. Le Page, L.M., et al., *Increasing pyruvate dehydrogenase flux as a treatment for diabetic cardiomyopathy: a combined 13C hyperpolarized magnetic resonance and echocardiography study.* Diabetes, 2015. **64**(8): p. 2735-2743.
346. Piao, L., et al., *The inhibition of pyruvate dehydrogenase kinase improves impaired cardiac function and electrical remodeling in two models of right ventricular hypertrophy: resuscitating the hibernating right ventricle.* Journal of molecular medicine, 2010. **88**: p. 47-60.
347. Kolwicz Jr, S.C. and R. Tian, *Glucose metabolism and cardiac hypertrophy.* Cardiovascular research, 2011. **90**(2): p. 194-201.
348. Samak, M., et al., *Cardiac Hypertrophy: An Introduction to Molecular and Cellular Basis.* Med Sci Monit Basic Res, 2016. **22**: p. 75-9.
349. Vahanian, A., et al., *2021 ESC/EACTS Guidelines for the management of valvular heart disease: Developed by the Task Force for the management of valvular heart disease of the European Society of Cardiology (ESC) and the European Association for Cardio-Thoracic Surgery (EACTS).* European Heart Journal, 2021. **43**(7): p. 561-632.
350. Minners, J., et al., *Inconsistencies of echocardiographic criteria for the grading of aortic valve stenosis.* European Heart Journal, 2007. **29**(8): p. 1043-1048.
351. Bohbot, Y., et al., *Usefulness of Cardiac Magnetic Resonance Imaging in Aortic Stenosis.* Circulation: Cardiovascular Imaging, 2020. **13**(5): p. e010356.
352. Nazir, M.S., et al., *Echocardiography versus Cardiac MRI for Measurement of Left Ventricular Ejection Fraction in Individuals with Cancer and Suspected Cardiotoxicity.* Radiol Cardiothorac Imaging, 2024. **6**(1): p. e230048.
353. Reis Santos, R., et al., *Cardiac magnetic resonance patterns of left ventricular remodeling in patients with severe aortic stenosis referred to surgical aortic valve replacement.* Scientific Reports, 2024. **14**(1): p. 7085.
354. Chen, H., et al., *Prognostic value of late gadolinium enhancement on CMR in patients with severe aortic valve disease: a systematic review and meta-analysis.* Clinical radiology, 2018. **73**(11): p. 983. e7-983. e14.
355. Debry, N., et al., *Prognostic significance of left ventricular concentric remodelling in patients with aortic stenosis.* Arch Cardiovasc Dis, 2017. **110**(1): p. 26-34.
356. Lang, R.M., et al., *Recommendations for Cardiac Chamber Quantification by Echocardiography in Adults: An Update from the American Society of Echocardiography and the European Association of Cardiovascular Imaging.* European Heart Journal - Cardiovascular Imaging, 2015. **16**(3): p. 233-271.
357. Truong, V.T., et al., *COEXISTENCE OF ASYMMETRIC SEPTAL HYPERTROPHY AND AORTIC STENOSIS.* Journal of the American College of Cardiology, 2023. **81**(8_Supplement): p. 1963-1963.
358. Bennett, J., et al., *Left Ventricular Hypertrophy in Aortic Stenosis: Early Cell and Matrix Regression 2 Months Post-Aortic Valve Replacement.* Circulation: Cardiovascular Imaging, 2024. **17**(12): p. e017425.
359. Barone-Rochette, G., et al., *Prognostic significance of LGE by CMR in aortic stenosis patients undergoing valve replacement.* J Am Coll Cardiol, 2014. **64**(2): p. 144-54.
360. Maltês, S., et al., *LGE prevalence and patterns in severe aortic stenosis: When "junctional" means the same.* Int J Cardiol, 2023. **378**: p. 159-163.
361. Treibel, T.A., et al., *Reappraising myocardial fibrosis in severe aortic stenosis: an invasive and non-invasive study in 133 patients.* Eur Heart J, 2018. **39**(8): p. 699-709.
362. Haaf, P., et al., *Cardiac T1 Mapping and Extracellular Volume (ECV) in clinical practice: a comprehensive review.* Journal of Cardiovascular Magnetic Resonance, 2016. **18**(1): p. 89.

363. Jaiswal, V., et al., *Cardiac amyloidosis and aortic stenosis: a state-of-the-art review.* European Heart Journal Open, 2023. **3**(6).
364. Cribier, A., et al., *Percutaneous Transcatheter Implantation of an Aortic Valve Prosthesis for Calcific Aortic Stenosis.* Circulation, 2002. **106**(24): p. 3006-3008.
365. Landmesser, U., *The Changing Landscape of Aortic-Valve Stenosis Management.* New England Journal of Medicine, 2023. **389**(21): p. 2008-2009.
366. Blanke, P., et al., *Computed Tomography Imaging in the Context of Transcatheter Aortic Valve Implantation (TAVI)/Transcatheter Aortic Valve Replacement (TAVR).* JACC: Cardiovascular Imaging, 2019. **12**(1): p. 1-24.
367. Antonides, C.F., M.J. Mack, and A.P. Kappetein, *Approaches to the role of the heart team in therapeutic decision making for heart valve disease.* Structural Heart, 2017. **1**(5-6): p. 249-255.
368. Dogosh, A.A., et al., *Comparison of Transcatheter Aortic Valve Implantation Devices in Aortic Stenosis: A Network Meta-Analysis of 42,105 Patients.* J Clin Med, 2022. **11**(18).
369. Hamilton-Craig, C.R., M.W. Strudwick, and G.J. Galloway, *T(1) Mapping for Myocardial Fibrosis by Cardiac Magnetic Resonance Relaxometry-A Comprehensive Technical Review.* Front Cardiovasc Med, 2016. **3**: p. 49.
370. Bloem, J.L., et al., *MR signal intensity: staying on the bright side in MR image interpretation.* RMD Open, 2018. **4**(1): p. e000728.
371. Taylor, A.J., et al., *T1 Mapping.* JACC: Cardiovascular Imaging, 2016. **9**(1): p. 67-81.
372. Robinson, A.A., K. Chow, and M. Salerno, *Myocardial T1 and ECV Measurement: Underlying Concepts and Technical Considerations.* JACC Cardiovasc Imaging, 2019. **12**(11 Pt 2): p. 2332-2344.
373. Piechnik, S.K., et al., *Shortened Modified Look-Locker Inversion recovery (ShMOLLI) for clinical myocardial T1-mapping at 1.5 and 3 T within a 9 heartbeat breathhold.* J Cardiovasc Magn Reson, 2010. **12**(1): p. 69.
374. Aquaro, G.D., et al., *Diagnostic Role of Native T1 Mapping Compared to Conventional Magnetic Resonance Techniques in Cardiac Disease in a Real-Life Cohort.* Diagnostics (Basel), 2023. **13**(14).
375. Iyad, N., et al., *Gadolinium contrast agents- challenges and opportunities of a multidisciplinary approach: Literature review.* Eur J Radiol Open, 2023. **11**: p. 100503.
376. Doltra, A., et al., *Emerging concepts for myocardial late gadolinium enhancement MRI.* Curr Cardiol Rev, 2013. **9**(3): p. 185-90.
377. Mewton, N., et al., *Assessment of myocardial fibrosis with cardiovascular magnetic resonance.* J Am Coll Cardiol, 2011. **57**(8): p. 891-903.
378. Satoh, H., et al., *Distribution of late gadolinium enhancement in various types of cardiomyopathies: Significance in differential diagnosis, clinical features and prognosis.* World J Cardiol, 2014. **6**(7): p. 585-601.
379. Pandey, T., et al., *Utility of the inversion scout sequence (TI scout) in diagnosing myocardial amyloid infiltration.* Int J Cardiovasc Imaging, 2013. **29**(1): p. 103-12.
380. Cholet, C., et al., *Quantification of Myocardial Enhancement on Cine-MRI: Diagnostic Value in Cardiac Amyloidosis.* Acad Radiol, 2019. **26**(6): p. e98-e107.
381. Lee, J.J., et al., *Myocardial T1 and extracellular volume fraction mapping at 3 tesla.* Journal of Cardiovascular Magnetic Resonance, 2011. **13**(1): p. 75.
382. White, S.K., et al., *T1 mapping for myocardial extracellular volume measurement by CMR: bolus only versus primed infusion technique.* JACC Cardiovasc Imaging, 2013. **6**(9): p. 955-62.
383. De Rubeis, G., et al., *Aortic valvular imaging with cardiovascular magnetic resonance: seeking for comprehensiveness.* Br J Radiol, 2019. **92**(1101): p. 20170868.
384. Nayak, K.S., et al., *Cardiovascular magnetic resonance phase contrast imaging.* Journal of Cardiovascular Magnetic Resonance, 2015. **17**(1): p. 71.

385. Smiseth, O.A., et al., *Myocardial Strain Imaging.* JACC: Cardiovascular Imaging. **0**(0).
386. Scatteia, A., A. Baritussio, and C. Bucciarelli-Ducci, *Strain imaging using cardiac magnetic resonance.* Heart Fail Rev, 2017. **22**(4): p. 465-476.
387. Marwick, T.H., *Measurement of Strain and Strain Rate by Echocardiography: Ready for Prime Time?* Journal of the American College of Cardiology, 2006. **47**(7): p. 1313-1327.
388. Cikes, M. and S.D. Solomon, *Beyond ejection fraction: an integrative approach for assessment of cardiac structure and function in heart failure.* European Heart Journal, 2015. **37**(21): p. 1642-1650.
389. Kammerlander, A.A., et al., *Global Longitudinal Strain by CMR Feature Tracking Is Associated With Outcome in HFPEF.* JACC: Cardiovascular Imaging, 2019. **12**(8, Part 1): p. 1585-1587.
390. Jørgensen, S., et al. *Hyperpolarized MRI–An update and future perspectives*. in *Seminars in nuclear medicine*. 2022. Elsevier.
391. Atherton, H.J.e.a., *Validation of the in vivo assessment of pyruvate dehydrogenase activity using hyperpolarised*

13C MRS. NMR Biomed., 2011.
392. Rabinowitz, J.D. and S. Enerbäck, *Lactate: the ugly duckling of energy metabolism.* Nature Metabolism, 2020. **2**(7): p. 566-571.
393. Cluntun, A.A., et al., *The pyruvate-lactate axis modulates cardiac hypertrophy and heart failure.* Cell Metabolism, 2021. **33**(3): p. 629-648.e10.
394. Slichter, C.P., *The discovery and renaissance of dynamic nuclear polarization.* Rep Prog Phys, 2014. **77**(7): p. 072501.
395. Equbal, A., et al., *Role of electron spin dynamics and coupling network in designing dynamic nuclear polarization.* Progress in Nuclear Magnetic Resonance Spectroscopy, 2021. **126**: p. 1-16.
396. Pinon, A.C., A. Capozzi, and J.H. Ardenkjær-Larsen, *Hyperpolarization via dissolution dynamic nuclear polarization: new technological and methodological advances.* Magnetic Resonance Materials in Physics, Biology and Medicine, 2021. **34**: p. 5-23.
397. Shah, A.S.V., et al., *Left Ventricular Hypertrophy With Strain and Aortic Stenosis.* Circulation, 2014. **130**(18): p. 1607-1616.
398. Lønnebakken, M.T., et al., *Left Ventricular Hypertrophy Regression During Antihypertensive Treatment in an Outpatient Clinic (the Campania Salute Network).* J Am Heart Assoc, 2017. **6**(3).
399. Appleby, C., et al., *Sex-related disparities in aortic stenosis from disease awareness to treatment: a state-of-the-art review.* J Thorac Dis, 2024. **16**(9): p. 6308-6319.
400. Basile, C., et al., *Arterial Hypertension in Aortic Valve Stenosis: A Critical Update.* J Clin Med, 2021. **10**(23).
401. de Wit-Verheggen, V.H.W., et al., *PCr/ATP ratios and mitochondrial function in the heart. A comparative study in humans.* Sci Rep, 2023. **13**(1): p. 8346.
402. Nollet, E.E., et al., *Mitochondrial dysfunction in human hypertrophic cardiomyopathy is linked to cardiomyocyte architecture disruption and corrected by improving NADH-driven mitochondrial respiration.* Eur Heart J, 2023. **44**(13): p. 1170-1185.
403. Smith, C.S., et al., *Altered Creatine Kinase Adenosine Triphosphate Kinetics in Failing Hypertrophied Human Myocardium.* Circulation, 2006. **114**(11): p. 1151-1158.
404. Levett, D.Z., et al., *Acclimatization of skeletal muscle mitochondria to high-altitude hypoxia during an ascent of Everest.* The FASEB Journal, 2012. **26**(4): p. 1431-1441.
405. Rosca, M.G. and C.L. Hoppel, *Mitochondrial dysfunction in heart failure.* Heart Fail Rev, 2013. **18**(5): p. 607-22.
406. Doenst, T., et al., *Decreased rates of substrate oxidation ex vivo predict the onset of heart failure and contractile dysfunction in rats with pressure overload.* Cardiovasc Res, 2010. **86**(3): p. 461-70.

407. Treibel, T.A., et al., *Reverse Myocardial Remodeling Following Valve Replacement in Patients With Aortic Stenosis.* J Am Coll Cardiol, 2018. **71**(8): p. 860-871.
408. Zile, M.R., et al., *Heart Failure With a Normal Ejection Fraction.* Circulation, 2001. **104**(7): p. 779-782.
409. Sorriento, D., E. Di Vaia, and G. Iaccarino, *Physical Exercise: A Novel Tool to Protect Mitochondrial Health.* Front Physiol, 2021. **12**: p. 660068.
410. Sahuquillo, J., et al., *Lactate and the lactate-to-pyruvate molar ratio cannot be used as independent biomarkers for monitoring brain energetic metabolism: a microdialysis study in patients with traumatic brain injuries.* PLoS One, 2014. **9**(7): p. e102540.
411. Ritterhoff, J. and R. Tian, *Metabolic mechanisms in physiological and pathological cardiac hypertrophy: new paradigms and challenges.* Nature Reviews Cardiology, 2023. **20**(12): p. 812-829.
412. Metra, M., et al., *Quality of life in patients with severe aortic stenosis undergoing transcatheter aortic valve implantation: tools and evidence.* J Cardiovasc Med (Hagerstown), 2024. **25**(4): p. 259-270.
413. Clark, M.A., et al., *Five-year clinical and economic outcomes among patients with medically managed severe aortic stenosis: results from a Medicare claims analysis.* Circ Cardiovasc Qual Outcomes, 2012. **5**(5): p. 697-704.
414. Green, P., et al., *Relation between six-minute walk test performance and outcomes after transcatheter aortic valve implantation (from the PARTNER trial).* Am J Cardiol, 2013. **112**(5): p. 700-6.
415. Caoimhe, T.R., et al., *Impact of gender, ethnicity and social deprivation on access to surgical or transcatheter aortic valve replacement in aortic stenosis: a retrospective database study in England.* Open Heart, 2023. **10**(2): p. e002373.
416. Aimo, A., et al., *Redefining the epidemiology of cardiac amyloidosis. A systematic review and meta-analysis of screening studies.* Eur J Heart Fail, 2022. **24**(12): p. 2342-2351.
417. Nitsche, C., et al., *Prevalence and Outcomes of Concomitant Aortic Stenosis and Cardiac Amyloidosis.* J Am Coll Cardiol, 2021. **77**(2): p. 128-139.
418. Généreux, P., et al., *Transcatheter Aortic-Valve Replacement for Asymptomatic Severe Aortic Stenosis.* New England Journal of Medicine, 2025. **392**(3): p. 217-227.
419. Nagaraja, V., et al., *What Is the Role of Cardiac Magnetic Resonance Imaging in Transcatheter Management of Aortic Valve Stenosis?* Structural Heart, 2021. **5**(3): p. 234-246.

Appendix 1: Kansas City Cardiomyopathy Questionnaire (KCCQ)

Cardiomyopathy Questionnaire (Kansas City)

The following questions refer to your **heart failure** and how it may affect your life. Please read and complete the following questions. There are no right or wrong answers. Please mark the answer that best applies to you.

1. **Heart failure** affects different people in different ways. Some may mainly feel shortness of breath while others mainly fatigue. Please indicate how limited you have been by **heart failure** (for example, shortness of breath or fatigue) in your ability to do the following activities over the past 2 weeks.

Please put an **X** in one box on each line

Activity	**Extremely** limited	**Quite a bit** limited	**Moderately** limited	**Slightly** limited	**Not at all** limited	**Limited for other reasons or did not do the activity**
Dressing yourself	☐	☐	☐	☐	☐	☐
Showering or having a bath	☐	☐	☐	☐	☐	☐
Walking 100 yards on level ground	☐	☐	☐	☐	☐	☐
Doing gardening, housework or carrying groceries	☐	☐	☐	☐	☐	☐
Climbing a flight of stairs without stopping	☐	☐	☐	☐	☐	☐
Jogging or hurrying (as if to catch a bus)	☐	☐	☐	☐	☐	☐

2. Compared with 2 weeks ago, have your symptoms of **heart failure** (for example, shortness of breath, fatigue, or ankle swelling) changed?

My symptoms of **heart failure** are now…

Much worse	Slightly worse	Not changed	Slightly better	Much better	I've had no symptoms over the last 2 weeks
☐	☐	☐	☐	☐	☐

Copyright ©1992 –2006 John Spertus, MD, MPH

KCCQ - UK/English

3. Over the past 2 weeks, how many times have you had **swelling** in your feet, ankles or legs when you woke up in the morning?

Every morning	3 or more times a week, but not every day	1-2 times a week	Less than once a week	Never over the past 2 weeks
☐	☐	☐	☐	☐

4. Over the past 2 weeks, how much has **swelling** in your feet, ankles or legs bothered you?

Extremely bothersome	**Quite a bit** bothersome	**Moderately** bothersome	**Slightly** bothersome	**Not at all** bothersome	I've had **no swelling**
☐	☐	☐	☐	☐	☐

5. Over the past 2 weeks, on average, how many times has **fatigue** limited your ability to do what you wanted?

All of the time	Several times a day	At least once a day	3 or more times a week but not every day	1-2 times a week	Less than once a week	Never over the past 2 weeks
☐	☐	☐	☐	☐	☐	☐

6. Over the past 2 weeks, how much has your **fatigue** bothered you?

Extremely bothersome	**Quite a bit** bothersome	**Moderately** bothersome	**Slightly** bothersome	**Not at all** bothersome	I've had **no fatigue**
☐	☐	☐	☐	☐	☐

7. Over the past 2 weeks, on average, how many times has **shortness of breath** limited your ability to do what you wanted?

All of the time	Several times a day	At least once a day	3 or more times a week but not every day	1-2 times a week	Less than once a week	Never over the past 2 weeks
☐	☐	☐	☐	☐	☐	☐

Copyright ©1992 –2006 John Spertus, MD, MPH

Appendix 2 Toronto Aortic Stenosis Quality of Life Questionnaire

Toronto Aortic Stenosis Quality of Life Questionnaire (TASQ)

This questionnaire helps us to better understand your heart problems, in particular aortic stenosis and how it has affected you. For each question, please circle the number that best describes your current health situation.

If the question does not apply to you, please circle the number '1' to indicate that this item has not been affected.

MASTER VERSION

1. ARE YOU SHORT OF BREATH?

NOT VERY MUCH 1 2 3 4 5 6 7 VERY MUCH

2. ARE YOU WORRIED ABOUT HAVING A HEART ATTACK OR DYING?

NOT VERY MUCH 1 2 3 4 5 6 7 VERY MUCH

3. DO YOUR HEART PROBLEMS INTERFERE WITH DOING DAILY CHORES?

NOT VERY MUCH 1 2 3 4 5 6 7 VERY MUCH

4. DO YOUR HEART PROBLEMS INTERFERE WITH GOING OUT TO VISIT FRIENDS OR SOCIAL EVENTS?

NOT VERY MUCH 1 2 3 4 5 6 7 VERY MUCH

5. DO YOUR HEART PROBLEMS INTERFERE WITH GOING OUT TO VISIT FAMILY?

NOT VERY MUCH 1 2 3 4 5 6 7 VERY MUCH

6. DO YOUR HEART PROBLEMS INTERFERE WITH BEING ABLE TO WALK WITHOUT RESTING?

NOT VERY MUCH 1 2 3 4 5 6 7 VERY MUCH

7. ARE YOU SHORT OF BREATH OR VERY TIRED WHEN EXERCISING?

NOT VERY MUCH 1 2 3 4 5 6 7 VERY MUCH

8. ARE YOU FRUSTRATED ABOUT HAVING TO STAY IN OR GO TO THE HOSPITAL BECAUSE OF HEART PROBLEMS?

NOT VERY MUCH 1 2 3 4 5 6 7 VERY MUCH

TASQ - United Kingdom/English - Version of 05 May 17

Copyright© 2017 R. Styra, in collaboration with IPPMed - The Institute for Pharmacology and Preventive Medicine

9. ARE YOU FEELING DISCOURAGED ABOUT BEING VERY TIRED?

NOT VERY MUCH 1 2 3 4 5 6 7 VERY MUCH

---

10. ARE YOU WORRIED ABOUT WHAT WILL HAPPEN TO YOUR FAMILY IF YOU DON'T GET BETTER?

NOT VERY MUCH 1 2 3 4 5 6 7 VERY MUCH

---

11. ARE YOU WORRIED ABOUT WHAT WILL HAPPEN FINANCIALLY?

NOT VERY MUCH 1 2 3 4 5 6 7 VERY MUCH

---

12. DO YOU FEEL YOU ARE UNABLE TO MAKE PLANS FOR THE FUTURE?

NOT VERY MUCH 1 2 3 4 5 6 7 VERY MUCH

---

13. IS YOUR ENJOYMENT OF LIFE LIMITED BY YOUR HEART HEALTH PROBLEMS?

NOT VERY MUCH 1 2 3 4 5 6 7 VERY MUCH

---

14. I WOULD RATE MY OVERALL HEART HEALTH TO BE:

☐ Excellent ☐ Very good ☐ Good ☐ Fair ☐ Poor ☐ Very Poor ☐ Terrible

---

15. COMPARED TO TWO MONTHS AGO, HOW WOULD YOU RATE YOUR ABILITY TO DO THINGS?

- ☐ Very much better than two months ago
- ☐ Much better than two months ago
- ☐ Somewhat better than two months ago
- ☐ About the same
- ☐ Somewhat worse than two months ago
- ☐ Much worse than two months ago
- ☐ Very much worse than two months ago

---

16. COMPARED TO TWO MONTHS AGO, DO YOU FEEL HOPEFUL THAT YOUR HEALTH WILL IMPROVE?

NOT VERY MUCH 1 2 3 4 5 6 7 VERY MUCH

MASTER VERSION

TASQ - United Kingdom/English - Version of 05 May 17

Copyright© 2017 R. Styra, in collaboration with IPPMed - The Institute for Pharmacology and Preventive Medicine

www.tasq-q.com

Appendix 3 Patient Global Impression of Change (PGI-I) and Patient Global Impression of Severity (PGI-S)

PGI-C

Please choose the response below that best describes the overall change in your symptom/overall status, etc. since you started taking the study drug.

☐ Much better

☐ A little better

☐ No change

☐ A little worse

☐ Much worse

PGI-S

Please choose the response below that best describes the severity of your symptom/overall status, etc. over the past week.

☐ None

☐ Mild

☐ Moderate

☐ Severe

☐ Very severe

Appendix 4 Borg Rating of perceived exertion and Dyspnoe Score

The Rating of Perceived Exertion Scale

6	
7	Very, very light
8	
9	Very light
10	
11	Fairly light
12	
13	Somewhat hard
14	
15	Hard
16	
17	Very hard
18	
19	Very, very hard
20	
Source: Borg GA. Perceived exertion. *Exerc Sport Sci Rev*. 1974;2:131-153.	

Modified Borg Dyspnoea Scale

Patient instructions: This is the scale that asks you to rate the difficulty of your breathing. It starts at number 0 where your breathing is causing you no difficulty at all and progresses through to number 10 where your breathing difficulty is maximal. How much difficulty is your breathing causing you right now?

0	Nothing at all
0.5	Very, very slight (just noticeable)
1	Very slight
2	Slight
3	Moderate
4	Somewhat severe
5	Severe
6	
7	Very severe
8	
9	Very, very severe (almost maximal)
10	Maximal
Source: Borg GA. Psychophysical bases of perceived exertion. *Med Sci Sports Exerc*. 1982;14(5):377-381.	